POLITECNICO DI MILANO

Department of Civil and Environmental Engineering
Doctoral School in Structural, Seismic and Geotechnical Engineering

Tensile structures: biaxial testing and constitutive modelling of coated fabrics at finite strains

by

Giada Colasante

A thesis submitted for the degree of
Doctor of Philosophy in
Structural, Seismic and Geotechnical Engineering

October 2014

Giada Colasante
Tensile structures: biaxial testing and constitutive modelling of coated fabrics at finite strains

e-mail:
info@giadacolasante.net

Doctoral School in Structural, Seismic and Geotechnical Engineering
Department of Civil and Environmental Engineering
Politecnico di Milano

XXVI cycle

Supervisor: Prof. Giorgio Novati

Faculty members

Prof. Roberto Paolucci (Co-ordinator)
Prof. Raffaele Ardito
Prof. Fabio Biondini
Prof. Gabriella Bolzon
Prof. Claudia Comi
Prof. Alberto Corigliano
Prof. Dario Coronelli
Prof. Claudio di Prisco
Prof. Marco di Prisco
Prof. Liberato Ferrara
Prof. Attilio Frangi
Prof. Elsa Garavaglia
Prof. Cristina Jommi
Prof. Pier Giorgio Malerba
Prof. Anna Pandolfi
Prof. Umberto Perego
Prof. Federico Perotti
Prof. Lorenza Petrini
Prof. Gianpaolo Rosati
Prof. Luigi Zanzi

page intentionally left blank

Politecnico di Milano – October 2014

Committee Members

Prof. Emmanuelle Vidal-Sallé

Prof. Stefano Lenci

Prof. Umberto Perego, Committee Chair

page intentionally left blank

To my family

page intentionally left blank

Abstract

This thesis deals with the mechanical characterisation and constitutive modelling of coated woven fabrics that are employed in tensile structures. These are made of thin surfaces that can carry only tension and no compression or bending, like membranes, cable nets or pneumatic structures. Tensile architecture is increasingly present in the urban environment, not only to cover large span spaces. An evolution towards a wider range of applications is noticeable today, which include canopies, solar shading structures, performance enhancing façades, photovoltaic integrated surfaces, and so on.

Tensile structures are highly efficient structural forms, which leave space to reduction of weight, costs and environmental impact. Since they are minimal, they require an accurate design, for which a considerable know-how is indispensable. Specific knowledge is needed also for the construction, which allows only for little tolerances. Moreover, new composite materials are being created every day; therefore, well-framed technical information is fundamental to keep up with the continuous innovation of this design branch. These are the reasons why only a few designers and constructors currently posses the expertise that is needed to build tensioned structures.

The increasing demand of the market on the one hand, and the need of a very specific expertise on the other hand, have led to the rise of projects that aim at connecting European researchers, engineers, architects, manufacturers and installers. They are all aware of the need of harmonising and standardising the design procedures and of coordinating the existing and future research to meet the stakeholders' requests for specific output. This thesis has been developed within one of these projects, which started in 2008 at Politecnico di Milano to promote the diffusion of lightweight structures in Italy, and to support the transfer of knowledge from the cutting-edge Italian sectors of membrane production and installation to the more traditional one of constructions. Several research groups have been gathered in a multi-disciplinary cluster on innovative textiles, named ClusTEX, with the aim of systematizing and enhancing their expertise on the subject of advanced composites.

The present thesis provides a series of contributions that are consistent with the ClusTEX objectives. First of all, an extensive literature review is carried out to assess the current state of the art about the design of tensile

structures. Besides the load analysis, which is common to all types of constructions, there are two phases that are typical of tensioned structures, namely form-finding and cutting pattern generation. The multiplicity of methods employed in these phases is described within a unified framework: this represents a first effort towards the homogenisation of the heterogeneous design procedures. The scarcity of references about the cutting pattern generation, which are very few if compared to the ones concerning form-finding, highlights the need of further research in this field; it may be partially attributed to the absence of an accurate constitutive model for coated fabrics, which is a prerequisite for the generation of cutting patterns.

Then, the thesis focus is placed on membrane materials for tensile structures. These are mainly composite materials made of a polymeric matrix, which is reinforced by means of woven yarns. The production process and the main technical characteristics of these composites are investigated, because they represent essential knowledge, in view of understanding their mechanical behaviour, which turns out to be extremely influenced by their internal meso-structure.

The mechanical behaviour of such materials is deeply explored in this thesis. First, the main mechanical characteristics of coated woven fabrics are inferred from the literature: anisotropy, nonlinearities, hysteresis are only some among the aspects that characterise their complex response. Subsequently, tests on coated fabrics directly performed by the author with the biaxial machine of ClusTEX are described, and their results commented. Among these tests are noticeable the ones performed under strain control, which employ a new testing procedure: this shows great potential as instrument to evaluate the compensation factors needed for the installation and retensioning of membranes, as well as to provide information that is complementary to the one of the typical stress controlled biaxial tests.

The last part of the thesis deals with the constitutive modelling of coated fabrics. An investigation about the existing constitutive models is presented, which highlights the difference between the ones used for research purposes and the ones employed by designers. The first are often too complex and computationally expensive; moreover, they involve many parameters, which are then difficult to calibrate. On the other hand, in the current design practice, the orthotropic linear elastic model is used, which is too rough to adequately reproduce the highly nonlinear behaviour of coated fabrics, as confirmed by the difficulties arisen during the identification of

the elastic moduli.

Hyperelastic modelling at finite strains seems to be promising to easily model the nonlinear behaviour of coated fabrics. The Holzapfel-Gasser-Ogden hyperelastic constitutive model for biological tissues is chosen first for the analogy between these materials and fibre reinforced composites. Then, a new energy term is added to capture the strong interaction between warp and fill yarns due to the weaving (crimp interchange). A validation of the new model is performed through some simple benchmark problems, of which the analytical solution is evaluated with a code developed within Mathematica. The comparison of the results with experimental data shows that the model can reproduce well the stress-strain behaviour of coated woven fabrics for bias and biaxial tests. The predictive capabilities of the new model are also assessed.

Finally, the proposed constitutive law is implemented into a FEM user subroutine for ABAQUS, and the same validation examples are solved numerically, with results that are consistent with the analytical solution. This implementation into a general purpose finite element software opens the doors to the application of this model to overall structural analysis. However, some numerical issues have still to be solved: extremely large stresses at very large strains, difficulty of Newton's method in predicting a reasonable displacement correction when the stiffness is low, discontinuous derivatives of the strain energy due to deactivation of the compressed fibres, are all aspects that should be considered for the development of an *ad hoc* solution algorithm able to overcome these difficulties.

page intentionally left blank

Acknowledgements

"To make something special you just have to believe it's special.
... There is no secret ingredient. It's just you."

— Mr. Ping to his son Po
(Kung Fu Panda movie)

This research has been founded by the Leo Finzi Memorial Scholarship, administered by "Istituto Lombardo - Accademia di Scienze e Lettere". I gratefully acknowledge the financial support from Finzi Family. Furthermore, I thank both Canobbio Textile Engineering (Castelnuovo Scrivia, Alessandria) and New Tech Targets (Fagnano Olana, Varese) for having provided the material employed in the experimental tests.

I wish to express my sincere thanks to my supervisor, Prof. Giorgio Novati, for his guidance and support throughout the course of this research. I would like to thank him for having introduced me to the extremely interesting research topic of tensile structures, but also for the kindness and patience he has demonstrated during these years.

Foremost, my deepest gratitude goes to Prof. Egidio Rizzi, of the University of Bergamo, because he has believed in me and encouraged me to start this beautiful Ph.D. experience. I know that he would not be thanked on top of others, because of his correctness, politeness and humility, but he would really deserve this reward for the stimulating chats and for remembering me continuously that passion is the secret ingredient of research.

I would also like to express my gratitude to Prof. Peter Gosling, who has hosted me for 5 months at Newcastle University. It has been one of the most exciting experiences I have ever had. I would like to thank him for his patience, humour, and for its advice, not only the scientific one (I spent wonderful days visiting the Lake District). On top of that, I am thankful to him for the precious contribution to my self-confidence growth.

Special thanks to Paolo Beccarelli and Carol Monticelli for the pleasing time we have spent together at the ClusTEX laboratory. I would like to thank also Prof. Alessandra Zanelli, the ClusTEX coordinator, for the times she popped in during the tests with her smile: it is nice to see that someone keeps always a positive attitude, especially the boss.

During my studies here in Milan, I had the opportunity to interact occasionally with some professors and researchers of the Department of

Civil and Environmental Engineering. I would like to thank all of them for the suggestions and the kind support. The enthusiasm that some of them have for research has been motivational to me; the passion and happiness of Prof. Giulio Maier, on top of others, are extremely contagious.

I have learnt very much from the interesting lectures by Prof. Anna Pandolfi. I am so much thankful to her for having provided me with the notions I needed to understand nonlinear mechanics and large strains theory. The basics about Holzapfel-Gasser-Ogden model that she taught me have turned out to be extremely useful for my research. I wish to thank her also for her kindness and professionalism.

I would also like to express my deepest gratitude to Prof. Gerard Holzapfel. Thanks for the quick answer to my e-mail and for the suggestions about possible sources of errors in the numerical implementation. It is always a honour to interact with the greatest scientists.

Furthermore, I warmly thank all my colleagues for the enjoyable time spent together: the ones in Milan, who have shared with me happiness and pain of doctoral studies at Politecnico di Milano, and the ones in Dalmine, for the chats in front of the best coffee of ever. I also thank Prof. Giuseppe Cocchetti for the pleasant and stimulating discussions at lunch time.

Last but not least, I would like to thank Andrea and my family for all their love and encouragement. Words will be never enough to express how much I have appreciated their faithful support, especially during the final stages of this wonderful experience. Thank you.

Giada Colasante
Politecnico di Milano
October 2014

Contents

List of Figures

List of Tables

LIST OF TABLES

1 Introduction

1.1 Context of the present research

The term *tensile* or *tension structures* describes a category of structures in which the load bearing capacity is achieved through an appropriate tension field combined with an adequate shape. Indeed all these structures show essentially two states: they are taut or slack depending on the presence or not of prestress, thus they are also named *taut structures* (Pauletti & Pimenta, 2008).

The above mentioned category covers a wide range of structures and applications. According to Lewis (2003), tension structures can be grouped into three main typologies: boundary tensioned membranes, pneumatic structures and pre-stressed cable nets. The first type of structures (Figure 1.1) is built by stretching a membrane (coated fabric or foil) to meet fixed boundaries; these boundaries can be assembled with flexible cables or rigid frame beams. Pneumatic structures (Figure 1.2) are thin membranes stressed by means of an internal air pressure, which may be subdivided into air-supported and air-inflated: the first typology consists of a single membrane that encloses a functionally useful space, whose internal pressure is slightly different from the external one; the second typology is realised with inflated building elements (e.g. cushions), while the internal volume of the building remains at atmospheric pressure. Finally, pre-stressed cable nets (Figure 1.3) represent a sort of discretised membrane structure, where cables can be tensioned directly using rigid supports (such as compression ring beams) or flexible edge cables.

Figure 1.1: *SAGA Headquarters Amenity Building, Folkston, UK, 2002 (from www.skyspan.com).*

Figure 1.2: *Allianz Arena in Munich, Germany, 2002 (from www.osram.it).*

Figure 1.3: *West German Pavillion at the 1967 Expo in Montreal, Canada, designed by Frei Otto and Rolf Gutbrod (from the National Archives of Canada).*

Tensile structures represent the most advanced result of a constant research of lightness and free forms in architecture. They are characterised by thin surfaces, whose shape is defined such that they are able to equilibrate the applied loads only by means of tensions, with no compression or bending. This results in highly efficient structural forms, where the ratio between the weight and the carried loads is extremely low.

Tents employed as protection against rain, wind and sun represent one of the earliest form of construction in the human history. Nevertheless, the first tensile structures as intended today were built in the fifties, when Frei Otto conducted an extensive experimental campaign about soap films and minimal surfaces, which provided architects and engineers with the first design tools for tensioned structures. Most of the earliest tensioned surfaces were realised as cable nets, sometimes covered with membranes. Some examples of cable net structures designed by Frei Otto are the West German Pavillion for the 1967 Expo in Montreal (Figure 1.3) and the Olympic Stadium built in 1972 in Munich (Figure 1.4).

Figure 1.4: *Olympic Stadium in Munich, Germany, 1972, designed by Frei Otto and Gunther Behnisch (from www.archdaily.com).*

Since that time, examples of tensile structures have been constructed

worldwide, especially in UK, Germany, Spain, France, USA, Australia, and, in the last years, China and Japan. Modern fabric structures employ polymeric fibre reinforced membranes, like PVC coated polyester fabrics and PTFE coated glass fabrics. These materials, which come from the aerospace industry, have been introduced in the construction sector only from the seventies. Today, membrane structures are increasingly employed as efficient solutions to cover large span areas with low weight, cost and environmental impact. One of the most popular applications is for sport arenas (Figure 1.5).

Figure 1.5: *Olympic Stadium in London, UK, 2012 (from www.wikipedia.org).*

At present, an evolutionary trend towards a wider range of applications of these membranes is noticeable. Technical textiles are incorporated into more complex hybrid structures, satisfying specific demands in terms of energy saving, sound absorption, translucency, flame retardancy, and so on. Multiple layer systems, ETFE cushions, air-inflated beams (Figure 1.6), performance enhancing textile façades (Figure 1.7), photovoltaic integrated

surfaces, are all products of continuous innovation in this field.

Figure 1.6: *Garage Park in Montreux, Switzerland, 2004, realised with Tensairty beams (from www.canobbio.com).*

Since tensile architecture is "minimal", a considerable know-how is needed for its design and construction. Specific knowledge is also required to keep up with the technical innovation of the advanced composite industry, which everyday introduces new materials in the market. These are the reasons why only a few designers and constructors currently possess the expertise that is needed to build tensioned structures.

Moreover, the rapid growth of this structural typology has led to the current heterogeneity of design procedures and to fragmentation of the technical knowledge that membrane producers have at their disposal. This situation is exacerbated by the absence of a European Standard for the regulation of the matter.

Within this context, new projects have been created to connect European researchers, engineers, architects, producers and installers. The main scope of these is to harmonise the design procedures and to coordinate the existing and future research, in order to meet the sector needs. The first association of this type, which is named TENSINET (www.tensinet.com),

Figure 1.7: *R&D center in Dogern, Switzerland, 2010 (from www.detail-online.com).*

was created in 2001 with the aim of shearing basic and multi-disciplinary information about tensile architecture and identifying gaps in the current knowledge about the topic, in order to stimulate the scientific research in those areas.

The TENSINET activity has represented a starting point for the institution of a European Committee for Standardization (CEN TC 250), which is currently preparing a preliminary document for the development of the Eurocodes for tensile membrane structures design (CEN/TC 250/WG5) and for testing and modelling of fibre reinforced polymer materials (CEN/TC 250/WG4).

Italy is trying to boost its competence and relevance in this field, by joining the aforementioned international activities. Despite its cutting-edge sector of membrane installers, tensile architecture is currently not widely employed in Italy. Some remarkable realisations include the Olympic Stadium in Rome (1927), the Palasport in Genova (1961, Figure 1.8), the membrane covering Piazza Italia during the Grand Exhibition of April in Milan (1986), the Delle Alpi Stadium in Turin (1988), the Juventus Sta-

dium in Turin (2011, Figure 1.9). Incidentally, Leo Finzi, to whom the memorial scholarship that has funded this research is devoted, was among the designers of Palasport in Genova (Maier, 1963a,b; Finzi & Maier, 1964).

Figure 1.8: *Palasport in Genova, Italy, 1961 (from genova.repubblica.it).*

To promote the development of lightweight structures in Italy, and to support the transfer of knowledge from the extremely competitive sectors of membrane production and installation to the more traditional one of constructions, a cluster has been created in 2008 at Politecnico di Milano. This multi-disciplinary cluster on innovative textiles is named ClusTEX, and it gathers several research groups and departments at Politecnico di Milano. It aims at systematizing and enhancing their expertise on the subject of textile materials and advanced composites and it manages a laboratory with one among the most advanced biaxial testing rigs currently available in Europe.

The present thesis is a contribution in line with the ClusTEX goals. Its objectives and structure are detailed in the next Sections 1.2 and 1.3.

Figure 1.9: *Juventus Stadium in Turin, Italy, 2011 (from wikimapia.org).*

1.2 Research objectives

Within the framework described in the previous Section 1.1, the main aim of this thesis is to increase the knowledge about the structural aspects of tensile structure design, with focus on coated woven fabrics that are employed as membranes. This objective may be particularised in the following specific goals:

- To carry out an extensive literature review, in order to assess the current state of the art about the design of membrane structures.
- To investigate the production process of the materials employed as membranes in tensile structures, in order to understand their technical and mechanical characteristics.
- To thoroughly characterise the mechanical behaviour of coated woven fabrics, by both employing data from the literature and performing biaxial tests of different types.

- To investigate the stress-strain behaviour of coated woven fabrics through a new typology of strain-controlled biaxial tests.
- To define the current framework of constitutive models available for coated fabrics.
- To implement the procedure of the MSAJ/M-02:1995 (1995) Japanese Standard for the identification of the elastic moduli and to apply it to the experimental data obtained from the previously performed biaxial tests, in order to highlight the issues related to this commonly adopted approach and to constitute a term of comparison for the more advanced constitutive model proposed in this thesis.
- To develop a modified version for coated woven fabrics of the HGO hyperelastic model, which was created by Holzapfel et al. (2000) for biological tissues. Such modified HGO model is characterised by the addition of a new term to the free-energy function, that aims at capturing the strong interaction between the yarns due to the so-called crimp interchange.
- To calibrate the parameters of the new hyperelastic model using the same biaxial test data previously employed for the identification of the orthotropic linear elastic model parameters, and to compare the obtained results.
- To validate the new hyperelastic model through some simple bias extension tests and cruciform biaxial tests, whose results will be compared to experimental data.
- To implement the new constitutive law into a general purpose finite element code, in order to make it useful for the overall analysis of membrane structures.

1.3 Thesis layout

The present thesis has the following structure:

- Chapter 2 contains an extensive literature review on the design procedures employed for tensile structures. More in detail, an attempt

is made of describing, within a unified framework, the heterogeneity of approaches currently used in the form-finding and cutting pattern generation phases, which are peculiar to tensioned membranes.

- Chapter 3 describes the main types of architectural membrane materials. Details are given concerning their technical properties. The production process is presented, together with the single components of these materials, which both contribute to their macroscopic mechanical behaviour.

- Chapter 4 investigates the main aspects of the mechanical behaviour of coated woven fabrics employed in textile architecture. In the first part of the chapter, this information is inferred from the literature about the topic. Additional knowledge is added in the second part, where uniaxial and biaxial tests performed directly by the author with the biaxial machine at ClusTEX laboratory are described, and their results commented. Several materials are tested and various testing procedures are employed. A new testing protocol, based on a strain-controlled loading profile, is proposed as an instrument for the evaluation of the compensation factors needed for the installation, as well as for furnishing information that is complementary to the one obtained from stress-controlled biaxial tests.

- Chapter 5 reports a summary of the existing constitutive models for coated fabrics, which are classified into mesostructural and continuum models. A least squares identification of the elastic moduli from biaxial test data is also performed, according to the current design practice, which employs the orthotropic linear elastic law to model coated fabric stress-strain behaviour.

- Chapter 6 presents a new hyperelastic constitutive model for coated fabrics at finite strains. First, the nonlinear continuum mechanics framework is described and a definition of the tensors and pertinent quantities employed is provided. Then, the Holzapfel-Gasser-Ogden (HGO) model for biological tissues is described and modified by adding a new energy term, which is intended to capture the strong transversal fibre interaction due to the weaving, namely the crimp interchange. Finally, the parameters of the new proposed model are

estimated with the use of least squares applied to the biaxial test data acquired from the previous Chapter 4.

- Chapter 7 describes the implementation of the new constitutive model into the general purpose finite element code ABAQUS. The developed user subroutine is illustrated and verification examples are provided to demonstrate the correctness of the coding.

- Chapter 8 validates the new model by comparing the analytical and numerical solutions of some simple biaxial and bias extension tests, with the available experimental data. The predictive capability of the model is also assessed through the results of some biaxial tests that are performed at constant values of warp to fill stress ratios not employed in the calibration of the material parameters.

- Chapter 9 summarises and comments the main results obtained with this work; future developments of the present research are also outlined.

- Appendix A collects the graphical representation of the experimental data concerning the biaxial tests performed in the context of this research.

2

Design of tensile structures

The design of tensile structures is a complex process, which involves several steps: shape definition, creation of the engineering model, form-finding, cutting pattern generation, load analysis, detailing and construction studies. Even though these phases follow each other in a linear fashion, many iterations may be required; thus, it often happens that going back and revisiting the previous phases becomes necessary.

In this Section the attention is put on the two design steps that are peculiar to tensile structures, namely form-finding and cutting pattern generation. Form-finding is the earliest engineering phase, which determines the shape that the membrane (or the cable net) must assume to equilibrate the prestress loads, while fitting the predefined boundaries. Cutting pattern generation is the process of defining the shape, direction and dimension of the strips that must be cut from the planar roll of membrane material, such that the final 3D surfaces can be reproduced once the strips have been positioned and prestressed.

The variety of methods currently employed to perform the aforementioned design phases has led to quite heterogeneous notations and approaches. An attempt is made here of systematising the current state of the art, by presenting them within a unified framework. Form-finding methods are described in Section 2.1, while cutting pattern generation is treated in Section 2.2.

2.1 Form-finding

Tensile structures belong to the category of *form active structures* (Veenendaal & Block, 2011; Beccarelli et al., 2011): these mechanical systems display the ability to alter their own configuration and form in response to possible changes of the environmental loads. In particular, the shape of membrane and pneumatic structures is not known a priori, since it depends on the applied prestress and on the boundary conditions. This peculiarity determines the need of a preliminary step in the design process, which is called *form-finding* or *shape-finding*. This aims at defining an appropriate reference prestressed configuration of the membrane, which is the shape that equilibrates the applied forces in a given boundary with respect to a certain stress state. Since the found equilibrated configuration is employed as initial or reference configuration for the subsequent load analysis, form-finding is sometimes called *initial equilibrium problem* in the technical literature (Haber & Abel, 1982a).

Form-finding is a complex process that must consider several factors simultaneously, as pointed out by Maurin & Motro (2013). First, the level of prestress has to be managed to avoid wrinkling, slackening or excessive tension, while providing the geometric stiffness that is needed to carry environmental loads. Second, boundary conditions (anchoring points and lines) must be defined on the basis of aesthetic reasons, but also in a way apt to satisfy architectural requirements and to allow water evacuation. According to Haber & Abel (1982a), the problem is further complicated by the fact that some of the loads acting in the reference configuration are shape-dependent, e.g. self-weight and inflation pressure (in the case of pneumatic structures). The solution must also satisfy all structural, architectural and constructional requirements.

The basic parameters involved in the initial equilibrium problem are: surface topology, body forces, surface tractions, geometry boundary conditions, internal stress distribution and surface geometry. The actual surface geometry is treated as unknown during the form-finding process, therefore boundary conditions are necessary to ensure a unique solution. Moreover, the initial pre-stress distribution is a crucial design parameter, since sufficient tensile stresses must be provided to avoid wrinkling and to produce the desired degree of stiffness (Haber & Abel, 1982a).

Once prestresses and boundary conditions are defined, the definition of the corresponding equilibrated membrane shape can be carried out using different methods. According to Lewis (2008), who provides a review of form-finding methods for fabric structures, prior to 1970 form-finding of tension membrane structures was based on the construction of physical models made of reduced-scale fabric or soap films. Then, in 1972, the design of the Munich Olympic Stadium marked the departure from the exclusive use of physical models in favour of computational form-finding techniques.

As described in the European Design Guide for Tensile Surface Structures (Forster & Mollaert, 2004), the art of form-finding with physical models (soap films, fabric and wire models) dates back to the 1950's, when architect Frei Otto started to realise membrane structures based on the concept of *minimal surfaces* (Otto et al., 1973). These are defined as the surfaces that have the smallest area within a particular set of boundaries, thus requiring the least amount of potential energy. Minimal surfaces show a uniform stress distribution, which is particularly convenient to avoid wrinkles and stress concentrations. Although physical modelling is cumbersome and may display limited accuracy, it is useful to the designer for the development of an intuitive understanding of membrane structure working principles. For example, by building physical models it is easy to understand that planar boundary configurations result in planar minimal surfaces, while doubly curved surfaces are obtained within three-dimensional boundaries. Moreover, curved surfaces are classified into synclastic (if the principal curvatures in two orthogonal directions have the same sign) and anticlastic (if the principal curvatures in two orthogonal directions display opposite signs): synclastic shapes can be obtained only for air inflated structures, while mechanically prestressed membranes always give rise to anticlastic shapes.

Currently, computational form-finding is the most widely used. In the last five decades several methods have been developed and implemented in commercial and research computer codes (Figure 2.1), which can be classified, according to Veenendaal & Block (2012), into three main categories:

- **Stiffness matrix methods**: also called transient stiffness methods (Lewis, 2008), they are based on using standard stiffness matrices, which are the sum of the elastic and geometric contributions;

- **Geometric stiffness methods**: only geometric stiffness is employed, therefore no material definition is needed;
- **Dynamic equilibrium methods**: the static equilibrium solution is obtained as steady-state of an equivalent dynamic problem.

In all these approaches the membrane is discretised into inter-connected elements (cable or surface elements) and different procedures are used to solve the initial equilibrium problem. Both the type of discretisation and the solution approach strongly influence the theoretical formulation of each form-finding method, as well as the accuracy of the solution. This has been confirmed by the extreme variability of the results obtained with the round robin exercise in Gosling et al. (2013).

Details about the existing shape-finding methods, divided by category, are given in the following subsections. Indications about their advantages and critical aspects are provided as well.

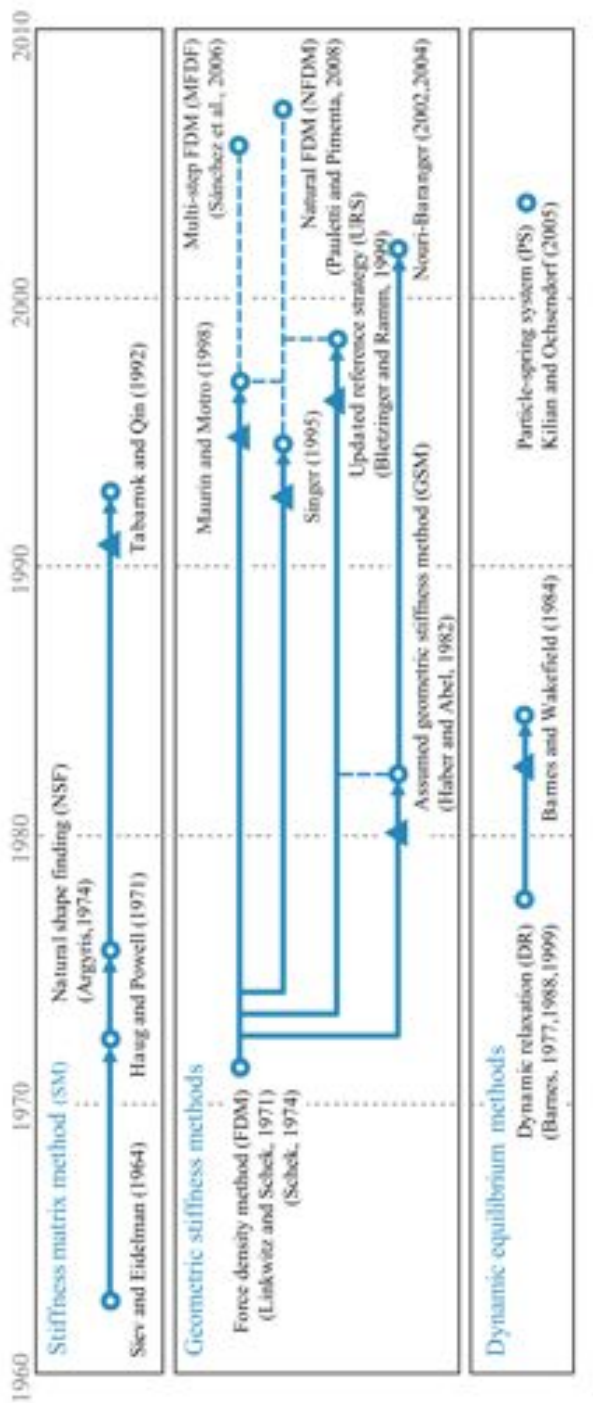

Figure 2.1: *Development and categorization of form finding methods with key references. Arrows denote descendence, dotted lines denote independent but related methods and triangles a first formulation using surface elements (from Veenendaal & Block, 2012).*

2.1.1 Stiffness matrix methods

The stiffness matrix methods are among the oldest form-finding approaches. This category is the least well-defined, especially because there is no consensus on how to name it in the existing literature: nonlinear network computation (Schek, 1974), Newton-Raphson iteration (Barnes, 1977), nonlinear displacement analysis (Haber & Abel, 1982a,b), transient stiffness (Lewis, 2003, 2008), Stuttgart direct approach (Linkwitz, 1999a,b), grid method (Siev & Eidelman, 1964). However, Veenendaal & Block (2012) claim that the references for stiffness matrix method (Siev & Eidelman, 1964; Argyris & Scharpf, 1972; Haug & Powell, 1972; Argyris et al., 1974a; Tabarrok & Qin, 1992) are largely equivalent.

According to Veenendaal & Block (2011), which presents a single computational framework for the comparison of different form-finding methods, each stiffness matrix method tries to minimize the residual force vector $\mathbf{r}$ to achieve static equilibrium. Vector $\mathbf{r}$ at each node is defined as the difference between the external loads (collected in vector $\mathbf{p}$) and the internal forces (vector $\mathbf{f}$):

$$\mathbf{r} = \mathbf{p} - \mathbf{f} \tag{2.1}$$

In a general network or membrane, which is not in equilibrium, $\mathbf{r}$ is different from the null vector. Applying Newton-Raphson's iterative method, the new configuration at time step $n+1$ can be evaluated starting from the known geometry at time step n, according to the following relation, until convergence is reached:

$$\mathbf{x}^{(n+1)} = \mathbf{x}^{(n)} + \mathbf{K}^{-1}\mathbf{r}^{(n)} = \mathbf{x}^{(n)} + \mathbf{K}^{-1}(\mathbf{p}^{(n)} - \mathbf{f}^{(n)}) \tag{2.2}$$

where $\mathbf{K}$ is the global stiffness matrix, which is the sum of elastic $\mathbf{K}^e$ and geometric $\mathbf{K}^g$ stiffness contributions (for the definition and construction of geometric and material (elastic) stiffness matrices see e.g. Zienkiewicz & Taylor (2000, vol. 1-2).

Linkwitz (1999a) particularizes Equations (2.1) and (2.2) to a network of branches and nodes. To achieve this, the structural topology is defined via the *connectivity matrix* ($\mathbf{C}$), sometimes also called *branch-node matrix*. For a network with m branches and n nodes in a three-dimensional space,

$\mathbf{C}$ is a $[3m \times 3n]$ matrix constructed as follows:

$$\mathbf{C} = \begin{bmatrix} \overline{\mathbf{C}} & & \\ & \overline{\mathbf{C}} & \\ & & \overline{\mathbf{C}} \end{bmatrix} \tag{2.3}$$

where the components of each submatrix $\overline{\mathbf{C}}$ are:

$$\overline{\mathbf{C}}_{ij} = \begin{cases} +1 & \text{if node } j \text{ is the head of branch } i \\ -1 & \text{if node } j \text{ is the tail of branch } i \\ 0 & \text{otherwise} \end{cases} \tag{2.4}$$

The connectivity matrix can be partitioned into two submatrices:

$$\mathbf{C} = [\mathbf{C}_i \quad \mathbf{C}_f] \tag{2.5}$$

where $\mathbf{C}_i$ and $\mathbf{C}_f$ contain the columns of $\mathbf{C}$ associated with the interior (i.e. free) and with the fixed nodes, respectively. Analogously, the $[3n \times 1]$ vector of nodal coordinates:

$$\mathbf{x} = \begin{bmatrix} \overline{\mathbf{x}} \\ \overline{\mathbf{y}} \\ \overline{\mathbf{z}} \end{bmatrix} = \begin{bmatrix} \overline{\mathbf{x}} & = [x_1 \; x_2 \; \dots \; x_n]^{\mathrm{T}} \\ \overline{\mathbf{y}} & = [y_1 \; y_2 \; \dots \; y_n]^{\mathrm{T}} \\ \overline{\mathbf{z}} & = [z_1 \; z_2 \; \dots \; z_n]^{\mathrm{T}} \end{bmatrix} \tag{2.6}$$

can be partitioned similarly:

$$\mathbf{x} = \begin{bmatrix} \mathbf{x}_i \\ \mathbf{x}_f \end{bmatrix} \tag{2.7}$$

Then, the coordinate difference vector $\mathbf{u}$ can be written as a function of $\mathbf{C}$ and $\mathbf{x}$:

$$\mathbf{u} = \begin{bmatrix} \overline{\mathbf{u}} \\ \overline{\mathbf{v}} \\ \overline{\mathbf{w}} \end{bmatrix} = \mathbf{C}\mathbf{x} = [\mathbf{C}_i \quad \mathbf{C}_f] \begin{bmatrix} \mathbf{x}_i \\ \mathbf{x}_f \end{bmatrix} \tag{2.8}$$

where $\overline{\mathbf{u}}$, $\overline{\mathbf{v}}$ and $\overline{\mathbf{w}}$ are vectors, each containing m coordinate differences in the corresponding Cartesian directions. Writing the internal forces $\mathbf{f}$ in terms of the branch forces $\mathbf{g}$, expressed as a function of coordinate differences $\mathbf{u}$, Equation (2.1) reads (Linkwitz, 1999a):

$$\mathbf{r} = \mathbf{p} - \mathbf{C}_i^{\mathrm{T}} \mathbf{g}(\mathbf{u}) \tag{2.9}$$

Therefore, by applying the Newton-Raphson method, the following solution is obtained (Linkwitz, 1999a):

$$\mathbf{x}^{(n+1)} = \mathbf{x}^{(n)} + [\mathbf{C}_i^{\mathrm{T}} \mathbf{J}_{\mathbf{g}}(\mathbf{x})]^{-1} [\mathbf{p}^{(n)} - \mathbf{C}_i^{\mathrm{T}} \mathbf{g}(\mathbf{u})^{(n)}] \tag{2.10}$$

where $\mathbf{J}_{\mathbf{g}}(\mathbf{x})$ is the Jacobian of the branch forces $\mathbf{g}$ with respect to the nodal coordinates $\mathbf{x}$. The analogy between Equations (2.2) and (2.10) shows that $\mathbf{C}_i^{\mathrm{T}} \mathbf{J}_{\mathbf{g}}(\mathbf{x}) = \partial \mathbf{f} / \partial \mathbf{x}$ is the global stiffness matrix of the system. The derivation of this matrix for a linear one-dimensional element can be found in Argyris & Scharpf (1972). The element elastic and geometric stiffness matrices can be written in global coordinates as follows:

$$\hat{\mathbf{k}}^e = \frac{\widehat{E}\widehat{A}}{\widehat{L}} \begin{bmatrix} \hat{\mathbf{a}}\hat{\mathbf{a}}^{\mathrm{T}} & -\hat{\mathbf{a}}\hat{\mathbf{a}}^{\mathrm{T}} \\ -\hat{\mathbf{a}}\hat{\mathbf{a}}^{\mathrm{T}} & \hat{\mathbf{a}}\hat{\mathbf{a}}^{\mathrm{T}} \end{bmatrix} \tag{2.11a}$$

$$\hat{\mathbf{k}}^g = \frac{\widehat{T}}{\widehat{L}} \begin{bmatrix} \mathbf{I} - \hat{\mathbf{a}}\hat{\mathbf{a}}^{\mathrm{T}} & -(\mathbf{I} - \hat{\mathbf{a}}\hat{\mathbf{a}}^{\mathrm{T}}) \\ -(\mathbf{I} - \hat{\mathbf{a}}\hat{\mathbf{a}}^{\mathrm{T}}) & \mathbf{I} - \hat{\mathbf{a}}\hat{\mathbf{a}}^{\mathrm{T}} \end{bmatrix} \tag{2.11b}$$

where the cap symbol denotes element quantities. More in detail, $\widehat{E}$ is the Young's modulus of the material, $\widehat{A}$ is the branch cross section area, $\widehat{L}$ is the element length, $\widehat{T}$ is the axial force inside the bar and $\hat{\mathbf{a}}$ is the unit vector that defines the branch direction (vector of direction cosines), written as:

$$\hat{\mathbf{a}}^{\mathrm{T}} = [\, \cos\alpha_x \quad \cos\alpha_y \quad \cos\alpha_z \,] \tag{2.12}$$

being α_x, α_y, α_z the angles between the bar and the global coordinate axis $\mathbf{e}_x$, $\mathbf{e}_y$, $\mathbf{e}_z$, respectively. All the element quantities can be grouped into diagonal matrices in which each row corresponds to one branch, thus $\overline{\mathbf{E}} = \mathrm{diag}(\widehat{E}_i)$, $\overline{\mathbf{A}} = \mathrm{diag}(\widehat{A}_i)$, $\overline{\mathbf{L}} = \mathrm{diag}(\widehat{L}_i)$ and $\overline{\mathbf{T}} = \mathrm{diag}(\widehat{T}_i)$. Then, it is possible to construct the global matrices $\mathbf{E}$, $\mathbf{A}$, $\mathbf{L}$ and $\mathbf{T}$ by following the same procedure previously employed for the connectivity matrix $\mathbf{C}$ in (2.3).

The last ingredient for the assembly of the global stiffness matrix consists in writing the global matrix of direction cosines as $\mathbf{U}\mathbf{L}^{-1}$, where it has been assumed that $\mathbf{U} = \mathrm{diag}(\mathbf{u})$. The global elastic and geometric stiffness matrices are finally obtained by the assembly:

$$\mathbf{K}^e = \mathbf{C}_i^{\mathrm{T}} \mathbf{L}^{-1} \mathbf{E} \mathbf{A} \mathbf{U}^2 \mathbf{L}^{-2} \mathbf{C}_i \tag{2.13a}$$

$$\mathbf{K}^g = \mathbf{C}_i^{\mathrm{T}} \mathbf{L}^{-1} \mathbf{T} (\mathbf{I} - \mathbf{U}^2 \mathbf{L}^{-2}) \mathbf{C}_i \tag{2.13b}$$

so that:

$$\mathbf{K} = \mathbf{C}_i^{\mathrm{T}} \mathbf{J}_{\mathbf{g}}(\mathbf{x}) = \mathbf{K}^e + \mathbf{K}^g \tag{2.14}$$

The stiffness matrix method solves the initial equilibrium problem (Equation (2.2) or (2.10)) within a Total Lagrangian Formulation, which means that variables are referred to the initial configuration Γ_0. Since the method assumes a linear dependence of deflections upon forces, it is critically dependent on the assumption of small displacements and rotations. Therefore large changes in geometry, which are common in the initial steps of form-finding, would results in lack of convergence. A transient stiffness matrix (Argyris & Scharpf, 1972; Argyris et al., 1974a; Lewis, 2008), which is updated at each iteration, can be used to improve convergence. However, to include material properties is unnecessary, computationally expensive and may lead to difficulties in reaching stable convergence (Barnes, 1977; Haber & Abel, 1982a; Nouri-Baranger, 2004; Lewis, 2008).

Another difficulty related to the use of stiffness matrix methods is that, to start the iterative algorithm, an initial geometry is required, which is usually unknown at this step of the design process. To partially overcome this problem in the case of cable nets, Linkwitz (1999a) suggests to partition the net into an interior and a boundary part. The internal elements have a fixed initial slack length (or cutting pattern length), while in the boundary zone cutting pattern lengths are unknown and can be evaluated by setting the tension values in the boundary elements. Only by trial and error, changing the forces in the boundary zone, it is possible to obtain a satisfactory tension distribution in the inner part. Anyway, Linkwitz (1999a) admits that "*many trials may be necessary until a figure of equilibrium satisfying both requirements of form and forces has been found*".

Geometric stiffness methods, discussed in the following section, can address the above described difficulties inherent to the use of the total stiffness matrix.

2.1.2 Geometric stiffness methods

Form-finding is in principle a geometric problem, thus material independent, even if some shape-finding methods (namely the stiffness matrix and the dynamic relaxation methods) require the designation of (sometime fictious) material properties. Geometric stiffness methods are based on this

observation, indeed they consider only the geometric stiffness contribution. Even if the methods belonging to this category have been developed independently, Veenendaal & Block (2012) conclude that the main references for geometric stiffness methods (Linkwitz & Schek, 1971; Linkwitz et al., 1974; Schek, 1974; Haber & Abel, 1982a; Singer, 1995; Maurin & Motro, 1998; Bletzinger & Ramm, 1999; Sánchez et al., 2007; Pauletti & Pimenta, 2008) are conceptually equivalent.

The force-density is the oldest geometric stiffness method, which was first introduced by Linkwitz for the form-finding of the cable roof of the Stadium for the 1972 Olympic Games in Munich. It was first published in Linkwitz & Schek (1971) and then extended by Linkwitz et al. (1974) and Schek (1974). Like in the stiffness matrix method applied to nets (Linkwitz, 1999a), the membrane is modelled as a system of straight bars and nodes, but with the force-density method it is possible to compute the coordinates of the free nodes, hence the structural geometry, solving the equilibrium equations without knowing any initial coordinates, but the ones of fixed nodes.

The force-density method performs a linearization of Equation (2.9) by introducing the definition of force density. The forces in a network of elastic bars are determined by an initial stress and an elastic term. If the elastic term is neglected, as typical of form-finding based on geometric stiffness, the element forces can be evaluated as follows:

$$\mathbf{f} = \mathbf{C}_i^{\mathrm{T}}\mathbf{g}(\mathbf{u}) = \mathbf{C}_i^{\mathrm{T}}\mathbf{U}\mathbf{L}^{-1}\mathbf{t} \tag{2.15}$$

where $\mathbf{t}$ is the vector that contains the tensile forces distribution. The so called *force densities* (Schek, 1974) or *tension coefficients* (Barnes, 1977) are defined as the force-to-length ratios:

$$\mathbf{q} = \mathbf{L}^{-1}\mathbf{t} \tag{2.16}$$

The coefficients of $\mathbf{q}$ depend on the actual lengths $\mathbf{L}$. Nevertheless, the linear force-density method assumes constant force densities, which are evaluated using the (updated) reference lengths $\mathbf{L}_{ref}$ and the prescribed forces $\mathbf{t}_0$:

$$\mathbf{q} = \mathbf{L}_{ref}^{-1}\mathbf{t}_0 \tag{2.17}$$

Using relation (2.8), $\mathbf{Q} = \mathrm{diag}(\mathbf{q})$ and the following identity:

$$\mathbf{U}\mathbf{q} = \mathbf{Q}\mathbf{u} \tag{2.18}$$

system (2.9) can be written as:

$$\mathbf{r} = \mathbf{p} - \mathbf{C}_i^{\mathrm{T}}\mathbf{U}\mathbf{q} = \mathbf{p} - \mathbf{C}_i^{\mathrm{T}}\mathbf{Q}\mathbf{C}_i\mathbf{x}_i - \mathbf{C}_i^{\mathrm{T}}\mathbf{Q}\mathbf{C}_f\mathbf{x}_f \tag{2.19}$$

By setting $\mathbf{D}_i = \mathbf{C}_i^{\mathrm{T}}\mathbf{Q}\mathbf{C}_i$ and $\mathbf{D}_f = \mathbf{C}_i^{\mathrm{T}}\mathbf{Q}\mathbf{C}_f$, Equation (2.19) becomes:

$$\mathbf{r} = \mathbf{p} - \mathbf{D}_i\mathbf{x}_i - \mathbf{D}_f\mathbf{x}_f \tag{2.20}$$

Since Equation (2.20) is now linear, iterative solution methods like Newton-Raphson are not further required. Thus, the coordinates of the internal nodes can be computed by solving the system of equilibrium $\mathbf{r} = \mathbf{0}$ with the classical methods used for linear systems. The symbolic solution is:

$$\mathbf{x}_i = \mathbf{D}_i^{-1}(\mathbf{p} - \mathbf{D}_f\mathbf{x}_f) \tag{2.21}$$

where it can be noted that only the coordinates of the fixed nodes must be provided as input, hence there is no need of knowing the initial slack lengths of the bars. After the solution in terms of nodal coordinates is known, the prestress can be computed a posteriori with the following expression:

$$\mathbf{s} = \overline{\mathbf{A}}^{-1}\mathbf{t} = \overline{\mathbf{A}\mathbf{L}}^{-1}\mathbf{q} \tag{2.22}$$

while the unstressed lengths are obtained as follows:

$$\overline{\mathbf{L}}_0 = \overline{\mathbf{L}}(\mathbf{I} + \overline{\mathbf{E}\mathbf{A}}^{-1}\mathbf{t})^{-1} \tag{2.23}$$

where $\mathbf{I}$ is the identity matrix of dimensions $[m \times m]$.

The number of shapes that can be generated with the force-density method is theoretically infinite. However, from the practical point of view, only networks with a more or less uniform stress distribution are acceptable. Since the stress field is evaluated only a posteriori (from Equation (2.22)), it is not possible to control the final stress distribution using the force density method. Moreover, it is clear that a constant value of force density in all the branches does not produce a uniform tension field, unless the calculated lengths of the elements happen to be constant. According to Schek (1974) and Linkwitz (1999a), values of force densities that produce reasonable stress distributions are equal to 1 for all inner cables and to a value inversely proportional to the length for boundary cables.

An extension of the force density method from cable nets to membrane surfaces has been proposed by Singer (1995) and Maurin & Motro (1998). In the first case, a fictitious stress variable is introduced, that represents the isotropic stress inside the triangular area delimited by three linear elements: the force densities are then expressed as a function of this new variable, thus allowing for the stress control during the form-finding procedure. In the second case, the membrane is discretised by means of triangular elements with isotropic Cauchy stress and the stress densities are defined as the stress to area ratios in each surface element. Both the strategies are useful to obtain a uniform isotropic plane stress distribution, which is conceptually equivalent to find a minimal surface (a surface characterised by the property of minimal area within a given boundary), as demonstrated by Bletzinger & Ramm (1999).

More recent modifications of the force density method that include the characteristic of preserving a constant tension field in the membrane are presented in Sánchez et al. (2007) and Pauletti & Pimenta (2008). On the one hand, Sánchez et al. (2007) maintain the branch-node discretisation, which is computationally advantageous, and introduce two alternative non-linear procedures aimed at adjusting the found shape to obtain a uniform force or stress distribution (these are respectively called multi-step force density method with force or stress adjustment). Since the use of iterative solution algorithms increases the calculation time, Sánchez et al. (2007) propose a technique to reduce the number of elements and nodes used in the shape-finding process: after the initial equilibrated shape has been found, parametric surfaces (NURBS) can be employed to obtain a smooth membrane surface by fitting of the net nodes. On the other hand, the natural force density method presented by Pauletti & Pimenta (2008) employs a cable element and a triangular element which are formulated sticking to the concept of natural strains introduced by Argyris et al. (1974b) for the finite element analysis of membranes. This method preserves the linearity that characterises the original force-density formulation and, at the same time, overcomes the difficulties in coping with irregular triangular finite element meshes. Nevertheless, to prescribe a uniform stress field it is once again necessary to invoke iterative solution procedures.

Further developments of the force-density method have been introduced to include additional constraints, such as the preservation of rectangular or equidistant meshes, fixed node distances, force constraints or fixed un-

strained lengths (Schek, 1974). In such cases, these conditions are introduced in the formulation by means of additional (usually nonlinear) equations: the number of these equations is identical to the number of additional restraints and independent of the number of nodes, therefore this nonlinear approach is more efficient than the nonlinear displacement method. Nevertheless, if the formulation becomes nonlinear, the force-density method loses some of its attractiveness.

The force-density method is a special case of the more general assumed geometric stiffness method presented by Haber & Abel (1982a). Once again, only the geometric stiffness matrix $\mathbf{K}^g$ is considered to write the equilibrium equations. The coefficients of $\mathbf{K}^g$ are in general nonlinear, since the geometric stiffness is a function of the unknown nodal coordinates. The assumed geometric stiffness method consists in prescribing the geometric stiffness element, so that they are no longer dependent on the coordinates: this linearises the system of equilibrium equations, which can be then solved directly. For a structure composed entirely of pin-joined bar elements, the definition of the geometric stiffness matrix coefficients is equivalent to selecting the force densities in the elements, i.e. the force to length ratios $\widehat{T}/\widehat{L}$ in matrix (2.11b). A common criticism to this method is that geometric stiffnesses (hence force densities) are not intuitive quantities, therefore the designer can hardly establish their values because the developed shape is not easily foreseeable and the stress distribution is difficult to be evaluated.

To overcome the drawbacks of the assumed geometric stiffness method, a more practical design approach, called iterative smoothing, is put forward by Haber & Abel (1982a), in which the designer prescribes only the stress distribution: the system of equilibrium equations remains nonlinear and iterative procedures are needed to find a solution. At each step, the geometric stiffness matrix is computed based on current values of coordinates, while an approximate solution for each of the unknown coordinates is obtained as a weighted average of the forces acting on the node and the coordinates of the adjacent nodes:

$$\mathbf{x}_i = \left[\mathbf{F}_i - \sum_{j=1}^{3(n-1)} \mathbf{K}^g_{ij} \mathbf{x}_j \right] \frac{1}{\mathbf{K}^g_{ii}} \qquad j \neq i \tag{2.24}$$

The method is named iterative smoothing because iterative coordinate averaging may be viewed as a surface smoothing technique. Haber & Abel

(1982a) claim that one apparent problem of this method is that it is difficult to predict the surface shape based on a prescribed stress pattern, therefore an interactive computer graphics environment has been implemented in Haber & Abel (1982b), that allows the designer to see the found shape at each iteration and to stop computations, if necessary, to alter the stress values.

At last, as pointed out by Bletzinger & Ramm (1999), the geometric stiffness matrix is singular with respect to tangential shape variations: the total area content of the membrane element or the total length of the cable are not altered by these shape modifications, since they would map the surface back to itself. As a consequence, shape variations cannot be chosen arbitrarily, while they must display a normal component at any point of the surface.

Bletzinger & Ramm (1999) present an alternative form-finding method, which is based on a different formulation called homotopy mapping. This is a mathematical method that is employed to approach a solution of a singular problem. If the problem consists in finding the minimum of a function $f(x)$ and this function is assumed to be singular at the solution, the related problem of finding the minimum of its derivative $f'(x)$ is not singular. The function $f'(x)$ can be then used to regularize the problem by mapping with the continuation factor λ, which varies from 0 to 1:

$$min f_\lambda(x) = min[\lambda f(x) + (1-\lambda) f'(x)] \tag{2.25}$$

The solution of the minimisation problem (2.25) approaches that of the original problem. The continuation factor λ determines for each step how the forces referred to the (updated) reference and actual configurations are interpolated. Different strategies are suggested by Bletzinger & Ramm (1999) to trace λ towards the optimal solution, but the one that shows the best convergence properties is the so-called update reference strategy, which employs the last calculated shape as a new updated reference configuration for the next step and uses a constant value of λ small enough to ensure regularity of the stiffness matrix.

2.1.3 Dynamic equilibrium methods

Dynamic relaxation is the king of dynamic equilibrium methods. It was developed to study marine streams and its first application to tensile struc-

tures and hanged roofs was carried out in 1965 by Day (1965). Then came the works of Barnes (Barnes, 1977, 1975, 1988, 1999) on form-finding of cable nets, membranes and inflatable structures. Currently the method has been applied to many fields of mechanics, such as tyre analysis (Oakley & Knight, 1995a,b; Oakley et al., 1995), form-finding of grid shells (Douthe et al., 2006; Tysmans et al., 2011), wrinkling (Zhang & Yu, 1989; Lee & Youn, 2006; Kashiwa & Onoda, 2009), biomechanical models for computing of intra-operative organ deformations (Joldes et al., 2011) and so on.

The main advantage of dynamic relaxation is that it does not require the estimation of the tangent stiffness matrix $\mathbf{K}$, which can be computationally expensive. Evaluation of $\mathbf{K}$ is usually needed for material/geometric nonlinear problems in order to solve the governing discretised equations for structural static equilibrium (2.2). This effort is not required with the dynamic relaxation method because it makes use of fictitious masses and damping to induce a pseudo-oscillation about the equilibrium position of the membrane. The trick is to obtain a static solution by integrating the damped equation of motion to find the steady state of an equivalent dynamic problem.

Let $\mathbf{x}^{(n)}$, $\dot{\mathbf{x}}^{(n)}$, $\ddot{\mathbf{x}}^{(n)}$ be the nodal displacement, velocity and acceleration vectors respectively at the n^{th} time step. The dynamic equilibrium equations read:

$$\mathbf{M}\ddot{\mathbf{x}}^{(n)} + \mathbf{C}\dot{\mathbf{x}}^{(n)} + \mathbf{K}\mathbf{x}^{(n)} = \mathbf{p}^{(n)} \tag{2.26}$$

where $\mathbf{M}$ is the lumped mass matrix, $\mathbf{C}$ is the damping coefficients matrix, $\mathbf{K}$ is the stiffness matrix and $\mathbf{p}^{(n)}$ is the external loads vector.

Equation (2.26) is integrated using the central difference explicit technique, because it shows, according to Krieg (1973) the best properties among the explicit time-stepping algorithms: it is simple to implement, it shows the largest stability limit for second-order accurate integration formulas and, in combination with the adoption of a lumped mass matrix, it permits the separate computation of each uncoupled component with no need for assembly or factorization. According to central difference integration method and supposing a constant time step Δt, the acceleration term is represented by the variation of velocities over the time interval, and the velocity term as an average over the same interval:

$$\ddot{\mathbf{x}}^{(n)} = \frac{\dot{\mathbf{x}}^{(n+1/2)} - \dot{\mathbf{x}}^{(n-1/2)}}{\Delta t} \tag{2.27a}$$

$$\dot{\mathbf{x}}^{(n)} = \frac{\dot{\mathbf{x}}^{(n+1/2)} + \dot{\mathbf{x}}^{(n-1/2)}}{2} \tag{2.27b}$$

Thus vector of residuals (2.1) can be evaluated using Equations (2.26) and (2.27):

$$\begin{aligned} \mathbf{r}^{(n)} &= \mathbf{p}^{(n)} - \mathbf{K}\mathbf{x}^{(n)} = \\ &= \mathbf{M}\frac{\dot{\mathbf{x}}^{(n+1/2)} - \dot{\mathbf{x}}^{(n-1/2)}}{\Delta t} + \mathbf{C}\frac{\dot{\mathbf{x}}^{(n+1/2)} + \dot{\mathbf{x}}^{(n-1/2)}}{2} \end{aligned} \tag{2.28}$$

Hence, from Equation (2.28), the linearised equation for the mid step velocity vector reads:

$$\dot{\mathbf{x}}^{(n+1/2)} = \left(\frac{\mathbf{M}}{\Delta t} + \frac{\mathbf{C}}{2}\right)^{-1} \left[\left(\frac{\mathbf{M}}{\Delta t} - \frac{\mathbf{C}}{2}\right)\dot{\mathbf{x}}^{(n-1/2)} + \mathbf{p}^{(n)} - \mathbf{K}\mathbf{x}^{(n)}\right] \tag{2.29}$$

and the incremental displacement at step $n+1$ is evaluated as follows:

$$\mathbf{x}^{(n+1)} = \mathbf{x}^{(n)} + \dot{\mathbf{x}}^{(n+1/2)}\Delta t \tag{2.30}$$

The iterative algorithm consists of a repetitive use of Equations (2.29) and (2.30) until the residuals are close to nought.

In the dynamic relaxation method mass matrix, damping matrix and time interval must be defined so as to guarantee stability and convergence. Since the central difference method is not unconditionally stable, the time interval Δt needs to be small to satisfy the Courant-Friedrichs-Levy condition (Courant et al., 1928). Δt must be selected as the smallest period of vibration of the system, so that the initial conditions may not be artificially amplified by the numerical algorithm. Barnes (1994) gives the following criterion for ensuring convergence of the solution:

$$\Delta t \leq \sqrt{2\frac{\mathbf{M}_{ij}}{\mathbf{K}_{ij}}} \tag{2.31}$$

Different choices of $\mathbf{M}$, $\mathbf{C}$ and Δt lead to different variants of the method. In Zhang et al. (1994) a critical review of the merits and disadvantages of the existent dynamic relaxation versions is presented and a physical approach is used to develop a modified adaptive algorithm with improved efficiency.

More in detail, concerning the evaluation of the mass matrix $\mathbf{M}$, Zhang et al. (1994) enumerate four methods to do it:

1. set $\mathbf{M} = \mathbf{I}$ (Rushton & Laing, 1968);
2. select different values $\mathbf{M}_{ii}$ of mass in different directions ($i = 1, 2, 3$) through the analysis of individual problems (Rushton, 1968);
3. assume that the value of $\mathbf{M}_{ii}$ in one direction is proportional to the corresponding diagonal stiffness matrix component $\mathbf{K}_{ii}$, which is equivalent to set the time interval in condition (2.31) as a constant value, usually equal to 1 (Brew & Brotton, 1971; Papadrakakis, 1981);
4. satisfy the inequality that guarantee the iteration stability according to Gerschgörin's theorem (Underwood, 1983; Zhang & Yu, 1989):

$$\mathbf{M}_{ii} \geq \frac{(\Delta t)^2}{4} \sum_{j=1}^{N} |\mathbf{K}_{ij}| \,. \tag{2.32}$$

Zhang et al. (1994) claim that 4 is the only mathematically reasonable method, because it is based on a stability condition that limits the enlargement of the fictitious time interval. More recently, Joldes et al. (2009) have proposed a diagonal lumped mass matrix which is scaled at each node to align the maximum eigenvalues of all the elements in the mesh: this improves the convergence rate by reducing the condition number of matrix $\mathbf{M}^{-1}\mathbf{K}$, leading to a decrease in the spectral radius, and guarantees the convergence by assuring that the maximum eigenvalue of the same matrix is an over-estimation of the actual one.

Also a proper selection of the fictitious damping can improve the convergence rate of the dynamic relaxation method. In its original form, first introduced in 1965 by Day (1965), the method makes use of viscous damping and a mass-proportional damping matrix $\mathbf{C} = c\mathbf{M}$ is assumed, according to Rayleigh formulation. Zhang et al. (1994) describe five main approaches that have been proposed in the published literature to estimate the damping factor c:

1. set $c = 2\omega_0$, where ω_0 is the lowest circular free-vibration frequency (Rushton & Laing, 1968; Frieze et al., 1978);
2. take $c = 2\omega_\lambda$ when

$$\lambda = \frac{\left\|\mathbf{x}^{(n+1)} - \mathbf{x}^{(n)}\right\|}{\left\|\mathbf{x}^{(n)} - \mathbf{x}^{(n-1)}\right\|} \tag{2.33}$$

approaches a constant value, where ω_λ is the lowest circular frequency corresponding to the constant λ (Papadrakakis, 1981);

3. calculate the lowest circular frequency at the n^{th} time step with the Rayleigh quotient for linear problems (Underwood, 1983):

$$c = 2\left[\frac{\mathbf{x}^{\mathrm{T}(n)}\overline{\mathbf{K}}^{(n)}\mathbf{x}^{(n)}}{\mathbf{x}^{\mathrm{T}(n)}\mathbf{M}^{(n)}\mathbf{x}^{(n)}}\right]^{1/2} \tag{2.34}$$

where $\overline{\mathbf{K}}^{(n)}$ is a diagonal matrix whose elements are evaluated as follows (summation over repeated index j):

$$\overline{\mathbf{K}}_{ii}^{(n)} = \frac{\mathbf{K}_{ij}\mathbf{x}_j^{(n)} - \mathbf{K}_{ij}\mathbf{x}_j^{(n-1)}}{\Delta t\dot{\mathbf{x}}_i^{(n-\frac{1}{2})}}; \tag{2.35}$$

4. assume that the critical damping factor at the n^{th} time step can be evaluated with the Rayleigh quotient as (Zhang & Yu, 1989):

$$c = \left[\frac{\mathbf{x}^{\mathrm{T}(n)}\mathbf{K}^{(n)}\mathbf{x}^{(n)}}{\mathbf{x}^{\mathrm{T}(n)}\mathbf{M}^{(n)}\mathbf{x}^{(n)}}\right]^{1/2}; \tag{2.36}$$

5. take a constant value of c throughout the whole process (Cassell & Hobbs, 1976; Turvey & Salehi, 1990).

According to Zhang et al. (1994), methods 3 and 4 are more reasonable, since they are based on the same idea of Rayleigh quotient, but 4 is much better because it does not require extra computation of matrix $\overline{\mathbf{K}}^{(n)}$ and practical applications show that it is more efficient and stable than 3. Moreover, an alternative to the use of viscous damping is represented by kinetic damping, introduced by Cassel et al. (1968). The idea behind kinetic damping is to stop the iterations as soon as a local kinetic energy peak is observed and to restart the analysis from the current configuration, setting to zero the initial velocity components. This approach relies on the observation that, in simple harmonic motion, a maximum of kinetic energy corresponds to a minimum of potential energy, therefore to an equilibrium configuration.

Another dynamic equilibrium method for form-finding has been proposed by Kilian & Ochsendorf (2006). This approximates the structure with a particle-spring system, which is composed of lumped masses, called particles, that are connected by linear elastic springs. Each spring has an assigned constant axial stiffness, an initial length and a damping coefficient. External forces are applied to the masses. The system is usually not in equilibrium when the simulation is started, hence masses move until the system reaches its equilibrium position. In the context of graphical statics, the particle-spring method is equivalent to finding a funicular polygon.

In conclusion, the main disadvantage of dynamic equilibrium methods is that they require too many parameters to control stability convergence. Moreover, mass and damping parameters are fictitious, therefore they may not be meaningful or easy to set. However, as pointed out by Lewis (2008), these methods perform a small amount of arithmetic operations at any one time, since the computations concern only one node in turn, rather than all nodes simultaneously: this minimises computational round-off errors and contributes to the accuracy of the solution.

2.2 Cutting pattern

The fabrication of the membrane shape resulting from the form-finding process is realised by assembling cut flat pieces of coated fabric. The definition of the cutting pattern, which is called *patterning*, is a complex process, where many parameters must be taken into account: definition of the cutting lines on the 3D shape, flattening of the curved strips and tension compensation by size reduction.

As summarised by Maurin & Motro (2013), the choice of the seam lines is a compromise between different parameters:

- *Technology*: size of the fabric roll (usually 1.8-3 m wide), welding equipment;
- *Cost*: a higher number of seams increases the accuracy but also the fabric cutting wastage;
- *Geometry*: to minimise deflection and distortion, the principal material directions (warp and weft) should coincide with the main direc-

tions of curvature (Figure 2.2) and smaller panels should be arranged where the surface curvature is high;

- *Mechanics*: to reduce the deflection under loading, warp direction (the stiffer one) should coincide with the main bearing direction (Figure 2.3);

- *Fabric behaviour*: usually orthotropic, with higher strength and rigidity in warp direction;

- *Aesthetics*: the pattern of seams should be aesthetically pleasing.

Two main strategies are used to determine the seam lines: geodetic lines or intersecting planes. According to the first one, the cutting lines should follow geodetic paths over the surface, which are the shortest routes between the two points of a curved surface (i.e. the equivalent of straight lines on plane surfaces). This method is recommended by the European Design Guide for Tensile Surface Structures (Forster & Mollaert, 2004) for reasons of material economy and accuracy and to avoid wrinkling in the final surface form (Figure 2.4). However, designers sometimes use intersecting planes to determine the cutting lines, which therefore result straight, like in the canopy for the German Federal Chancellery Court of Honour (Brew & Lewis, 2013). According to Gründig et al. (2000), there are some situations where intersecting planes may be the best choice, e.g. in symmetrical surfaces, central strips running along the symmetry axes, cloth areas close to connections with rectilinear supports. Automated procedures for cutting pattern generation usually allows the user to define either geodesic or non-geodesic lines (see, e.g., Gründig et al., 1996).

Once the 3D strips have been defined, these must be flattened, since the fabricator cuts them out of a 2D fabric roll. As shown in Figure 2.5, the projection results in plane strips with curved edges: these are convex for surfaces with positive Gaussian curvature (synclastic) and concave for surfaces with negative Gaussian curvature (anticlastic). Synclastic surfaces can be developed exactly, but most of the fabric membranes are doubly curved (anticalstic), therefore it is impossible to map them onto a 2D plane without distortion. As pointed out by Maurin & Motro (2013), the solution proposed to map the Earth demonstrate this impossibility, since they can

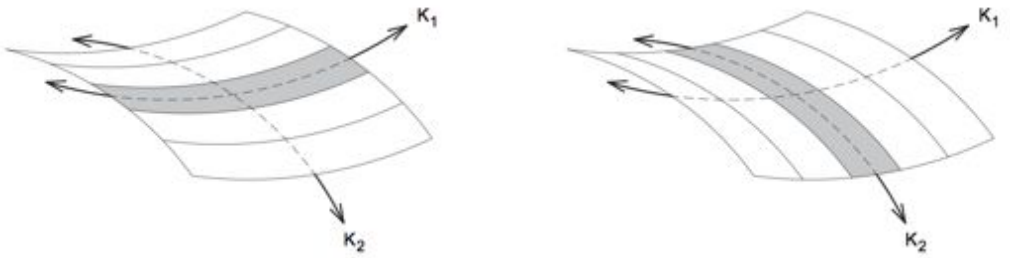

Figure 2.2: *Layouts with strips in the main directions of curvature (from Seidel, 2009).*

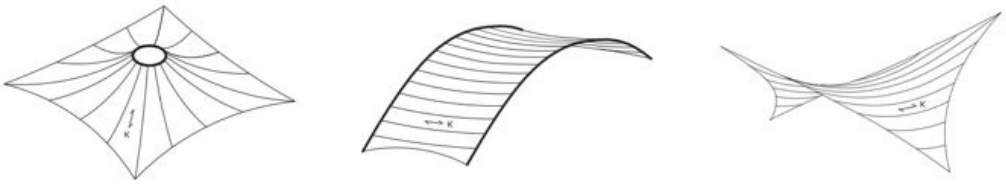

Figure 2.3: *Strips layout with warp in the main bearing direction (from Seidel, 2009).*

Figure 2.4: *Comparison of non-geodesic (orange) and geodesic (blu) cutting pattern generation (from Forster & Mollaert, 2004).*

preserve either areas (equivalent flattening), distances (equidistant flattening) or angles (conformal flattening), but never all of them simultaneously. As a consequence, one of the main patterning issues is to find the cutting pattern that minimises the final distortion.

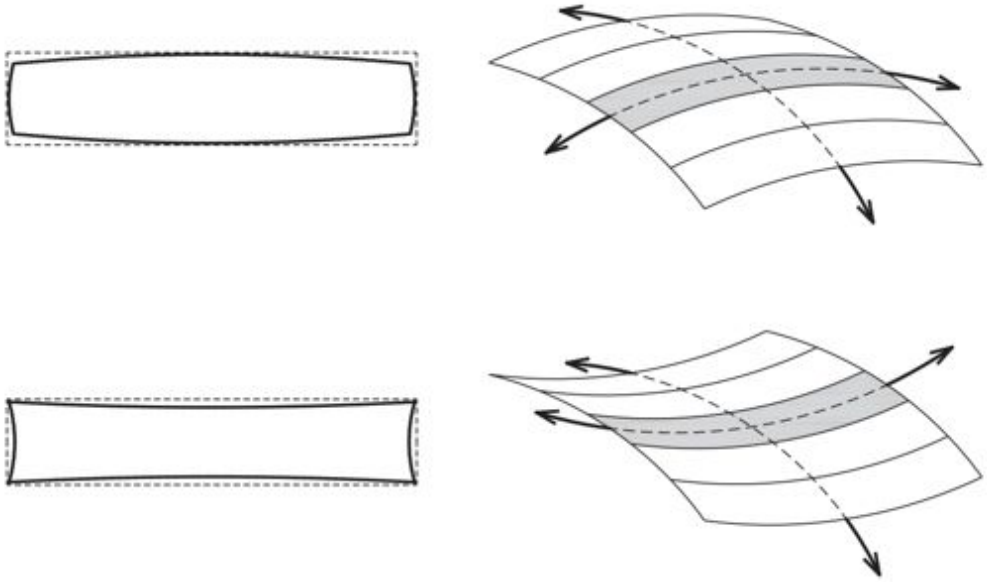

Figure 2.5: *Curved strips for synclastic (top) and anticlastic (bottom) surfaces (from Seidel, 2009).*

The last step of the patterning process is named compensation and consists in a reduction in size of the planar panels. This is necessary because, if the strip sizes were not modified, there would be no pretension in the 3D assembled membrane. Compensation (or sometimes decompensation) values depend on the material properties, hence they are generally different for warp and weft and usually lower along warp direction. Stretch values vary along a strip, thus they are typically graded along the panel. Moreover, where the strips are connected to boundary cables or rigid elements, the compensation is removed at the boundary (decompensation) and then gradually increased over a short length, so that after 1 m into the panel the full compensation value is applied.

According to Maurin & Motro (1999), the most common methods for cutting pattern generation employ decomposition into two distinct oper-

ations: a first step of flattening followed by a reduction of the strip. For example, this is the case of the Simple Triangulation Method (STM), which performs a triangulation of the 3D surface and then flattens it by keeping unvaried the triangle side lengths, as it has been described by Maurin & Motro (1999) and by Ishii (1999). Another method consists in determining the geometry of the strips on the 3D surface and then flattening them onto the plane (Ishii, 1999).

Different algorithms have been proposed for the flattening, which aim at reducing distortions by minimising errors: such techniques include both purely geometric criteria and use of minimum strain energy (Gründig & Bäuerle, 1990; Yu et al., 2000). Some advanced features allow the user to handle darts (i.e. removal of material) and gussets (i.e. insertion of material), for instance the algorithm presented by McCartney et al. (1999). However, constitutive law of the material and stress distribution in the strip are not considered by these approaches: they are only introduced during the subsequent step of compensation.

Separation of the flattening and reduction phases leads to lost of information about the stress field generated in the membrane after installation. Moreover, the reduction is usually related to the experience of the engineer, so that significant errors may occur. To overcome these drawbacks, an alternative approach has been proposed by Maurin & Motro (1999), named Stress Composition Method (SCM), which combines the operations of flattening and reduction. The problem of minimising the difference between the desired prestress and the stress field arising from installation has inspired also the cutting pattern procedure presented by Ishii (1999).

One of the most recent approaches to cutting pattern generation is the one by Brew & Lewis (2013). It presents some interesting enhancements of the existing methods. Firstly, it assures compatibility between adjacent panels by forcing the stresses along the their edges to be equal to the design values. Secondly, it minimises distortions by projecting the 3D surface onto a closer developable surface, instead of a plane. Finally, it employs splines to describe the panels, which enables flattening solutions to be generated in analytical form.

Concluding, cutting pattern generation requires further research, as demonstrated by the scarcity of references. Most of the available articles are from conference proceeding, therefore they are not easily accessible. One of the causes could be the fact that this stage is usually in charge of

the installer, not of the designer, so that it is essentially based on experience. Moreover, an accurate estimation of the cutting pattern involves the use of reliable material models, whose development is cutting-edge research at present.

3

Membrane materials for tensile structures

Membrane materials employed for tensile structures may be essentially classified into two categories: films and coated woven fabrics (Figure 3.1). Even if foils are increasingly used in tensile architecture (e.g. ETFE foils), these are not treated in this thesis, where the focus is on the mechanical behaviour of coated woven fabric membranes.

Architectural membranes usually consist of a polymeric matrix that may be reinforced with fibres in the form of laminates or fabrics. Coated woven fabrics are the most widely used, since the weaving increase the loading capability and eliminates delamination issues. There exists single-component coated fabrics, like PTFE coated PTFE woven fabrics (Tenara®Gore), and multi-component coated fabrics, like Silicone or PTFE coated glass fabrics and PVC coated polyester fabrics.

When selecting a membrane for structural purposes, the most important qualities to consider are the mechanical tensile strength and the elastic properties. On the basis of these properties, PVC/polyester and PTFE/glass fabrics are classified according to Figure 3.2 (Forster & Mollaert, 2004). Other aspects that are fundamental in the material selection include durability, insulation, light transmission, fire protection, foldability and cost. For instance, glass fabrics are not suitable to be employed for deployable systems (Mollaert et al., 2006; De Temmerman et al., 2007; De Laet et al., 2009; Van Mele et al., 2010), because of the brittleness of glass yarns.

Coated fabrics are composite materials, hence their constitutive be-

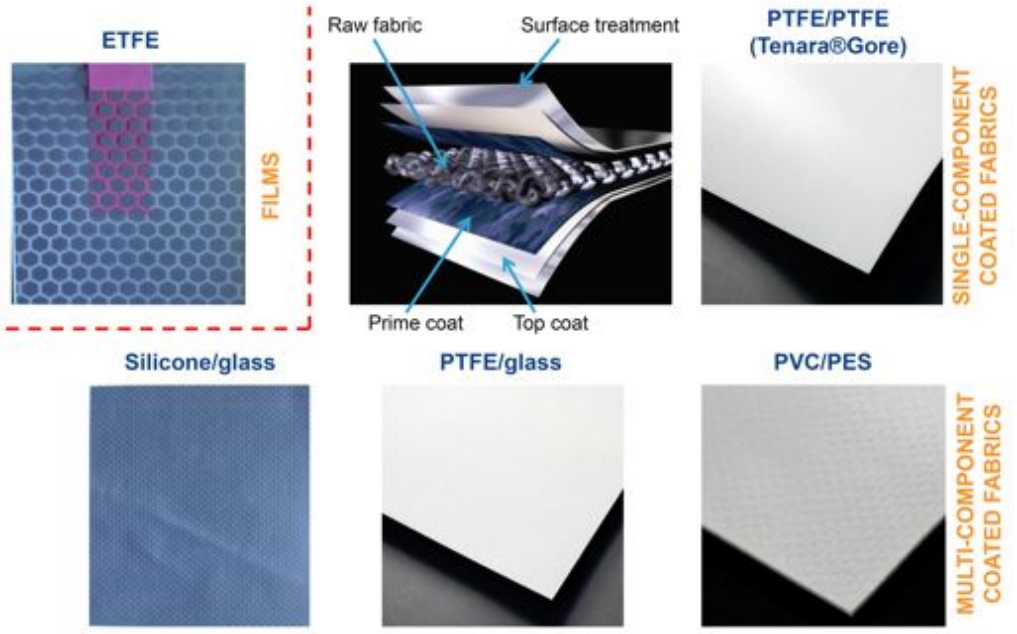

Figure 3.1: *Membrane materials for tensile structures.*

haviour and their properties depend on the mechanical characteristics of each component and on their mutual interaction. These will be discussed in the following Section.

3.1 Architectural membrane components

Coated fabrics used for architectural purposes are made of different layers, as shown in Figure 3.3. The middle layer is the raw fabric, which is realized interlacing yarns with different techniques (weaving, braiding, knitting, stitching). Then, the fabric is covered with a prime coat that stabilises the geometry and protects yarns against environmental sources of damage, like rainwater, pollution, UV rays, abrasion, and so on. A second thin and chemically distinct coating, named top coat, is added to protect the prime coat. Finally, the outer layer consists of a surface treatment that allows the sealing or printing, where necessary, by chemical compatibility of the components.

Type	1	2	3	4	5
Surface weight (g/m²)					
French design guide	720	1 000	1 200	1 400	2 000
WG Messe Frankfurt	800	900	1 050	1 300	1 450
Yarn linear density (dtex)					
French design guide					
WG Messe Frankfurt	1 100	1 100	1 670	1 670	2 200
Tensile strength warp/weft (kN/m)					
French design guide	60/60	84/80	110/104	120/130	160/170
WG Messe Frankfurt	60/60	88/79	115/102	149/128	196/166
Trapezoïdal test warp/weft (N)					
French design guide					
WG Messe Frankfurt	310/350	520/580	800/950	1 100/1 400	1 600/1 800
Yarn number per cm warp/weft					
French design guide					
WG Messe Frankfurt	9/9	12/12	10.5/10.5	14/14	14/14

(a) PVC/polyester types

Type	G1	G2	G3	G4	G5	G6	G7
Tensile strenght warp/weft (kN/m)	26/22	43/28	70/70	90/72	124/100	140/120	170/158
Filament diameter (micrometer)	9	6	3	6	3	3 or 6	3
Surface weight (g/m²)	500	420	800	1 000	1 200	1 500	1 600
Trapezoïdal tear warp/weft (N)			300/300	300/300	400/400	500/500	450/450

(b) PTFE/glass types

Figure 3.2: *Categorization of coated fabrics based on their mechanical properties (adapted from Forster & Mollaert, 2004).*

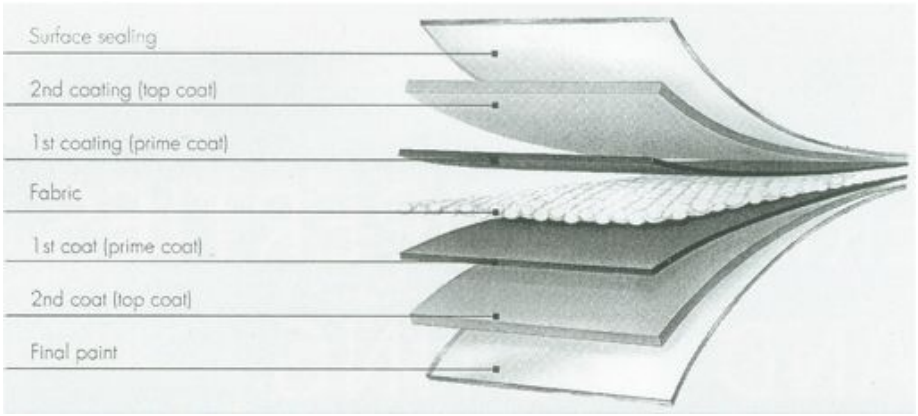

Figure 3.3: *Architectural membrane layers (from Forster & Mollaert, 2004).*

Among the thousands of coated fabrics that are on the market, the most commonly used for tensile structures are PVC (Poly Vinyl Chloride) coated polyester fabrics and PTFE (Poly Tetra Fluoro Ethylene) or Silicone coated glass fabrics. More recently, PTFE coated PTFE fabrics have been adopted in some cases. The choice of which type of coated fabric has to be used in a membrane structure realization is based on several factors: durability, structural lifespan, deformability, cleanability, fire resistance, toxicity of some components. All these aspects will be breafly discussed later on.

In the next Sections each coated fabric component will be described in detail, following the hierachical organization of architectural membranes: yarns, fabric, coating.

3.1.1 Yarns

Yarns are realized with natural or chemical fibres of small diameter (between 3 and 25 μm): the first ones have a limited length, so they are bound up in strands; the second ones have pontentially endless length and are called filaments (Houtman & Orpana, 2000). Two or more yarns can be twisted together to obtain a thread of higher strength.

As pointed out by Houtman & Orpana (2000), it is almost always difficult to determine the transversal area of very small fibres. Therefore, an average cross section can be calculated by multipling the specific weight of the material by a quantity named titer or count, which is provided by the

Material	**Density**	**Tensile strength**	**Extension at break**	**Elasticity modulus**
	[g/cm^3]	[GPa]	[%]	[GPa]
Polyester	1.38-1.41	0.97-1.17	11-15	12-15
Glass	2.6	2.4	4.5	73
Aramid	1.45	3.32	1.5	160
Nylon	1.14	1.0	15-20	5-6
LCP	1.4	3.28	2.5	104
Cotton	1.5	0.35-0.7	6-15	4.5-9
PTFE	2.1-2.3	0.16-0.38	2-4	130-150

Table 3.1: *Mechanical properties of yarns.*

producers. The count is the weight of a fibre with a certain length and its unit of measure in the International System of Units is tex: 1 tex is the weight in g per 1000 m length. In USA and UK denier is more commonly used as unit of measure for the linear mass density of fibres: 1 denier is the weight in g per 9000 m length.

Another important aspect that influence the mechanical behaviour of a yarn is the twisting. The more the thread is twisted around its centre the more its elastic compliance decreases compared to the one of the fibres. Information about the number of twists per meter and their direction (s is for left-hand twist, z is for right-hand twist) is usually added to the fibre description. Hence, a thread is characterized by its count and number of fibres, followed by the twists (t0 if it is not twisted). For example, a thread that is designated with 2200 dtex f200 z60 has a titer of 2200 dtex, made out of 200 fibres, and it is right-hand twisted 60 times per meter.

Different kind of fibres can be applied in membrane structures. Polyester and glass fibres are the most widely used and are obtained from extrusion spinning. Other yarns that are used in this field are polyamides (aramid or, more rarely, nylon) and LCP (Liquid Crystal Polymer based on aromatic polyester), which are made from a solution. Moreover, cotton fibres are sometimes used for short term constructions due to their susceptibility to staining and moisture. Finally, PTFE fibres have been adopted more recently. Table 3.1 shows the properties of these yarns.

Polyester yarns

Synthetic polymer fibres that constitute the base of polyester fabrics are made of PET (Poly Ethylene Terephthalate), which is also named PES in textile jargon: actually, this is incorrect, because in material science PES already stands for thermoplastic Poly Ether Sulphone. Together with fibreglass, PET yarns are the most common standard product in textile architecture.

As described by Seidel (2009) and in the European Design Guide for Tensile Surface Structures (Forster & Mollaert, 2004), to produce polyester yarns, the granulate is melted and sent to a heated spinning manifold. Then the melted mass is pressed at high temperature through a spinning shaft that forms it into filaments. After that, filaments are solidified by air blowing and elongated with a variable-speed roller system: during this step, crystallisation and orientation of macromolecular chains occurs that increases filaments strength and tenacity. Finally, fibres are twisted together to form a yarn. The process is depicted in Figure 3.4.

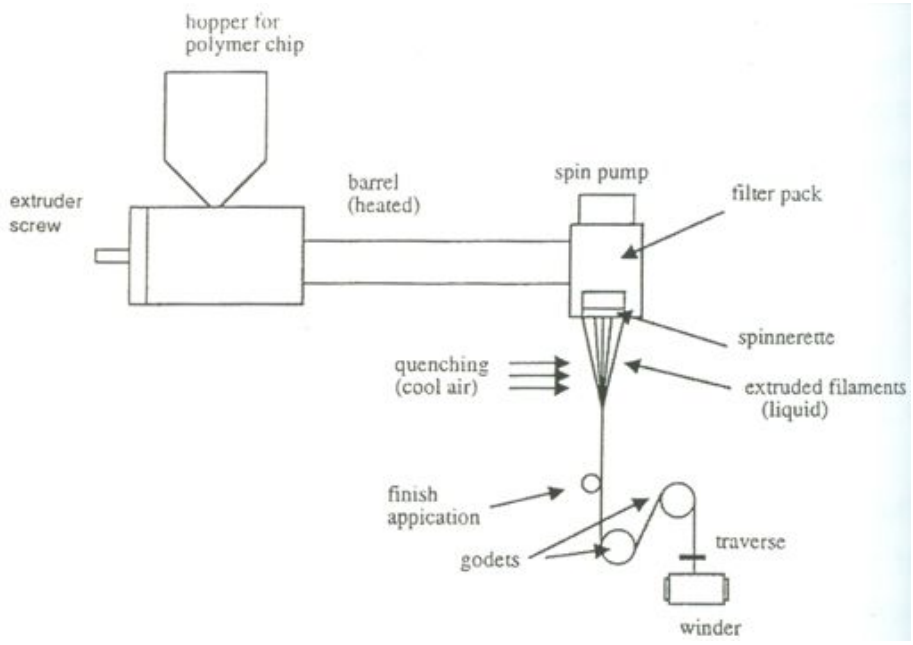

Figure 3.4: *Polyester fibres method of production (from Forster & Mollaert, 2004).*

Polyester yarns have high tenacity and they are characterized by a tensile strength of at least 0.97 GPa. This material permits small corrections during installation, thanks to its considerable elongation before yielding (Houtman & Orpana, 2000), but it tends to creep over time, a phenomenom that is common to all polymers. PET yarns have high flexibility and buckling resistance, thus they are often used for ropes, belts and sewing threads, besides coated fabric membranes.

Figure 3.5 shows the force-extension curve of a PET yarn. Three regions can be identified, which correspond to changes in the material stiffness: this is typical of all polymers, whose behaviour is called rubbelike elasticity. Region I delimits the zone of linear elasticity. Region II is characterised by a relatively low stiffness, which corresponds to the uncoiling of elastomer chains. Once the chains have been completely uncrimped, higher forces are required to stretch also the primary chemical bonds, thus resulting in a stiffer stress-strain behaviour in region III.

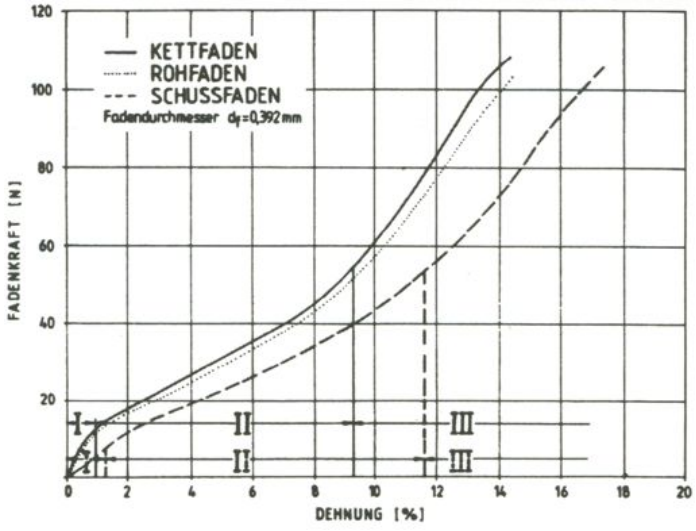

Figure 3.5: *Force-extension diagram of polyester yarns (from Forster & Mollaert, 2004).*

Regarding the behaviour of the material against light and high temperatures, polyester fibres exhibit the typical properties of polymers. They present low resistance to UV radiation, which causes ageing and deteriorates the mechanical properties. Moreover, they are flammable at high

temperatures, even if they self esinguish after ignition. All these disadvantages may be reduced with a PVC coating.

Finally, polyester is sensitive to hydrolysis, since it is an organic material characterized by an ester group. PVC coating represents again a barrier that protects PET yarns from oxidation. Alternatively, fibres are sometimes treated with a substance that prevents water absorption (hydrophobic treatment). As described in the European Design Guide for Tensile Surface Structures (Forster & Mollaert, 2004), when the coating shows pinholing or does not penetrate into the cloth, a phenomenon named *wicking* may appear, which consists in the migration of water between yarns, resulting in yellow or brown lines due to growth of bacteria and fungi. This leads to a reduction of adhesion that may cause seam problems or delamination of the coating.

Glass yarns

Fiberglass is one of the most utilized materials in textile architecture, together with polyester yarns. It is produced with the melt spinning process depicted in Figure 3.6. The glass raw components are melted down in a furnace over several days, homogenised and forced trough spinning nozzles. Then, using a winding machine that rotates fast, filaments are stretched to about 40000 times their original length.

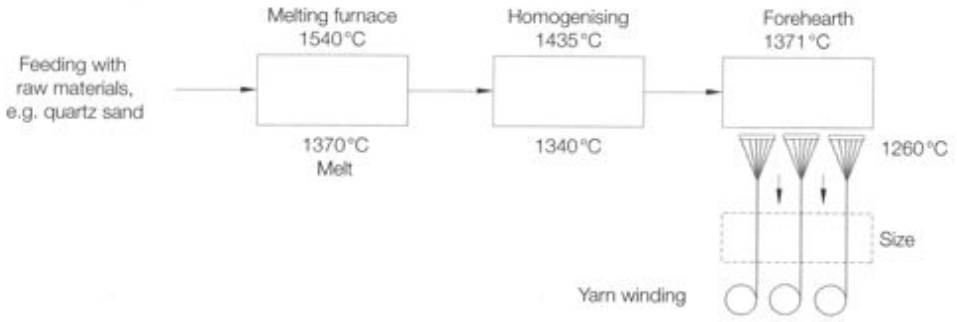

Figure 3.6: *Glass fibres method of production (adapted from Knippers et al., 2011).*

Glass yarns are isotropic, therefore they exhibit the same mechanical properties in longitudinal and transversal directions. Figure 3.7 shows the

force-extension behaviour of glass fibres, which is linear elastic up to brittle failure. Thanks to the small diameter they are flexible, even if they are rather sensitive to buckling in comparison with other fibres.

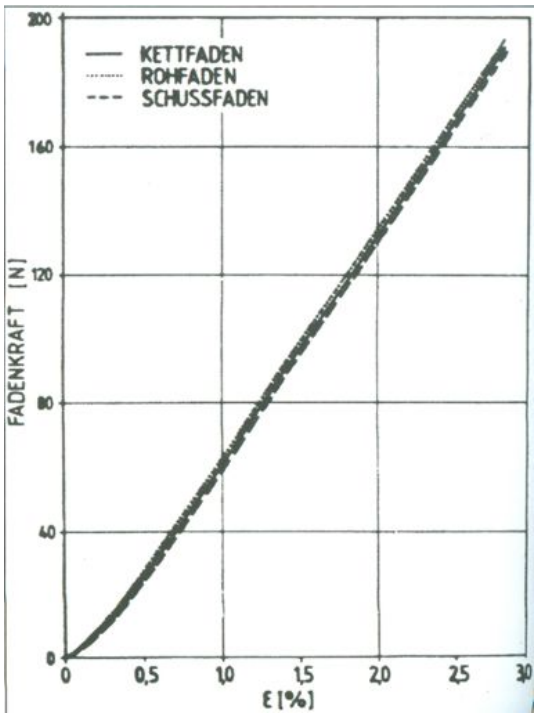

Figure 3.7: *Force-extension diagram of glass yarns (from Forster & Mollaert, 2004).*

The strength of glass filaments depends on their diameter (3-5 μm), since they are produced by cooling a melt substance. As a result, outer layers cool faster than inner ones, thereby compressive residual strains in the axial direction arises that strengthen the yarns core with respect to tensile loading. This means that glass fibres with large diameter can carry higher tensile loads, because they have a larger prestressed cross section. Nevertheless, fibreglass brittleness is higher for large diameter filaments, thus yarns used in textile architecture have a diameter of no more than 3 μm.

Moreover, brittleness of this kind of fibres is partially overcome with the polymeric coating that is added to the glass fabric, usually consisting

of PTFE or Silicon. Covering prevents also reduction of the yarns tensile strength due to moisture. Therefore, coating makes the lifetime of glass fabrics longer.

Finally, glass is resistant to high temperatures, UV light and wether. Like all inorganic fibres, glass filaments show good dimensional stability since they exhibit very little creep. Last but not least, glass fibres do not burn if exposed to fire.

Aramid yarns

According to the definition reported by Knippers et al. (2011), aramid fibres are very lightweight fibres that consists of aromatic polyamides. They are strong synthetic fibres which were discovered simultaneously by Akzo (Twaron fibre) and DuPont (Kevlar fibre).

As described by Knippers et al. (2011) and illustrated in Figure 3.8, aramid fibres are not produced with a melt spinning process, since they do not exhibit a distinct melting behaviour. Instead, aromatic polyamide is dissolved with an acid ad spun to form fibres.

Aramid yarns have high tensile strength, but their compressive strength is much lower than the tensile one (asymmetric mechanical behaviour), hence they are suitable for applications involving only tension (ropes and membranes). However, they are only rarely employed in the building industry because they are too tough and therefore difficult to machine.

Lastly, aramid threads are chemically resistant and their characteristic failure behaviour enables them to absorb impact energy. As drawbacks, they present low strain at break and bad resistance against UV light and high temperature. In addition, they tend to absorb moisture.

Nylon yarns

Polyamide 6.6 (Nylon) fibres, which are produced with the melt spinning method, were used in the first membrane structures. Nowaday they are not of great importance in textile architecture, since they have several disadvantages: bad resistance against UV rays and high temperatures, swelling in length when they absorbs moisture and, more important, they are subjected to severe elongation, that causes drop in the prestress. Instead,

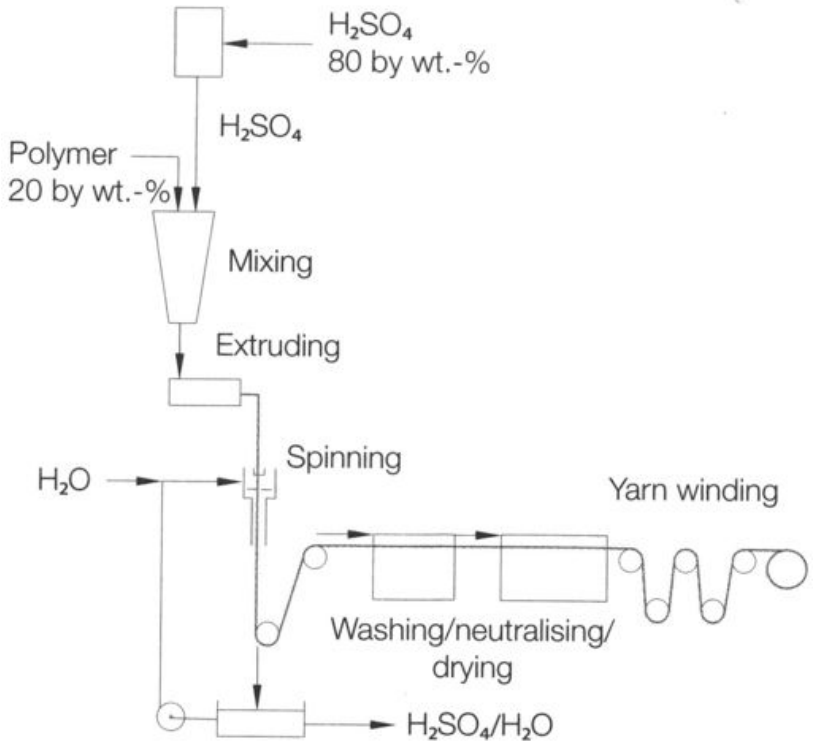

Figure 3.8: *Aramid fibres method of production (adapted from Knippers et al., 2011).*

Nylon fibres are more largely applied in the sailing industry thanks to their lightness and high strength.

LCP yarns

Liquid Crystal Polymers (LCP) are a class of aromatic polyester polymers that exhibit order similar to an ordinary solid crystal. As described by Hearle (2001), these polymers are thermotropic (or melt-orienting). This means that, in a molten state they consist of very rigid chain-like molecules positioned into randomly oriented domains, as shown in Figure 3.9. Extrusion through very small holes and subsequent cooling down cause high orientation of the internal material structure, which results in a high tensile strength and modulus of the fibres. Because of this high orientation,

drawing after spinning is not necessary.

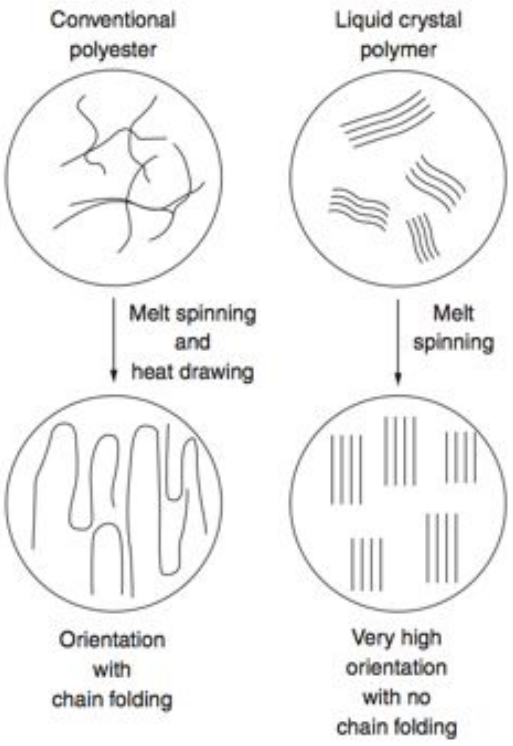

Figure 3.9: *Molecular chain structure of standard and liquid crystal polymers (from Hearle, 2001).*

Typically, LCP fibres have a high mechanical strength at high temperatures, extreme chemical resistance, inherent flame retardancy, and good weatherability.

Cotton yarns

Cotton represents the only organic fibre used in membrane structures. In the past, it was largely used by Frei Otto to realize its tensile structures and nowadays it is applied for some tents. Since it is an organic material, its lifespan is very short (about 4 years) because it is sensitive to moisture and fungi.

PTFE yarns

In comparison with other polymeric yarns, PTFE fibres have lower strength, but they show a high tear propagation resistance, which is a very useful property in membrane structures realization. Moreover, the high light trasmittance of PTFE fabrics (up to 40 %) is particulary important for architectural design. The high flexibility and resistance to bending, as well as the tendency to creep under costant loading, are all factors that contribute to prefer their utilisation for convertible roofs rather than for permanent structures.

Other characteristics of PTFE fibres are high resistance to chemicals and moisture, good UV stability and self-cleaning (anti-adhesive) surface. Finally, they are not readily combustible in air.

3.1.2 Fabrics and foils

Woven fabrics

A woven fabric is produced interlacing weft yarns between two layers of warp yarns at 90° with respect to the weft yarns. The weaving process consists in the repetition of five steps, described by Sen & Damewood (2001):

1. The first step is the *shedding* of the warp threads. These are kept in a harness and divided into two layers: the sequence of threads in the upper and lower layers (e.g. one up one down, two up two down, ect.) determines the type of weave pattern.

2. One weft thread is passed through the enclosure between the upper and lower layers.

3. The third step is named *beating up*: the new weft thread is pushed against the already made fabric and the intensity of the force used to do this influences the surface weight of the fabric (measured in g/m^2).

4. The position of upper and lower harnesses is exchanged. As a consequence, the new weft thread is enclosed by the warp threads.

5. The procedure is repeated from the second step, with a new weft thread, untill the fabric is completed.

During the weaving process, the completed fabric is winded on a roll at a certain speed, which depends on the weaving velocity. Hence, in the final roll the warp threads are positioned along the longitudinal direction, while the weft threads are in the transversal direction.

As anticipated before, the configuration of threads in the harnesses determines the type of weave. The types of weaving used to make fabrics for membrane constructions are plain weave and 2-2 basket weave (or panama), which is a sort of modified plain weave (Figure 3.10). The yarns crimp is lower in panama weave (Forster & Mollaert, 2004).

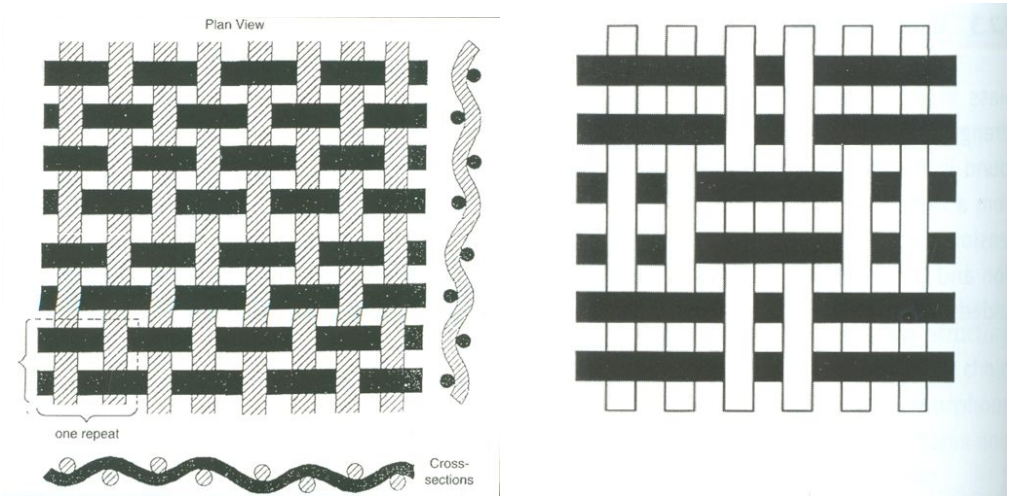

(a) Plain weave (b) Basket or panama weave

Figure 3.10: *Weave patterns used for membrane constructions (from Forster & Mollaert, 2004).*

Independently of the type of weave pattern, the warp threads in a fabric have a more streched profile, while the weft ones are more crimped. This is due to the weaving process, beacuse warp yarns are kept under tension during the fabric realisation. As a result, the weft stress-strain curves show a lower slope than the warp ones, at least at low stresses, thus giving rise to an orthotropic behaviour of the fabric at the macroscale.

The French manufacturing company Serge Ferrari adopts the so called Précontraint® system, that can provide more balanced fabrics. Using this techinque, which was initially developed to produce fabrics with the same

level of crimp in warp and fill directions, it is possible to realize membranes with a level of crimp in the two weaving directions that is specified in order to obtain a certain prestress for a given structure and a specific assembling procedure. As claimed by Bridgens (2005), the Précontraint® system is useful especially when the fill prestress is introduced by restraining the fabric in the fill direction and then tensioning it in the warp direction: this may result in negative fill strains and raising of fill stress and the use of a Précontraint® fabric can solve the problem.

Knitted fabrics

Knitting is the second most used technique in textile production, even if it is less used in techical textile applications (Kuusisto, 2010). A knitted fabric is produced interlooping one or more yarns to form a continuous structure. As a consequence, yarns are subjected to lower stress than in woven fabrics and this allows the use of delicate fibres, like aramid and glass.

If compeared to other types of manufacturing, knitting seems to be more versatile and rapid. This technique can easily meet every design requirements (shape, dimension, details) without waste of material and at a low cost. Nevertheless, knitted architectural fabrics are still rare: they are seldom used for sun shade membranes.

Multiaxial multiply fabrics

The European standard EN 13473 defines a multiaxial multiply fabric as follow:

> "*A textile structure constructed out of one or more laid parallel non-crimped not-woven thread plies with the possibility of different orientations, different thread densities of single thread plies and possible integration of fibre fleeces, films, foams or other materials, fixed by loop systems or chemical binding systems. Threads can be oriented parallel or alternating crosswise. These products can be made on machines with insertion devices (parallel- weft or cross-weft) and warp knitting machines or chemical binding systems.*".

The so called weft-inserted warp-knitted fabrics, sometimes used for textile architecture, belong to this category of textile materials. They are realized superimposing two layers of warp and weft yarns to form a web and then fixing them with a thin knitted yarn. Hence their production makes use of a machine that is composed by two main parts: a weft insertion device and a knitting unit. In this kind of fabrics the yarn crimp is very low, thus the mechanical strength is improved, but the shear resistance is reduced with respect to woven fabrics.

Nonwoven fabrics

Nonwoven fabrics are membranes that are produced bonding the base material chemically, mechanically or thermally. Nonwoven fabrics provide specific functions, so possible applications are filters, geotextiles, insulation. They are not used as architectural membranes.

As described by Kuusisto (2010), nonwovens manufacturing consists of three stages: web or batt forming, web bonding and finishing. Web forming can make use of different techniques: drylaid (from textile industry), wetlaid (from paper industry), spunlaid or polymerlaid. The second step is the bonding: this may be chemical, mechanical, thermal, or even a combination of these techniques. The type of bonding influences the final properties of the nonwoven, such as the finishing, which can be dry or wet.

ETFE Foils

ETFE is a copolymer of Ethylene and TetraFluoroEthylene with a melting temperature of 250 °C and very good chemical resistance. It is used to create large thin sheets, named foils or films, with a thickness of 50 to 300 μm. These are the most employed films in the building industry for loadbearing enclosing components.

As described by Knippers et al. (2011) and Seidel (2009), ETFE foils are manufactured with a thermoplastic process called extrusion. The granulate is melted at temperatures above 380 °C, then it is trasported in a heated metal barrel containing a rotating plasticising screw that generates a pressure and forces the material through a die. Depending on the die geometry, two types of products can be obtained: on the one hand flat foils, manufactured with a wide slot die and downstream chill rolls; on the other

hand tubolar foils, obtained passing the molten resin through an annular die and expanding it into a tube by air blowing. Figure 3.11 illustrates the two types of extrusion processes. Blown films present lower quality, worse homogenity and more thickness variations, hence they are not used very often in the building industry.

ETFE films have high traslucency (up to 90%) and high absorption of sun radiation, which makes them excellent for green houses. Their mechanical behaviour is elastic and isotropic. Moreover, they are very resistant to aggressive environments (acids, alkalis, UV radiation, ...). All these benefits makes ETFE ideal for membrane and tensile structures.

Finally, ETFE foils can be used in single or multi-layer applications. A multilayer ETFE cladding is obtained by clamping and sealing two ore more ETFE films together and inflating the space between the foils to create a cushion. Furthermore, welding is used to join together pieces of ETFE foil in order to obtain a larger sheet. The welding does not require chemical substances, but it is done applying heat (approximatively 280 °C) and pressure to a 10 to 15 mm overlap between two foils. Hence weldability represents another characteristic that makes ETFE film very suitable for the realisation of membrane structures.

3.1.3 Coatings

Before applying the coating, the fabric is protected with a finish, usually on both sides. This increases the compatibility between fabric and coating, which means a good wettability of the fibers by the liquid resin and then a good adhesion between fabric and coating. Hence, the choice of the type of finishing depends on both the fabric and the coating. For instance, polyester fabrics finish has a hydrophobic compound that avoids moisture diffusion at the fibre/resin interface; PTFE base coat is applied to provide flexibility; aramid fabrics need a special chemical modification of the fibres surface to avoid delamination with the coating (Forster & Mollaert, 2004).

The coating function is to protect the base fabric against moisture, UV radiation, fire, fungi attack and so on. In addition, it influences the mechanical properties of the final composite material. Three types of coating are usually employed for architectural textiles: PVC, PTFE and Silicone.

Finally, a top coating is added to ensure good cleanability, weldability, waterproofness, resistance against fungi attacks, and to offer a barrier for

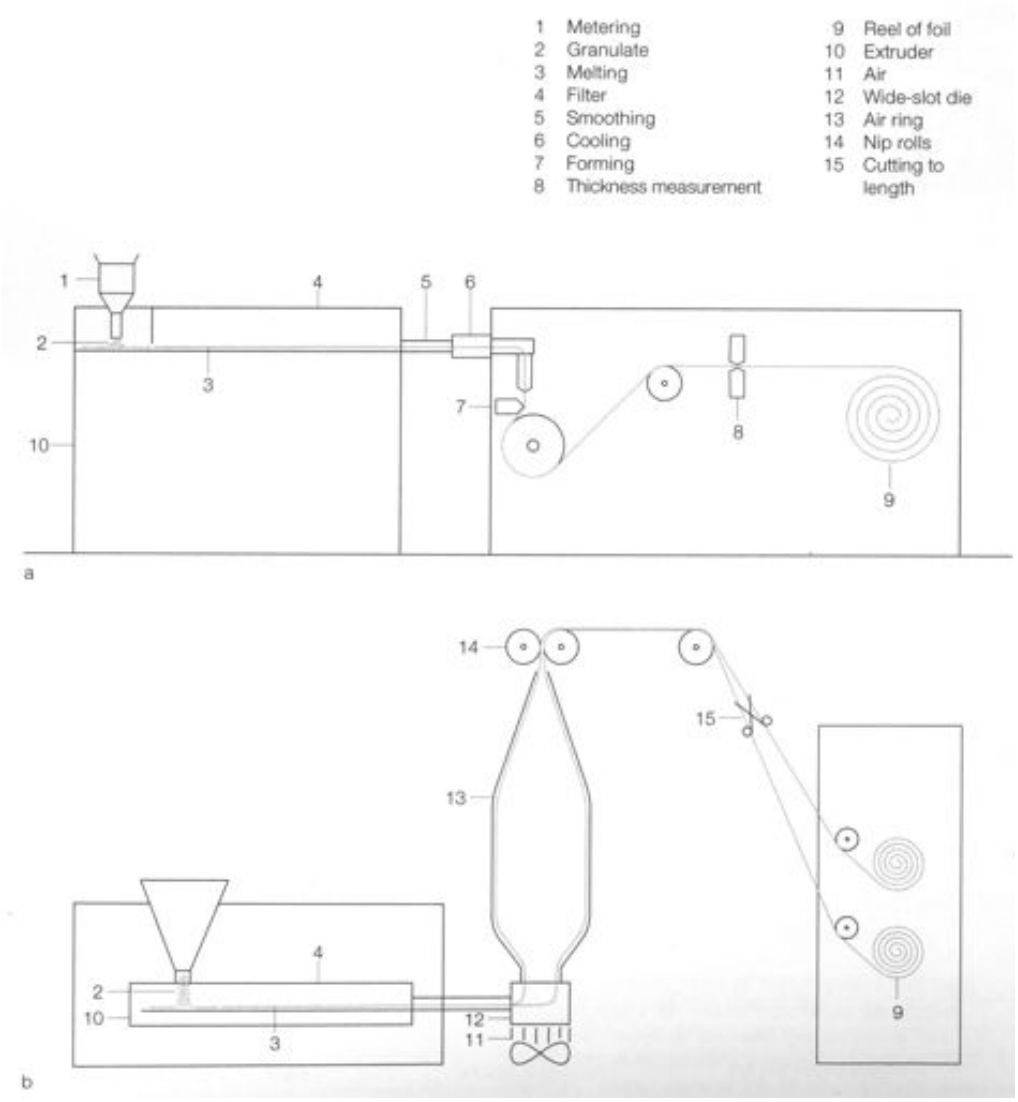

Figure 3.11: *Foil extrusion: (a) flat foil (b) tubolar (blown) foil (adapted from Knippers et al., 2011).*

plasticiser migration to the surface and weather influences. For PVC coated fabrics the top coat may be of acrylics, PVDF (PolyVinyliDene Fluoride), PVDF/acrylic mixtures, PVD (PolyVinyl Fluoride), while for PTFE coated fabrics FEP (FluoroEthylenePropylene copolymer) is mostly used.

PVC coating

PVC coating has different components, described in the European Design Guide for Tensile Surface Structures (Forster & Mollaert, 2004). The main one is the PVC paste, which is an emulsion containing significant quantities of emulgators, whose concentration and type have a strong impact on the thermal and cleaning properties of the surface. The second major component is the plasticiser, that determines the flame retardant properties as weel as the dirt pickup. Phosphates are the most efficient plasticisers in term of flame retardancy, but they have a high tendency to migrate to the surface and are subjected to biological attack. On the other hand, phtalates have a very good compatibility with PVC that makes them the most widely used plasticisers, even if they are also subjected to migration and hydrolysis. Chlorinated paraffines are a third type of plasticisers used, with good flame retardant properties, but they have a strong tendency to migrate to the surface, resulting in dirt pickup.

Most of the times, PVC coating is pigmented, usually in white. Pigments are not added merely to color the fabric, but they play an important role in the UV stability and opacity, thus they affect the light stability of the material. Moreover, stabilisers are often added to the emultion to overcome oxidation, UV ray degradation, dirt pickup and thermal effects. Also flame retardant additives are sometimes used.

PVC coated fabrics can be recycled with a process patented by Solvay. Using a selctive chemical solvent (ketonic solvent) at 115 °C, the PVC is dissolved and PET fibres remain in suspension. Then the fibres are separated by filtration and drying, while the PVC solution is precipitated at room temperature, so both the components may be reused.

PTFE (Teflon) coating

PTFE coating is applied by dipping the glass fabric in a PTFE dispersion, then drying and sintering at 350-380 °C (sintering is a process for fusing particles together by helding the powdered material in a mold and then heating it below the melting point). Compared to the raw PTFE fabrics, the coated ones are weldable and watertight. However, PTFE shows high tendency to creep, thus the pretensioning values must be low and the spans limited (Knippers et al., 2011).

As claimed in the European Design Guide for Tensile Surface Structures (Forster & Mollaert, 2004), PTFE is a material with outstanding properties. Firstly, it has one of the strongest bonds in organic chemistry, since its structure is characterised by long chain molecules with a carbon based core and an outer sheath of fluorine atoms that shields the core against chemical attack. Secondly, it can resist to temperatures from $-200\,°C$ to $+260\,°C$ and temperature variations have no influence on its lifespan. Moreover, it is inflammable, insulating, inert against all the environmental polluttants. PTFE coating is anti-adhesive, hence it is self cleaning and water repellent. Finally, its hydrophobic properties protect the glass yarns against moisture, preventing the loss of thensile strength due to humidity exposure.

Silicone coating

Silicone coating is based on silicone rubber, which shows mechanical resistance in a wide range of temperatures ($-50\,°C$ to $+200\,°C$) even in aggressive atmospheres (Forster & Mollaert, 2004). This is particulary advantageous for the use in hot climate countries. Moreover, silicone is very resistant to ageing thanks to its extraordinary chemical resistance.

As pointed out by Knippers et al. (2011), silicone coating presents some positive characteristics if compared with PTFE or PVC coatings. One of them is the high flexibility, that makes the fabrics coated with silicone easy to handle and more resistant to flectional cracking than PTFE coated fabrics. Compared to PVC, silicone coating shows a light tranmittance which is three times higher.

Despite the above mentioned advantages, there are some factors that limit the use of silicone in the building industry (Knippers et al., 2011). First of all, it tends to attract static electric charges, thus it is subjected to soiling. Secondly, silicone is not weldable since it does not have a distinct melting point; as a consequence, joints must be realised with vulcanisation or gluing, which are both complex and expensive methods. Finally, because of the additives used for siclicone coating, this can only be classified as readily flammable, despite the fact that silicone itself is incombustible.

4

Mechanical properties and testing of coated fabrics

Coated fabrics producers provide datasheets containing the main characteristics and properties of their products. An example of how one of these sheets looks like is shown in Figure 4.1. The information that is typically provided may be subdivided into the following categories:

- technical characteristics of the base fabric, yarns, coating and coated fabric (e.g. material, weight, yarn count, thickness, ...);
- mechanical characteristics of the coated fabric (e.g. tensile strength, elongation at break, tear strength, coating adhesion, ...);
- other important properties (e.g. fire reaction, light transmission, ageing, seamability, ...).

Characteristics provided in datasheets are evaluated through the procedures described in International (ISO, International Organization for Standardization) and European (EN, European Norm) standards when available. Otherwise, national standards are used as reference; for instance, NF (France), DIN (Germany), BS (United Kingdom), ASTM (United States of America). Moreover, laboratories have their internal protocols to determine some characteristics that are usually not reported in datasheets, but are anyway very important to understand the mechanical behaviour of coated fabrics. The complete list of standards employed for this aim is given in Tables 4.1 to 4.3.

UK	Type IV		B 18059
Base fabric			Glass fibre EC 3/4
Coating			PTFE – polytetrafluoroethylene
Total weight (g/m²)	DIN EN ISO 2286-2		1550
Width (cm)	DIN EN ISO 2286-1		470
Tensile strength (N/5 cm)	DIN 53354	warp/weft	8000/7000
Tear resistance (N)	DIN 53363	warp/weft	500/500
Adhesion (N/5 cm)	DIN 53357		100
Translucency at 550 nm (%)	DIN 5036		11
Flame retardancy	DIN 4102		B1*

Note: Product must not be sewn, but hot-bar welded. *Additional certificates available on request. Subject to change regarding technical upgrades. Values indicated without tolerance levels are nominal values with a tolerance range ± 5%. All data presented here is given to the best of our current knowledge for guidance purposes and is not legally binding. Translucency refers to bleached version.

Figure 4.1: *Example of a coated fabric datasheet.*

The main international standards cited in Tables 4.1 to 4.3 are mostly focused on uniaxial tests, due to the relatively simple and common testing equipment that is required. The values of ultimate tensile strength, tear resistance and adhesion are easily determined by means of uniaxial tests and commonly reported in the technical datasheets.

However, an adequate characterisation of the mechanical behaviour of coated fabrics is possible only through biaxial tests, which are carried out with specific testing equipments able to pull both warp and fill directions at the same time.

Moreover, the information contained in the current datasheets often does not match the designer needs, because it is not sufficient to correctly model the mechanical response of coated fabrics. This is reflected by the high factors of safety (between 5 and 10) used in the current tensile structure design practice (Bridgens et al., 2004b).

In consideration of all these aspects, further research is needed to broaden the knowledge about coated fabrics, in order to enhance the modelling of their mechanical behaviour. This is the aim of the present Chapter, which has been structured in two parts:

- Section 4.1 reports information about the mechanical characterisation of coated fabrics collected from the literature.
- Section 4.2 contains a description of a series of uniaxial and biaxial tests that have been performed at Politecnico di Milano, together with some provided by Newcastle University, and comments on their results.

	Technical characteristics	Unit	EN standards	ISO standards	National standards
Base fabric/yarn	Material				
	Weight	[g/m^2]	EN 22286	ISO 2286-2	
	Weave style			ISO 9354	NF G 07155
	Nb of yarns/cm (warp, weft)			ISO 7211-2	DIN 53853; NF EN 1049-2
	Yarn count	[dtex]	EN 1973		DIN 53830
	Filaments diameter	[μm]	EN 1973		DIN 53830
	Twist, turns per meter, sizing	[tpm]			
	Yarn tensile strength	[N/tex]	EN ISO 2062	EN ISO 2062	
	Yarn elongation	[%]	EN ISO 2062	EN ISO 2062	
Coating	Material				
	Weight	[g/m^2]	EN 22286	ISO 2286-2	
	Total thickness			ISO 2286-3	
	Thickness (top fabric)	[mm]			
	Top coat (material, weight)				
Coated f.	Weight	[g/m^2]		ISO 2286-2	
	Thickness	[μm]	EN 22286	ISO 2286-3	
	Available width	[m]			
	Color				

Table 4.1: *Standards for coated fabrics: technical characteristics (adapted from Forster & Mollaert, 2004)*

	Technical characteristics	Unit	EN standards	ISO standards	National standards
Coated fabric	Tensile strength (warp, weft)	[daN/5 cm]	EN ISO 4674-2	EN ISO 1421	NF G 37103; BS 3424-4 method 6; DIN 53354; ASTM D 4851
	Tear strength (warp, weft)	[N]			NF G 37130; BS 7304-44; DIN 53363; ASTM D 4851
	Elongation at break (tensile test)	[%]		EN ISO 1421	NF G 37103
	Coating adhesion	[daN/5 cm]		EN ISO 2411 ISO 5978	NF G 37107; BS 3424 part 7; DIN 53357

Table 4.2: *Standards for coated fabrics: mechanical characteristics (adapted from Forster & Mollaert, 2004)*

	Technical characteristics	EN standards	ISO standards	National standards
Fire reaction	Noncombustibility of substrate		ISO 3941	NFP 92 503; ASTM E-136; DIN 4102; BS 7837
	Intermittent flame, spread of flame			ASTM E-108
	External fire exposure roof test			BS 476-3
	Fire propagation			BS 476-6
	Spread of flame			BS 476-7
Physical prop.	Infra-red emissivity and absorbance			ASTM C 423-89
	Acoustic insulation, absorption			
	Light transmission			NFP 38511; ASTM D 1494; ASTM E-903
	Solar transmission reflectance			ASTM E 424-71; ASHRAE 74-73

Continued on next page

Table 4.3: *Standards for coated fabrics: other characteristics (adapted from Forster & Mollaert, 2004)*

Continued from previous page

	Technical characteristics	EN standards	ISO standards	National standards
Other properties	Accelerated ageing	NF EN 12280-1/2/3	DIN EN ISO 4892	
	Seams (strip tensile test)		ISO 1421	
	Hydrostatic resistance	EN 20811	ISO 811	NF EN 1734
	Cold crack	EN 1876-2		
	Burst			NF G 37116
	Crease			NF G 37131
	Puncturing			
	Gas permeability			NF G 37114
	Hydrolysis resistance			NF G 37122
	Volatile organic content			
	Cleaning ability			
	Recyclability			
	Quality insurance		ISO 9002	

Table 4.3: *Standards for coated fabrics: other characteristics (adapted from Forster & Mollaert, 2004)*

4.1 Mechanical properties of coated fabrics

4.1.1 Uniaxial tensile behaviour

The generalised load-extension curve of an uncoated fabric subjected to uniaxial loading is shown in Figure 4.2(a). It displays three regions where the behaviour of the fabric is governed by different mechanisms. First, the initial high stiffness is mainly due to the frictional resistance to bending of the threads. Once the friction is overcome, a relatively low slope is recorded, which is governed by the force needed to unbend the yarns in the direction of the load; at the same time, the yarns in the direction transversal to the applied load increase their crimp (see Figure 4.3), according to a process called *crimp interchange* (Freeston et al., 1967; Treloar, 1977; Testa & Yu, 1987; Bridgens et al., 2004a). When the crimp of the threads aligned with the force cannot decrease any more, the load rises very steeply and, as a result, the stiffness of the fabric is mainly due to the load-extension properties of the yarns themselves.

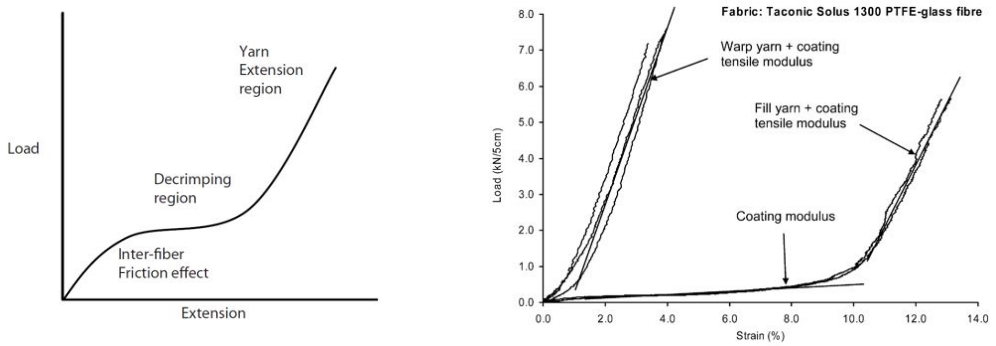

(a) Uncoated fabric

(b) Coated fabric

Figure 4.2: *Typical uniaxial load-extension curves of uncoated (from Lin, 2010) and coated (from Bridgens & Gosling, 2008) fabrics.*

The uniaxial behaviour of a coated fabric is slightly different, even if the same basic mechanisms must be present. As the coating inhibits the movement between the yarns, the crimp interchange starts immediately, as it can be figured out by looking at Figure 4.2(b), which reports the results of two uniaxial tests in warp and fill direction performed on a coated fabric.

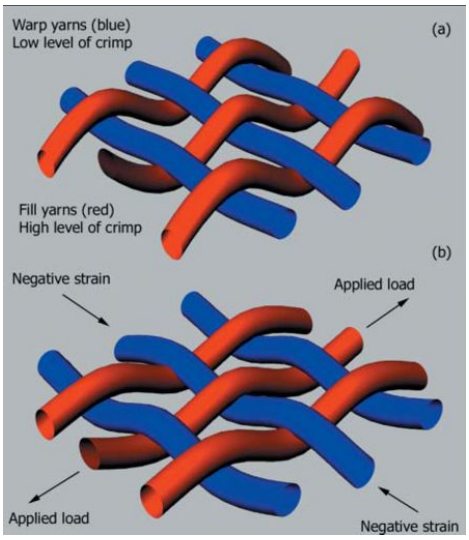

Figure 4.3: *Crimp interchange (from Bridgens et al., 2004a).*

It can be noticed that the decrimping region is narrow for warp threads, as they are initially almost straight in the virgin fabric, because of the weaving process. Moreover, the addition of the coating produces some resistance to crimp interchange, which is overcome only gradually as the load level increases (Testa & Yu, 1987); therefore the stiffness of the fabric in the decrimping region is mostly related to the one of the coating.

Uniaxial tensile behaviour of architectural coated fabrics strongly depends on the direction of loading. More in detail, if the loading direction is increasingly biased against the principal directions of the material (warp and weft), the initial stiffness and the tensile strength become lower, while the corresponding breaking strain increases.

Figure 4.4 illustrates the test results obtained by Chen et al. (2007). A group of seven specimens of a polyester woven fabric with PVC coating were tested until tensile failure: the warp direction was biased 0°, 15°, 30°, 45°, 60°, 75° and 90° against the loading direction. The material behaviour is consistent to the one described earlier. It can be noted that, although the fabric count was the same in warp and fill direction, the tensile behaviour is different (0° and 90° curves): this is due to the weaving and coating processes, in which the fabric is held uniformly in warp direction, leaving fill direction free of tension (hence more crimped).

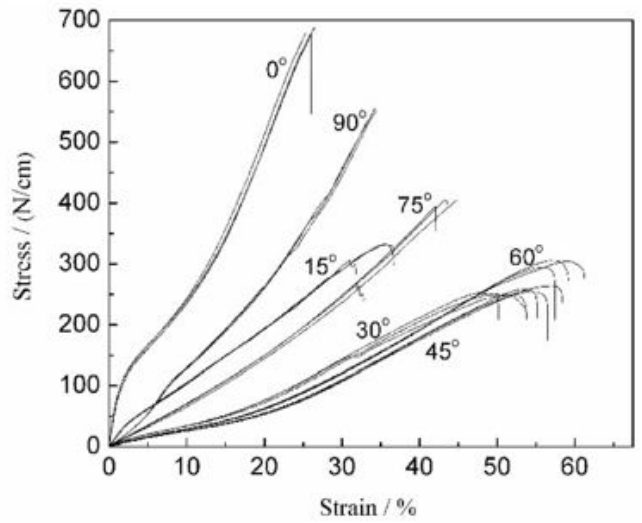

Figure 4.4: *Stress-strain behaviour of a PVC-coated polyester fabric under bias tensile loading (from Chen et al., 2007).*

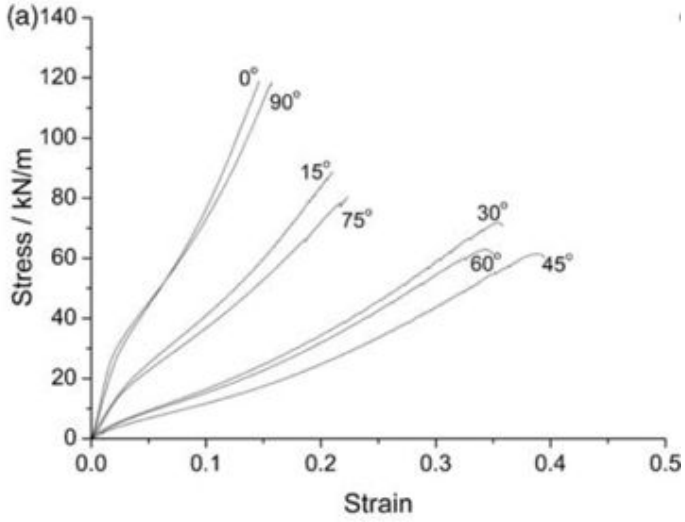

Figure 4.5: *Stress-strain behaviour of a PVC-coated polyester fabric with Précontraint® technology under bias tensile loading (from Zhang et al., 2012).*

The same bias tensile test was carried out in Zhang et al. (2012) on a polyester fabric coated with PVC using Précontraint® technology. As shown in Figure 4.5, the difference between warp and weft (0° and 90° curves) is not significant, which is contrary to the results obtained by Chen et al. (2007). The reason for this come from the Précontraint® coating technology, that holds both warp and weft threads during the manufacturing process, leading to a reduction of the difference between the mechanical behaviours along the two principal material directions.

Figure 4.6 illustrates the test results obtained in a previous work (Zhang et al., 2010) on a PTFE coated glass woven fabric. The behaviour is close to the one of PVC/polyester fabrics, with tensile strength and modulus gradually decreasing, and breaking strain increasing, with increasing bias angles. It must be noticed that, contrary to what is done in Figures 4.4 and 4.5, the bias angles in Figure 4.6 are referred to the weft directions, thus warp curve is indicated with 90° and fill with 0°. Again the warp and weft curves are different because of the weaving process and, more in detail, warp direction is stiffer than fill.

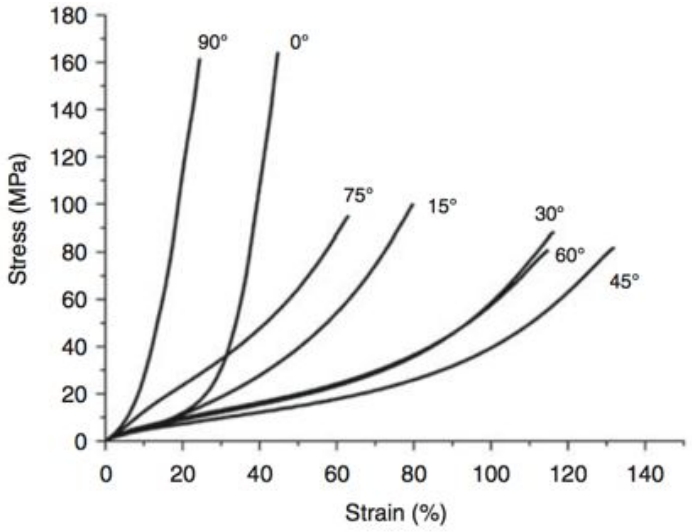

Figure 4.6: *Stress-strain behaviour of a PTFE-coated glass fabric under bias tensile loading (from Zhang et al., 2010).*

Three types of failure mechanisms in the specimens subjected to bias tensile loading are observed by Chen et al. (2007) and Zhang et al. (2010,

2012): pure tensile failure, pure shear failure and mixed shear and tensile failure. The first one takes place in the samples that are loaded along the material principal directions, where the crack propagation is perpendicular to the loading direction. Pure shear failure is shown in 45° samples: failure happens at the interface between fibres and coating and yarns are pulled out from the matrix. The mixed failure mechanism is observed for intermediate bias angles, where part of the yarns are drawn out from the coating and the remaining yarns break when their tensile strength is reached. It can be concluded that the shear strength becomes the dominant strength component for intermediate angles of orientation: in this case coating plays an important role, since it provides the fabric with a shear resistance, which would be otherwise null.

Moreover, Chen et al. (2007) and Zhang et al. (2010, 2012) show that the strength of coated woven fabrics under uniaxial load can be predicted by the Tsai-Hill criterion (see Figure 4.7. Among the several strength criteria used for composite materials, the Tsai-Hill criterion (Tsai, 1968) is the most appropriate, since it takes into account the interaction between the longitudinal and transverse direction and it satisfies the requirements of coordinate trasformation, but its mathematical equation is nethertheless simple. It represents a particularisation of the Hill yield criterion for metals (Hill, 1948) to composite laminae, which are transversally isotropic and subjected to plane stress states.

For what concern the dependence on loading rate of the uniaxial tensile response of coated fabrics, it has been ascertained, for example by Galliot & Luchsinger (2011a), that it is not significant. Figure 4.8 displays the results form uniaxial tensile tests in warp and fill directions, which have been carried out at different loading velocities. They show that the strain rate has a certain influence on the material behaviour, but it is actually negligible.

4.1.2 Biaxial and multiaxial behaviour

Service loads acting on architectural membranes induce complicated stress fields, that arise not only from the applied prestress but also from the natural environment (snow, rain, wind, ...). Therefore, investigation about how the tensile strength of coated fabrics is affected by the multiaxiality of applied loads is a particularly important issue. Nevertheless, only a

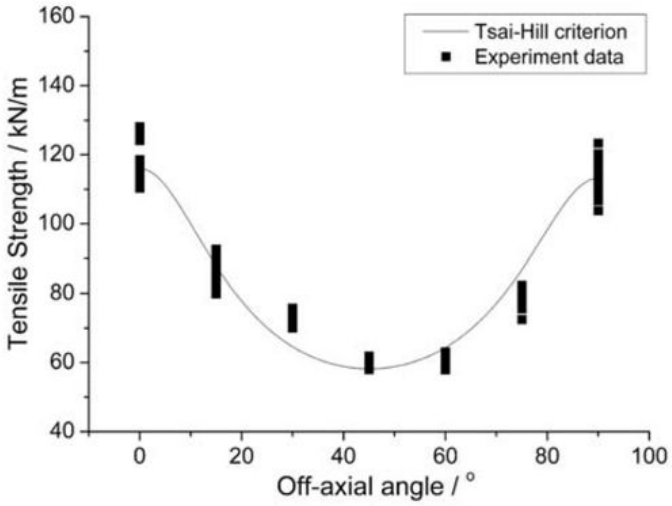

Figure 4.7: *Comparison of the experiment data and prediction of Tsai-Hill criterion (from Zhang et al., 2012).*

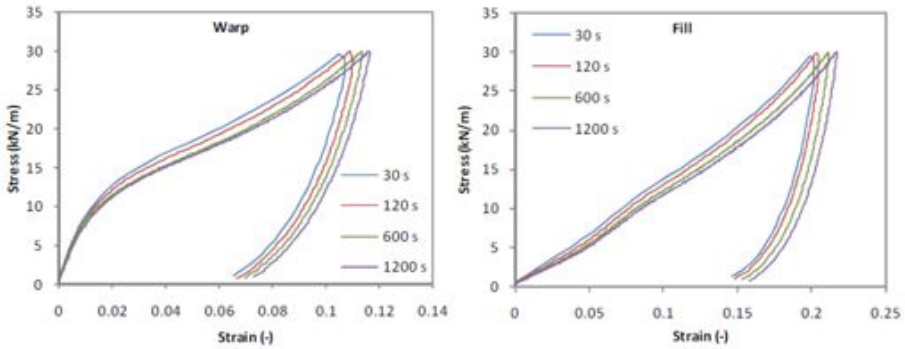

Figure 4.8: *Influence of the loading rate measured with uniaxial tensile tests in warp and fill directions (from Galliot & Luchsinger, 2011a).*

little work has been done until now and the performance of architectural membranes is still expressed through the uniaxial tensile strength in warp and weft directions.

A test that could be used to determine the biaxial strength of membranes is the bursting test, also called bubble inflation test. A circular specimen is clamped along its edge and this flat membrane is deformed by means of a lateral air pressure into a spherical shape until the sample bursts. Anyway, this type of test is not suitable for fabrics because it shows several drawbacks if applied to anisotropic materials, as outlined by Reinhardt (1976) and in the European Design Guide for Tensile Surface Structures (Forster & Mollaert, 2004). First, the ratio between warp and weft stresses cannot be varied. Second, the deformed shape only approximate a sphere, so the assumptions on which the stress and strain calculation is based are not completely correct. For these reasons the bursting test is not widely used to test coated fabrics, while it is sometimes applied to foils (Figure 4.9).

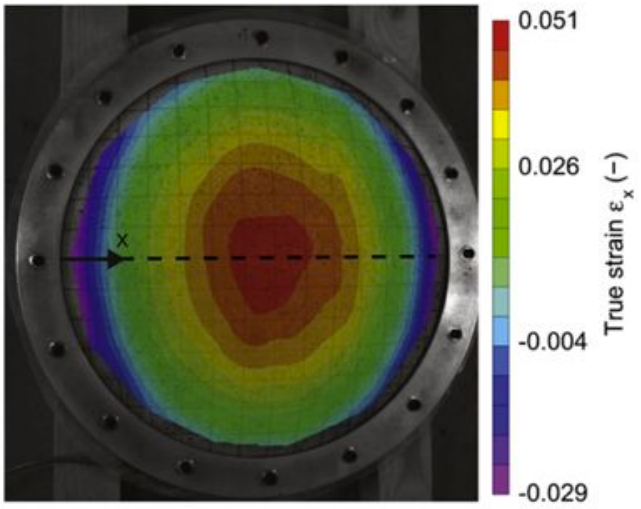

Figure 4.9: *Bubble inflation test carried out on an ETFE foil (adapted from Galliot & Luchsinger, 2011b).*

Another test that is suitable to investigate the biaxial behaviour of membranes is the cylinder test (Figure 4.10). This employs cylindrical specimens that are subjected to axial tension and inflated: the ratio be-

tween the stress components can be easily varied, since the axial tension and air pressure are independent of each other. The cylinder test has been often used in the past to study the mechanical properties of fabrics, e.g. by Alley & Faison (1972), but, as pointed out by Reinhardt (1976), one or two symmetrical seams must be realised to create the specimen, that strongly influence the test results.

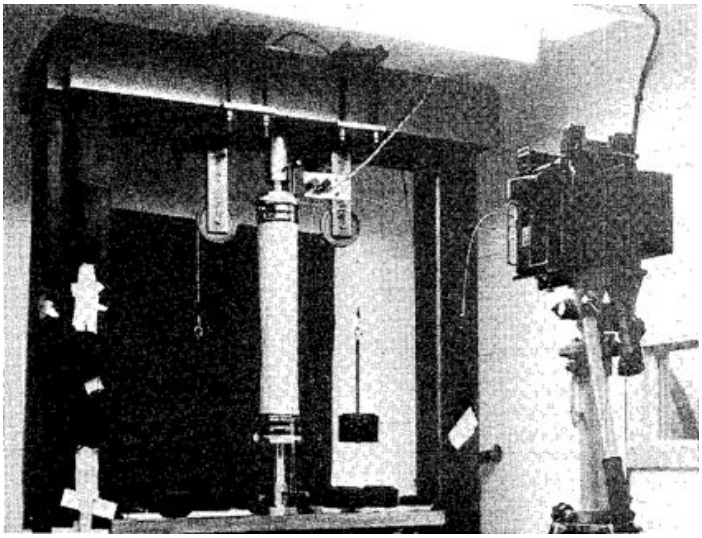

Figure 4.10: *Cylindrical test carried out on a coated fabric (from Alley & Faison, 1972).*

The plain biaxial test is selected by Reinhardt (1976) as the most suitable method to determine the biaxial strength. Moreover, in that article it is claimed that, with a slitted cruciform specimen like the one in Figure 4.11, the fracture runs trough the biaxially stretched central square of the sample, hence the true biaxial strength can be evaluated. The author concludes that the value of biaxial strength obtained with the slitted cruciform sample is equal to the uniaxial strength. Nonetheless, the failure load of biaxial specimens does not coincide with the failure strength of the material, as pointed out by Zhang et al. (2012), since the failure always starts from one of the slits, thus it is due to a concentration of stress at the end of the cut. This is confirmed in the European Design Guide for Tensile Surface Structures (Forster & Mollaert, 2004, p. 305), where it is highlighted that biaxial tests are not intended for strength measurement.

In Zhang et al. (2012) the biaxial failure load *of the samples* is evaluated with a cruciform specimen with slits, but the ratio between the applied warp and weft loads is 1, while in Reinhardt (1976) it is 1.1.

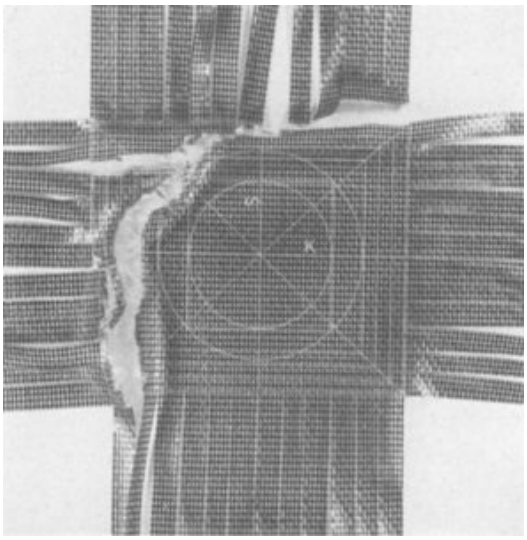

Figure 4.11: *Fractured slitted cruciform specimen (from Reinhardt, 1976).*

An interesting modification of the sample shape that allows multiaxial plane loading of the membrane is proposed by Chen et al. (2008). It is a gear shaped specimen with short and large arms, like the one in Figure 4.12, that guarantees a uniform strain distribution in the central part and a good interaction between the loading directions, which is instead dramatically reduced if long arms are used. Figures 4.13 to 4.15 from Chen et al. (2008) show the results obtained on a PVC coated polyester fabric subjected to uniaxial, biaxial (with warp to fill loading ratio of 1) and multiaxial plane loading. It can be outlined that the tensile strength and elongation at break is always higher under uniaxial loading than those under biaxial and multiaxial loading: this confirms that it is not possible to evaluate the strength of structural membranes on the base of their uniaxial tensile strength in warp and fill direction. Moreover, the stiffness of the material increases under biaxial and multiaxial loading, therefore the tensile performance of construction membrane materials takes advantage of the interaction between warp and fill yarns that arise when the membrane is loaded along more than one direction.

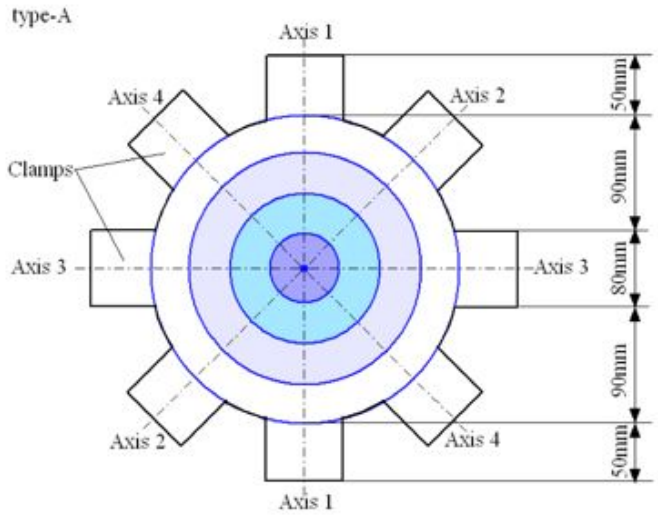

Figure 4.12: *Gear shaped specimen for multiaxial tensile tests (from Chen et al., 2008).*

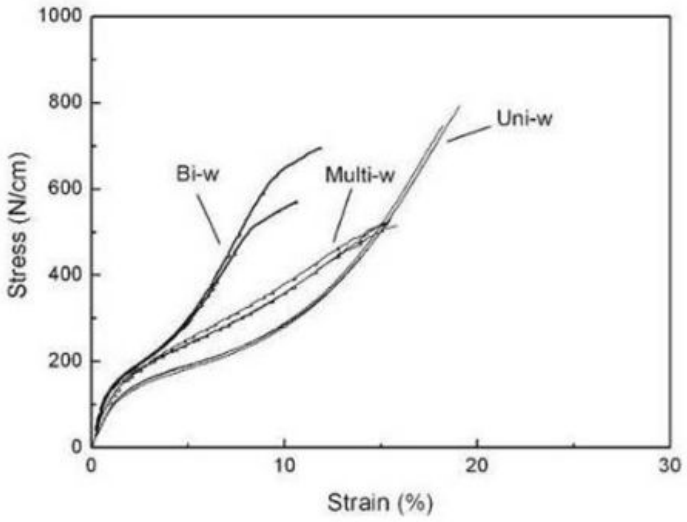

Figure 4.13: *Stress-strain curves in warp direction under uni-, bi- and multi-axial tensile loads (adapted from Chen et al., 2008).*

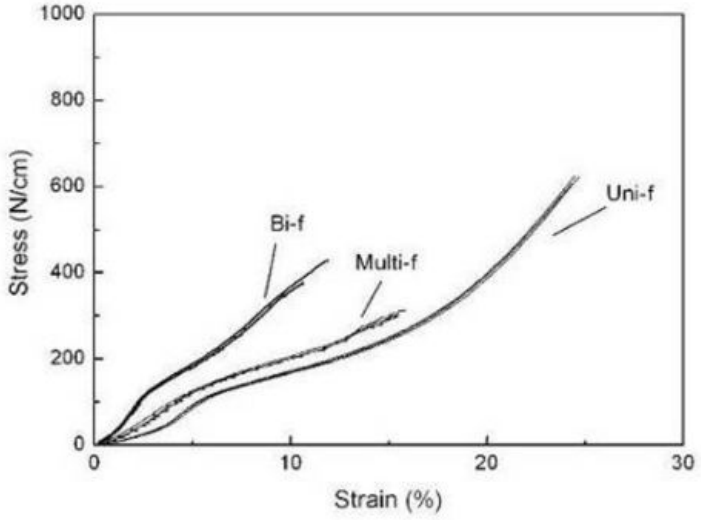

Figure 4.14: *Stress-strain curves in fill direction under uni-, bi- and multi-axial tensile loads (adapted from Chen et al., 2008).*

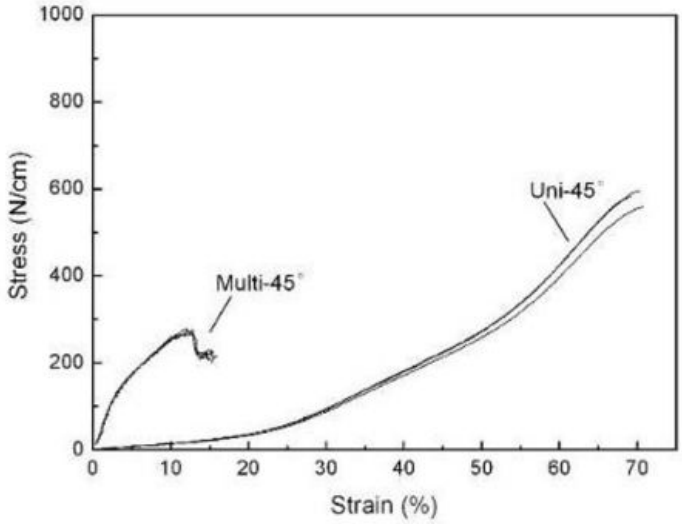

Figure 4.15: *Stress-strain curves in 45° direction under uni- and multi-axial tensile loads (adapted from Chen et al., 2008).*

The results of biaxial and multiaxial tests on coated fabrics have shown that the stress-strain curves of these materials depend on the load ratio (or stress ratio) in warp and fill direction (see, e.g., Testa & Yu, 1987; Bridgens et al., 2004a; Galliot & Luchsinger, 2009, 2011a). The reason is that when the yarn directions are loaded simultaneously, both warp and fill fibres try to straighten, but this cannot happen independently, because of the weaving. Therefore, coated fabrics show a sort of Poisson's effect, which causes the deformation in one direction to be influenced by the force applied in the transversal direction. This behaviour is consistent with the practice of characterising their biaxial behaviour by employing several stress-strain diagrams, which are obtained at different load ratios Figure 4.16.

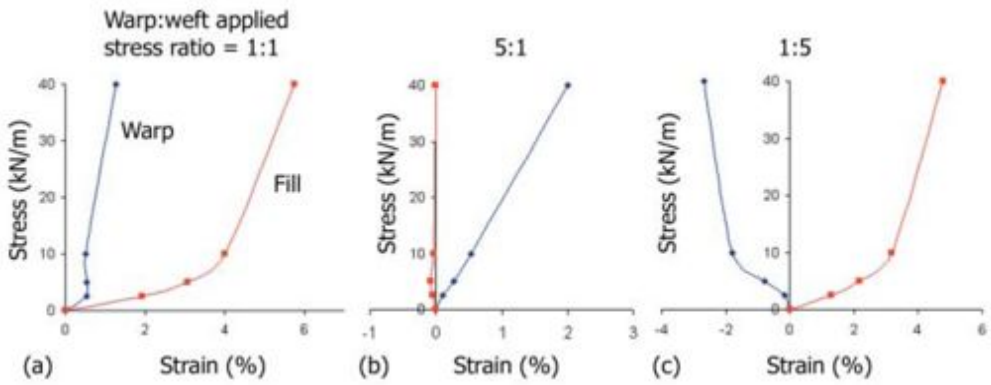

Figure 4.16: *Initial stress-strain behaviour of a PTFE coated glass fabric reproduced by the work of Day (1986) (from Bridgens et al., 2004a).*

The biaxial response of a coated fabric is also dependent on the load history. Because of the crimp interchange effect, the previously applied loads determine the configuration of the fibres in terms of crimp, which can be of three types:

- straight warp yarns and curved fill yarns, resulting in a stiffer behaviour of warp direction;
- straight fill yarns and curved warp yarns, resulting in a stiffer behaviour of fill direction;
- an intermediate configuration, between the previous two.

If several cycles are repeated at the same load ratio, after 3-5 cycles the residual strain after the unloading becomes negligible, and the response of the coated fabric can be considered repeatable (until the load ratio is varied). This is shown in Figure 4.17, where the effect of cycle repetition on a PVC coated polyester fabric is represented.

Moreover, Figure 4.17 displays that coated fabrics loading/unloading behaviour is characterised by hysteresis. This can be attributed to the loss of energy due to the friction between fibres and between the yarns and the coating (Bridgens et al., 2004a).

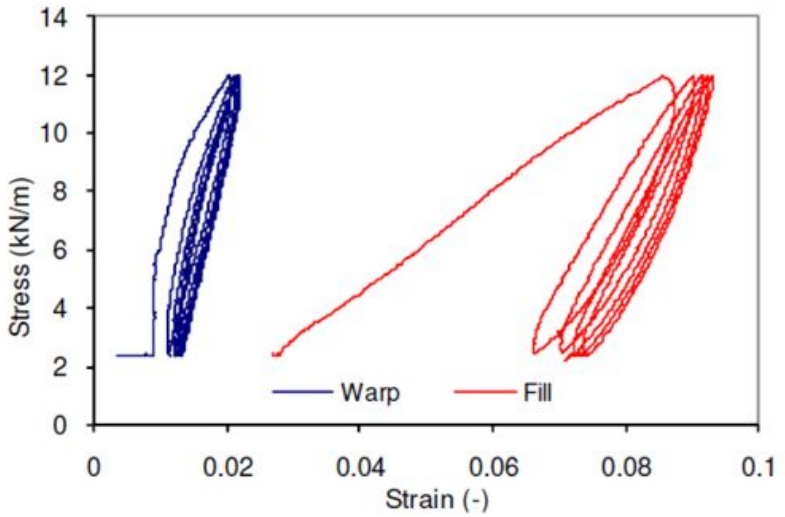

Figure 4.17: *Influence on a PVC/PES fabric of cyclic loading at 1:1 load ratio (from Galliot & Luchsinger, 2011a).*

Finally, since membranes are flexible, they have no bending stiffness, hence they can only support tension. To guarantee that the membrane will not experience compressions when subjected to various environmental loads, a prestress is applied during installation (Bridgens et al., 2004b). Galliot & Luchsinger (2011a) studied the influence of prestress level on coated fabric behaviour. A higher prestress leads to a stiffer material behaviour in fill direction during the first loading, as demonstrated by Figure 4.18. However, the warp yarns seems to be not influenced by the initial prestress level: the cause is in the weaving geometry of the virgin fabric. In fact, fill fibres are initially more crimped, hence they require the application

of a tensile load to be straightened, while the warp fibres are yet straight in the unstressed configuration.

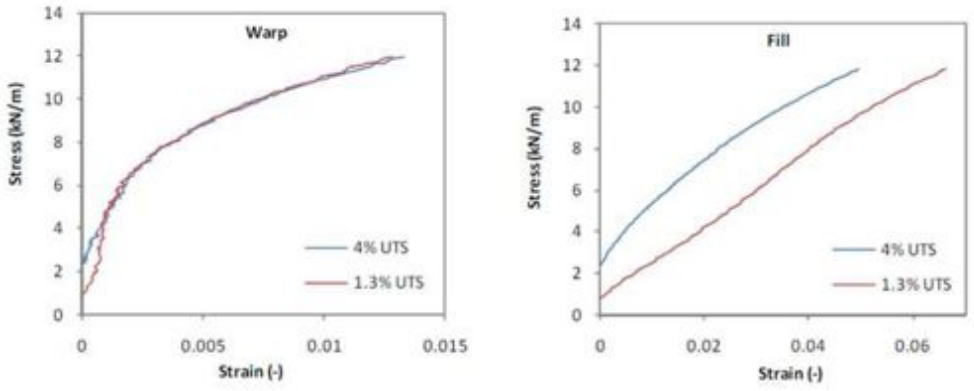

Figure 4.18: *Influence of the initial prestress level in warp and fill directions on a coated fabric biaxially loaded at 1:1 load ratio for the first time (from Galliot & Luchsinger, 2011a).*

4.1.3 Shear behaviour

Even if the most suitable stress field for a coated fabric does not involve shear, there exist several cases where real membrane structures experience shear loading conditions. For instance, the the shear deformations allow flat fabric patterns to be developed into complex forms. In addition, inflated beams show large shear deformations under bending loads (Cavallaro et al., 2003). Therefore, an accurate estimation of the shear stiffness of architectural coated fabrics is fundamental to correctly predict their behaviour.

Despite the importance of the shear issue in structural engineering, very few studies have been done so far on the coated fabric shear response. Currently, most of the works that are present in the literature treat the problem for raw fabrics (Skelton, 1976; Potluri et al., 2006; Cao et al., 2008; Hivet et al., 2012), because in-plane shear is the dominant deformation mode for woven fabrics during industrial processes of composite forming (Potluri et al., 2006; Cao et al., 2008). These studies demonstrate that the shear resistance of uncoated woven fabrics is negligible with respect to their biaxial tensile strength.

Whereas uncoated fabrics offer almost no resistance to shear deformation, in coated fabrics this deformation is resisted by the coating. Testa & Yu (1987) comments the results of an off-axis (45°) uniaxial tensile test performed on a Teflon (PTFE) and a silicone coated fabrics, which are reported in Figure 4.19. Testa & Yu (1987) claims that it is not surprising that the shear responses are found to be essentially elastic, since the resistance to shear deformations arises almost entirely from the coating.

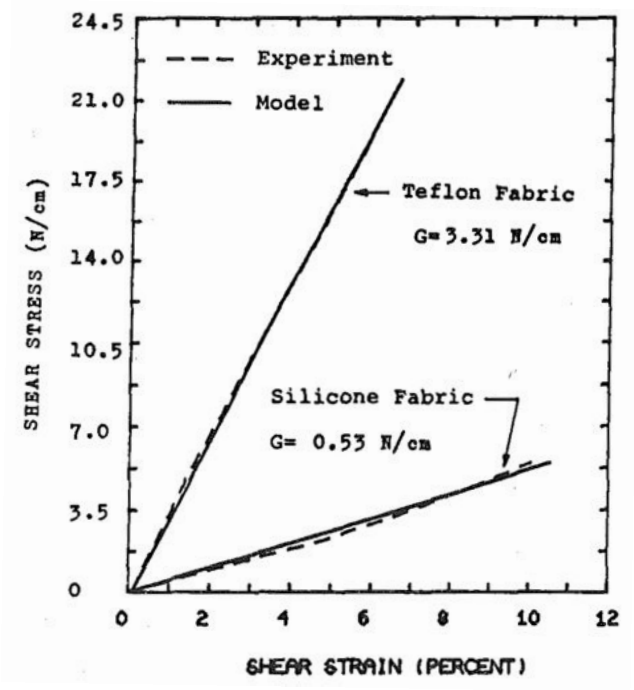

Figure 4.19: *Shear response of a Teflon and a Silicone coated fabrics (from Testa & Yu, 1987).*

According to Galliot & Luchsinger (2010b), most of the present studies focused on coated fabrics provide not a single value of the shear stiffness, but a range of possible values. From these results, it appears that PTFE coated glass fabrics have a shear modulus of 30-70 kN/m, while for PVC coated polyester fabrics it lies in the range 10-50 kN/m. The majority of the considered studies furnished a single value of shear stiffness, which is equivalent to consider the shear response as linear elastic. However, as pointed out by Galliot & Luchsinger (2010b), only in one of them (Testa &

Yu, 1987) the measured stress-strain curve was linear. Indeed, fabric shear response is nonlinear and hysteretic (Bridgens et al., 2004a).

Several test methods have been developed to investigate the shear behaviour of coated and uncoated fabrics. A summary of these methods is provided by Galliot & Luchsinger (2010a), who states that the bias extension test and the picture frame test are probably the most popular among the others. These are illustrated in Figure 4.20. In both the two the sample is loaded at 45° with respect to the yarn directions, in order to get a trellis shear deformation in the sample. The bias test is the simplest, but the obtained shear strain is not uniformly distributed in the sample: the trellis shear deformation mode is localised in region 3 of Figure 4.20(a). On the other hand, the tangential strain field developed by the picture frame method is almost homogeneous within the sample.

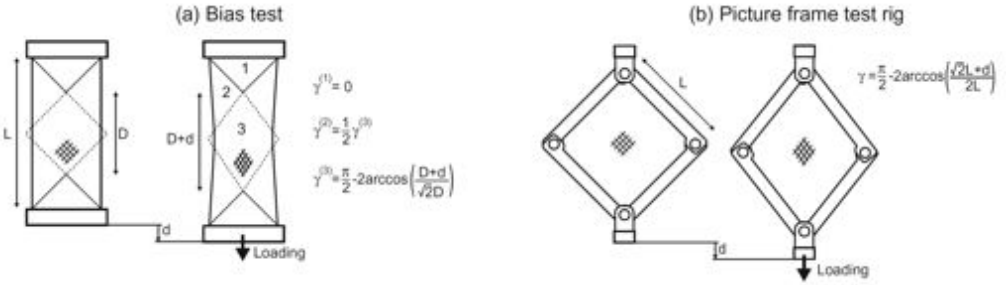

Figure 4.20: *Test methods used for the investigation of the fabric shear response (adapted from Galliot & Luchsinger, 2010a).*

The bias test have been utilised, for example, by Chen et al. (2007) and Zhang et al. (2010, 2012) to investigate the behaviour of PVC/PES and PTFE/glass fabrics for several angles of application of the tensile force. The results of these tests have been previously commented in Section 4.1.1. Although the bias test is really simple and requires small specimens to be carried out, the picture frame is the method suggested by the MSAJ/M-01:1993 Japanese Standard for the determination of the in-plane shear stiffness of membrane materials.

For architectural coated fabrics, a modification of the picture frame test has been proposed by Jackson et al. (2009). According to the described test protocol (see Figure 4.21), a cruciform specimen is first prestressed and

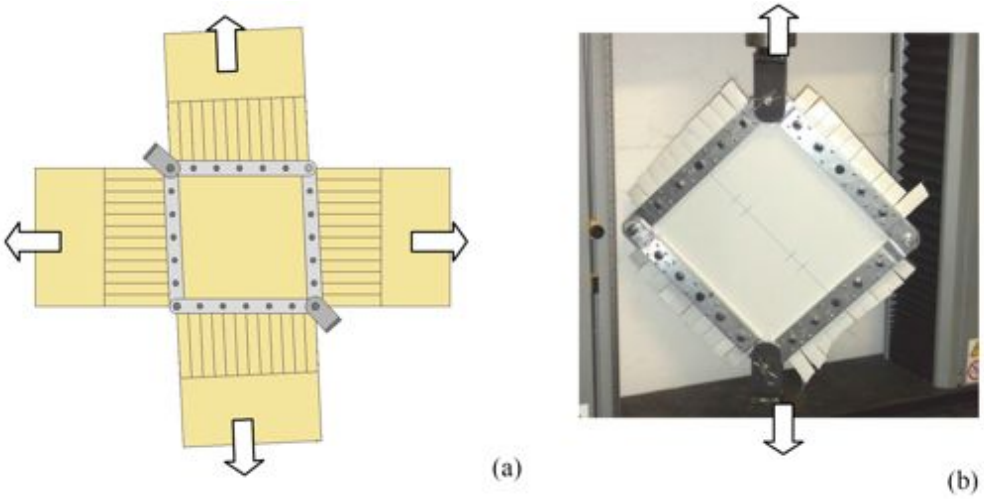

Figure 4.21: *Biaxial and shear protocol for architectural fabrics: (a) previous biaxial loading and (b) subsequent picture frame test (from Jackson et al., 2009).*

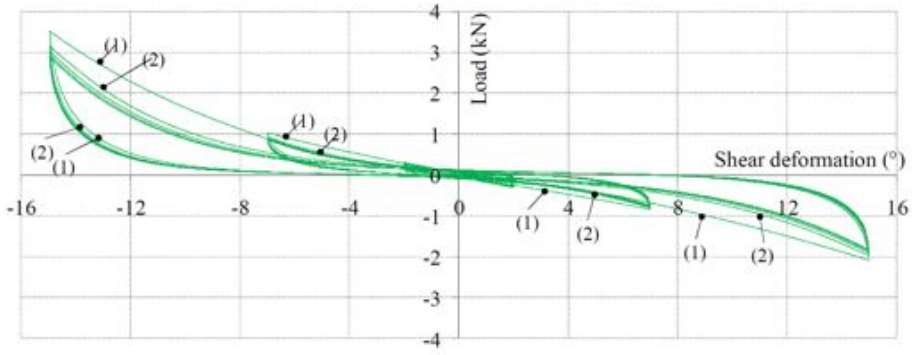

Figure 4.22: *Load-extension curves obtained from picture frame tests of different coated fabrics (adapted from Jackson et al., 2009).*

conditioned with a standard biaxial testing rig. Then, a frame is installed on the conditioned specimen, which is removed and tested with the classical picture frame procedure. As pointed out by Jackson et al. (2009), the most significant advantage of this modified picture frame method is that any biaxial stress state can be applied to the test specimen through the conditioning, and then maintained during the shear testing.

The experimental results presented in Jackson et al. (2009) show that the coated fabric behaviour is nonlinear and hysteretic (see Figure 4.22). The shape of the hysteretic curve was found to be similar for all the tests, and more influenced by the loading history than by the loading rate.

Finally, a new shear testing methodology, which is named shear ramp, has been proposed by Galliot & Luchsinger (2010a,b). It consists in the bixial loading of a cruciform sample, where the forces are applied so that stresses along each side of the central square vary linearly Galliot & Luchsinger (2010a). This allows the simultaneous determination of yarn-parallel and shear properties of a coated fabric with a single sample and a unique test.

The results obtained with the shear testing procedure have been compared by Galliot & Luchsinger (2010b) with the ones of an equivalent off-axis biaxial tests of a specimen with 45° rotated fibres (Figure 4.23). The resulting stress-strain curves for repeated cycles confirm that the shear behaviour of coated fabrics is hysteretic. Moreover, the measured loading curves illustrated in Figure 4.24 underline the characteristic nonlinearity of the shear response, which is typical of several coated fabrics.

4.2 Coated fabric testing

4.2.1 Uniaxial testing

In absence of European standards on biaxial testing, the tensile strength of coated fabrics is currently determined by means of uniaxial tensile tests. As reported in Table 4.1, the tensile strength and elongation at break of coated fabrics can be measured according to several national and international standards, where the most widely used is EN ISO 1421:1998 *"Rubber- or plastics-coated fabrics – Determination of tensile strength and elongation at break"*.

Two testing methods are described in the EN ISO 1421:1998 Stan-

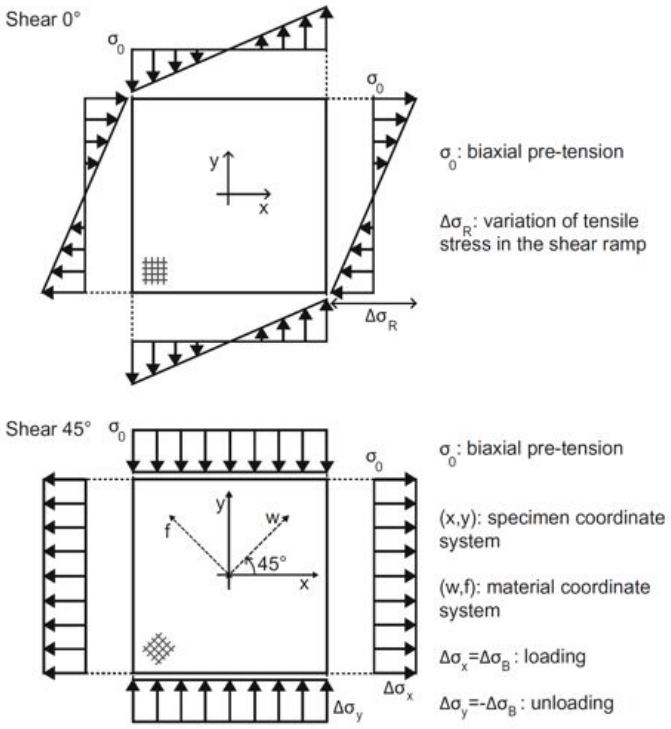

Figure 4.23: *The shear ramp test method (Shear 0°) and the equivalent off-axis biaxial test (Shear 45°) proposed by Galliot and Luschinger (from Galliot & Luchsinger, 2010b).*

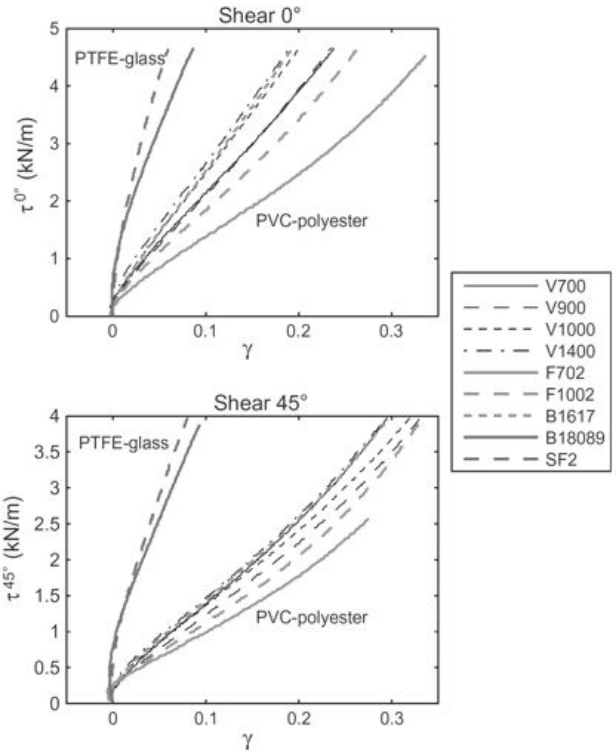

Figure 4.24: *Stress-strain curves obtained with the shear ramp test method (Shear 0°) and with the equivalent off-axis biaxial test (Shear 45°) for different coated fabrics (from Galliot & Luchsinger, 2010b).*

dard: the strip test and the grab test, whose samples are illustrated in Figure 4.25(a) and Figure 4.25(b), respectively. The first method tests a strip of material gripped in the jaws for the full width and provides both the Ultimate Tensile Strength (UTS) and the elongation at break. The second technique, called grab test, performs the tensile test on a sample that is gripped in the jaws only in its central part and it is limited to the determination of the tensile strength.

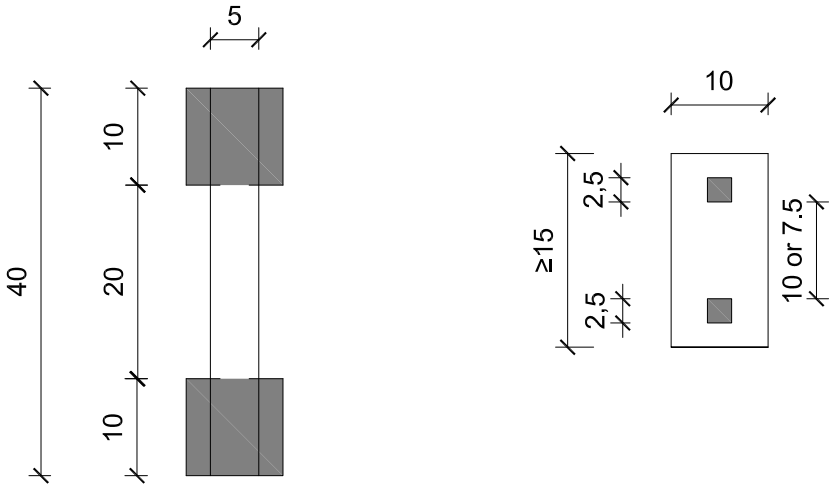

(a) Strip method (b) Grab method

Figure 4.25: *The specimens employed for uniaxial tensile tests, according to EN ISO 1421:1998 Standard.*

The strip test has been employed to perform the uniaxial tests described in this Section 4.2.1. According to this methodology, two sets of samples must be cut form the roll: one set of five pieces in the longitudinal (warp) direction and the other one in the transversal (fill) direction. Each specimen shall be 50 ± 0.5 mm wide and of sufficient length to allow a distance of 200 ± 1 mm between tha jaws of the test machine, as illustrated in Figure 4.25(a).

Each sample is then gripped in the jaws of a constant rate of extension (CRE) tensile testing machine and loaded with a pretension of 2 -10 N that

makes it tight. The uniaxial tests described in this Section have been performed with the biaxial testing rig that belongs to the Research Cluster on "Innovative Textiles" (ClusTEX) of Politecnico di Milano, which will be described in detail in the next Section 4.2.2.

After the pretensioning, the clamps are moved apart at a constant rate of 100 ± 10 mm/min, until the sample breaks. The force at break and the correspondent maximum elongation are recorded. Then, the test is repeated for all the other specimens.

Once the test has been performed on each of the five specimens in both the longitudinal and transversal direction, the mean values in each direction are determined: these correspond to the UTS and to the maximum elongations in warp and fill directions. Any test result where the test piece breaks within 5 mm of the face of a jaw should be disregarded.

The values of UTS and elongation at break in warp and fill directions are usually evaluated by the producers and provided within the technical datasheet available with most of the coated fabrics on the market. The majority of the fabrics tested for this thesis are commercial products, therefore there were no need of uniaxial testing. However, part of the biaxial tests described in the next Section 4.2.2 have been performed for research purposes on four new types of Polyurethane (PU) coated polyester fabrics (PU/PES), which are named material A, B, C, and D hereafter.

In order to mechanically characterise these new types of coated fabrics, and to determine the warp and fill UTS values to be employed in the construction of the biaxial loading profiles, a series of uniaxial tensile tests have been performed on each of the four materials (A, B, C, and D), whose results are reported in Tables 4.4 to 4.7.

The estimated values of UTS for materials A, B and D (Tables 4.4, 4.5 and 4.7) are similar to the ones of a PVC/polyester of Type I, therefore possible applications of these materials in the structural field are canopies and shade structures with a limited span. In consideration of their waterproof property, they could be used also to realise pneumatic structures with a limited internal pressure. Material C has a very low weight ($400\,\mathrm{g/m^2}$) and, consequently, a low UTS (see Table 4.6), which is comparable to the one of blinds for internal solar protection.

Direction	Sample	Force at break	UTS	Elongation at break	Mean elongation
		[daN/5 cm]	[daN/5 cm]	[%]	[%]
Warp	1	300		70.39	
	2	280		72.24	
	3	288	276	71.97	73.50
	4	251		75.89	
	5	262		77.00	
Fill	1	267		74.24	
	2	280		72.22	
	3	269	268	72.58	73.10
	4	Failed		Failed	
	5	256		73.35	

Table 4.4: *Uniaxial test results (material A).*

Direction	Sample	Force at break	UTS	Elongation at break	Mean elongation
		[daN/5 cm]	[daN/5 cm]	[%]	[%]
Warp	1	295		70.97	
	2	293		71.72	
	3	282	283	70.80	72.52
	4	286		72.94	
	5	261		76.17	
Fill	1	272		72.59	
	2	Failed		Failed	
	3	269	269	72.05	72.58
	4	264		73.12	
	5	269		72.56	

Table 4.5: *Uniaxial test results (material B).*

Direction	Sample	Force at break	UTS	Elongation at break	Mean elongation
		[daN/5 cm]	[daN/5 cm]	[%]	[%]
Warp	1	Failed		Failed	
	2	139		17.01	
	3	170	157	20.16	18.70
	4	171		20.05	
	5	149		17.61	
Fill	1	102		19.80	
	2	94		18.30	
	3	120	113	22.50	21.13
	4	120		21.31	
	5	130		23.76	

Table 4.6: *Uniaxial test results (material C).*

Direction	Sample	Force at break	UTS	Elongation at break	Mean elongation
		[daN/5 cm]	[daN/5 cm]	[%]	[%]
Warp	1	274		22.87	
	2	286		23.54	
	3	Failed	285	Failed	23.44
	4	278		22.85	
	5	304		24.51	
Fill	1	244		21.87	
	2	284		23.23	
	3	271	263	22.42	22.43
	4	Failed		Failed	
	5	255		22.20	

Table 4.7: *Uniaxial test results (material D).*

4.2.2 Biaxial testing

Currently, there are no international standards or design codes in Europe concerning plane biaxial testing. In spite of that, biaxial tests are fundamental for the design and realisation of tensile structures: they are commonly employed for material quality control, evaluation of compensation values, determination of tear strength and strain measurement under prescribed loadings and thermal conditions. Furthermore, biaxial tests are essential for researchers to assess validity and reliability of material models.

Biaxial tests of coated fabrics are usually performed on cruciform specimens with a central area bigger than (160×160)mm. According to Beccarelli et al. (2011), biaxial testing rigs that are apt to carry out this kind of tests are relatively not common and based on different operating principles. At present, the European testing centres that own these types of apparatuses are (see Figure 4.26):

1. Research Cluster on "Innovative Textiles" (ClusTEX), Politecnico di Milano (I);
2. Newcastle University (UK);
3. Centre for Synergetic Structures at Swiss Federal Laboratories for Materials Science Technology (EMPA), Dübendorf (CH);
4. Laboratorium Blum, Stuttgart (D);
5. University of Duisburg-Essen (D);
6. City University of London (UK);
7. Universität Stuttgart (D);
8. Bauer Membranbau, Freising (D).

Not only the listed testing centres have biaxial machines based on different operating principles, but they have developed their own internal protocols for the definition of the biaxial testing procedure. This is mainly due to the absence of international standards that would define a unique biaxial testing protocol, so that several approaches for the mechanical characterisation of coated fabrics and foils are currently employed.

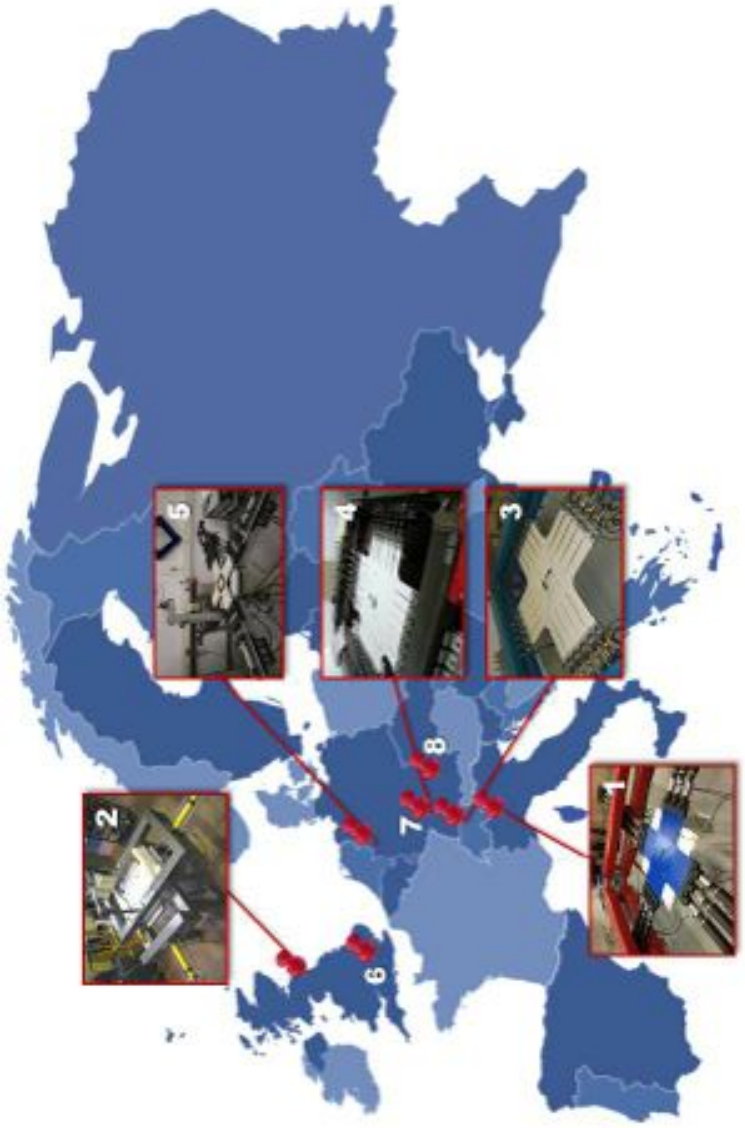

Figure 4.26: *European testing centres with biaxial machines: 1) Politecnico di Milano 2) Newcastle University (from Bridgens et al., 2004a) 3) EMPA (from Beccarelli et al., 2011) 4) Laboratorium Blum (from Bridgens et al., 2012) 5) University of Duisburg-Essen (from Beccarelli et al., 2011) 6) City University of London 7) Universität Stuttgart 8) Bauer Membranbau.*

The level of reproducibility of a test represents an important aspect, especially in this case of extreme variability of approaches. An important contribute to the definition of the reproducibility of biaxial tests in the European contest is given by the round-robin exercise presented in Beccarelli et al. (2011). It consists in a biaxial test that was carried out with a unique loading profile and on samples cut out from the same batch of PVC coated polyester fabric 1302 produced by Serge Ferrari S.A.S. The cruciform specimens were cut out and tested according to the internal protocols adopted by each laboratory. Finally, the test results were compared to asses the level of accuracy of biaxial information commonly used in the design ad realisation of membrane structures. The experiment has recorded a level of precision equal to the one commonly present in the design of tensile structures, even if the testing apparatuses were completely different. The Research Cluster on "Innovative Textiles" (ClusTEX) of Politecnico di Milano has taken part to the round-robin exercise, but the results concerning this test are not presented by Beccarelli et al. (2011) because it has been performed after the publication of the article since the biaxial testing rig was under construction at that time. However, the results have shown a level of accuracy which is in line with the one of the other involved testing centrers.

At present, the only national standards available as reference for the development of biaxial testing protocols are the Japanese MSAJ/M-02:1995 *"Testing Method for Elastic Constant of Membrane Materials"* and MSAJ/M-01:1993 *"Testing Method for In-plane Shear Stiffness of Membrane Materials"*. The procedure established by the Membrane Structure Association of Japan is generally applied with slight variations, which aim at improving the experimental results and customising the test on the base of its scope.

Some of the biaxial tests presented in this thesis were carried out by the author with the biaxial testing rig belonging to the Research Cluster on "Innovative Textiles" (ClusTEX) of Politecnico di Milano, while part of them were kindly provided by the research team of Prof. Peter Gosling at Newcastle University (UK), where the author spent the period from the beginning of April to the end of August 2013 as visiting Ph.D. student.

Sampling procedure

The testing protocol adopted by the author starts from the definition of the sampling procedure. Biaxial tests have been performed on cruciform specimens with slits. The Japanese standard MSAJ/M-02:1995 prescribes the minimum dimensions of the cross and imposes the use of slitted arms that improve the load transfer from the clamps to the centre of the specimen (see Figure 4.27). According to these prescriptions, the cross samples employed by the author have a central square area of (300×300)mm and a clamp interval of 900 mm, with two slits for each arm, as shown in Figure 4.28.

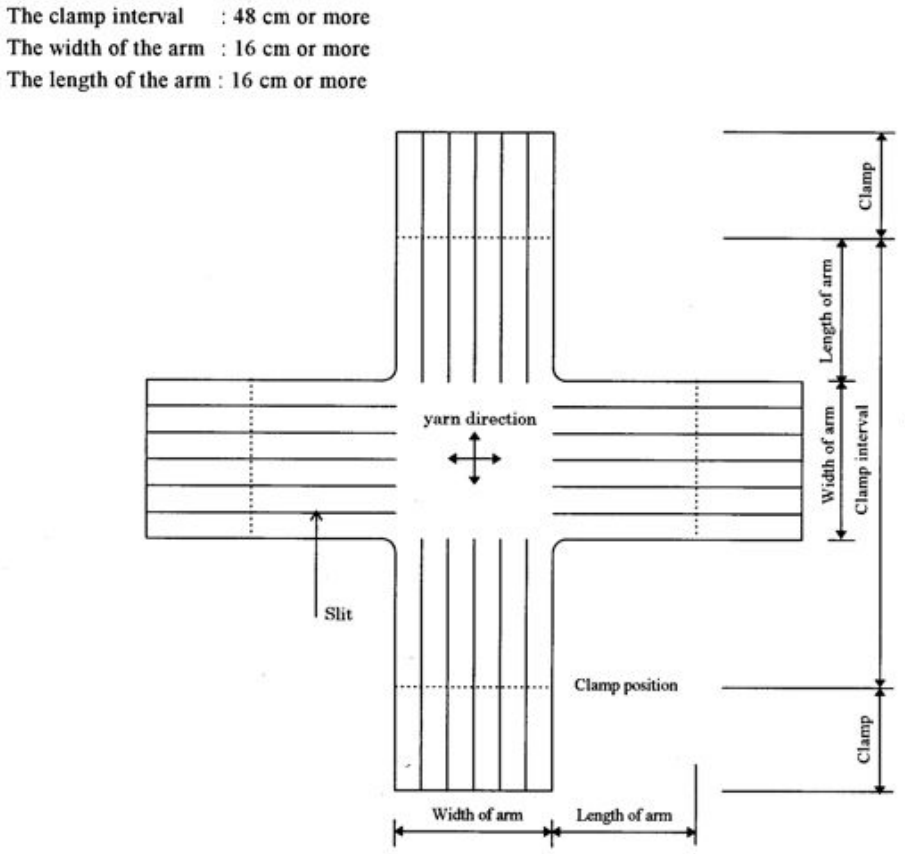

Figure 4.27: *Slitted cross-shaped specimen according to the Japanese standard MSAJ/M-02:1995 (from MSAJ/M-02:1995).*

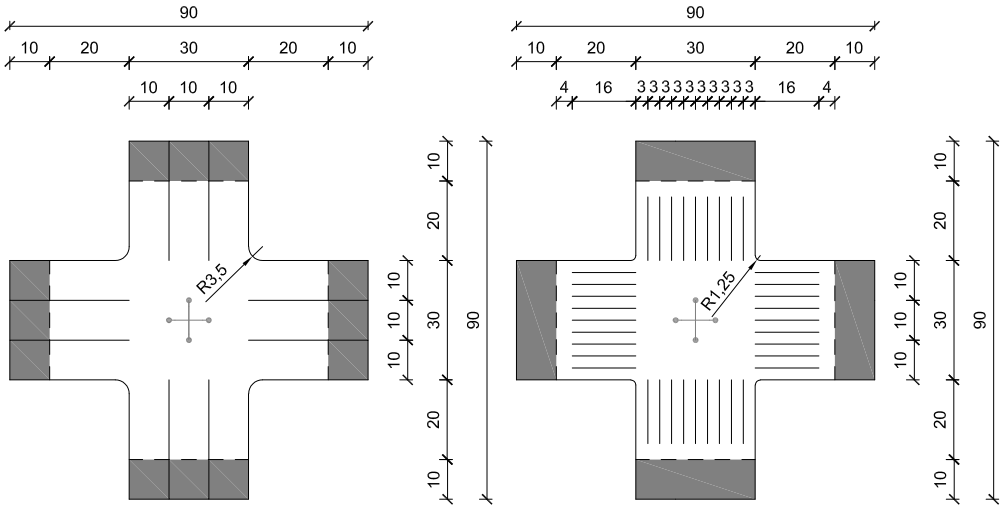

(a) Politecnico di Milano (b) Newcastle University

Figure 4.28: *Slitted cross-shaped specimen employed at Politecnico di Milano (Polimi) and at Newcastle University (NCL).*

It has been widely demonstrated that slitted cross-shaped specimens can effectively reproduce a homogeneous stress distribution in the central area of the sample (Reinhardt, 1976; Bridgens, 2005; Galliot & Luchsinger, 2009). Moreover, as pointed out by Bridgens (2005), the use of full-length slits with arm strips clamped independently solves the problem of large shear deformations in the arms, even if it results in slightly higher variation in stress across the central square of the cruciform. The solution adopted in this thesis is the one with 2 slits and independent clamps, while the tests carried out at Newcastle University employed 9 slits and a single clamp for each arm (see Figure 4.28).

Even if cross samples with slits have been accepted as the best shape for plane biaxial test, there is still a wide variety of dimensions for both the central area and the clamp interval, as well as in the number of slits. The dimension of the central area adopted by the author has been chosen according to Bridgens (2005), who demonstrates that a length of 300 mm is large enough to ensure that a sufficient number of yarns have been included to obtain a good distribution of yarn properties and to ensure that the contribution of any single yarn is negligible. Moreover, Bridgens (2005) claims

that a larger cross specimen would led to practical problems if tested until failure, because of the increased rig dimensions and high loads required. However, some testing centres adopt different, e.g. EMPA (500×500)mm, University of Duisburg-Essen (200×200)mm (see Beccarelli et al., 2011; Beccarelli, 2010).

For what concern the number of specimens, the Japanese standard MSAJ/M-02:1995 recommends a minimum of three samples for each weaving direction. These should be cut out from the part of the roll which is 1/10 of the overall width from each selvage, and excluding more than 100 cm from either edge. However, the number of tests depends on the objective: to obtain average values of the material properties three tests are enough, whereas a significantly greater number of tested specimens is required to establish the 5 % fractile.

Test rig and experimental setup

Part of the tests presented in this thesis have been performed by the author at Politecnico di Milano with the biaxial machine in Figure 4.29, that belongs to the Research Cluster on "Innovative Textiles" (ClusTEX). This has been designed by Paolo Beccarelli (Beccarelli, 2010) to test fabrics and foils used in structural applications.

The above mentioned test rig has a rigid square frame realised by means of steel profiles with a rectangular hollow section. The frame, with a net internal distance of 1852 mm, is designed to counterbalance an estimated maximum force of 140 kN on each side.

Each side of the frame has a battery of three independent servomotors, which consist of an electromechanical motor that controls a ball screw[1] (actuator) coupled with a sensor for position feedback (transducer). The tensile force is applied to the membrane sample by means of these actuators, which are equipped with:

- load cells, that provide a tension force from 1 up to 25 kN for each clamp (100 mm wide);
- force transducers, which measure the force applied at each clamp.

[1] A ball screw is a mechanical linear actuator, which is made with a screw inserted in a planetary gearbox: it is employed to translate rotational motion into linear motion with little friction.

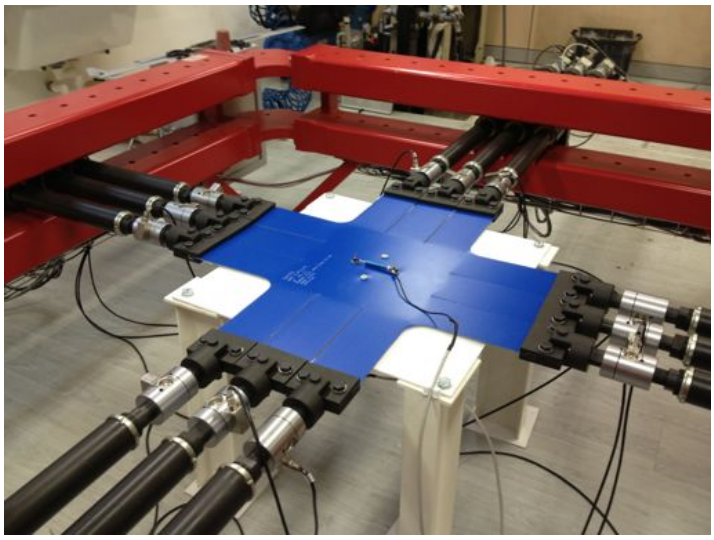

Figure 4.29: *Biaxial testing rig of the Research Cluster on "Innovative Textiles" (ClusTEX), Politecnico di Milano.*

The motors allow a maximum speed of 240 mm/min and a maximum stroke of 512 mm.

The above described actuators are free to move along the side of the frame and to rotate around an axis perpendicular to the sample plane. The first degree of freedom is allowed thanks to a couple of low friction rollers for each actuator. The out-of-plane rotation is released by means of a ball joint placed at the extremity of each ball screw. This type of kinematics assures that only axial forces and no bending moment are applied to the components.

The clamping system is composed by two superimposed grooved steel plates 100 mm wide for each actuator, one fixed and the other removable in order to easily place the sample inside the hem sleeve. Each arm strip is wound up around a steel bar and held within the enclosure formed between the two bolted plates.

Once the slitted cruciform specimen has been positioned, the sample equilibrium is achieved by balancing the total force applied on each side through the computerised control system. A master/slave option is available, which automatically satisfies this requirement, but there is also the possibility of moving each electric motor independently (all master): this

option can be useful for asymmetric tests, e.g. of structural details or seams.

Elongations (hence strains) in the central square of the cross-shaped specimen are acquired through two contact extensometers, which are positioned along warp and weft directions with an initial base of about 100 mm. The base length is chosen so that, on the chance that a fracture started from one of the slits propagates across the central square, the tear would pass exactly through the gauge position avoiding the damage of the extensometer. More in detail, the biaxial machine is equipped with four potentiometers Penny & Giles SLS095/0030/1.2K/R/50 with a closed size of 90 mm and a maximum stroke of 30 mm.

Instead, the biaxial tests provided by Newcastle University (UK) have been performed with a biaxial testing rig that represents a *unicum* in this field (Figure 4.30). It has been developed by Architen Landrell (Chepstow, UK; www.architen.com) and the School of Civil Engineering & Geosciences of the University. Its design is based on the *floating frame* concept: loads are applied in warp and weft directions by two reaction frames, of which the lower one is fixed and the upper one is mounted on four spherical bearings that make it free to move in the plane of the fabric.

Figure 4.30: *Biaxial testing rig of Newcastle University (from Bridgens et al., 2004a).*

The floating frame approach allows the spontaneous alignment of the uniaxial load with the weaving directions, which are not always orthogonal because the fabric manufacturing process results in bowing of the weft yarns. This aspect is particularly important, since the weaving directions represent the material principal directions, hence the alignment of the load with them is fundamental to exclude unwanted shear effects. The same result is obtained in the biaxial testing rig of Politecnico di Milano thanks to the translational and rotational degrees of freedom of the actuators described above.

The design adopted for the biaxial machine of Newcastle University is particularly convenient from the economical point of view, because it leads to a considerable optimisation of the testing equipment. Indeed, the tensile loads are applied by means of only two hydraulic actuators, one for each direction, which are connected to an external hydraulic pump able to develop a maximum force of 150 kN. The force is applied to two sides of the cruciform specimen, while the stress on the opposite sides are generated through the reaction forces provided by the frame. Each actuator is equipped with a pancake load cell, which measures the force transmitted by the actuator to the clamps.

The clamping system is based on the same principle of the one described above for the biaxial machine of Politecnico di Milano. The only difference is that there is a single clamp 300 mm wide for each side, therefore the arm strips are clamped together and not separately.

Also the extensometers employed for the strain measurement are the same, even if at Newcastle University there is the possibility of using scanning laser extensometers (Hounsfield 500L) if a more accurate non-contact strain measurement is required. This is particularly advantageous when a material with a low fracture energy is tested, because the holes made by the gauges could cause the propagation of tears. Moreover, the use of optical strain measurement equipment is fundamental to test very thin membranes or materials with a little number of yarns per cm, because in these cases the contact extensometers could be unstable, thus providing inaccurate measurements.

Test outline

The scope of a test represents one of the most crucial aspects in developing a testing protocol. Indeed, mechanical behaviour of foils and coated fabrics is different in the initial stage, during service life, at break, as well as in long term (creep) and dynamic conditions. Therefore the loading profile and the type of control that are employed in a test must be selected according to its aim.

Tables 4.8 and 4.9 provide an outline of the biaxial tests that have been carried out during this research, together with some that have been provided by Newcastle University (UK). According to their aim, such tests may be grouped as follows:

1. Test VUB 001 A has been performed to investigate the effect of the preconditioning cycles prescribed by the MSAJ/M-02:1995 Standard.

2. Tests F702 MSAJ and B18089 MSAJ aim at recording the mechanical response of two types of coated fabric, a PVC/PES and a PTFE/glass fibre, when subjected to the loading profile that is in accordance with the MSAJ/M-02:1995 Standard prescriptions.

3. Tests F1202T2 ALR and B18059 ALR contain additional cycles with respect to the MSAJ/M-02:1995 loading profile, which investigate the material behaviour for loading ratios that are intermediate between the ones considered by the Japanese Standard.

4. Tests NTT 011 1 BX, NTT 010 2 BX, NTT 001 A BX, NTT 002 A BX, NTT 001 B BX and NTT 002 B BX have been realised (according to the MSAJ/M-02:1995 Standard) on several new types of Polyurethane (PU) coated polyester fabrics with the intent of mechanically characterising the new materials and establishing their potential applications and target.

5. Tests TEN 008 A, TEN 015 A, TEN 018 A and TEN 019 A represent an innovative typology of biaxial tests, which are strain-controlled (a strain history is assigned in the central part of the specimen) and have the scope of furnishing additional information about the material behaviour that may be meaningful for the installation process.

6. Test TEN 001 A is a stress-controlled biaxial test that has been carried out according to the MSAJ/M-02:1995 loading profile, but at lower value of stress, coinciding with the one currently employed in the pretensioning of structural membranes; it constitutes a preliminary phase intended to estimate the compensation factors (see Section 2.2) and to set up the strain loading profile to be used for tests TEN 008 A, TEN 015 A, TEN 018 A and TEN 019 A.

The force-controlled biaxial tests from 1 to 4 will be described and commented in Section 4.2.3, while the strain-controlled biaxial tests 5 and their corresponding preliminary force-controlled test 6 will be presented in Section 4.2.4.

Test ID	Testing center	Tested fabric	Material type	Strip tensile strength [kN/m]		Stress/strain histories
				Warp	Fill	
VUB 001 A	Polimi	Naizil Big Cover	PVC/PES Type II	80	80	Figure A.1
F702 MSAJ	Newcastle	Ferrari 702	PVC/PES Type I	56	56	Figure A.2
B18089 MSAJ	Newcastle	Verseidag B18089	PTFE/glass Type G6	140	120	Figure A.3
F1202T2 ALR	Newcastle	Ferrari 1202T2	PVC/PES Type III	112	112	Figure A.4
B18059 ALR	Newcastle	Verseidag B18059	PTFE/glass Type G6	160	140	Figure A.5
TEN 001 A	Polimi	Ferrari 1002 W/B 538 OP	PVC/PES Type II	84	80	Figure A.12

Continued on next page

Table 4.8: *Outline of force-controlled biaxial tests.*

Continued from previous page

Test ID	Testing center	Tested fabric	Material type	Strip tensile strength [kN/m]		Stress/strain histories
				Warp	Fill	
NTT 011 1 BX	Polimi	NTT Material A	PU/PES -	55	54	Figure A.6
NTT 010 2 BX	Polimi	NTT Material B	PU/PES -	57	54	Figure A.7
NTT 001 A BX	Polimi	NTT Material C	PU/PES -	31	23	Figure A.8
NTT 002 A BX	Polimi	NTT Material C	PU/PES -	31	23	Figure A.9
NTT 001 B BX	Polimi	NTT Material D	PU/PES -	57	53	Figure A.10
NTT 002 B BX	Polimi	NTT Material D	PU/PES -	57	53	Figure A.11

Table 4.8: *Outline of force-controlled biaxial tests.*

Test ID	**Testing center**	**Tested fabric**	**Material type**	**Strip tensile strength [kN/m]**		**Stress/strain histories**
				Warp	**Fill**	
TEN 008 A	Polimi	Ferrari 1002 W/B 538 OP	PVC/PES Type II	84	80	Figure A.13
TEN 015 A	Polimi	Ferrari 1002 W/B 538 OP	PVC/PES Type II	84	80	Figure A.14
TEN 018 A	Polimi	Ferrari 1002 W/B 538 OP	PVC/PES Type II	84	80	Figure A.15
TEN 019 A	Polimi	Ferrari 1002 W/B 538 OP	PVC/PES Type II	84	80	Figure A.16

Table 4.9: *Outline of strain-controlled biaxial tests.*

4.2.3 Force-controlled biaxial tests

Tests F702 MSAJ and B18089 MSAJ have been carried out according to the MSAJ/M-02:1995 Japanese Standard loading profile (see Figure A.2(a) and Figure A.3(a)). This is intended to estimate the elastic constants of a linear orthotropic elastic material model, which aims at reproducing the fabric service behaviour. For this reason, a cyclic load pattern is employed, which would simulate the loading conditions of an in situ membrane that has been prestressed during erection and exposed to environmental loads (e.g. wind and snow).

As prescribed by the MSAJ/M-02:1995 Standard, the load is applied up to a maximum level of 25 % UTS (ultimate tensile strength, see Section 4.2.1), that Happold et al. (1987) demonstrated to be the load at which approximately tear propagation occurs. Moreover, this range of load covers the one of membrane materials in use, since 4 is currently the worldwide accepted minimum factor of safety for the design of tensioned membranes (Bridgens et al., 2004b).

A minimum load is applied to the cruciform specimen in order to remove the slackness, which would distort the strain measurement in the central part of the sample. Different values of prestress have been adopted in the literature (and in the tests here presented), ranging from 1.3 % UTS for PVC coated polyester fabrics to 2.5 % UTS for PTFE coated glass fabrics (see, e.g., Bridgens et al., 2012). A lower prestress value is usually associated with PVC/polyester fabrics, because these show residual strains of 5-10 % at the end of a biaxial test, which are not as high as the 15 % typically recorded for a highly crimped PTFE/glass fabric (Bridgens et al., 2012). Although sometimes higher values of prestress have been used, for instance in test VUB 001 A, these are never larger than 10 % UTS, which is the safety factor employed by the designers for simulations of the installation process (Bridgens et al., 2004b).

A constant rate of extension of 2-4 mm/min is prescribed for the whole test by the MSAJ/M-02:1995 Standard. However, this requirement can be checked only after the test, because in coated fabrics stiffness varies with load and significant deformation occurs in the cruciform arms, hence the actual rate of extension in the central part of the specimen can be evaluated only *a posteriori*.

The MSAJ/M-02:1995 Standard prescribes to attach the slitted cruci-

form sample to the biaxial testing machine so that warp and weft directions are aligned with the loading axes. Then, the suggested testing procedure consists of the following steps:

1. A minimum load is applied to remove the slackness without occurrence of crimp interchange, which can be achieved by using the so-called *natural force ratio* (Testa & Yu, 1987)[1] between warp and weft directions.

2. While maintaining a warp to fill load ratio of 1:1, a biaxial load is applied at a constant rate up to 25 % of the UTS in the weaker weaving direction (fill), and then removed at the same rate and load ratio. This cycle should be repeated three times (preconditioning cycles).

3. The load is applied and removed again at a constant predetermined load ratio of interest. The maximum load coincides with the 25 % UTS of the weaving direction that currently has the larger load applied. The forces and strains measured during this step are the ones employed for the stress-strain curves construction and for the estimation of the material model parameters.

4. The procedure 2-3 is repeated throughout the sequence of predetermined load ratios. The MSAJ/M-02:1995 Standard suggests to employ the sequence of load ratios in Table 4.10.

It may be worth noticing that step 3 might be reproduced more than once, in order to investigate the material behaviour under cyclic loading. This has been done in tests F702 MSAJ and B18089 MSAJ, as well as in test VUB 001 A. Anyway, only the first cycle can be employed in the estimation of the material model parameters, since it starts from a fixed reference configuration of yarn crimp, which coincides with the one obtained after 3 cycles at 1:1 load ratio (step 2).

[1] According to (Testa & Yu, 1987), a *natural crimp state* is a curve that uniquely defines the crimp strain in a fabric that is loaded from the reference state, either at constant warp to fill load ratio and monotonically increasing load level, or at constant load level and monotonically increasing load ratio of fill to warp stress. By extension, a *natural force ratio* is a load ratio that does not change the crimp state in fabric, either for increasing or decreasing applied loads.

Direction of yarns	Load ratios				
Warp direction	1	2	1	1	0
	:	:	:	:	:
Fill direction	1	1	2	0	1

Table 4.10: *Combination of load ratios which should be used in biaxial tests according to the MSAJ/M-02:1995 Japanese Standard.*

With reference to step 2, preconditioning is a commonly employed procedure that attempts to simulate the effect of cyclic environmental loads. It is employed for that materials that show an initial behaviour which is completely different from the mechanically conditioned one. In fact, the initial behaviour of a virgin coated fabric that is loaded for the first time tends to be not repeatable. Therefore, the stress-strain response during the subsequent load cycles is typically different. The initial behaviour is usually established by *ad hoc* "compensation tests" to determine the parameters for patterning and installation (see Section 2.2), whereas preconditioning is needed if the repeatable service behaviour of a coated fabric has to be investigated for medium and long-term structural design purposes. To better understand the importance of this aspect, a test have been performed on a PVC coated polyester fabric (VUB 001 A, Figure A.1(a-b)), which follows the MSAJ/M-02:1995 Standard procedure with removing of the preconditioning cycles: the results will be commented in the next subsection.

In addition, the load ratios in Table 4.10 are such that the space of feasible stress states for the fabric is wholly explored by means of radial load paths, as shown by Figure A.2(b) and Figure A.3(b), which correspond to two biaxial tests that have been performed in accordance with the MSAJ/M-02:1995 Standard prescriptions. This approach does not exclude the possibility of investigating other load ratios. For example, tests F1202T2 ALR and B18059 ALR, whose loading profiles are reported in Figure A.4(a-b) and Figure A.5(a-b) respectively, have considered four additional load ratios (0.3:1 (path F), 1:0.3 (path G), 0.7:1 (path H), 1:0.7 (path I)), which are intermediate between the ones in Table 4.10. The scope of these two tests is providing further information on the coated fabric mechanical behaviour, which will be useful to validate the predictive capability of a model calibrated with the cycles associated with the stan-

dard load ratios in Table 4.10.

Lastly, NTT 011 1 BX, NTT 010 2 BX, NTT 001 A BX, NTT 002 A BX, NTT 001 B BX and NTT 002 B BX have been performed on a series of anonymous PU coated polyester fabrics. These are not among the most utilised materials for membrane structures, mainly because of their impossibility to be welded, which leads to the more expensive use of glued joints between panels. Anyway, they are waterproof materials, thus suitable to be employed, for instance, in air-inflated structures. Moreover, their use for little structures, which do not require welding, is growing. The load profile for these tests has been prepared in accordance to the MSAJ/M-02:1995 Standard (see Figures A.6(a-b) to A.11(a-b)). They aim at identifying in a quite standard manner the mechanical characteristics of these new types of materials, in order to establish their potential applications.

Discussion on force-controlled test results

Classical stress-strain plots have been produced using results from the previously described tests. More in detail, separate graphics have been extracted for each (first) loading curve that is subsequent to the group of three preconditioning cycles. This means that the stress-strain plots presented here represent the mechanical behaviour of the coated fabric when loaded along one of the radial paths in Figures A.1(b) to A.11(b).

Along these paths the load ratio between the warp and fill directions has been considered constant. Actually, this is not correct, because the radial load paths start from the prestress, rather than from zero. However, since the prestress value is low, considering that loads are applied at a fixed warp to fill stress ratio leads to negligible errors.

Separate stress-strain curves have been constructed for warp and fill directions. Since the constitutive modelling that will be presented in Chapter 6 is based on the large strain theory, it is here fundamental to specify which kind of stress and strain have been employed. The graphs have been built by using nominal stresses and engineering strains, calculated as specified further on.

On the one hand, the nominal stress has been evaluated through the division between the force applied by the actuators along one direction of the cruciform sample and the width of the arm (0.3 m, see Section 4.2.2). This value has been multiplied by a reduction factor (sometimes also called

cruciform factor) of 0.95, which accounts for the fact that the stress level in the central square is less than the one applied at the clamps, because part of the load is absorbed by the arms (Bridgens, 2005; Bridgens et al., 2004a; Galliot & Luchsinger, 2009).

On the other hand, the engineering strain has been computed by the relation $\varepsilon = \Delta L/L_0 = (L - L_0)/L_0$, where L_0 and L are the initial and final lectures of the extensometers. To permit the comparison between the stress-strain curves associated to different load ratios, the residual strain at the end of each group of preconditioning cycles has been removed from the test data of the subsequent loading cycle.

The stress-strain behaviours of a PVC/polyester fabric (test F702 MSAJ) and of a PTFE/glass fabric (B18089 MSAJ) for different fixed load ratios are shown in Figure 4.31 and Figure 4.32, respectively. The characteristics of the two typologies are different, but they both show high nonlinearity and anisotropy. The key features of the fabric response are (Bridgens et al., 2004a):

- sudden changes in gradient;
- multiple values of stress for a given strain;
- negative strains, even when tensile loads are applied.

Initial large strains at low stresses are due to the crimp interchange and to the initial slackness of the yarns. Then, an increase of the tensile stiffness occurs when the crimp interchange is complete and the yarn stretching becomes the dominant deformation mechanism. This behaviour is more evident in the PTFE coated glass fabrics (Figure 4.32), because glass yarns are initially more crimped than polyester yarns (see Figure 4.33): this expedient is employed by the coated fabric producers to make the glass fabrics appear more stretchable, otherwise they would break at very low strains.

Another important characteristic that is highlighted by Figures 4.31 and 4.32 is that the material response is hysteretic. Due to the coating and fibre properties and to the frictional effects between yarns, the unloading stress-strain curves follow a different path with respect to the loading ones, which results in residual strains at the end of each cycle.

Lower values of residual strain are recorded, if the preconditioning cycles are performed before. A comparison between the experimental results

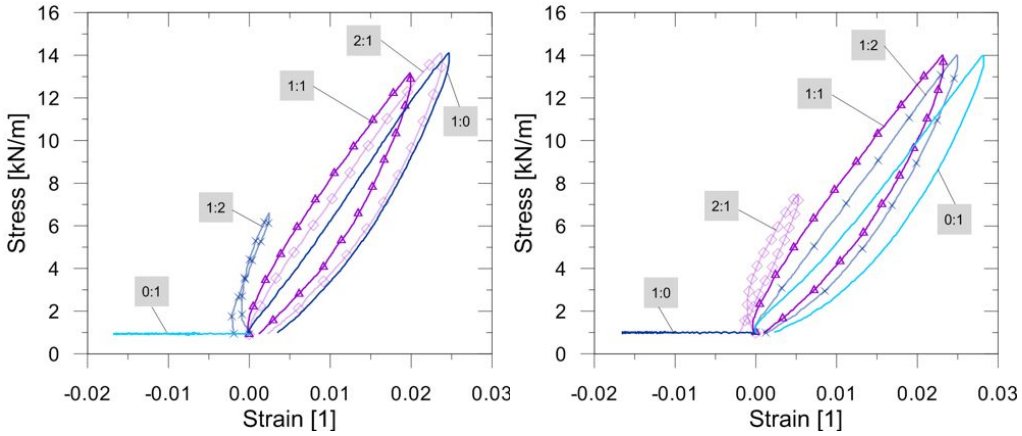

(a) Warp (b) Fill

Figure 4.31: *Stress-strain curves of a PVC/PES fabric for different warp to fill load ratios (test F702 MSAJ).*

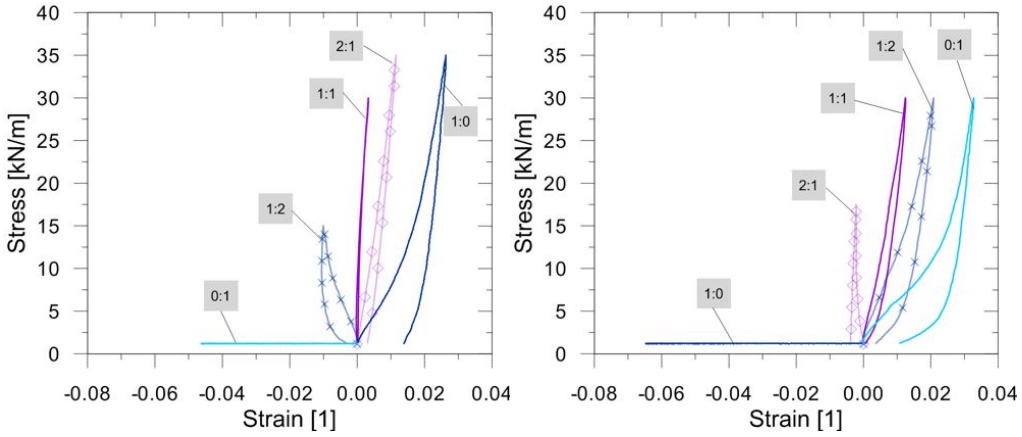

(a) Warp (b) Fill

Figure 4.32: *Stress-strain curves of a PTFE/glass fabric for different warp to fill load ratios (test B18089 MSAJ).*

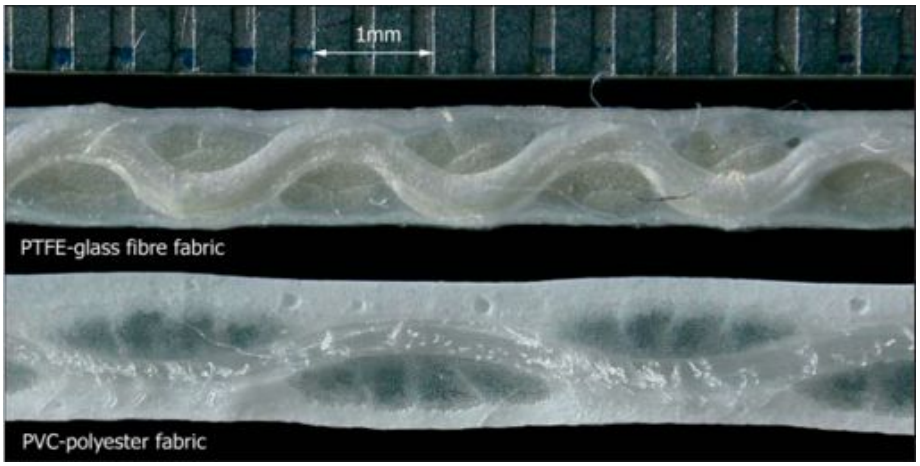

Figure 4.33: *Cross section of a PTFE/glass and a PVC/polyester virgin fabrics: glass yarns show a more severe crimp. (from Bridgens et al., 2004a).*

obtained from tests VUB 001 A (Figure 4.34) and F702 MSAJ (Figure 4.31) may clarify this point. Both the tests have been performed on a PVC/PES fabric, but the hysteretic behaviour recorded in Figure 4.34 seems to be extremely emphasized, if compared to the one in Figure 4.31. The reason is in the absence of preconditioning cycles, which have been eliminated from the loading profile of test VUB 001 A.

Moreover, preconditioning is employed to make the fabric response repeatable. Again with reference to tests VUB 001 A and F702 MSAJ, Figure 4.35 shows a plot of the warp and weft stress-strain curves for three repeated cycles at load ratio 1:1. More in detail, these curves have been constructed using the test data from cycles 1-3 in Figure A.1(a) for test VUB 001 A, and from cycles 4-6 in Figure A.2(a) for test F702 MSAJ. It is evident that the preconditioning guarantees the repeatability of the stress-strain behaviour, as demonstrated by the low values of residual strain measured in Figure 4.35(a). This condition is obtained through an internal arrangement of the yarns, which reach an equilibrated state of crimp after the preconditioning cycles. In addition, Figure 4.35(b) displays the large discrepancy between the first and the subsequent loading behaviours, typical of coated fabrics.

Like tests F702 MSAJ and B18089 MSAJ, tests F1202T2 ALR and B18059 ALR have been performed on a PVC/PES and a PTFE/glass fa-

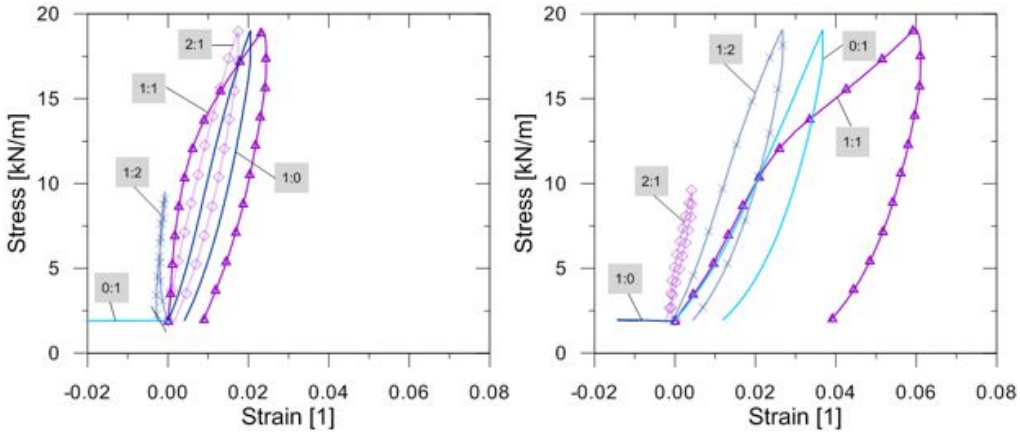

(a) Warp (b) Fill

Figure 4.34: *Stress-strain curves of a PVC/PES fabric for different warp to fill load ratios, obtained without preconditioning (test VUB 001 A).*

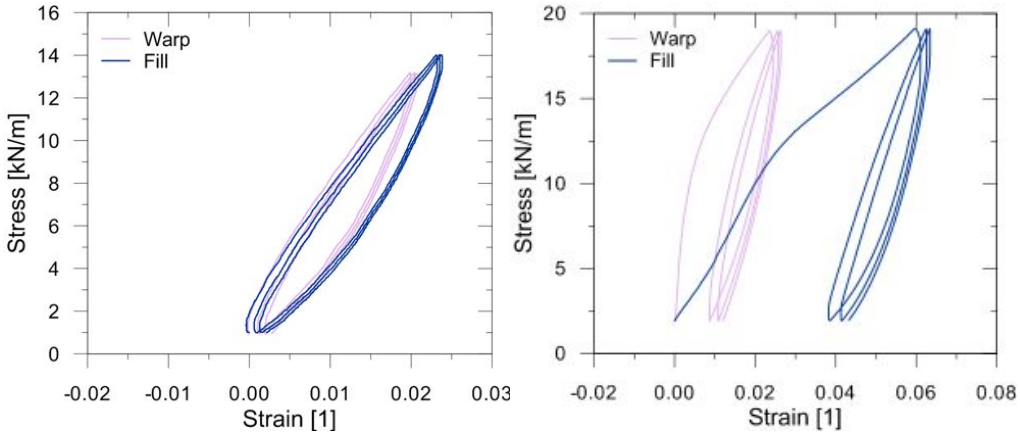

(a) With preconditioning (b) Without preconditioning

Figure 4.35: *Warp and fill stress-strain curves of a PVC/PES fabric for three repeated cycles at 1:1 load ratio, obtained with and without preconditioning (tests F702 MSAJ and VUB 001 A, respectively).*

bric, respectively. Their load profile has been constructed according to the MSAJ/M-02:1995 Standard, but four additional load ratios (0.3:1, 1:0.3, 0.7:1, 1:0.7), which are intermediate between the ones in Table 4.10, have been added. In Figures 4.36 and 4.37 are reported the stress-strain curves associated with the traditional five load ratios in Table 4.10: the same observations made for Figures 4.31 and 4.32 are still valid.

Figures 4.38 and 4.39 depict the mechanical behaviour of the same fabrics for the additional stress ratios. As expected, the obtained stress-strain curves are intermediate between the ones associated with the traditional five load ratios (reported in gray in the graphics). This supplementary information about the fabric behaviour will be useful to validate the predictive capability of the new model presented in Section 6.4.

Finally, Figures 4.40 to 4.45 illustrate the stress-strain curves of four types of PU coated polyester fabrics, which have been named material A, B, C and D. The behaviour of these materials is qualitatively similar to the one of PVC coated polyester fabrics. In materials A and B, the energy dissipated because of internal friction is higher than for PVC coating, as shown by the larger area of the hysteresis loops in Figures 4.40 and 4.41. All the tested PU/PES woven fabrics present strains after unloading that are greater that the ones of PVC/PES fabrics, which means that PU offers a weaker resistance to crimp interchange thanks to its higher compliance. In conclusion, PU coated polyester fabrics could be employed in place of PVC/PES in applications where it is required that the membrane could be stretched by applying low tension forces, for instance in tents.

4.2.4 Strain-controlled biaxial tests

As previously commented, the testing procedure for biaxial tests is currently described by few national Standards, namely MSAJ/M-02:1995 and ASCE55-10, and, due to the absence of a widely recognised procedure, laboratories and engineers have developed their own internal protocols. The procedures are generally based on stress profiles, which reproduce the level of prestress assumed in the design phase and/or the expected stress due to the external loads, such as wind and snow.

In addition, some procedures prescribe a predetermined displacement rate (see, e.g., MSAJ/M-02:1995), like it is commonly required for uniaxial displacement driven tests. However, due to the cruciform shape, the speed

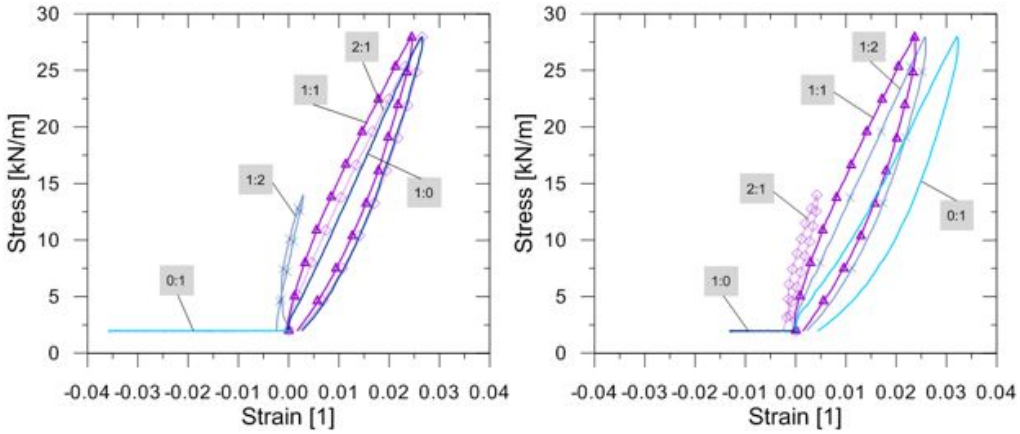

(a) Warp (b) Fill

Figure 4.36: *Stress-strain curves of a PVC/PES fabric for different warp to fill load ratios (test F1202T2 ALR).*

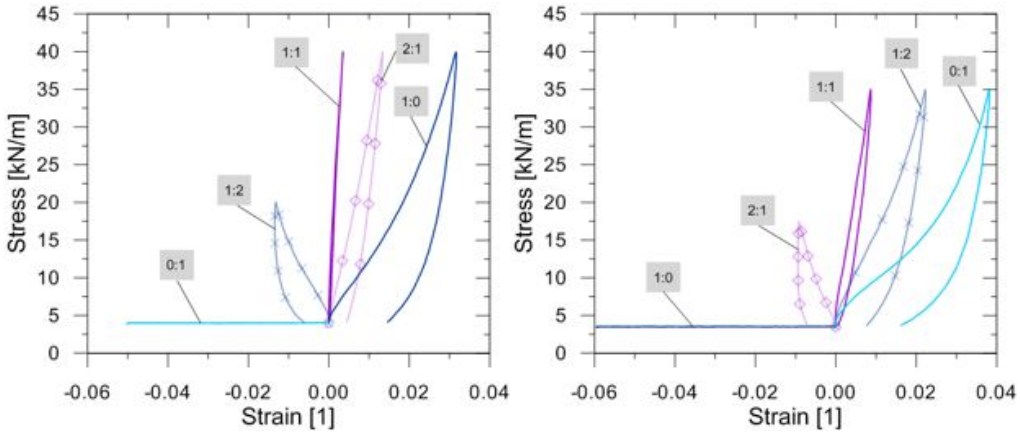

(a) Warp (b) Fill

Figure 4.37: *Stress-strain curves of a PTFE/glass fabric for different warp to fill load ratios (test B18059 ALR).*

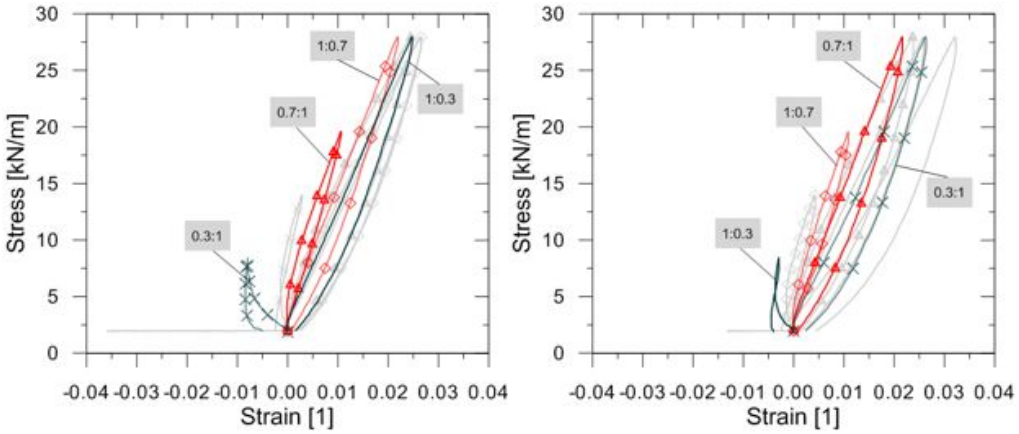

(a) Warp (b) Fill

Figure 4.38: *Stress-strain curves of a PVC/PES fabric for some warp to fill load ratios additional to the ones in Figure 4.36, which are here reported in gray (test F1202T2 ALR).*

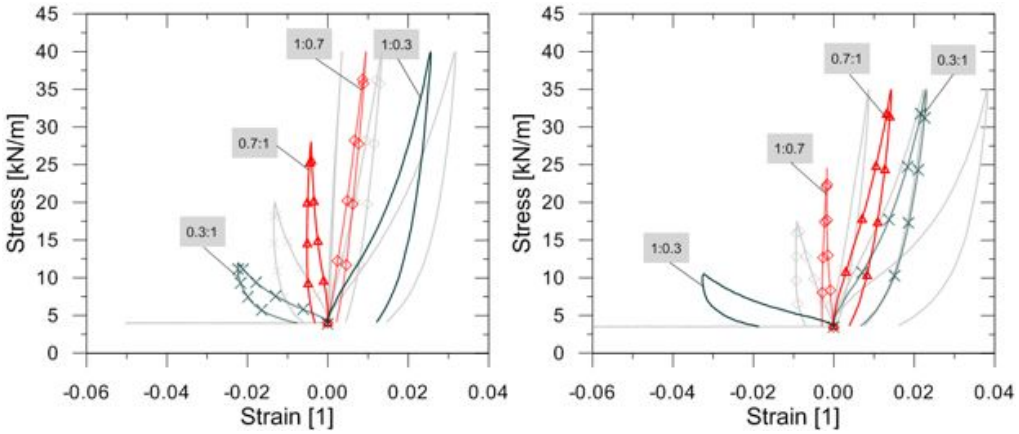

(a) Warp (b) Fill

Figure 4.39: *Stress-strain curves of a PTFE/glass fabric for some warp to fill load ratios additional to the ones in Figure 4.37, which are here reported in gray (test B18059 ALR).*

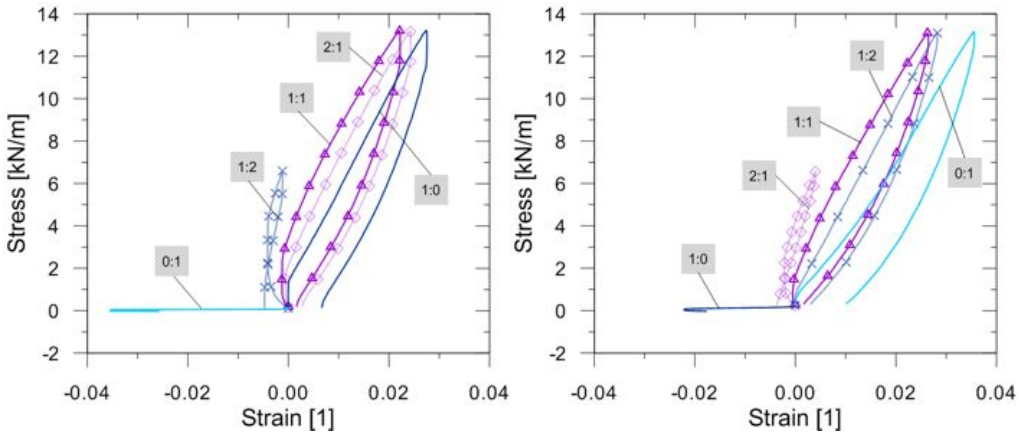

(a) Warp (b) Fill

Figure 4.40: *Stress-strain curves of a PU/PES fabric (material A) for different warp to fill load ratios (test NTT 011 1 BX).*

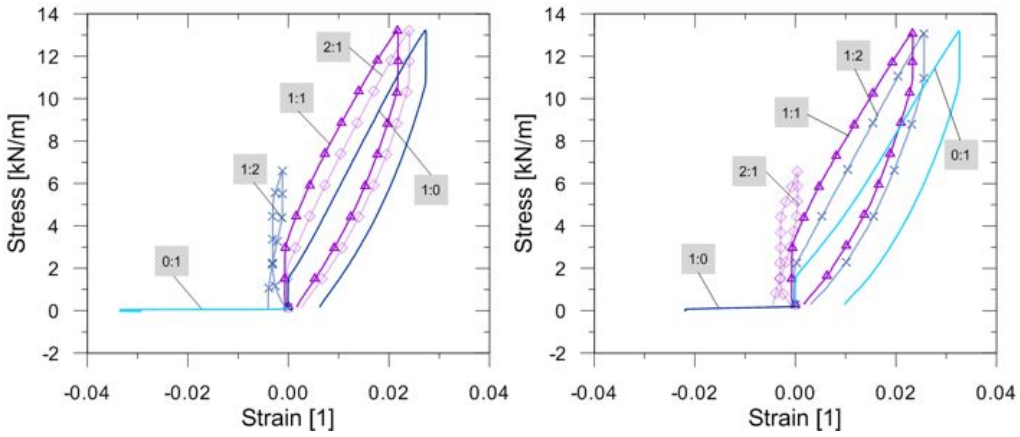

(a) Warp (b) Fill

Figure 4.41: *Stress-strain curves of a PU/PES fabric (material B) for different warp to fill load ratios (test NTT 010 2 BX).*

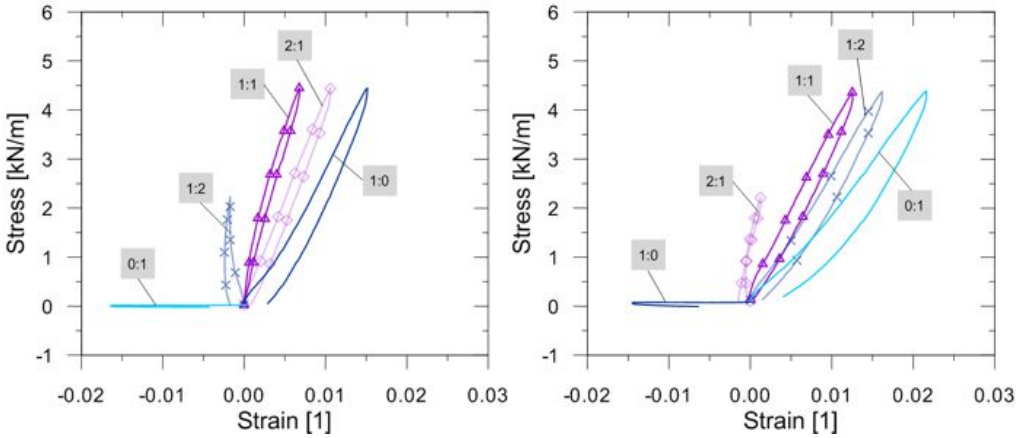

(a) Warp (b) Fill

Figure 4.42: *Stress-strain curves of a PU/PES fabric (material C) for different warp to fill load ratios (test NTT 001 A BX).*

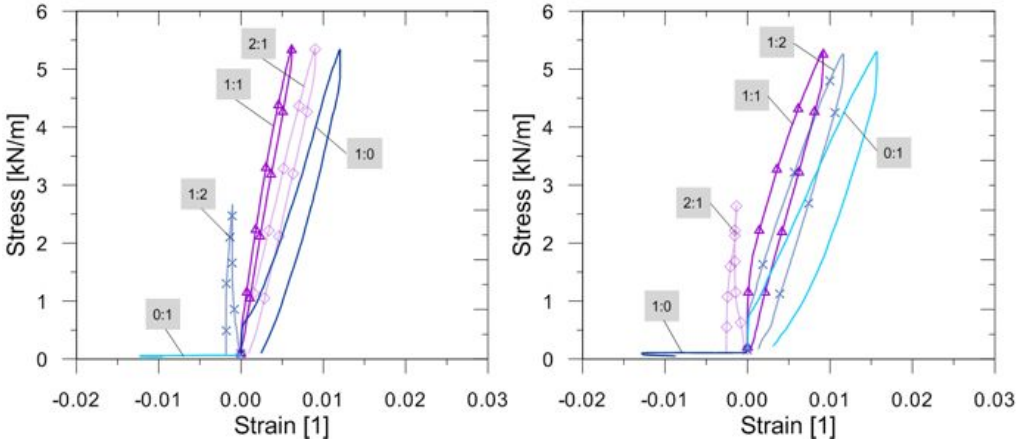

(a) Warp (b) Fill

Figure 4.43: *Stress-strain curves of a PU/PES fabric (material C) for different warp to fill load ratios (test NTT 002 A BX).*

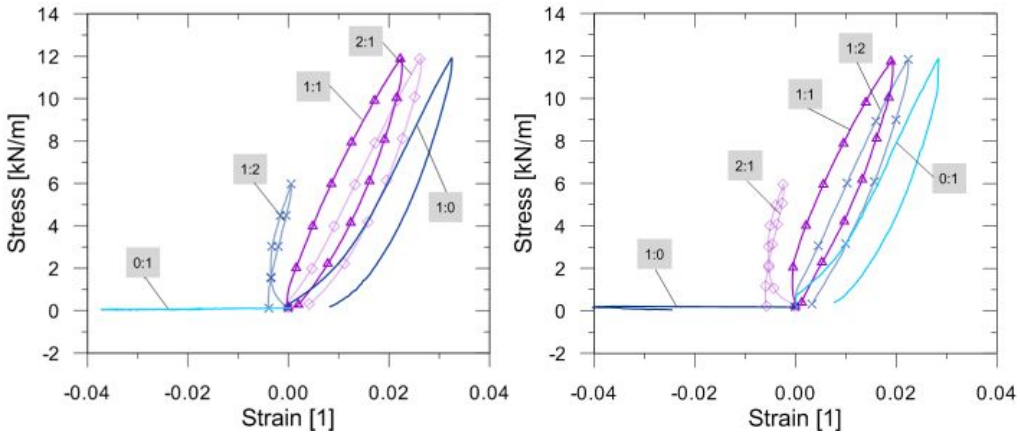

(a) Warp (b) Fill

Figure 4.44: *Stress-strain curves of a PU/PES fabric (material D) for different warp to fill load ratios (test NTT 001 B BX).*

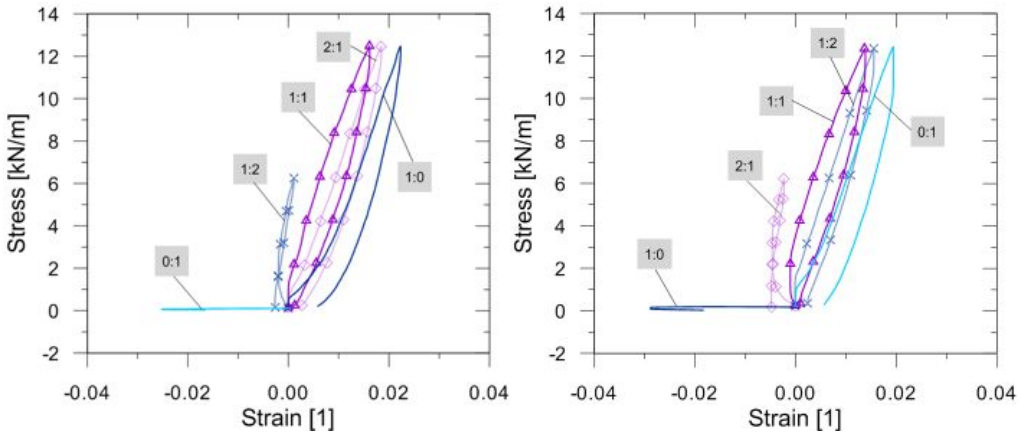

(a) Warp (b) Fill

Figure 4.45: *Stress-strain curves of a PU/PES fabric (material D) for different warp to fill load ratios (test NTT 002 B BX).*

of the actuators is not directly related to the strain rate in the centre of the sample. The displacements that occur at the clamps are mainly absorbed by the arms of the specimen, with potential discordant strain between the centre and the arms.

The tests illustrated in this Section represent an innovative contribution to the field of biaxial testing, which has been presented at the Tensinet Symposium 2013 (Beccarelli et al., 2013). The novelty is in the type of control: these are biaxial tests in which the strain histories in a central portion of the specimen are prescribed. This approach has the advantage that the "loads" are applied directly on the portion of the cruciform sample that is of interest for the measurements, because there the stress and strain fields may be considered homogeneous. Moreover, the results obtained by such new experimental procedure can provide further insight into the mechanical behaviour of coated fabrics and can give valuable information in connection with membrane installation processes. For example, the knowledge of the stress level achieved in a membrane when it is stretched by following specific strain paths, is certainly of interest for both installation and load analyses.

Focusing on the installation process, accurate knowledge of the material properties is needed to estimate how much smaller the unstressed textile panels must be with respect to their final dimensions, in order to obtain the desired prestress. Indeed, as previously discussed in Chapter 2, prestress in tensile structures is essential to ensure that the membrane, which can carry load only by means of tensile stress, remains in tension under all loading conditions, and to reduce deflections. In the current practise, biaxial stress-controlled testing of samples from each roll of fabrics are carried out at prestress loading to determine the percentage length reduction (compensation factors, see Section 2.2) required in warp and fill direction at installation (Bridgens et al., 2004b).

A simple case of installation of a flat membrane that must be fixed to a rectangular rigid frame has been considered here (Figure 4.46). First, the coated fabric is stretched along one of the material directions (warp or fill) and fixed to the rigid support. Then, the membrane is stretched parallel to the other weaving direction and fixed to the boundary frame. Therefore, two different loading paths have been utilised: in tests of type A (TEN 008 A and TEN 015 A in Table 4.9) the direction that is stretched first is warp, in tests of type B (TEN 018 A and TEN 019 A in Table 4.9)

is fill.

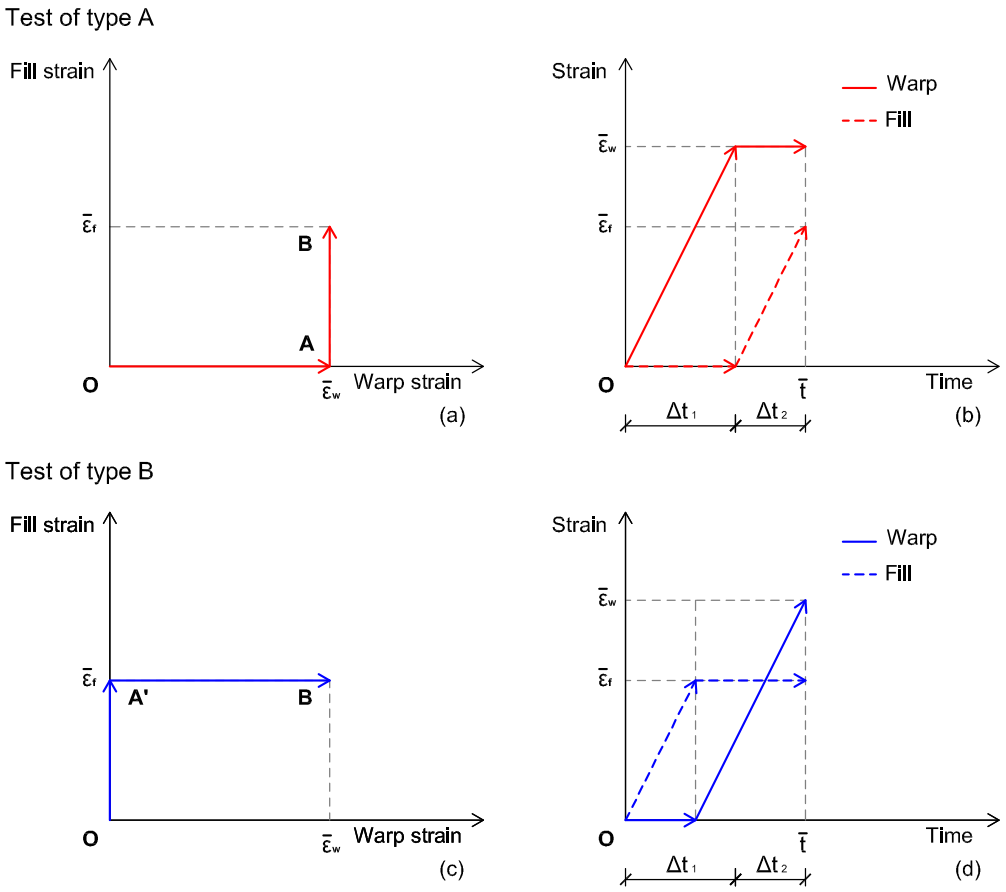

Figure 4.46: *Imposed strain-paths (a,c) and histories (b,d) for tests of type A and B.*

A preliminary stress-controlled biaxial test (TEN 001 A in Table 4.8) has been performed up to an established prestress level to estimate the compensation factors. A value of 2 kN/m, which is equal to 2.5 % of the UTS in the weakest direction of the tested material, has been employed as feasible value of prestress, according to the current design rules (see Forster & Mollaert, 2004, p. 192-193). As shown in Figure A.12(a-b), the cruciform sample has been loaded with five cycles from 0.1 kN/m to 2 kN/m at a constant rate (0.1 kN/s) and using a load ratio of 1:1 between warp and fill

direction. The resulting strain histories are plotted in Figure A.12(c): the maximum values of warp and fill strains turned out to be equal to 0.33 % and 0.21 %, respectively. It can be noticed that these values remain almost constant for repeated load cycles. They have been employed as final values of strain to be imposed during installation to the ideal initially unstressed membrane panel (compensation factors).

In the strain-controlled tests (Table 4.9), a strain rate of 0.001 % per second has been adopted in both warp and fill directions, which implies that the final strain state ($\bar{\varepsilon}_w = 0.33\,\%$, $\bar{\varepsilon}_f = 0.21\,\%$) is reached at time $\bar{t} = 540\,\mathrm{s}$. The actual strain profiles adopted in the experiments have been extended in time beyond $\bar{t} = 540\,\mathrm{s}$, by enforcing five cycles in order to investigate the gradual stabilisation of the material behaviour (see Figures A.13 and A.16). As previously stated, the strain histories employed for tests of type A (TEN 008 A and TEN 015 A) and B (TEN 018 A and TEN 019 A) differentiate themselves thanks to the first loaded direction, which is warp for type A (Figure A.13(a) and Figure A.14(a)) and fill for type B (Figure A.15(a) and Figure A.16(a)).

For each test, deformations in the central part of the specimen and forces at the clamps have been measured with a frequency of 2 Hz. The recording began immediately after the initial tensioning of the membrane at a very low stress level (0.2 kN/m), which is necessary to make the sample tight and to enable the extensometers to measure the deformation correctly.

The employed testing procedure requires a dedicated feedback control system: the strains measured by the extensometers are compared (in real time) to the assigned, programmed values and the loading system automatically adjusts to minimise the discrepancy. This type of control is integrated in the biaxial machine belonging to the Research Cluster on "Innovative Textiles" (ClusTEX), at Politecnico di Milano. At present, it represents a *unicum* among the facilities offered by the existing European biaxial testing rigs.

The mentioned control system is based on the following strategy: the strain to be imposed along each of the material directions drives the displacements at the clamps of the two specimen arms aligned with the direction in point. This avoids the ambiguity linked to the fact that the strain in one direction may be changed by means of a stretch applied in either the same or the transversal direction (because of the Poisson's effect).

Finally, the three clamps at the end of each arm have been made to

have the same displacement. This implies that the corresponding forces are slightly different; however, the effect on the stress distribution in the central area of the specimen (where the strain are measured) is negligible.

Discussion on strain-controlled test results

Although it is common practice (Bridgens et al., 2004a; Galliot & Luchsinger, 2009) to apply a reduction coefficient to the applied stresses at the ends of the arms in order to obtain the ones in the central area, this approach has not been adopted for the strain-controlled biaxial tests here presented. In the following results, stresses are evaluated from the measured forces at the clamps, without any reduction. The approximation implied in this choice is comparable to other uncertainties inherent in the adopted testing procedure.

As previously illustrated, two kinds of tests, labelled A and B, have been performed: in tests of type A (B) the specimen is first stretched in the warp (fill) direction, while keeping a null value of the fill (warp) strain; then, the fill (warp) direction is stretched, while keeping constant the warp (fill) strain. Two tests of type A (TEN 008 A and TEN 015 A) and two of type B (TEN 018 A and TEN 019 A) have been carried out, as outlined in Table 4.9.

The obtained stress responses are shown in Figures A.13(c) to A.16(c). Both kinds of test show a behaviour that is qualitatively the same in each cycle, with maximum stress values that remain almost constant. The strain-controlled linear loading in warp (fill) direction induces a nearly linear increment of the stresses. Moreover, it can be noticed that the change of loading direction determines a modification of the stress curves slopes: the change in slope is evident also during unloading, and it is more marked in the fill direction.

By comparing tests of the same type, namely Figure A.13(c) to Figure A.14(c) and Figure A.15(c) to Figure A.16(c), it may be noticed that the obtained results in term of stresses are more variable along the fill direction, especially during the first loading. In addition, this variability between the measured stresses of different specimens is larger for tests of type A. This unevenness of the results is due to the fabric weaving, characterised by a greater crimp in the weft direction. Indeed, when the fill yarns are stretched first (test of type B), the stress response is less vari-

able, thanks to the crimp interchange, which reduces the level of crimp of the weft yarns. The highlighted phenomenon might be even more marked for coated fabrics that are manufactured using the Précontraint® technology (that consists in applying the coating under tension, thus reducing the differences between the behaviour along the principal material directions).

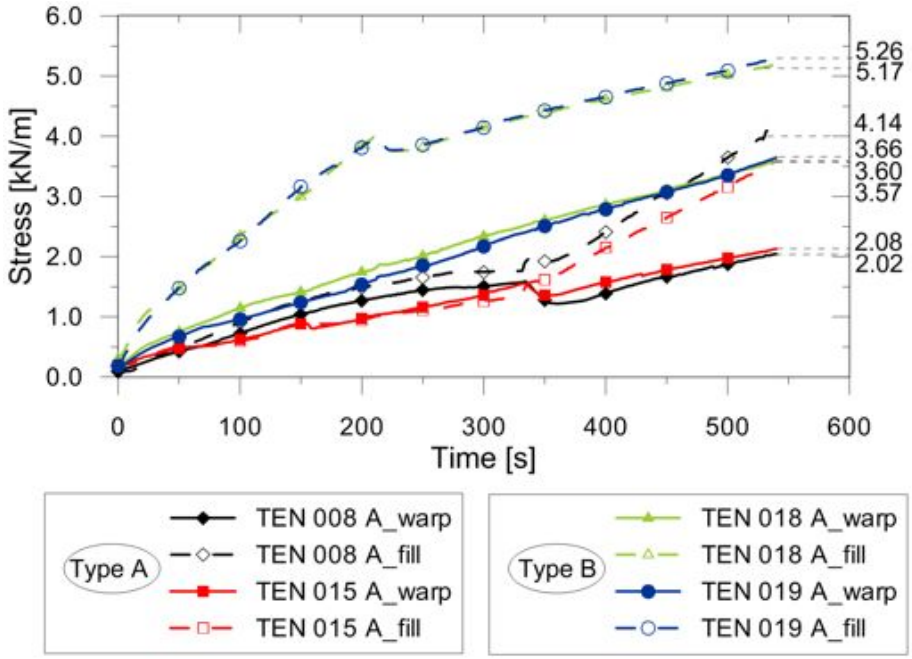

Figure 4.47: *Warp and fill stress histories at first loading of a PVC/PES fabric subjected to strain controlled biaxial tests of type A and B.*

Figure 4.47 shows the stress responses at first loading, i.e. until time $\bar{t} = 540\,\mathrm{s}$. This time interval is the one corresponding to the installation process, which starts loading the fabric from its virgin state. Experimental results indicate that higher stresses are required to achieve the prescribed strains if the fill direction is stretched first (test of type B). In fact, a maximum warp stress of $2.02\,\mathrm{kN/m}$ and $2.08\,\mathrm{kN/m}$ and a maximum fill stress of $4.14\,\mathrm{kN/m}$ and $3.57\,\mathrm{kN/m}$ have been recorded in tests TEN 008 A and TEN 015 A; on the other hand, a maximum warp stress of $3.60\,\mathrm{kN/m}$ and $3.66\,\mathrm{kN/m}$ and a maximum fill stress of $5.17\,\mathrm{kN/m}$ and $5.26\,\mathrm{kN/m}$ have been recorded in tests TEN 018 A and TEN 019 A.

Furthermore, the stress ratio between the warp and weft directions is variable during the strain loading. The final value of such ratio represents the final state of prestress at the completion of the installation procedure, therefore the prestress value to be imposed in the structural analyses. It may be observed that the mean stress ratio required in order to achieve the prescribed maximum value of strain is:

- 0.54 in tests of type A ($2.02/4.14 = 0.49$ for test TEN 008 A and $2.08/3.57 = 0.58$ for test TEN 015 A);
- 0.7 in tests of type B ($3.06/5.17 = 0.70$ for test TEN 018 A and $3.66/5.26 = 0.70$ for test TEN 019 A).

Therefore, none of the type of tests considered has induced a balanced prestress (load ratio of 1:1), which is usually the most suitable condition for a membrane, because it is the closest to a minimal surface obtained with a soap bubble (Otto et al., 1973; Gosling, 1992).

Anyway, if the fill direction is stretched first (tests of type B), the final load ratio is higher, which would suggest to employ this sequence for the installation. However, other factors should be considered in addition, to determine the optimal sequence of tensioning to be used in the erection (Seidel, 2009): for instance, how large are the forces required in warp and weft direction. According to Seidel (2009), to determine the primary tensioning direction, it should be considered how large the force necessary to pull the tensioning travel is and how much the associated erection cost is.

Finally, Figures 4.48 and 4.49 display the stress-strain curves resulting from the strain-controlled biaxial tests presented here. The first loading curves, in both warp and fill directions, have a slope that is slightly different from the one of the subsequent cycles: this is reasonable, since the crimp interchange in the material is not stabilised yet. However, one loading/unloading is sufficient to reach the stabilised condition for that specific stress level. Loading and unloading segments have the same slope, which confirms that the material can be treated as elastic in a certain stress/strain range, even if residual strains are show up at the end of the experiment.

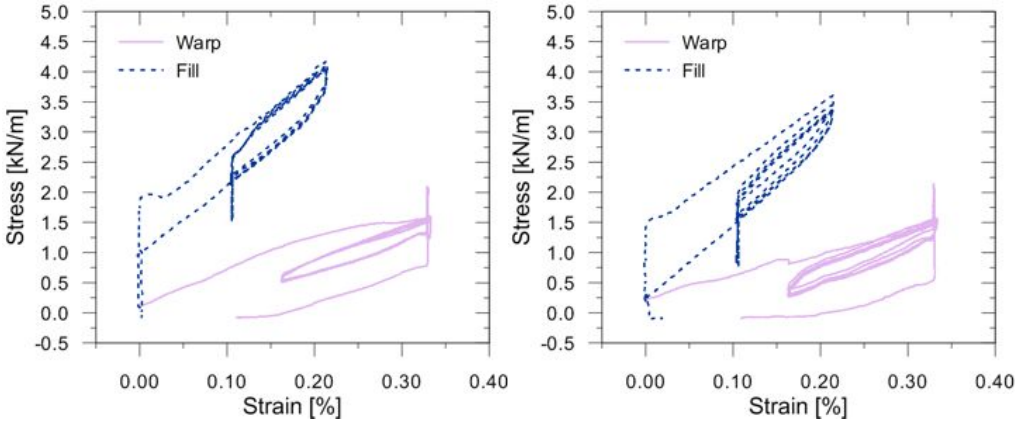

(a) TEN 008 A (b) TEN 015 A

Figure 4.48: *Stress-strain curves of a PVC/PES fabric from two strain-controlled biaxial tests of type A (TEN 008 A and TEN 015 A), where the warp direction is stretched first.*

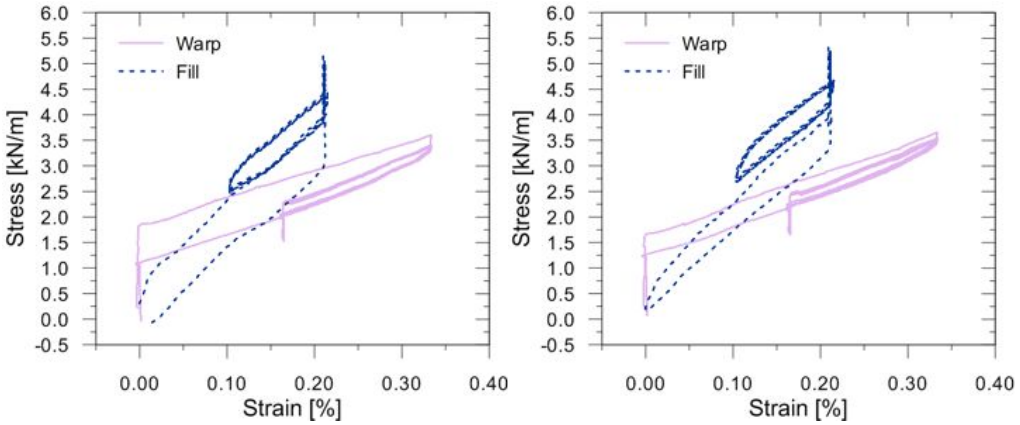

(a) TEN 018 A (b) TEN 019 A

Figure 4.49: *Stress-strain curves of a PVC/PES fabric from two strain-controlled biaxial tests of type B (TEN 018 A and TEN 019 A), where the fill direction is stretched first.*

page intentionally left blank

5

Constitutive models for coated fabrics

Coated fabrics are composite materials that belong to the category of fibre-reinforced materials. As described in Chapter 4, they display a quite complex mechanical behaviour, which is chiefly affected by the local weaving geometry. This makes the mechanical response of these membranes not only nonlinear, but highly dependent on the way the membrane is stretched. Considering the close relationship between the global mechanical response and the internal structure of fabrics, most of the available constitutive models are built starting at least from the meso-scale, which is a scale that is intermediate between the micro- (yarns) and the macro- (coated fabric) scales (Figure 5.1). Indeed, it is very difficult to capture the deformation mechanisms that are typical of coated and uncoated fabrics (e.g. the crimp interchange effect) without considering the interaction between the threads.

Although coated woven fabrics shall be considered as very complex materials, since they show high degree of anisotropy and nonlinearity, only simple material models are often used to represent their mechanical behaviour in relevant numerical simulations. This is mainly due to the fact that existing nonlinear models for fabrics require a large computational time or, in some cases, expensive experimental tests. The mechanical behaviour of raw and coated fabrics has been modelled with different approaches, which can be grouped into two main categories:

- *Mesostructural models*: based on the fabric structure, they emphasize the influence of local wave geometry and mechanisms on the global behaviour. Almost always, they turn out prohibitively computationally expensive, if used for the analysis of large membrane structures.

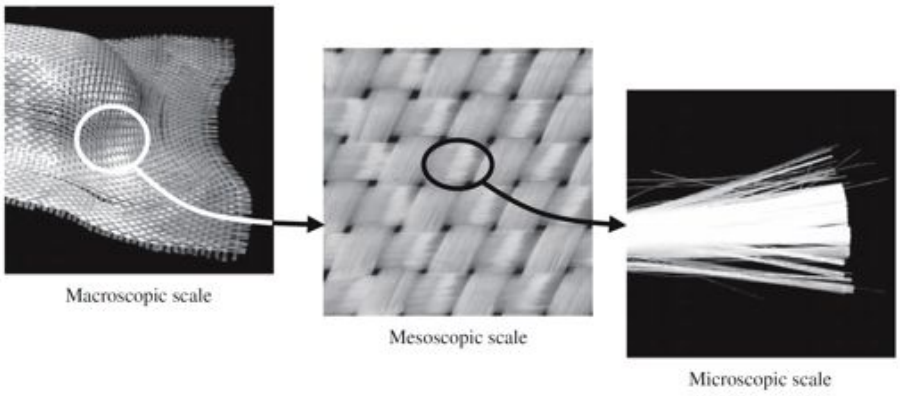

Figure 5.1: *The three scales of a reinforced composite (from Charmetant et al., 2011).*

- *Continuum models*: they treat fabrics as a continuum, usually by deriving a strain-energy function or a potential energy function from the underlying mesostructure, or sometimes using homogenization techniques. In the current engineering design practice orthotropic linear elastic models under the plane stress assumption are widely used for the computational analysis of membrane structures: these do not require large computational time, but need a lot of test data to be calibrated and some of them are too rough to satisfactorily describe the complex behaviour of coated fabrics.

The following subsections describe the main mechanical models developed for coated and uncoated fabrics, divided into the two categories outlined above. In addition, the Orthotropic Linear Elastic (OLE) model with the plane stress assumption, which is the most widely used in the current design practice, is then calibrated using biaxial test data on PVC/polyester and PTFE/glass fabrics from Section 4.2. The identification of OLE model parameters is conducted using least squares. The solutions found by means of both classical differential approach and pattern search method are then compared. Such a calibration highlights the already known limits of using OLE model for coated fabrics, and provides results that are useful for comparison purposes, with respect to the new constitutive model that is presented in the next chapter.

5.1 Mesostructural models

Mesostructural models are based on the description of the fabric mesostructure. They describe the behaviour of a unit cell[1], which should be representative of the whole membrane. If calibrated through experimental test data, these kind of models are usually able to satisfactorily represent the mechanical behaviour of coated woven fabrics. Nevertheless, they require a computational effort which looks too large for their engineering application. In addition, all these models are too much strictly related to particular geometries and loading conditions and their extension to account for more general conditions would probably lead to extreme complications.

The model developed by Peirce (1937) is usually cited as the first mathematical treatment of the mechanical behaviour of fabrics. It provides a mathematical description of the fabric geometry, where yarns are supposed to display two-dimensional trajectories and circular transverse cross sections (Figure 5.2). Yarns are considered as elastic, axially rigid and without bending capacity. Although Peirce's assumptions oversimplify the true fabric response, his model allows the crimp interchange effect to be studied.

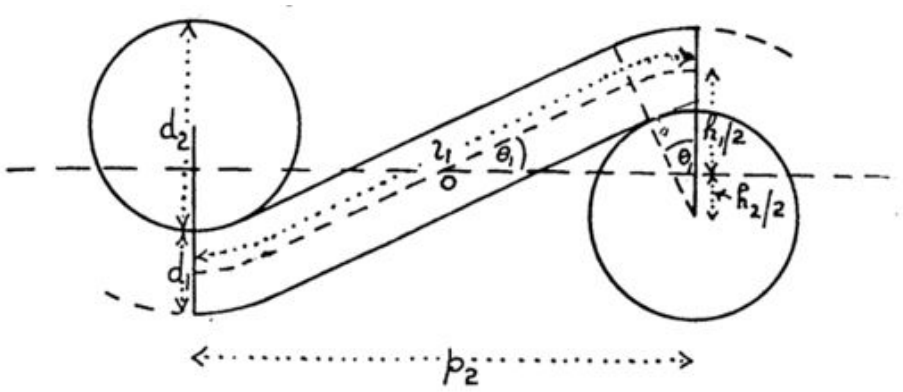

Figure 5.2: *Yarn geometry adopted by Peirce (from Peirce, 1937).*

Several researchers have developed models based on that by Peirce, introducing modifications to account for the nonlinear mechanical characteristics of fabrics. For instance, models that include yarn extension and

[1] The *unit cell* is the smallest repeated unit in the fabric. For plain woven fabrics it consists of two crossed yarns, of which half wavelength is considered.

bending are the ones by Olofsson (1964, 1966), Freeston et al. (1967), Testa et al. (1978), Huang (1979a,b) and Leaf & Anandjiwala (1985). Various forms of material inelasticity (resulting from yarn and coating viscoelasticity, plastic deformations and dissipative mechanisms) have been also considered by several authors (Freeston et al., 1967; Thomas & Stubbs, 1984; Kato et al., 1997, 1999; Pargana et al., 2007). Moreover, several nonlinear mechanical characteristics of fabrics, such as noncircular or deformable cross sections, different yarn waveforms (specifically polynomial), yarn extension and bending effects, have been incorporated into a Peirce's geometry-based model by Sagar et al. (2003). In Sagar et al. (2003) the deformed configuration of the fabric is then found by minimization of the potential energy.

Concerning the yarn cross section, it is known from direct observation that the hypothesis of being it circular is actually invalid. Peirce (1937) considers also the case of elliptic threads, but not in a rigorous manner: the same equations derived using circular yarns are employed and the diameter of the circular threads is merely replaced with the minor axis of the elliptic cross section. To reduce the errors due to approximation of the yarn geometry, alternative shapes for the yarn cross section have been proposed. For instance, Kemp (1958) makes use of a section that is rectangular with semi-circular ends, termed the racetrack section (Figure 5.3). Pargana et al. (2007) and Bridgens & Gosling (2008) employ a rhombus, which provides more accurate representation of the flat yarns used in architectural fabrics, as claimed by Bridgens (2005).

Another key aspect of the models derived from the one by Peirce (1937) is the yarn waveform. The yarn path is influenced by the way the contact between yarns is modelled, as a point or as a finite contact length (Peirce, 1937). A point contact combined with negligible bending stiffness gives rise to the family of the sawtooth models (Menges & Meffert, 1976; Stubbs & Fluss, 1980; Pargana et al., 2007; Bridgens & Gosling, 2008): this assumption enables the crimp interchange to be treated by the equilibrium of forces, but it results in lack of geometric consistency between the warp and fill yarns. The former type of contact is employed also by Wang (2002) and Bridgens & Gosling (2008), who propose a sinusoidal shape for the yarn path, in order to minimise the discrepancy between the actual and the modelled yarn lengths, thus capturing the crimp interchange more accurately. A finite contact length at yarn crossovers (Figure 5.4) is adopted by

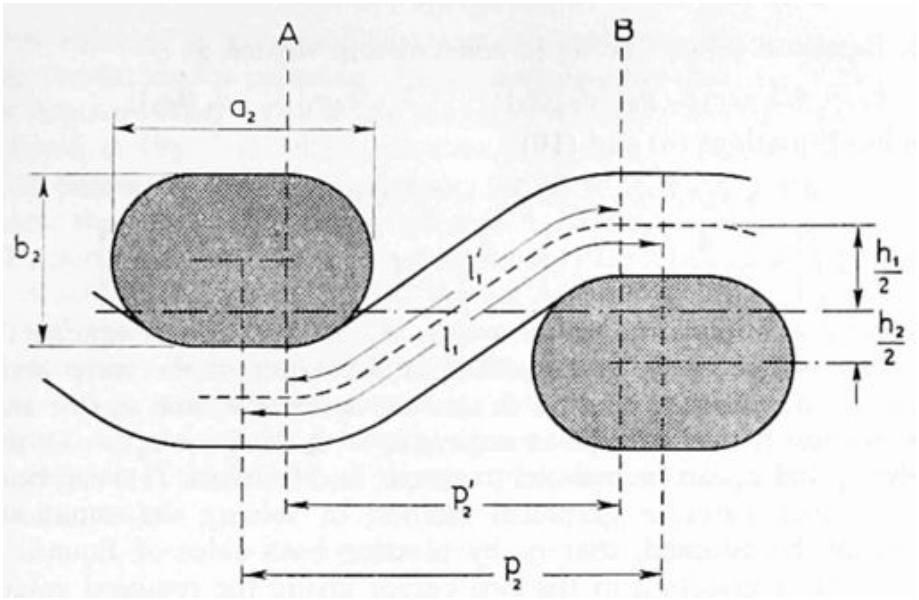

Figure 5.3: *Racetrack yarn cross section adopted by Kemp (from Kemp, 1958).*

Olofsson (1964, 1966), who developed a model with a yarn weave geometry that is not fixed a priori, but the result of the load application on the initial set (i.e. the configuration of the yarns in terms of crimp at the beginning of the loading). By employing finite contacts, the yarn weaveform fits the orthogonal yarn cross section throughout the contact length (Figure 5.5), so that the model can be considered geometrically consistent (Boisse et al., 2001; Hivet & Boisse, 2008; Wendling et al., 2014).

Since Pierce geometry is fairly detailed, other authors have proposed simpler models based on the representation of yarns through truss elements (sawtooth models). In Kawabata et al. (1973), for example, a simple pin-joined truss geometry is used to build a series of models able to describe biaxial, uniaxial and shear deformation of fabric membranes. The authors demonstrated that the compressibility of yarns has a great influence on the tensile properties of the fabric. They state that the yarn compressibility is related not only to the crushing force, but also to the applied tension; therefore, they model this coupled behaviour by assuming that the yarn crushing mechanism is a function that interpolates the yarn responses under the lowest and highest level of tension. Replacement of the smooth Peirce

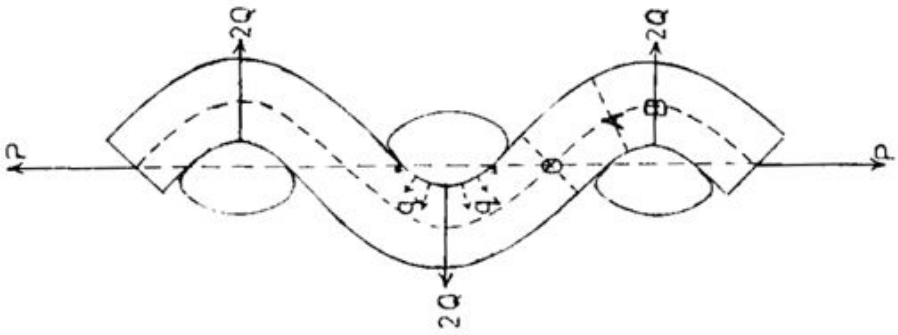

Figure 5.4: *Olofsson's fabric model with finite contact length (adapted from Olofsson, 1964).*

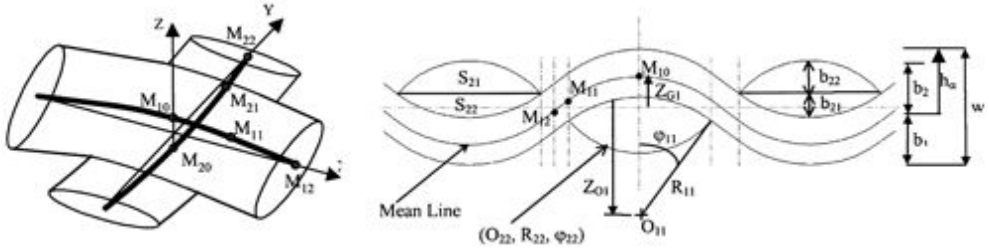

Figure 5.5: *Geometrically consistent fabric model by Boisse et al. (adapted from Boisse et al., 2001).*

geometry with a sawtooth profile simplifies the mathematical treatment and makes the model more efficient, but Kawabata's model does not look very accurate, probably because the crushing response modelling is too simple to capture the real material behaviour.

Another model that takes into account yarn crushing is presented in Kato et al. (1997, 1999). Short and long term behaviour of a PTFE coated glass fibre fabric are investigated through a nonlinear constitutive model that considers material viscosity. More in detail, the unit cell of the fabric is reproduced with a series of trusses (fabric lattice model, Figure 5.6), some of them representing the yarns (active only in tension) and some representing the coating (active both in tension and in compression). Each truss displays a viscoelastic mechanical behaviour: trilinear for the axial behaviour of yarns and bilinear for the crushing elements. It is shown that the model reproduces very well the experimental stress-strain curves, despite the fact that it neglects the effect of axial yarn tension upon yarn crushing. Some considerations on the long term relaxation are presented as well. The drawback of the fabric lattice model is that it needs measurements of the geometry and knowledge of the mechanical response of the fabric components, which are not easily obtainable. Moreover, if large structures are modelled, the large amount of elements makes the model computationally prohibitive.

Also in Pargana et al. (2007) the unit cell consists of a series of trusses (Figure 5.7). Three kinds of elements are considered to model the yarns (nonlinear elastic, frictional elements and rigid links), all having a nonlinear mechanical behaviour. An isotropic plate is then employed for the coating. The yarn crushing is modelled by Pargana et al. (2007) with nonlinear crushing elements located at the yarn crossover point, which cause the transverse cross section and the axial stiffness of the yarns to change. It is shown that this model appears able to faithfully represent the main deformation mechanisms of fabrics, namely crimp interchange, yarn extension and crushing, friction, coating deformation and shear.

Most of mesostructural fabric models do not account for the coating. The presence of the coating significantly influences the fabric behaviour, for example by enhancing the shear resistance, which is almost absent in uncoated fabrics. In addition, it reduces crimp interchange and slippage between yarns. As already stated, Pargana et al. (2007) model the coating as an isotropic linear elastic plate. Another approach consists in repre-

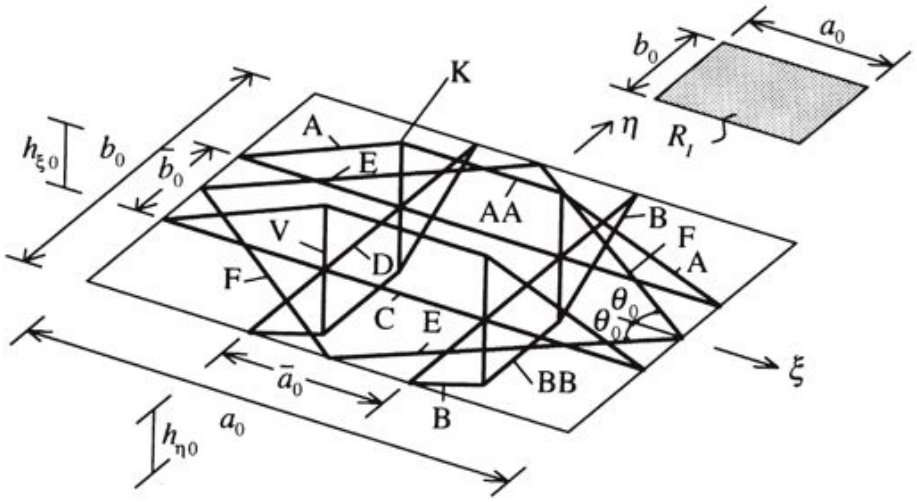

Figure 5.6: *Fabric lattice model by Kato et al. (from Kato et al., 1999).*

senting the coating by using springs (Figure 5.8) that are placed between crossovers (Menges & Meffert, 1976; Bridgens & Gosling, 2008).

Two simplified mesostructural models are presented in Bridgens & Gosling (2008). Both a sawtooth and a sinusoidal model are used to represent the fabric unit cell, while springs between crossovers represent the coating. One advantage of these models is that there is no need to know the yarn crushing stiffness, since a constant cross-sectional area is adopted. Despite the fact that the sinusoidal model represents the fabric geometry in a more realistic way than the sawtooth model, it does not provide results that display the same good correlation with test data. The authors claims that probably this is due to the fact that the sawtooth model compensates the absence of out-of-plane restraint provided by the coating with a shorter yarn length, which leads to underestimate the decrimping strains. They add that also the yarn bending stiffness, which is not considered in these models, may induce significant effects on the scale of the unit cell. Since the models presented in Bridgens & Gosling (2008) are not calibrated for a specific fabric, while they try to be truly predictive of the behaviour of PTFE-glass fibres and PVC-polyester fibres membranes in general, it is not surprising that they cannot reproduce the coated fabric behaviour exactly, because of the high degree of approximation. Improvements introducing the coating

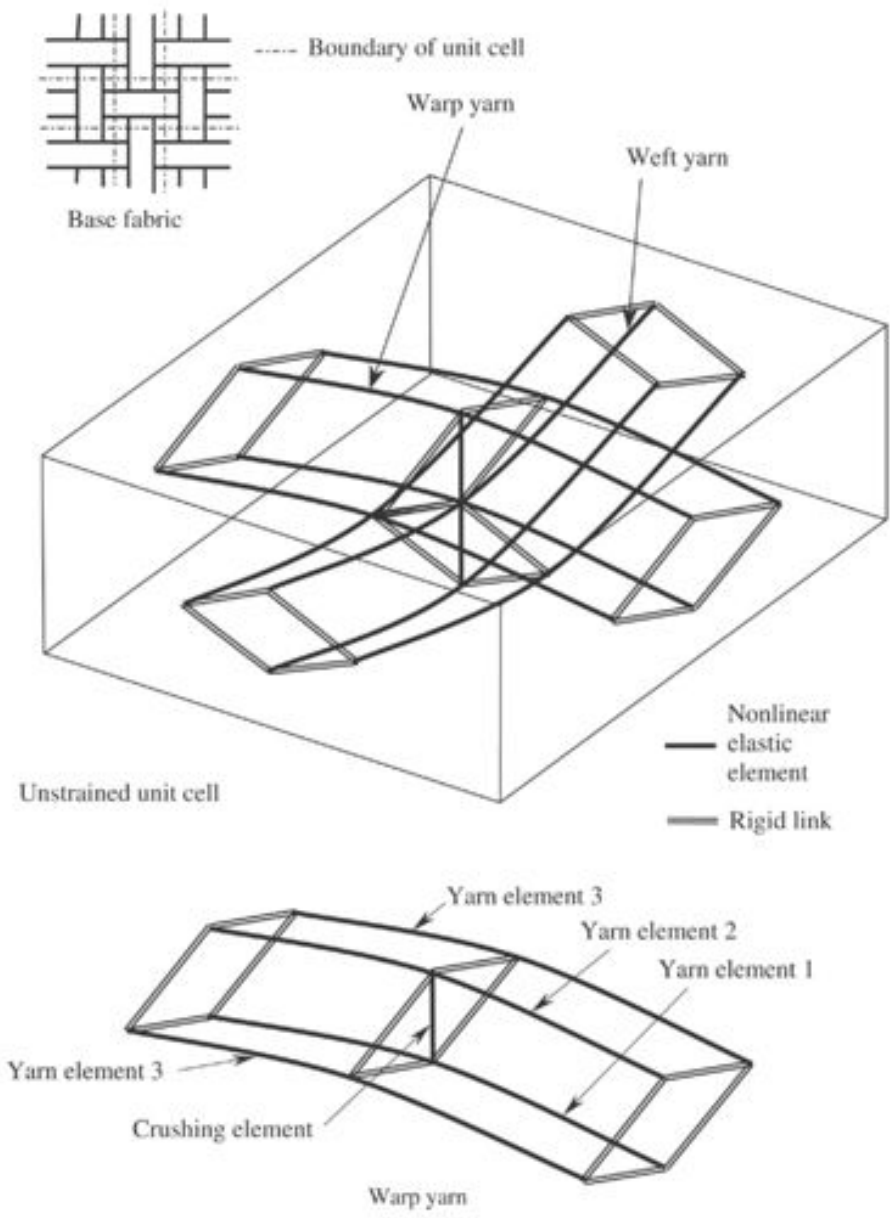

Figure 5.7: *Coated fabric model proposed by Pargana (from Pargana et al., 2007).*

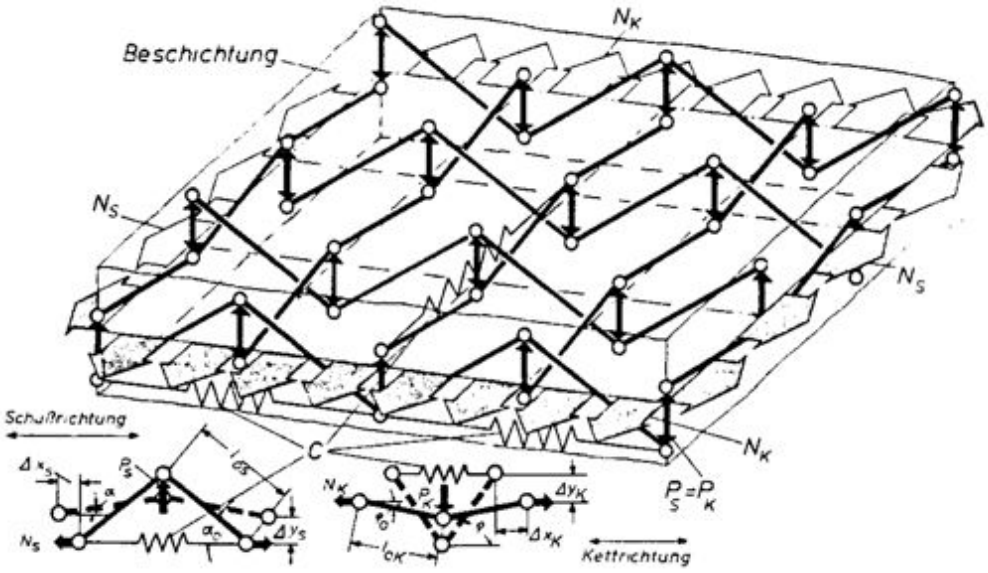

Figure 5.8: *Menges & Meffert's model with springs representing the coating (from Menges & Meffert, 1976).*

out-of plane restraint and the yarn bending may be useful to obtain results closer to the experimental data, but would inevitably complicate the model and might make it not useful for the large amount of tests needed for the parameter estimation.

Finally, the most recent application of mesostructural models for coated fabrics consists in the unit cell finite element modelling (Bigaud & Hamelin, 1997; Glaessgen et al., 1996; Gasser et al., 2000; Boisse et al., 2001; D'Amato, 2001; Tarfaoui et al., 2001; Tarfaoui & Akesbi, 2001; Zhu, 2003; Durville, 2008; Chen et al., 2011). Finite elements provide a powerful tool for modelling coated fabrics, because they allow for higher detail. Indeed, both the yarn geometry (Gasser et al., 2000; Boisse et al., 2001; Durville, 2008) and the contact between yarns (Tarfaoui et al., 2001; Tarfaoui & Akesbi, 2001) can be faithfully modelled. Moreover, it is possible to easily represent complex weaving patterns (D'Amato, 2001). The finite element approach can be used to explore and predict the mechanical behaviour of coated fabrics (Chen et al., 2011), without the need of expensive experimental testing; moreover, it represents a basic feature for the homogenisation techniques

described in the following section.

5.2 Continuum models

The pioneering works of Testa & Yu (1987) and Day (1986) represent a first attempt to model the complex mechanical behaviour of coated fabrics. In both articles, the shear and tensile responses are assumed to be uncoupled, because the stresses are defined in a coordinate system whose axes coincide with the principal material directions, namely warp and fill (or weft).

On the one hand, Testa & Yu (1987) suggest to additively split the strain into an elastic component (due to the fibre stretching) and an inelastic component (related to the crimp interchange). Elastic strains are derived from a complementary strain energy function in polynomial form: the use of the complementary energy is justified with the observation that it is more convenient to express strains as a function of stresses, since the stresses are varied independently in biaxial tests. An exponential evolution law for the calculation of the inelastic strains is then provided, which is based on the experimental evidence that crimp depends on the warp to fill load ratio and on the load level. Moreover, shear strains are assumed to be linearly dependent on the shear stresses by Testa & Yu (1987).

On the other hand, in the article by Day (1986) the mean stresses and strains $\sigma_a = (\sigma_w + \sigma_f)/2$ and $\varepsilon_a = (\varepsilon_w + \varepsilon_f)/2$ are related to stress and strain differences, namely $\tau = (\sigma_w - \sigma_f)/2$ and $\gamma = (\varepsilon_w - \varepsilon_f)/2$. As described by Bridgens & Gosling (2004), the biaxial tensile behaviour of coated woven fabrics is approximated by Day (1986) by the following equations:

$$\sigma_a = f^1(\varepsilon_a) + f^2(\gamma) \tag{5.1}$$

$$\tau = f^3(\varepsilon_a) + f^4(\gamma) \tag{5.2}$$

where f^1, f^2, f^3 and f^4 are four nonlinear functions, while shear stress and strain are related by an independent linear function f^5:

$$\sigma_{wf} = f^5(\varepsilon_{wf}) \tag{5.3}$$

The five functions f^1 to f^5 are determined by fitting experimental data, e.g. using polynomials or a linear interpolation between data points. In both articles by Day (1986) and Bridgens & Gosling (2004) it is demonstrated

that Day's model is able to fit well the experimental stress-strain curves for the load ratios employed in the definition of the five functions f^1 to f^5. Moreover, Bridgens & Gosling (2004) try to analyse the predictive capability of Day's model by considering additional load ratios: in the absence of test data, the response curves for these new load ratios are derived by linear interpolation. The comparison of these pseudo-experimental data with the response surfaces generated using the model shows that Day's equations give highly unpredictable results if load ratios other then the ones used in the calibration are considered. Anyway, further investigation with real experimental data is needed to asses the validity of the model proposed by Day (1986).

Despite that the works of Testa & Yu (1987) and of Day (1986) show that coated woven fabrics present a marked nonlinear behaviour, in the current design practice, the most widely used continuum material model for architectural membranes is the plane stress orthotropic linear elastic. The main reasons for that are its numerical efficiency and the fact that it employs parameters that are compatible with the available structural analysis software. Moreover, the lack of an extensive set of experimental data does not facilitate the constitutive modelling of coated fabrics, which requires further research. The fact that many articles (Blum, 2002; Forster & Mollaert, 2004; Bridgens & Gosling, 2004, 2010; Minami, 2006; Gosling, 2007) describe how to fit the compliance (or stiffness) matrix to the experimental data to obtain the material elastic constants confirms this design practice. Prescriptions about that are provided also in the American guidelines for tensile membrane structures (ASCE55-10) and in the Japanese guidelines for the evaluation of elastic constants of membrane materials (MSAJ/M-02:1995).

Besides the fact that an orthotropic linear elastic model cannot represent well the behaviour of a strongly anisotropic material, such as the one used for architectural fabrics, another tricky aspect of fitting orthotropic elastic models to experimental data on membranes is the symmetry of the compliance matrix. Unconstrained fitting provides four independent elastic parameters, i.e. two Young's moduli and two Poisson's ratios, which do not satisfy the reciprocity relationship $\nu_{fw}/E_w = \nu_{wf}/E_f$. It is possible to force the compliance matrix to be symmetric, but this operation causes loss of fitting accuracy, as demonstrated by Bridgens & Gosling (2010). However, Gosling (2007) argued that a compliance matrix not satisfying the reci-

procity constraint is admissible, considering that coated woven fabrics are not homogeneous, hence the obtained matrix coefficients may be regarded as arbitrary parameters that define a best fit plane, more than elastic constants with a mechanical meaning. Even if this approach provides a good correlation with experimental data on PTFE-glass and PVC-polyester fabrics, nonetheless the unconstrained identification of the elastic moduli can only be regarded as a fitting and not as a constitutive model.

As proposed by Minami (2006) and in the Japanese guidelines MSAJ/M-02:1995, it is possible to perform a multi-step linear approximation of the so-called response surfaces (see Figure 5.9). These are the surfaces that the biaxial test data, consisting in orthogonal stresses (σ_w, σ_f) and strains $(\varepsilon_w, \varepsilon_f)$, create in the stress-stress-strain coordinate systems $(\sigma_w - \sigma_f - \varepsilon_w$ and $\sigma_w - \sigma_f - \varepsilon_f)$. Their multi-step linear approximation is conducted dividing them into several quadrilaterals or triangles. In each area the material is assumed to be orthotropic linear elastic and subjected to a plane stress state; hence, four compliance matrix coefficients can be estimated within each zone. The main disadvantages of this method are the large computational time and the high amount of test data required to accurately describe the material behaviour. In addition to these drawbacks, the multi-step linear approximation provides snapshots of the coated fabric behaviour and is not suitable for computer analysis without interpolation.

In Galliot & Luchsinger (2009) a simple modification of the orthotropic linear elastic model is proposed to describe the biaxial tensile behaviour of PVC-coated polyester fabrics for an efficient use in finite element analysis. Since the stress-strain behaviour of the material varies depending on the load ratio between warp and fill directions, Young's moduli are expressed as linear functions of the normalized load ratios γ_w and γ_f, which are defined as follows:

$$\gamma_w = \frac{\sigma_w}{\sqrt{\sigma_w^2 + \sigma_f^2}} \ , \qquad \gamma_f = \frac{\sigma_f}{\sqrt{\sigma_w^2 + \sigma_f^2}} \tag{5.4}$$

The material model proposed by Galliot & Luchsinger (2009) has been implemented in the finite element software ANSYS and a comparison of the results with the classical linear orthotropic response shows that the new model can better predict the mechanical behaviour of PVC-coated fabrics, especially in the case of load ratios different from 1:1. Due to its simplicity and efficiency, the model is particularly adequate for its use in

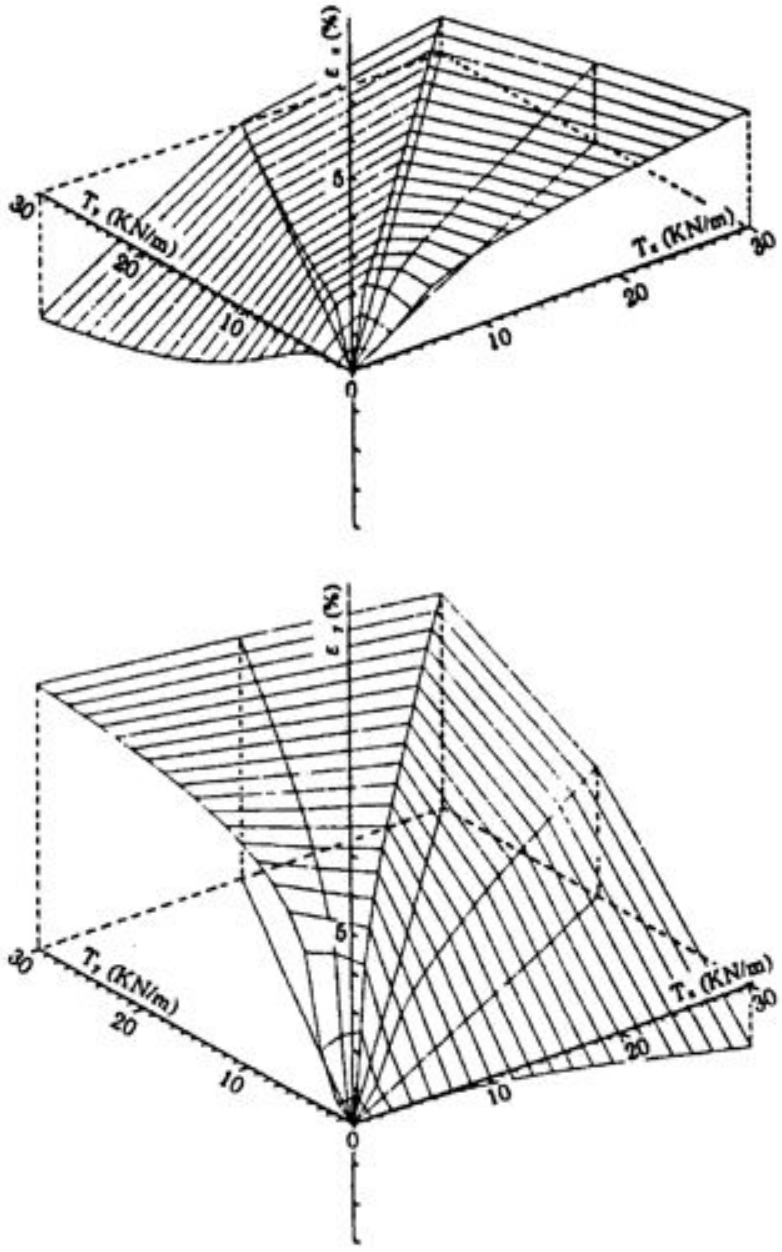

Figure 5.9: *Biaxial stress-stress-strain response surfaces (from Minami, 2006).*

finite element analysis of membrane structures.

Another procedure for predicting the effective nonlinear elastic moduli of textile composites is by homogenization (Dasgupta et al., 1996; Takano et al., 1999; Byström et al., 2000; Peng & Cao, 2000; Carvelli & Poggi, 2001; Ivanov & Tabiei, 2001; Peng & Cao, 2002; Yu et al., 2002). A summary of this technique is given by Takano et al. (1999), who explain that this method is based on a hierarchical modelling of the considered material, thus it is also called multi-scale material characterization approach. The process is illustrated in Figure 5.10. First, the effective elastic constants of the yarns (which are regarded as unidirectional composites) are predicted by homogenization of the fibre properties. A unit cell (also named reference volume) is then built to enclose the characteristic periodic pattern of the textile composite. Numerical tests are performed on the unit cell and on a single finite element (usually a shell element) with the same outer size of the reference volume. By correlating the obtained force-displacement curves, the effective nonlinear stiffness tensor of the homogenized composite can be obtained.

The homogenization method has been successfully applied to the prediction of the mechanical behaviour (Peng & Cao, 2000, 2002; Carvelli & Poggi, 2001) and thermal properties (Dasgupta et al., 1996) of textile reinforced composites. Homogenization techniques guarantee convergence and can allow for mesoscopic fracture in fibre bundles and matrix, including filament cracking, matrix cracking, debonding, and so on (Takano et al., 1999). Despite the accuracy of the method, a huge computational cost limits its application. Moreover, an exact knowledge of the geometrical and mechanical characteristics of the representative unit cell is needed, which requires difficult measurements with specific devices that are not always available. As demonstrated by Byström et al. (2000), the first scale predictions, which are the tow properties, are the most critical, because uncertainties in this information may cause large differences in the results obtained from the final homogenized model.

A homogenisation technique has been used also by Yu et al. (2002) to develop a non-orthogonal constitutive model for woven fabrics reinforced thermoplastic composites. Non-orthogonal constitutive laws take into account the effect that the modification of the angle between warp and weft yarns induces on the material response; this aspect is particularly important for uncoated textiles, but it still exists in coated woven membranes, even if

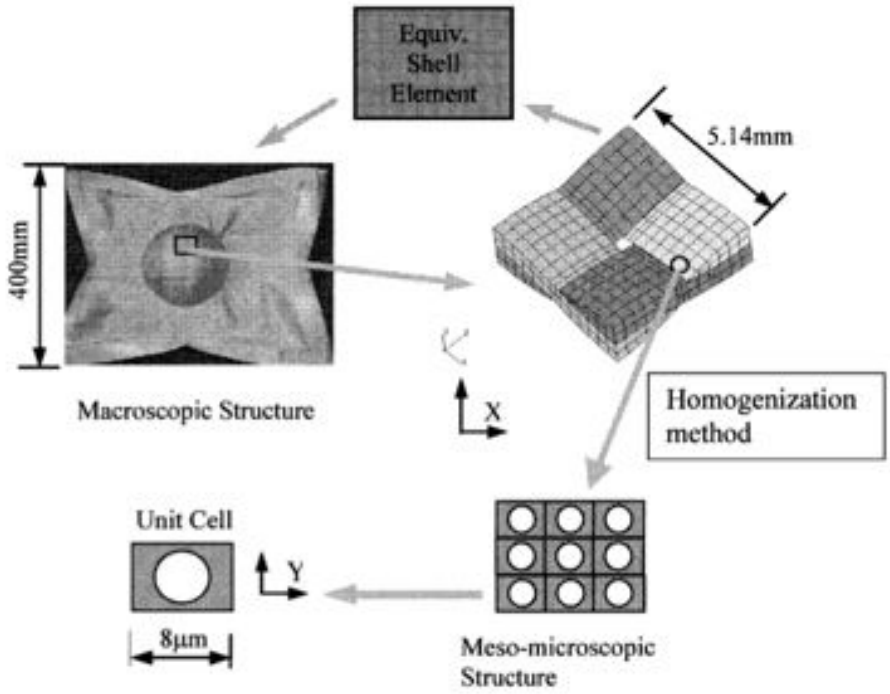

Figure 5.10: *Multi-scale material characterization approach (from Peng & Cao, 2002).*

mitigated by the presence of the coating. In Yu et al. (2002) a structural net composed of warp and weft fibres is considered and the matrix is supposed to be attached to the yarns at the net intersection points. Then, stresses are calculated by homogenization, starting from the structural parameters and the fibre properties, while the material stiffness (relating stresses and strains) is created using the kinematics and the force equilibrium of the net.

A validation of the analytical model presented by Yu et al. (2002) demonstrates that it properly accounts for the effect of the differences in fibre strength and orientation on the anisotropic behaviour. For validation purposes, the model was implemented as a material user subroutine (VUMAT) in the finite element code ABAQUS. Investigations about in-plane shear, pure shear, uniaxial extension and 3D draping problems ware perfomed, with good results concerning the capability of the model to predict

the material mechanical behaviour, according to the authors. However, as stated by Peng & Cao (2005), the derivation by Yu et al. (2002) is based on a small deformation assumption and the paper does not present the stress distributions and characteristic force-displacement responses obtained in the numerical analyses: therefore, further validation would be needed.

A non-orthogonal constitutive model for woven composite fabrics that is not based on the small strain assumption is the one presented by Xue et al. (2003). Three coordinate systems are considered by Xue et al. (2003): a global Cartesian (i.e. orthogonal) reference frame and two local coordinate systems, one orthogonal and having the x-axis aligned with the warp direction and one non-orthogonal, with the two in-plane directions aligned with the warp and fill threads. The relationship between stresses and strains in the global coordinate system is obtained with a rigid body rotation of the material matrix, written in the local Cartesian coordinate system, which is derived with a stress and strain analysis conducted in both the orthogonal and non-orthogonal local coordinate systems. The nonlinear coefficients of the material matrix are evaluated by fitting experimental data from biaxial and shear tests: a definition of effective strain is introduced to allow the expression of the material elastic matrix coefficients as functions of one variable only, without losing the biaxial interaction between the weaving directions. A comparison between numerical results and experimental data from a shear test on a plane weave composite sheet confirms the validity of the model. Nevertheless, the physical meaning of the stress definition in the non-orthogonal system is not very clear, as outlined by Peng & Cao (2005).

An alternative non-orthogonal constitutive model for woven fabrics under large deformation is presented by Peng & Cao (2005). As pointed out by the authors, a nonlinear constitutive model based on a non-orthogonal coordinate system is indispensable to correctly characterize the anisotropic behaviour of fabrics during forming, since the effective elastic properties of these materials in conventional Cartesian coordinates are very sensitive to the fibre orientation. Moreover, woven fabrics experience large angular variation between warp and weft during deformation. Even if architectural membranes are less subjected to variation of the angle between the weaving directions thanks to the coating, orthogonality between warp and weft threads may be modified by shear loading; hence, the model proposed by Peng & Cao (2005) looks still applicable.

The material model by Peng & Cao (2005) (as the one by Xue et al. (2003)) is based on the assumption that direct and shear stresses are uncoupled. This results in a convenient block-partitioned elastic matrix, thus facilitating the identification of the nonlinear matrix components by uniaxial and bias tensile tests. The assumption of a partitioned contravariant elastic matrix is justified by experimental evidence, which has confirmed the uncoupling between direct and shear stresses for woven fabrics (Boisse et al., 2001; Buet-Gautier & Boisse, 2001).

Again, in Peng & Cao (2005) the equivalent material properties are obtained by fitting experimental data of tensile and bias extension tests. A model validation is provided, by comparing numerical results with experimental data of bias extension tests and shear tests. The obtained results are quite close to the real material behaviour in the considered examples, but the effect that changing the biaxial warp to fill load ratio has on the deformation response was not investigated. Moreover, the model presented in Peng & Cao (2005) does not consider the presence of a coating material, which supplies a fundamental contribute to the shear resistance of real architectural fabrics.

Standard continuum constitutive models are unable to capture yarn-level-based deformations. Indeed, many of the typical aspects of the fabric behaviour, such as crimp interchange and locking, are difficult to be modelled with a continuum approach, because they are essentially due to the yarn interaction. Parallel multiscale models (Boljen & Hiermaier, 2012), also called mesostructurally-based analytical models (King et al., 2005), are particularly advantageous, since they combine the robustness and simplicity of continuum constitutive laws with the capacity of capturing some characteristics that are strictly related to the kinematics of yarns. In this type of modelling, from the deformation of an integrated kinematic model representing the fabric mesostructure, the macroscopic response of the fabric is derived, in terms of effective deformation gradient. Then, a continuum constitutive model calculates the effective stress tensor.

Within the framework of parallel multiscale modelling, an approach for developing continuum models for the mechanical behaviour of woven fabrics based on the mesostructure is proposed by King et al. (2005). Firstly, it is necessary to select a geometric model for the representative unit cell, coupled with a constitutive model of the yarns mechanical behaviour. Secondly, the fabric structural configuration is defined starting from the unit

cell defined previously. Once the fabric configuration is known, it is related to the macroscopic deformation by an energy minimisation method, and it is used to calculate the loads carried by the yarns, which are then employed to estimate the macroscopic stresses. In the article by King et al. (2005) it is demonstrated how a mesostructurally-based continuum model can capture the effects of yarns configuration on the macroscopic reponse, with an application to a Kevlar® plane weave fabric.

A drawback of the method described by King et al. (2005) is the huge number of parameters involved. The configuration of the plain weave fabric analysed in the article requires five parameters to be defined, but more complicated representative geometries will have a larger number of free parameters. As a consequence, the conditional free-energy function associated with the unit cell configuration may not have a single global minimum, which means that a given state of macroscopic deformation corresponds to more than one stable state at the meso-scale. Moreover, a high number of parameters results in greater computational time, which makes its application to the finite element analysis of large structures not convenient.

Another disadvantage of the approach discussed in King et al. (2005) is the fact that most of the parameters are related to the internal structure of the fabric. Therefore, they require measurements of quantities at the meso-scale, that are not always simple to be achieved, since they need specific devices. These instruments are not always available and information about the weaving geometry is not complete in the datasheets provided by the producers. Thus, the difficulties that arise in the calibration of the corresponding constitutive laws make this kind of modelling unsuitable for structural engineering applications.

Other parallel multiscale models for fabrics are presented by Boljen & Hiermaier (2012) and Antonietti et al. (2011). The kinematic model employed by Boljen & Hiermaier (2012) uses sixteen degrees of freedom, which are reduced to six by introducing internal kinematic constraints. Material parameters for three different aramid woven fabrics have been identified and it is shown that the model is able to reproduce some specific aspects of aramid fabrics behaviour, such as rate dependency of aramid fibres, crimp interchange, yarns trellising and shear locking. The constitutive model presented by Antonietti et al. (2011) is characterized by an effective strain energy functional obtained by superposition of a matrix contribute and two contributes related to the fibres (two families of yarns with different

mechanical properties). The equilibrated configuration of the fabric is determined by minimizing the associated strain energy function with respect to the position of the internal nodes. It is shown that this method can easily deal with complex textile topologies, like the tricot textile (a type of warp knitting shown in Figure 5.11).

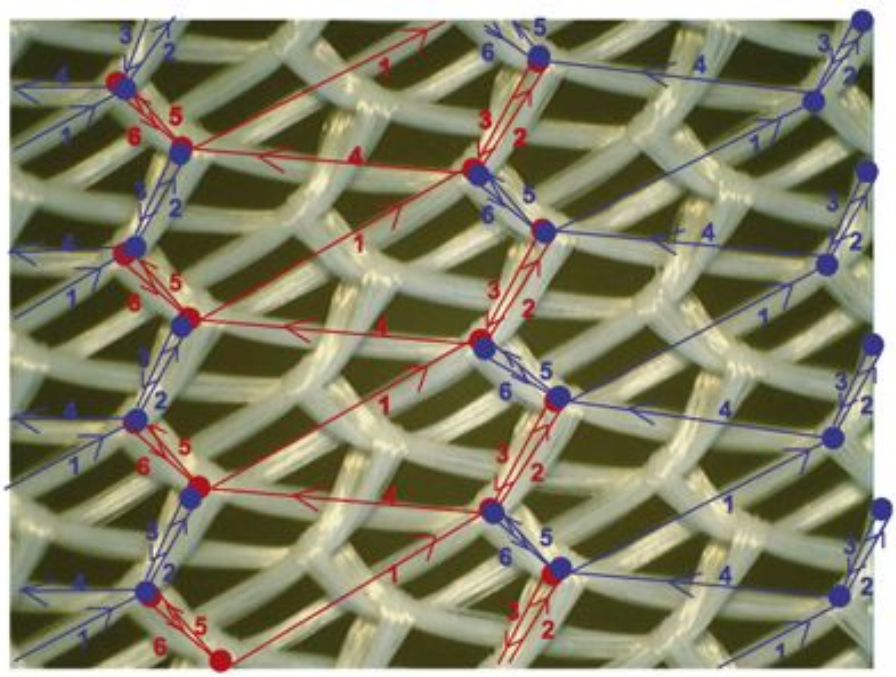

Figure 5.11: *Tricot textile (from Antonietti et al., 2011).*

In the current literature, plasticity is not often included in the modelling of the macro-mechanical behaviour of coated woven fabrics. One among few articles about this topic is that by Odegard et al. (2001), where a continuum elastic-plastic constitutive law for woven fabric/polymeric matrix composites is proposed. The model is formulated within a large strain framework and it makes use of a plane stress assumption. A scalar hardening parameter, function of the applied stress state, is introduced to determine the plastic strain increment. The authors show that the proposed model is able to accurately describe the nonlinear mechanical behaviour of two different coated woven fabrics, for different biaxial stress states, using experimental data from the literature. Nevertheless, the constitutive law presented by

Odegard et al. (2001) displays a lot of parameters; thus, it can be very hard to estimate their values, especially if there is not a large amount of available experimental data.

Finally, creep behaviour is another topic that is not very popular in the present literature about constitutive modelling of coated fabric membranes. As pointed out by Yu et al. (2006), due to the polymeric nature of the coating material and, in some cases, of the textile reinforcement, coated fabrics deform gradually over time, at constant stress and temperature. Therefore, it is extremely important to include the creep behaviour into constitutive laws for textile reinforced composites; for example, n view of evaluating the tension that must be applied to compensate the excessive creep deformation after some time from the installation of the structure. The multi-axial anisotropic creep model for coated textiles proposed by Yu et al. (2006) is based on a three-parameter potential which is used to derive the creep strain rate. Moreover, an associated flow rule links the effective creep strain rate to the conjugate effective stress, as in the theory of plasticity. Lastly, an expression that relates the creep strain rate to the effective stress through four experimentally-determined functions completes the creep model, enabling to calculate the proportional factor that appears in the flow rule. It is shown that the presented model is able to reproduce the anisotropic creep behaviour of coated polymeric textiles under uniaxial stress states (bias tensile tests). The possibility of predicting the creep deformation under multi-axial stress states is also discussed by Yu et al. (2006).

5.3 Identification of Orthotropic Linear Elastic (OLE) model parameters

Biaxial test data are often employed to estimate Young's moduli and Poisson's ratios, which are needed to model coated fabrics as an orthotropic linear elastic material. As commented by Bridgens & Gosling (2010), this enables the complex non-linear behaviour of coated fabrics to be approximated by parameters that are compatible with available structural analysis software. Indeed, even if general purpose finite element software generally includes more complex material laws, analysis of tensile structures presents

characteristic phases (form-finding, cutting pattern generation), as illustrated in Chapter 2, which require tailored software, wherein only simple material constitutive equations are often implemented.

In the hypothesis of small strains, the well-known linear elastic constitutive law can be expressed as:

$$\boldsymbol{\sigma} = \mathbb{C} : \boldsymbol{\varepsilon} \ , \qquad \sigma_{ij} = \mathbb{C}_{ijhk}\varepsilon_{hk} \tag{5.5}$$

where $\boldsymbol{\sigma}$ and $\boldsymbol{\varepsilon}$ are the nominal stress and infinitesimal strain tensors, while $\mathbb{C}$ is the fourth-order elasticity tensor. The inverse constitutive relationship is therefore:

$$\boldsymbol{\varepsilon} = \mathbb{C}^{-1} : \boldsymbol{\sigma} \ , \qquad \varepsilon_{ij} = \mathbb{C}^{-1}_{ijhk}\sigma_{hk} \tag{5.6}$$

where $\mathbb{C}^{-1}$ is the compliance tensor. Both $\mathbb{C}$ and $\mathbb{C}^{-1}$ are fully symmetric (minor and major symmetries) and positive definite. Equations (5.5) and (5.6) can be rewritten in Voigt's notation as follows:

$$\begin{bmatrix} \sigma_{11} \\ \sigma_{22} \\ \sigma_{33} \\ \sigma_{12} \\ \sigma_{13} \\ \sigma_{23} \end{bmatrix} = \begin{bmatrix} \mathbb{C}_{1111} & \mathbb{C}_{1122} & \mathbb{C}_{1133} & \mathbb{C}_{1112} & \mathbb{C}_{1113} & \mathbb{C}_{1123} \\ \mathbb{C}_{2211} & \mathbb{C}_{2222} & \mathbb{C}_{2233} & \mathbb{C}_{2212} & \mathbb{C}_{2213} & \mathbb{C}_{2223} \\ \mathbb{C}_{3311} & \mathbb{C}_{3322} & \mathbb{C}_{3333} & \mathbb{C}_{3312} & \mathbb{C}_{3313} & \mathbb{C}_{3323} \\ \mathbb{C}_{1211} & \mathbb{C}_{1222} & \mathbb{C}_{1233} & \mathbb{C}_{1212} & \mathbb{C}_{1213} & \mathbb{C}_{1223} \\ \mathbb{C}_{1311} & \mathbb{C}_{1322} & \mathbb{C}_{1333} & \mathbb{C}_{1312} & \mathbb{C}_{1313} & \mathbb{C}_{1323} \\ \mathbb{C}_{2311} & \mathbb{C}_{2322} & \mathbb{C}_{2333} & \mathbb{C}_{2312} & \mathbb{C}_{2313} & \mathbb{C}_{2323} \end{bmatrix} \begin{bmatrix} \varepsilon_{11} \\ \varepsilon_{22} \\ \varepsilon_{33} \\ \varepsilon_{12} \\ \varepsilon_{13} \\ \varepsilon_{23} \end{bmatrix} \tag{5.7}$$

$$\begin{bmatrix} \varepsilon_{11} \\ \varepsilon_{22} \\ \varepsilon_{33} \\ \varepsilon_{12} \\ \varepsilon_{13} \\ \varepsilon_{23} \end{bmatrix} = \begin{bmatrix} \mathbb{C}^{-1}_{1111} & \mathbb{C}^{-1}_{1122} & \mathbb{C}^{-1}_{1133} & \mathbb{C}^{-1}_{1112} & \mathbb{C}^{-1}_{1113} & \mathbb{C}^{-1}_{1123} \\ \mathbb{C}^{-1}_{2211} & \mathbb{C}^{-1}_{2222} & \mathbb{C}^{-1}_{2233} & \mathbb{C}^{-1}_{2212} & \mathbb{C}^{-1}_{2213} & \mathbb{C}^{-1}_{2223} \\ \mathbb{C}^{-1}_{3311} & \mathbb{C}^{-1}_{3322} & \mathbb{C}^{-1}_{3333} & \mathbb{C}^{-1}_{3312} & \mathbb{C}^{-1}_{3313} & \mathbb{C}^{-1}_{3323} \\ \mathbb{C}^{-1}_{1211} & \mathbb{C}^{-1}_{1222} & \mathbb{C}^{-1}_{1233} & \mathbb{C}^{-1}_{1212} & \mathbb{C}^{-1}_{1213} & \mathbb{C}^{-1}_{1223} \\ \mathbb{C}^{-1}_{1311} & \mathbb{C}^{-1}_{1322} & \mathbb{C}^{-1}_{1333} & \mathbb{C}^{-1}_{1312} & \mathbb{C}^{-1}_{1313} & \mathbb{C}^{-1}_{1323} \\ \mathbb{C}^{-1}_{2311} & \mathbb{C}^{-1}_{2322} & \mathbb{C}^{-1}_{2333} & \mathbb{C}^{-1}_{2312} & \mathbb{C}^{-1}_{2313} & \mathbb{C}^{-1}_{2323} \end{bmatrix} \begin{bmatrix} \sigma_{11} \\ \sigma_{22} \\ \sigma_{33} \\ \sigma_{12} \\ \sigma_{13} \\ \sigma_{23} \end{bmatrix} \tag{5.8}$$

Architectural coated fabrics are typically modelled in a plane stress framework, so that Equations (5.7) and (5.8) become:

$$\begin{bmatrix} \sigma_{11} \\ \sigma_{22} \\ \sigma_{12} \end{bmatrix} = \begin{bmatrix} \mathbb{C}_{1111} & \mathbb{C}_{1122} & \mathbb{C}_{1112} \\ \mathbb{C}_{2211} & \mathbb{C}_{2222} & \mathbb{C}_{2212} \\ \mathbb{C}_{1211} & \mathbb{C}_{1222} & \mathbb{C}_{1212} \end{bmatrix} \begin{bmatrix} \varepsilon_{11} \\ \varepsilon_{22} \\ \varepsilon_{12} \end{bmatrix} \tag{5.9}$$

$$\begin{bmatrix} \varepsilon_{11} \\ \varepsilon_{22} \\ \varepsilon_{12} \end{bmatrix} = \begin{bmatrix} \mathbb{C}^{-1}_{1111} & \mathbb{C}^{-1}_{1122} & \mathbb{C}^{-1}_{1112} \\ \mathbb{C}^{-1}_{2211} & \mathbb{C}^{-1}_{2222} & \mathbb{C}^{-1}_{2212} \\ \mathbb{C}^{-1}_{1211} & \mathbb{C}^{-1}_{1222} & \mathbb{C}^{-1}_{1212} \end{bmatrix} \begin{bmatrix} \sigma_{11} \\ \sigma_{22} \\ \sigma_{12} \end{bmatrix} \tag{5.10}$$

Finally, coated fabrics are almost always orthotropic: the two material directions coincide with the weaving warp (index 11) and weft (index 22) directions. Therefore, one gets:

$$\begin{bmatrix} \sigma_{11} \\ \sigma_{22} \\ \sigma_{12} \end{bmatrix} = \begin{bmatrix} \dfrac{E_1}{1-\nu_{12}\nu_{21}} & \dfrac{E_1\nu_{21}}{1-\nu_{12}\nu_{21}} & 0 \\ \dfrac{E_2\nu_{12}}{1-\nu_{12}\nu_{21}} & \dfrac{E_2}{1-\nu_{12}\nu_{21}} & 0 \\ 0 & 0 & 2G_{12} \end{bmatrix} \begin{bmatrix} \varepsilon_{11} \\ \varepsilon_{22} \\ \varepsilon_{12} \end{bmatrix} \tag{5.11}$$

$$\begin{bmatrix} \varepsilon_{11} \\ \varepsilon_{22} \\ \varepsilon_{12} \end{bmatrix} = \begin{bmatrix} \dfrac{1}{E_1} & -\dfrac{\nu_{21}}{E_2} & 0 \\ -\dfrac{\nu_{12}}{E_1} & \dfrac{1}{E_2} & 0 \\ 0 & 0 & \dfrac{1}{2G_{12}} \end{bmatrix} \begin{bmatrix} \sigma_{11} \\ \sigma_{22} \\ \sigma_{12} \end{bmatrix} \tag{5.12}$$

where E_1 and E_2 are Young's moduli in the warp and weft directions respectively, ν_{12} and ν_{21} are Poisson's ratios and G_{12} the in-plane shear modulus. More in detail, ν_{12} (ν_{21}) represents the opposite of the fill (warp) strain caused by a unit strain in the warp (fill) direction.

More than one method has been proposed to evaluate the elastic moduli (E_1, E_2, ν_{12}, ν_{21} and G_{12}) from biaxial test data. Laboratorium Blum has developed its internal testing protocol and identification method, which are described in detail in the European Design Guide for Tensile Surface Structures (Forster & Mollaert, 2004, pp. 305-315). The Japanese Standard MSAJ/M-02:1995 suggests various approaches, namely the least squares, the minimax and the multistep linear approximation methods. The least squares approximation of biaxial test data is also prescribed by the American Standard ASCE55-10. At present, it has not been established yet which one of the proposed estimation procedures meets the real structural behaviour best, but research activity is being performed on the topic (Uhlemann et al., 2014).

The determination of the elastic constants has been carried out in this thesis according to the MSAJ/M-02:1995 Standard and following the recommendations contained in an interesting conference paper by Bridgens & Gosling (2010), who comment on the effects of some choices on the result of the least squares identification, which will be explained in Section 5.3.1.

5.3.1 Least squares identification of OLE model parameters

The least squares method is a standard method used for fitting. It consists in minimising a function (objective or discrepancy function) that is the sum of squared residuals, a residual being the difference between measured data and calculated values provided by a model. The model employed in this paragraph is the Orthotropic Linear Elastic (OLE), as suggested by the Japanese Standard MSAJ/M-02:1995, whose constitutive relationships have been previously recalled (Equation (5.11), in terms of stress, or Equation (5.12), in terms of strain).

As described in Section 4.2.2, during a biaxial test performed with the procedure prescribed by MSAJ/M-02:1995, the loads are aligned with the warp and weft directions. Since the weaving directions coincide with the principal material directions, the responses to normal and shear stresses are uncoupled and can be considered separately. This means that the biaxial test procedure described in MSAJ/M-02:1995 is specifically studied to determine only Young's moduli and Poisson's ratios (E_1, E_2, ν_{12}, ν_{21}); the shear modulus G_{12} can be estimated separately, by using another typology of test, which is illustrated in the MSAJ/M-01:1993 Japanese Standard. Hence, the following reduced forms of Equations (5.11) and (5.12) have been employed in the identification procedure presented in this paragraph:

$$\begin{bmatrix}\sigma_{11}\\ \sigma_{22}\end{bmatrix} = \begin{bmatrix}\mathbb{C}_{1111} & \mathbb{C}_{1122}\\ \mathbb{C}_{2211} & \mathbb{C}_{2222}\end{bmatrix}\begin{bmatrix}\varepsilon_{11}\\ \varepsilon_{22}\end{bmatrix} = \begin{bmatrix}\dfrac{E_1}{1-\nu_{12}\nu_{21}} & \dfrac{E_1\nu_{21}}{1-\nu_{12}\nu_{21}}\\ \dfrac{E_2\nu_{12}}{1-\nu_{12}\nu_{21}} & \dfrac{E_2}{1-\nu_{12}\nu_{21}}\end{bmatrix}\begin{bmatrix}\varepsilon_{11}\\ \varepsilon_{22}\end{bmatrix} \tag{5.13}$$

$$\begin{bmatrix}\varepsilon_{11}\\ \varepsilon_{22}\end{bmatrix} = \begin{bmatrix}\mathbb{C}^{-1}_{1111} & \mathbb{C}^{-1}_{1122}\\ \mathbb{C}^{-1}_{2211} & \mathbb{C}^{-1}_{2222}\end{bmatrix}\begin{bmatrix}\sigma_{11}\\ \sigma_{22}\end{bmatrix} = \begin{bmatrix}\dfrac{1}{E_1} & -\dfrac{\nu_{21}}{E_2}\\ -\dfrac{\nu_{12}}{E_1} & \dfrac{1}{E_2}\end{bmatrix}\begin{bmatrix}\sigma_{11}\\ \sigma_{22}\end{bmatrix} \tag{5.14}$$

The symmetry of the elasticity tensor implies that Young's moduli and Poisson's ratios are not independent, rather constrained by the reciprocity relationship:

$$\mathbb{C}_{1122} = \mathbb{C}_{2211} \quad \Rightarrow \quad \frac{\nu_{21}}{E_2} = \frac{\nu_{12}}{E_1} \tag{5.15}$$

The MSAJ/M-02:1995 Standard applies this constraint to the calculation of the elastic moduli. Gosling & Bridgens (2008) argued that the enforcement of the reciprocity constraint, which is an energetic requirement, is not compulsory for coated fabrics, since they are not homogeneous materials, but show energy losses due to frictional effects at crossovers, inelastic yarn crushing and inelastic coating extension. Therefore, the identification of elastic moduli should be intended as a best-fitting of biaxial test data, more than a constitutive modelling procedure. However, Bridgens & Gosling (2010) demonstrated that inclusion of the reciprocity restraint only makes a small difference to the estimated elastic constant values. Since the identification that has been carried out in this thesis aims at comparing OLE model results to the ones of the new hyperelastic model later presented in Chapter 6, the symmetry of the elasticity tensor has been enforced in the following calculations.

The first step of the least squares method is the choice of the objective function. Residuals can be written in terms of stress or of strain. In the former case, the objective function $\Phi(\boldsymbol{\sigma})$ expressed in terms of stress is:

$$\Phi(\boldsymbol{\sigma}) = \sum_{i=1}^{N} (\sigma^c_{11,i} - \sigma^m_{11,i})^2 + \sum_{i=1}^{N} (\sigma^c_{22,i} - \sigma^m_{22,i})^2 \tag{5.16}$$

where c stands for *calculated*, m for *measured* and N is the number of experimental points that are used for the calibration procedure. The stress values are evaluated with Equation (5.13), so that:

$$\begin{aligned} \Phi(\boldsymbol{\sigma}) = &\sum_{i=1}^{N} (\mathbb{C}_{1111}\varepsilon^m_{11,i} + \mathbb{C}_{1122}\varepsilon^m_{22,i} - \sigma^m_{11,i})^2 + \\ &+ \sum_{i=1}^{N} (\mathbb{C}_{1122}\varepsilon^m_{11,i} + \mathbb{C}_{2222}\varepsilon^m_{22,i} - \sigma^m_{22,i})^2 \end{aligned} \tag{5.17}$$

where the reciprocity constraint has been already enforced. Analogously,

the objective function $\Phi(\boldsymbol{\varepsilon})$ can be expressed in terms of strain as:

$$\Phi(\boldsymbol{\varepsilon}) = \sum_{i=1}^{N}(\varepsilon^c_{11,i} - \varepsilon^m_{11,i})^2 + \sum_{i=1}^{N}(\varepsilon^c_{22,i} - \varepsilon^m_{22,i})^2 \tag{5.18}$$

that, using Equation (5.14) to determine the calculated strains and enforcing the elasticity tensor symmetry, becomes:

$$\begin{aligned}\Phi(\boldsymbol{\varepsilon}) = &\sum_{i=1}^{N}(\mathbb{C}^{-1}_{1111}\sigma^m_{11,i} + \mathbb{C}^{-1}_{1122}\sigma^m_{22,i} - \varepsilon^m_{11,i})^2 + \\ &+ \sum_{i=1}^{N}(\mathbb{C}^{-1}_{1122}\sigma^m_{11,i} + \mathbb{C}^{-1}_{2222}\sigma^m_{22,i} - \varepsilon^m_{22,i})^2\end{aligned} \tag{5.19}$$

Once the objective function has been defined, the second step is its minimisation, which determines the best fitting values of the searched parameters. The minimisation can be carried out either analytically or numerically: the first approach is illustrated in the MSAJ/M-02:1995 Standard. The analytical procedure consists in evaluating the derivatives of the objective function with respect to the parameters, and in setting these derivatives equal to nought in order to obtain a system of equations, whose solution renders the best fitting values of the parameters. If the objective function is written in terms of stresses (Equation (5.17)), the final system becomes:

$$\begin{cases}\dfrac{\partial\Phi(\boldsymbol{\sigma})}{\partial\mathbb{C}_{1111}} = 0 \\ \dfrac{\partial\Phi(\boldsymbol{\sigma})}{\partial\mathbb{C}_{1122}} = 0 \\ \dfrac{\partial\Phi(\boldsymbol{\sigma})}{\partial\mathbb{C}_{2222}} = 0\end{cases} \tag{5.20}$$

where:

$$\frac{\partial\Phi(\boldsymbol{\sigma})}{\partial\mathbb{C}_{1111}} = 2\sum_{i=1}^{N}(\mathbb{C}_{1111}\varepsilon^m_{11,i} + \mathbb{C}_{1122}\varepsilon^m_{22,i} - \sigma^m_{11,i})\varepsilon^m_{11,i} \tag{5.21}$$

$$\frac{\partial \Phi(\boldsymbol{\sigma})}{\partial \mathbb{C}_{1122}} = 2\sum_{i=1}^{N}(\mathbb{C}_{1111}\varepsilon_{11,i}^{m} + \mathbb{C}_{1122}\varepsilon_{22,i}^{m} - \sigma_{11,i}^{m})\varepsilon_{22,i}^{m} + \\ + 2\sum_{i=1}^{N}(\mathbb{C}_{1122}\varepsilon_{11,i}^{m} + \mathbb{C}_{2222}\varepsilon_{22,i}^{m} - \sigma_{22,i}^{m})\varepsilon_{11,i}^{m} \tag{5.22}$$

$$\frac{\partial \Phi(\boldsymbol{\sigma})}{\partial \mathbb{C}_{2222}} = 2\sum_{i=1}^{N}(\mathbb{C}_{1122}\varepsilon_{11,i}^{m} + \mathbb{C}_{2222}\varepsilon_{22,i}^{m} - \sigma_{22,i}^{m})\varepsilon_{22,i}^{m} \tag{5.23}$$

If the objective function is written in terms of strains (Equation (5.19)), the final system is:

$$\begin{cases} \dfrac{\partial \Phi(\boldsymbol{\varepsilon})}{\partial \mathbb{C}_{1111}^{-1}} = 0 \\ \dfrac{\partial \Phi(\boldsymbol{\varepsilon})}{\partial \mathbb{C}_{1122}^{-1}} = 0 \\ \dfrac{\partial \Phi(\boldsymbol{\varepsilon})}{\partial \mathbb{C}_{2222}^{-1}} = 0 \end{cases} \tag{5.24}$$

where:

$$\frac{\partial \Phi(\boldsymbol{\varepsilon})}{\partial \mathbb{C}_{1111}^{-1}} = 2\sum_{i=1}^{N}(\mathbb{C}_{1111}^{-1}\sigma_{11,i}^{m} + \mathbb{C}_{1122}^{-1}\sigma_{22,i}^{m} - \varepsilon_{11,i}^{m})\sigma_{11,i}^{m} \tag{5.25}$$

$$\frac{\partial \Phi(\boldsymbol{\varepsilon})}{\partial \mathbb{C}_{1122}^{-1}} = 2\sum_{i=1}^{N}(\mathbb{C}_{1111}^{-1}\sigma_{11,i}^{m} + \mathbb{C}_{1122}^{-1}\sigma_{22,i}^{m} - \varepsilon_{11,i}^{m})\sigma_{22,i}^{m} + \\ + 2\sum_{i=1}^{N}(\mathbb{C}_{1122}^{-1}\sigma_{11,i}^{m} + \mathbb{C}_{2222}^{-1}\sigma_{22,i}^{m} - \varepsilon_{22,i}^{m})\sigma_{11,i}^{m} \tag{5.26}$$

$$\frac{\partial \Phi(\boldsymbol{\varepsilon})}{\partial \mathbb{C}_{2222}^{-1}} = 2\sum_{i=1}^{N}(\mathbb{C}_{1122}^{-1}\sigma_{11,i}^{m} + \mathbb{C}_{2222}^{-1}\sigma_{22,i}^{m} - \varepsilon_{22,i}^{m})\sigma_{22,i}^{m} \tag{5.27}$$

The measured stresses and strains can be collected in vectors, such that:

$$\boldsymbol{\sigma}_{\mathbf{11}}^{\boldsymbol{m}} = [\sigma_{11,1}^{m}\ \sigma_{11,2}^{m}\ \dots\ \sigma_{11,N}^{m}]^{\mathrm{T}} \tag{5.28}$$

$$\boldsymbol{\sigma}_{\mathbf{22}}^{\boldsymbol{m}} = [\sigma_{22,1}^{m}\ \sigma_{22,2}^{m}\ \dots\ \sigma_{22,N}^{m}]^{\mathrm{T}} \tag{5.29}$$

$$\boldsymbol{\varepsilon}_{\mathbf{11}}^{\boldsymbol{m}} = [\varepsilon_{11,1}^{m}\ \varepsilon_{11,2}^{m}\ \dots\ \varepsilon_{11,N}^{m}]^{\mathrm{T}} \tag{5.30}$$

$$\boldsymbol{\varepsilon}_{\mathbf{22}}^{\boldsymbol{m}} = [\varepsilon_{22,1}^{m}\ \varepsilon_{22,2}^{m}\ \dots\ \varepsilon_{22,N}^{m}]^{\mathrm{T}} \tag{5.31}$$

In terms of these vectors, the sums in previous Equations (5.21) to (5.23) and (5.25) to (5.27) can be restated as dot products. For instance:

$$\sum_{i=1}^{N} \varepsilon_{11,i}^{m} \varepsilon_{11,i}^{m} = \boldsymbol{\varepsilon}_{\mathbf{11}}^{\boldsymbol{m}} \cdot \boldsymbol{\varepsilon}_{\mathbf{11}}^{\boldsymbol{m}} \tag{5.32}$$

Therefore Equations (5.21) to (5.23) become:

$$\frac{\partial \Phi(\boldsymbol{\sigma})}{\partial \mathbb{C}_{1111}} = 2\left(\mathbb{C}_{1111}\boldsymbol{\varepsilon}_{\mathbf{11}}^{\boldsymbol{m}} \cdot \boldsymbol{\varepsilon}_{\mathbf{11}}^{\boldsymbol{m}} + \mathbb{C}_{1122}\boldsymbol{\varepsilon}_{\mathbf{22}}^{\boldsymbol{m}} \cdot \boldsymbol{\varepsilon}_{\mathbf{11}}^{\boldsymbol{m}} - \boldsymbol{\sigma}_{\mathbf{11}}^{\boldsymbol{m}} \cdot \boldsymbol{\varepsilon}_{\mathbf{11}}^{\boldsymbol{m}}\right) \tag{5.33}$$

$$\begin{aligned} \frac{\partial \Phi(\boldsymbol{\sigma})}{\partial \mathbb{C}_{1122}} = {} & 2\left(\mathbb{C}_{1111}\boldsymbol{\varepsilon}_{\mathbf{11}}^{\boldsymbol{m}} \cdot \boldsymbol{\varepsilon}_{\mathbf{22}}^{\boldsymbol{m}} + \mathbb{C}_{1122}\boldsymbol{\varepsilon}_{\mathbf{22}}^{\boldsymbol{m}} \cdot \boldsymbol{\varepsilon}_{\mathbf{22}}^{\boldsymbol{m}} - \boldsymbol{\sigma}_{\mathbf{11}}^{\boldsymbol{m}} \cdot \boldsymbol{\varepsilon}_{\mathbf{22}}^{\boldsymbol{m}}\right) + \\ & + 2\left(\mathbb{C}_{1122}\boldsymbol{\varepsilon}_{\mathbf{11}}^{\boldsymbol{m}} \cdot \boldsymbol{\varepsilon}_{\mathbf{11}}^{\boldsymbol{m}} + \mathbb{C}_{2222}\boldsymbol{\varepsilon}_{\mathbf{22}}^{\boldsymbol{m}} \cdot \boldsymbol{\varepsilon}_{\mathbf{11}}^{\boldsymbol{m}} - \boldsymbol{\sigma}_{\mathbf{22}}^{\boldsymbol{m}} \cdot \boldsymbol{\varepsilon}_{\mathbf{11}}^{\boldsymbol{m}}\right) \end{aligned} \tag{5.34}$$

$$\frac{\partial \Phi(\boldsymbol{\sigma})}{\partial \mathbb{C}_{2222}} = 2\left(\mathbb{C}_{1122}\boldsymbol{\varepsilon}_{\mathbf{11}}^{\boldsymbol{m}} \cdot \boldsymbol{\varepsilon}_{\mathbf{22}}^{\boldsymbol{m}} + \mathbb{C}_{2222}\boldsymbol{\varepsilon}_{\mathbf{22}}^{\boldsymbol{m}} \cdot \boldsymbol{\varepsilon}_{\mathbf{22}}^{\boldsymbol{m}} - \boldsymbol{\sigma}_{\mathbf{22}}^{\boldsymbol{m}} \cdot \boldsymbol{\varepsilon}_{\mathbf{22}}^{\boldsymbol{m}}\right) \tag{5.35}$$

while Equations (5.25) to (5.27) become:

$$\frac{\partial \Phi(\boldsymbol{\varepsilon})}{\partial \mathbb{C}_{1111}^{-1}} = 2\left(\mathbb{C}_{1111}^{-1}\boldsymbol{\sigma}_{\mathbf{11}}^{\boldsymbol{m}} \cdot \boldsymbol{\sigma}_{\mathbf{11}}^{\boldsymbol{m}} + \mathbb{C}_{1122}^{-1}\boldsymbol{\sigma}_{\mathbf{22}}^{\boldsymbol{m}} \cdot \boldsymbol{\sigma}_{\mathbf{11}}^{\boldsymbol{m}} - \boldsymbol{\varepsilon}_{\mathbf{11}}^{\boldsymbol{m}} \cdot \boldsymbol{\sigma}_{\mathbf{11}}^{\boldsymbol{m}}\right) \tag{5.36}$$

$$\begin{aligned} \frac{\partial \Phi(\boldsymbol{\varepsilon})}{\partial \mathbb{C}_{1122}^{-1}} = {} & 2\left(\mathbb{C}_{1111}^{-1}\boldsymbol{\sigma}_{\mathbf{11}}^{\boldsymbol{m}} \cdot \boldsymbol{\sigma}_{\mathbf{22}}^{\boldsymbol{m}} + \mathbb{C}_{1122}^{-1}\boldsymbol{\sigma}_{\mathbf{22}}^{\boldsymbol{m}} \cdot \boldsymbol{\sigma}_{\mathbf{22}}^{\boldsymbol{m}} - \boldsymbol{\varepsilon}_{\mathbf{11}}^{\boldsymbol{m}} \cdot \boldsymbol{\sigma}_{\mathbf{22}}^{\boldsymbol{m}}\right) + \\ & + 2\left(\mathbb{C}_{1122}^{-1}\boldsymbol{\sigma}_{\mathbf{11}}^{\boldsymbol{m}} \cdot \boldsymbol{\sigma}_{\mathbf{11}}^{\boldsymbol{m}} + \mathbb{C}_{2222}^{-1}\boldsymbol{\sigma}_{\mathbf{22}}^{\boldsymbol{m}} \cdot \boldsymbol{\sigma}_{\mathbf{11}}^{\boldsymbol{m}} - \boldsymbol{\varepsilon}_{\mathbf{22}}^{\boldsymbol{m}} \cdot \boldsymbol{\sigma}_{\mathbf{11}}^{\boldsymbol{m}}\right) \end{aligned} \tag{5.37}$$

$$\frac{\partial \Phi(\boldsymbol{\varepsilon})}{\partial \mathbb{C}_{2222}^{-1}} = 2\left(\mathbb{C}_{1122}^{-1}\boldsymbol{\sigma}_{\mathbf{11}}^{\boldsymbol{m}} \cdot \boldsymbol{\sigma}_{\mathbf{22}}^{\boldsymbol{m}} + \mathbb{C}_{2222}^{-1}\boldsymbol{\sigma}_{\mathbf{22}}^{\boldsymbol{m}} \cdot \boldsymbol{\sigma}_{\mathbf{22}}^{\boldsymbol{m}} - \boldsymbol{\varepsilon}_{\mathbf{22}}^{\boldsymbol{m}} \cdot \boldsymbol{\sigma}_{\mathbf{22}}^{\boldsymbol{m}}\right) \tag{5.38}$$

Using this compact vectorial notation, the system 5.20, which minimises the objective function written in terms of stress, can be reformulated in a convenient matrix form:

$$\begin{aligned} \begin{bmatrix} \boldsymbol{\varepsilon}_{\mathbf{11}}^{\boldsymbol{m}} \cdot \boldsymbol{\varepsilon}_{\mathbf{11}}^{\boldsymbol{m}} & \boldsymbol{\varepsilon}_{\mathbf{11}}^{\boldsymbol{m}} \cdot \boldsymbol{\varepsilon}_{\mathbf{22}}^{\boldsymbol{m}} & 0 \\ \boldsymbol{\varepsilon}_{\mathbf{11}}^{\boldsymbol{m}} \cdot \boldsymbol{\varepsilon}_{\mathbf{22}}^{\boldsymbol{m}} & \boldsymbol{\varepsilon}_{\mathbf{11}}^{\boldsymbol{m}} \cdot \boldsymbol{\varepsilon}_{\mathbf{11}}^{\boldsymbol{m}} + \boldsymbol{\varepsilon}_{\mathbf{22}}^{\boldsymbol{m}} \cdot \boldsymbol{\varepsilon}_{\mathbf{22}}^{\boldsymbol{m}} & \boldsymbol{\varepsilon}_{\mathbf{11}}^{\boldsymbol{m}} \cdot \boldsymbol{\varepsilon}_{\mathbf{22}}^{\boldsymbol{m}} \\ 0 & \boldsymbol{\varepsilon}_{\mathbf{11}}^{\boldsymbol{m}} \cdot \boldsymbol{\varepsilon}_{\mathbf{22}}^{\boldsymbol{m}} & \boldsymbol{\varepsilon}_{\mathbf{22}}^{\boldsymbol{m}} \cdot \boldsymbol{\varepsilon}_{\mathbf{22}}^{\boldsymbol{m}} \end{bmatrix} \begin{bmatrix} \mathbb{C}_{1111} \\ \mathbb{C}_{1122} \\ \mathbb{C}_{2222} \end{bmatrix} = \\ = \begin{bmatrix} \boldsymbol{\sigma}_{\mathbf{11}}^{\boldsymbol{m}} \cdot \boldsymbol{\varepsilon}_{\mathbf{11}}^{\boldsymbol{m}} \\ \boldsymbol{\sigma}_{\mathbf{11}}^{\boldsymbol{m}} \cdot \boldsymbol{\varepsilon}_{\mathbf{22}}^{\boldsymbol{m}} + \boldsymbol{\sigma}_{\mathbf{22}}^{\boldsymbol{m}} \cdot \boldsymbol{\varepsilon}_{\mathbf{11}}^{\boldsymbol{m}} \\ \boldsymbol{\sigma}_{\mathbf{22}}^{\boldsymbol{m}} \cdot \boldsymbol{\varepsilon}_{\mathbf{22}}^{\boldsymbol{m}} \end{bmatrix} \end{aligned} \tag{5.39}$$

System 5.39 can be solved analytically or numerically to get the best fitting values (in terms of stress) of $\mathbb{C}_{1111}$, $\mathbb{C}_{1122}$ and $\mathbb{C}_{2222}$, which are the elasticity tensor components. In addition to the already considered symmetry, the following additional constraints have been imposed:

$$\mathbb{C}_{1111} > 0 \tag{5.40a}$$
$$\mathbb{C}_{2222} > 0 \tag{5.40b}$$
$$\mathbb{C}_{1111}\mathbb{C}_{2222} - (\mathbb{C}_{1122})^2 > 0 \tag{5.40c}$$

which guarantee the positive definiteness of the elasticity tensor. Using the estimated values of $\mathbb{C}_{1111}$, $\mathbb{C}_{1122}$ and $\mathbb{C}_{2222}$, Young's moduli and Poisson's ratios can be obtained as follows:

$$E_1 = \mathbb{C}_{1111} - \frac{(\mathbb{C}_{1122})^2}{\mathbb{C}_{2222}} \tag{5.41a}$$
$$E_2 = \mathbb{C}_{2222} - \frac{(\mathbb{C}_{1122})^2}{\mathbb{C}_{1111}} \tag{5.41b}$$
$$\nu_{21} = \frac{\mathbb{C}_{1122}}{\mathbb{C}_{1111}} \tag{5.41c}$$
$$\nu_{12} = \frac{\mathbb{C}_{1122}}{\mathbb{C}_{2222}} \tag{5.41d}$$

Analogously, the system 5.24, which minimises the objective function written in terms of strain, can be reformulated as follows:

$$\begin{bmatrix} \boldsymbol{\sigma}^m_{\mathbf{11}} \cdot \boldsymbol{\sigma}^m_{\mathbf{11}} & \boldsymbol{\sigma}^m_{\mathbf{11}} \cdot \boldsymbol{\sigma}^m_{\mathbf{22}} & 0 \\ \boldsymbol{\sigma}^m_{\mathbf{11}} \cdot \boldsymbol{\sigma}^m_{\mathbf{22}} & \boldsymbol{\sigma}^m_{\mathbf{11}} \cdot \boldsymbol{\sigma}^m_{\mathbf{11}} + \boldsymbol{\sigma}^m_{\mathbf{22}} \cdot \boldsymbol{\sigma}^m_{\mathbf{22}} & \boldsymbol{\sigma}^m_{\mathbf{11}} \cdot \boldsymbol{\sigma}^m_{\mathbf{22}} \\ 0 & \boldsymbol{\sigma}^m_{\mathbf{11}} \cdot \boldsymbol{\sigma}^m_{\mathbf{22}} & \boldsymbol{\sigma}^m_{\mathbf{22}} \cdot \boldsymbol{\sigma}^m_{\mathbf{22}} \end{bmatrix} \begin{bmatrix} \mathbb{C}^{-1}_{1111} \\ \mathbb{C}^{-1}_{1122} \\ \mathbb{C}^{-1}_{2222} \end{bmatrix} = \\ = \begin{bmatrix} \boldsymbol{\varepsilon}^m_{\mathbf{11}} \cdot \boldsymbol{\sigma}^m_{\mathbf{11}} \\ \boldsymbol{\varepsilon}^m_{\mathbf{11}} \cdot \boldsymbol{\sigma}^m_{\mathbf{22}} + \boldsymbol{\varepsilon}^m_{\mathbf{22}} \cdot \boldsymbol{\sigma}^m_{\mathbf{11}} \\ \boldsymbol{\varepsilon}^m_{\mathbf{22}} \cdot \boldsymbol{\sigma}^m_{\mathbf{22}} \end{bmatrix} \tag{5.42}$$

System 5.42 can be solved analytically or numerically to get the best fitting values (in terms of strain) of $\mathbb{C}^{-1}_{1111}$, $\mathbb{C}^{-1}_{1122}$ and $\mathbb{C}^{-1}_{2222}$, which are the compliance tensor components. Once again the positive definiteness of the compliance tensor is guaranteed by imposition of the following constraints:

$$\mathbb{C}^{-1}_{1111} > 0 \tag{5.43a}$$
$$\mathbb{C}^{-1}_{2222} > 0 \tag{5.43b}$$
$$\mathbb{C}^{-1}_{1111}\mathbb{C}^{-1}_{2222} - (\mathbb{C}^{-1}_{1122})^2 > 0 \tag{5.43c}$$

which guarantee the positive definiteness of the elasticity tensor. Using the estimated values of $\mathbb{C}^{-1}_{1111}$, $\mathbb{C}^{-1}_{1122}$ and $\mathbb{C}^{-1}_{2222}$, Young's moduli and Poisson's ratios can be obtained as follows:

$$E_1 = \frac{1}{\mathbb{C}^{-1}_{1111}} \tag{5.44a}$$
$$E_2 = \frac{1}{\mathbb{C}^{-1}_{2222}} \tag{5.44b}$$
$$\nu_{21} = -\frac{\mathbb{C}^{-1}_{1122}}{\mathbb{C}^{-1}_{2222}} \tag{5.44c}$$
$$\nu_{12} = -\frac{\mathbb{C}^{-1}_{1122}}{\mathbb{C}^{-1}_{1111}} \tag{5.44d}$$

The MSAJ/M-02:1995 Standard recommends disregarding warp data for the 0:1 load ratio and fill data for the 1:0 load ratio because they results in errors if a differential solution method (e.g. the analytical approach previously described) is used to minimise the objective function. However, as pointed out by Bridgens & Gosling (2010), these load ratios are relevant for membrane structure design, because anticlastic membranes becomes highly tensioned in one direction and almost slack in the other if subjected to extreme load conditions. To obviate the removal of part of the data, the minimisation should be carried out with a numerical method that does not require the computation of the objective function derivatives, e.g. the *patternsearch* algorithm employed by Bridgens & Gosling (2010). Both the differential solution (DS) and patternsearch (PS) methods have been employed in this thesis in order to compare the discrepancy between the results obtained with the two methods.

More in detail, the numerical minimisation has been performed using the *patternsearch* algorithm available in MATLAB. Pattern search is a family of numerical optimisation methods that do not require the gradient of the problem to be optimised. These methods finds a local minimum by the

following procedure, which is called *polling*. The search starts at an initial point (i.e. the vector containing the initial guess of the elastic moduli values). In the first step the current point is set coincident to the initial point, then:

1. A pattern of points is generated, which is centered on the current point. This is typically plus and minus the coordinate directions, times a mesh size.

2. The objective function is evaluated at each point in the pattern.

3. If the objective function value at some point in the pattern is lower than the value at the current point, then the poll is successful, and the following happens:

   (a) The minimum point becomes the current point.

   (b) The mesh size is incremented (usually it is doubled).

   (c) The algorithm proceeds from Step 1.

4. If the poll is not successful, then the following happens:

   (a) The mesh size is reduced (usually it is halved).

   (b) If the mesh size is below a threshold, the iterations stop.

   (c) Otherwise, the current point is retained, and the algorithm proceeds from Step 1.

Using the methods previously described, calibration of the OLE model has been performed on the experimental data from the following biaxial tests (see Section 4.2):

- **Test A**: B18089 MSAJ;
- **Test B**: B18059 ALR;
- **Test C**: F702 MSAJ;
- **Test D**: F1202T2 ALR;
- **Test E**: VUB 001 A.

As described in Section 4.2.2, tests A-B have been performed on PTFE coated glass fabrics, while tests C-E have been performed on a PVC coated polyester fabric. Only the first loading curves have been considered for each load ratio. The residual strain and the prestress have been removed at the beginning of each load ratio of interest. This is possible because the fabric is in a known state of crimp and stress, which is the one setted by the conditioning cycles. Therefore, the calibrated OLE model will approximate the elastic behaviour of the membrane when it is loaded starting from this known reference state. For each loading curve, a number of 21 experimental points equally spaced in time have been considered. This reduction in the number of data points with respect to the measured ones facilitates the identification procedure, since it reduces both the time required for the calculations and the measurement noise, without loosing information about the stress-strain curve trend.

	Test	$\mathbf{E_1}$	$\mathbf{E_2}$	$\boldsymbol{\nu_{21}}$	$\boldsymbol{\nu_{12}}$	RSS
		[kN/m]	[kN/m]	[1]	[1]	[kN^2/m^2]
DS	A	2498	1545	0.33	0.53	8.30E+03
	B	2604	1825	0.46	0.66	1.13E+04
	C	555	494	0.23	0.26	1.40E+02
	D	970	969	0.24	0.24	7.06E+02
	E	852	400	0.09	0.19	1.61E+03
PS	A	3417	1931	0.31	0.55	3.13E+05
	B	2016	1234	0.39	0.65	1.18E+05
	C	442	396	0.40	0.45	5.71E+02
	D	564	807	0.57	0.40	4.22E+03
	E	560	346	0.28	0.45	2.64E+03

Table 5.1: *Values of the elastic moduli obtained by minimising the objective function written in terms of stress and employing both the differential solution (DS) and pattern search (PS) methods.*

Table 5.1 shows the results of the identification procedure carried out with the objective function written in terms of stress. For each test the table reports the estimated values of the elastic parameters and the value assumed by the Residual Sum of Squares (RSS), which is a measure of the

quality of fit defined as follows:

$$\mathrm{RSS} = \sum_{i=1}^{N} (Y_i^c - Y_i^m)^2 \tag{5.45}$$

where N is the number of experimental points, Y_i^m are the measured values (of stress, in this case), and Y_i^c are the corresponding calculated values, which are predicted using the estimated values of the model parameters. In the present context, RSS assumes the same value of the objective function in Equation (5.17) when evaluated at the solution point. Both the results obtained with the differential solution (with removal of 0:1 warp and 1:0 fill data) and patternsearch (no data removal) methods are presented.

First of all, looking at Table 5.1, it can be noticed that Young's moduli of PTFE/glass fabrics (tests A and B) resulted to be greater that the ones of PVC/polyester fabrics (tests C to E). This result was expected, since glass fibres are initially more crimped than polyester yarns (Figure 4.33) and this causes an apparent higher tensile stiffness during the crimp interchange. Moreover, glass is notoriously stiffer than polyester, therefore the trend is confirmed also at large strains, when the crimp interchange has been completed. In additon, the difference between the warp (E_1) and weft (E_2) Young's moduli is lower for tests C and D, which are performed on PVC/polyester fabrics produced with Précontraint® technology. Indeed, this method of production is intended to reduce the level of anisotropy of the coated textile (see Section 4.1.1).

In Table 5.1, there are some cases of Poisson's ratio greater than 0.5: these are indispensable to model the strong interaction between warp and fill threads, which causes large negative strains in the woven fabric under some biaxial loads. Moreover, values of Poisson's ratio in excess of 0.5, or even larger than 1, are common for composites (see, e.g., Sun & Sacks, 2005; Peel, 2007; Uhlemann et al., 2014). As it is well known, such values of this parameter are thermodinamically inadmissible for isotropic materials, because they lead to negative strain energy under certain loads. However, Lempriere (1968) demonstrated that the limit of Poisson's ratio smaller than 0.5 does not hold for orthotropic materials. In that case, the aforementioned thermodynamic constraint, which is equivalent to the positive definitiveness of the elasticity matrix, is expressed by the following

constraints on the elastic moduli (plane stress assumption):

$$E_1, E_2, G_{12} > 0 \tag{5.46a}$$

$$|\nu_{21}| - (E_2/E_1)^{1/2} < 0 \tag{5.46b}$$

$$|\nu_{12}| - (E_1/E_2)^{1/2} < 0 \tag{5.46c}$$

$$0 < \frac{1}{2}[1 - \nu_{21}^2(E_1/E_2)] < \frac{1}{2} \tag{5.46d}$$

These constraints are all satisfied by the material parameters in Table 5.1, hence the thermodynamic requirements are not violated.

Concerning the comparison between the differential solution and the pattern search methods, the last one generally estimated slightly lower values of Young's moduli and higher values of Poisson's ratios. This result is opposite to the one obtained by Bridgens & Gosling (2010), but in that article the fitting was performed by minimising an objective function written in terms of strain, so that a direct comparison is not possible. In Bridgens & Gosling (2010), as well as in this thesis, the pattern search method produced higher values of RSS, which means a worse quality of fit. However, the differential solution is only apparently better, since it improves the correlation by neglecting part of the experimental data.

Figures 5.12 to 5.16 show the comparison between the calibrated OLE model stress-strain curves and the experimental data. These graphics are useful to check the quality of the fit. It can be noticed that the OLE model can reproduce satisfactorily the mechanical behaviour of PVC coated polyester fabrics (tests C and D), but is unsuitable to model the behaviour of PTFE coated glass fabrics (tests A and B), which show a higher degree of nonlinearity due to the more severe crimp of glass yarns. This fact is confirmed by the extreme sensibility of the numerical solution (i.e. the elastic moduli values) to the choice of the initial guess employed to start the pattern search algorithm.

Despite the fact that the OLE model is usually easier to calibrate in the case of PVC/polyester fabrics, Figure 5.16 seems to contradict this statement. The result is confirmed by the high objective function values shown in Table 5.1 for each identification method applied to test E. The cause is in the testing procedure, since test E was performed without preconditioning cycles. This highlights again the extreme importance of preconditioning to obtain repeatable stress-strain curves and to create a unique initial refer-

ence state (in terms of crimp and prestress) for each loading cycle that will be employed in the calibration procedure.

Finally, Figures 5.12 to 5.16 show that the pattern search method does not improve appreciably the quality of the fit with respect to the differential solution: the curves with positive strain are worse approximated, while no significant improvement in the fitting of the curves with negative strain is obtained. This is the reason why the differential solution identification is employed in the following chapters for the comparison with the new model presented in Chapter 6.

Although the identification results obtained with the objective function written in terms of strains are not reported, the same considerations can be made. The strain approach usually results in a better fit, but is not applicable for nonlinear constitutive models, which are not invertible. Since the new model presented in Chapter 6 is nonlinear, only the stress approach can be employed in its calibration. An attempt of using the objective function written in terms of strains was made, but it was too computationally expensive, since an iterative algorithm was required for the computation of the strains values at each point and for each trial value of the model parameters. Therefore only the OLE model calibrated with the stress approach, which has already been presented, will be used later for comparison.

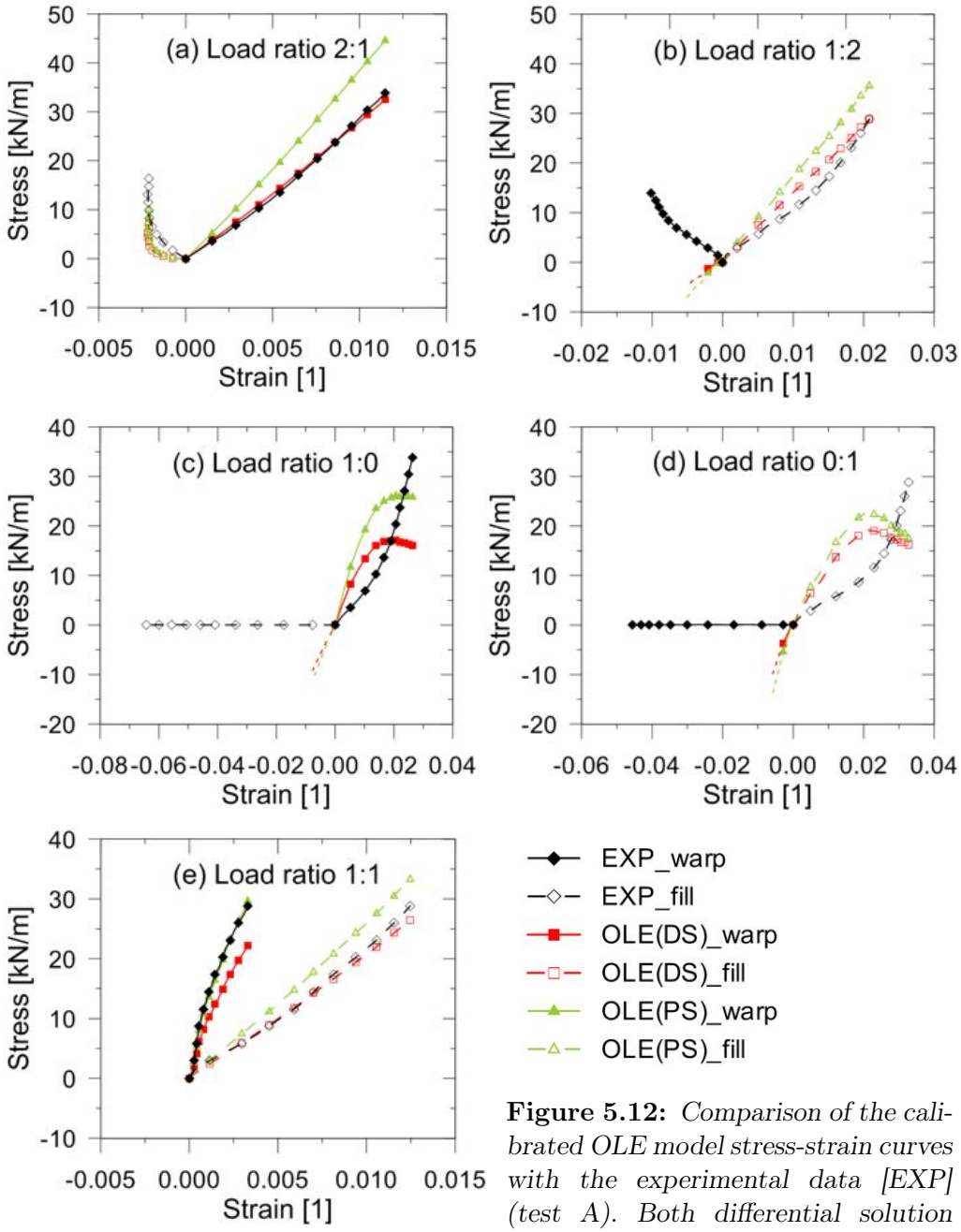

Figure 5.12: *Comparison of the calibrated OLE model stress-strain curves with the experimental data [EXP] (test A). Both differential solution [OLE(DS)] and pattern search solution [OLE(PS)] are displayed.*

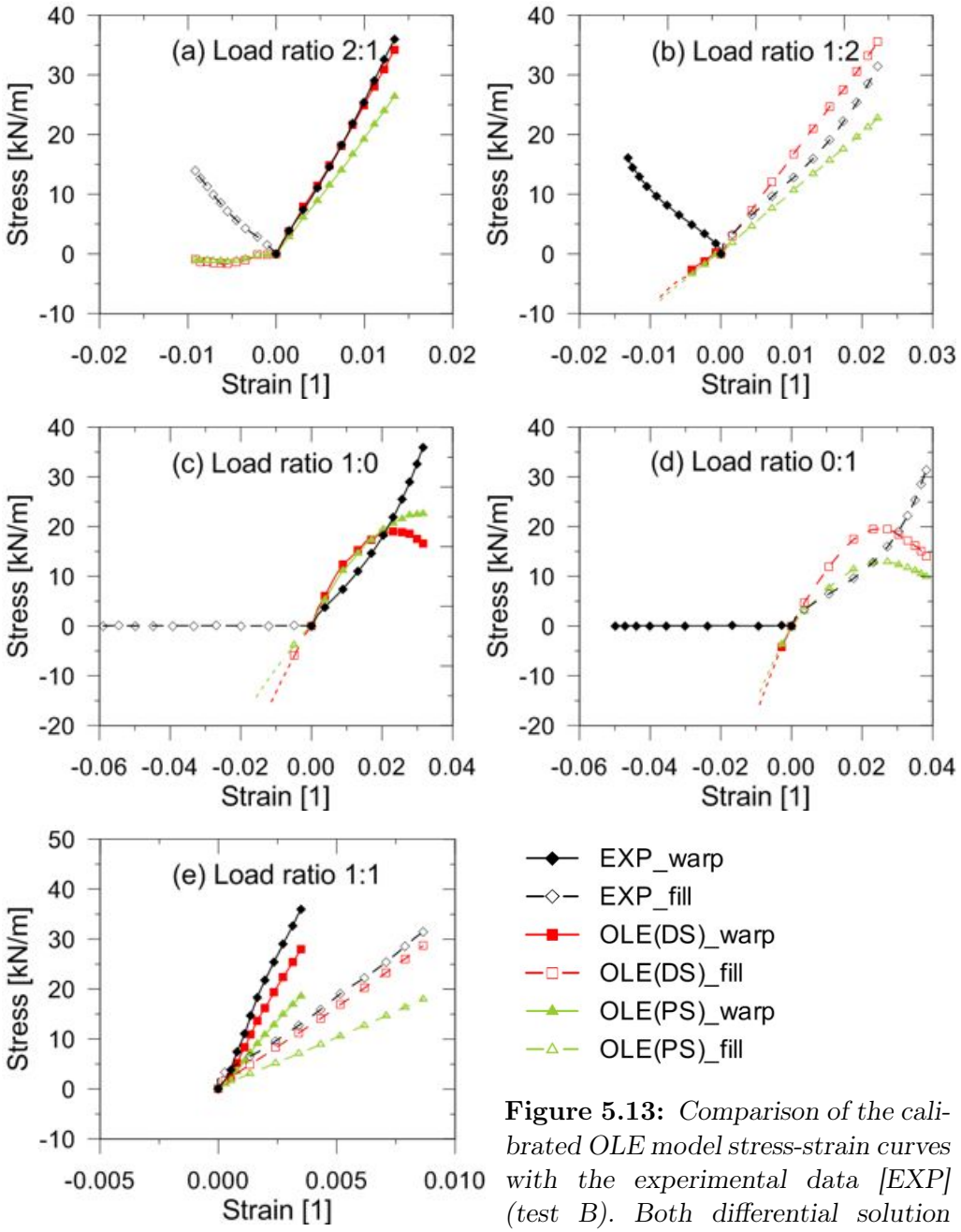

Figure 5.13: *Comparison of the calibrated OLE model stress-strain curves with the experimental data [EXP] (test B). Both differential solution [OLE(DS)] and pattern search solution [OLE(PS)] are displayed.*

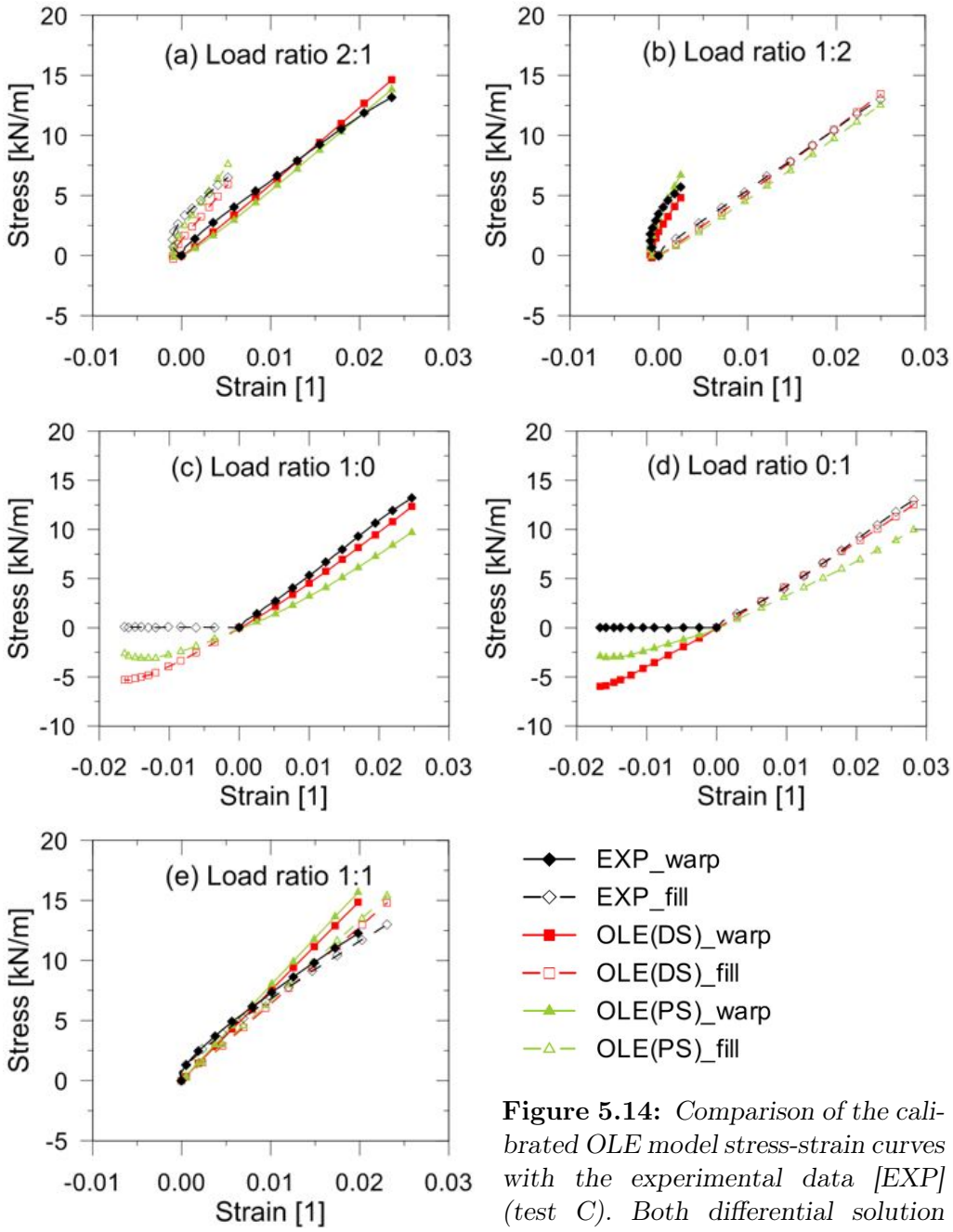

Figure 5.14: *Comparison of the calibrated OLE model stress-strain curves with the experimental data [EXP] (test C). Both differential solution [OLE(DS)] and pattern search solution [OLE(PS)] are displayed.*

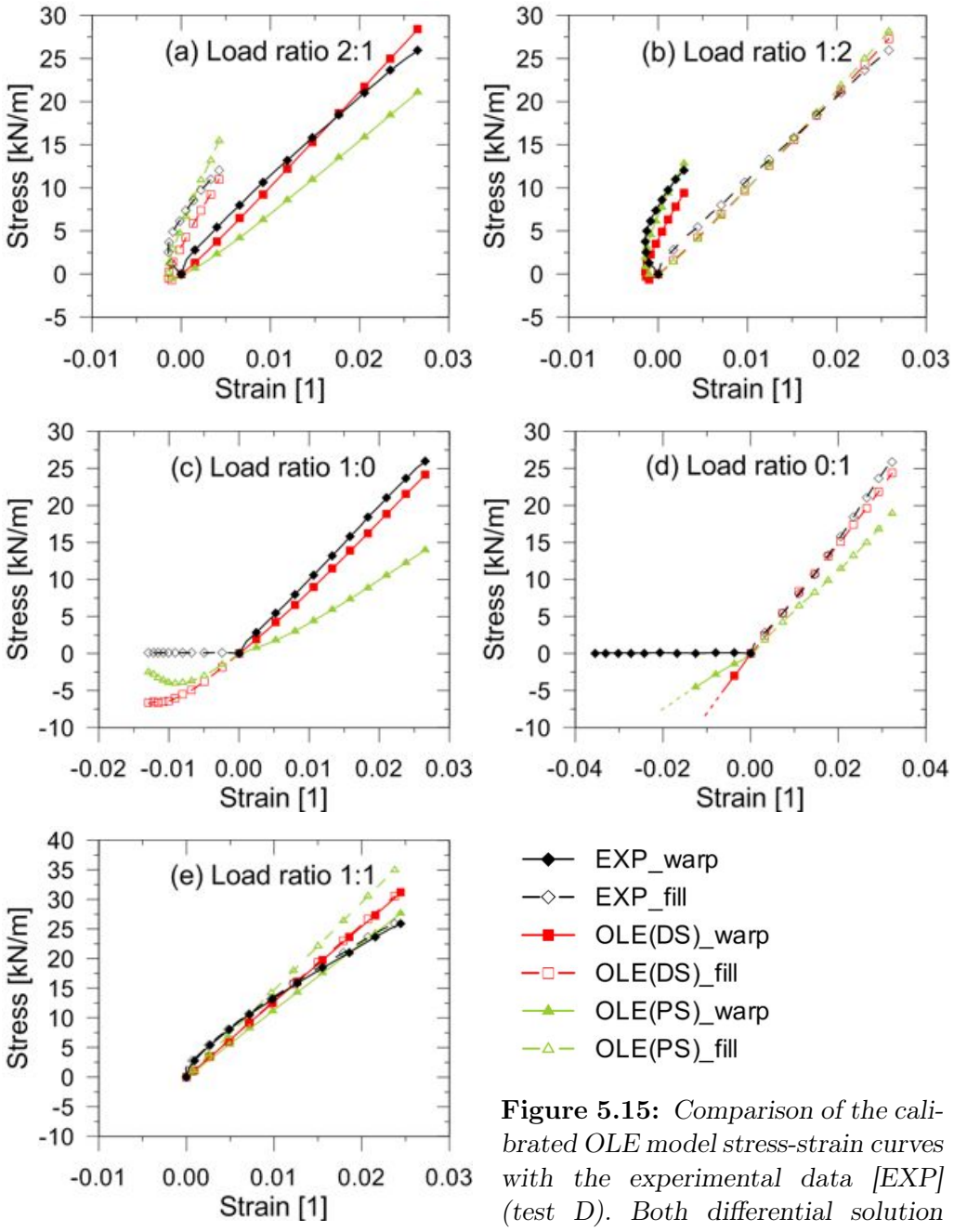

Figure 5.15: *Comparison of the calibrated OLE model stress-strain curves with the experimental data [EXP] (test D). Both differential solution [OLE(DS)] and pattern search solution [OLE(PS)] are displayed.*

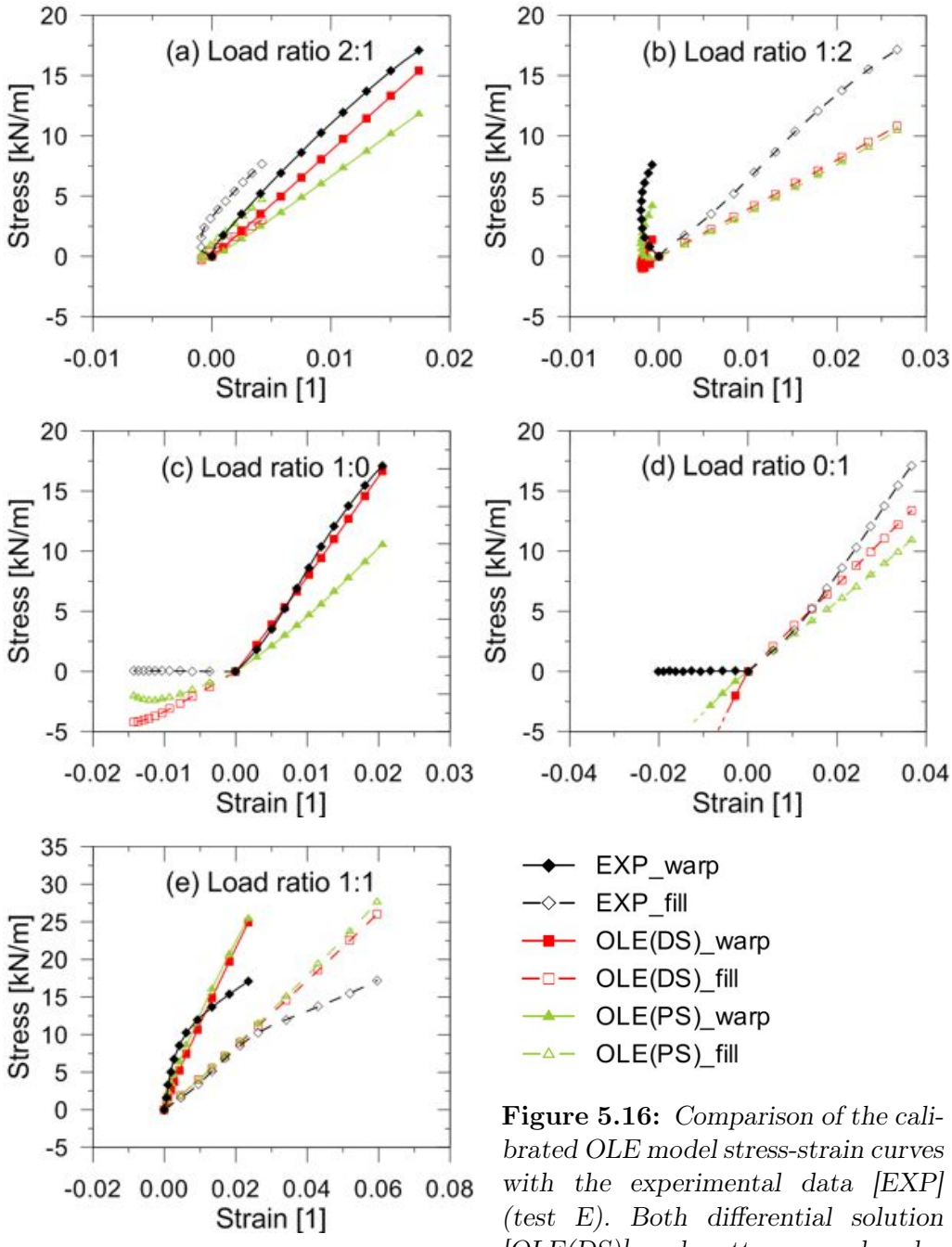

Figure 5.16: *Comparison of the calibrated OLE model stress-strain curves with the experimental data [EXP] (test E). Both differential solution [OLE(DS)] and pattern search solution [OLE(PS)] are displayed.*

6

A new hyperelastic constitutive model for coated fabrics at finite strains

Coated fabrics experience large deformations when subjected to uniaxial loading. Moreover, in the biaxial tests described in Section 4.2.2, engineering strains that are higher than 2 % have been measured; by considering that the applied loads were only up to one fourth of the ultimate tensile strength of the tested materials, it can be easily understood that coated fabrics should be realistically modelled within a large strain framework.

This aspect is well-known in the field of forming analyses. In fact, during the forming process, the fabric reinforcement undergoes large displacements and large strains, both in terms of extension and of modification of the angle between the yarns. Hyperelastic modelling at finite strains has been claimed to be particularly suitable to model anisotropic large displacement behaviour (Vidal-Sallé et al., 2014). It has been recently successfully employed in forming analyses of raw fabrics (Aimene et al., 2008, 2009; Boisse et al., 2010; Charmetant et al., 2011, 2012).

Nevertheless, on the top of the author's knowledge, this kind of approach has not been applied to coated fabrics yet, at least in the structural field, as it has emerged from the literature review on constitutive models reported in Chapter 5. In this Chapter, a new hyperelastic constitutive model for coated fabrics is presented.

First, the framework of nonlinear continuum mechanics is briefly summarised in Section 6.1. Then, the Holzapfel-Gasser-Ogden (HGO) hyperelastic constitutive model for soft tissues, which is based on Spencer's theory

for strongly anisotropic solids (described in Section 6.2), is chosen as suitable to model coated woven fabrics mechanical behaviour. Details about HGO model are provided in Section 6.3. After that, HGO model is modified, to account for the strong interaction between warp and fill directions due to the weaving, and the effects of such modification are illustrated (Section 6.4). Finally, in Section 6.5, the parameters of the new proposed model are estimated for different materials, through the use of experimental biaxial test results from Section 4.2.2.

6.1 Nonlinear continuum mechanics framework

In this section a framework of continuum mechanics at large strains is briefly presented in order to introduce the notation to be used subsequently. For a more extensive treatment of this topic the reader is referred e.g. to the books of Holzapfel (2000), Ogden (2003) and Gurtin et al. (2010).

6.1.1 Kinematics and strain measures

A body $\mathcal{B}$ embedded in a three-dimensional Euclidean space is considered (Figure 6.1). According to the continuum or macroscopic approach, a body $\mathcal{B}$ is conceived as a continuous (or at least piecewise continuous) distribution of matter in space and time and is composed by a set of particles $P \in \mathcal{B}$, which are named material points. The position of each particle in the Euclidean space can be described by means of a position vector, whose components are expressed with respect to a reference frame: this consists in an orthonormal right-handed basis, centered at a fixed origin O, whose unit basis vectors are labeled $\mathbf{e}_i,\ i = 1, 2, 3$.

At time $t = 0$ the considered body occupies a region Ω_0, named initial configuration. The initial configuration of a body is usually assumed to be the undeformed or reference (fixed) configuration. Then the body moves from Ω_0 to occupy a region Ω at time t: this is named current or deformed configuration. Consequently, the generic particle $P \in \mathcal{B}$ moves from the point described by the reference position vector $\mathbf{X}$ to the one described by the current position vector $\mathbf{x}$. The two position vectors can be expressed as $\mathbf{X} = X_I \mathbf{E}_I$ and $\mathbf{x} = x_i \mathbf{e}_i$, where X_I and x_i are the material (or referential) and the spatial (or current) coordinates, respectively. More in general,

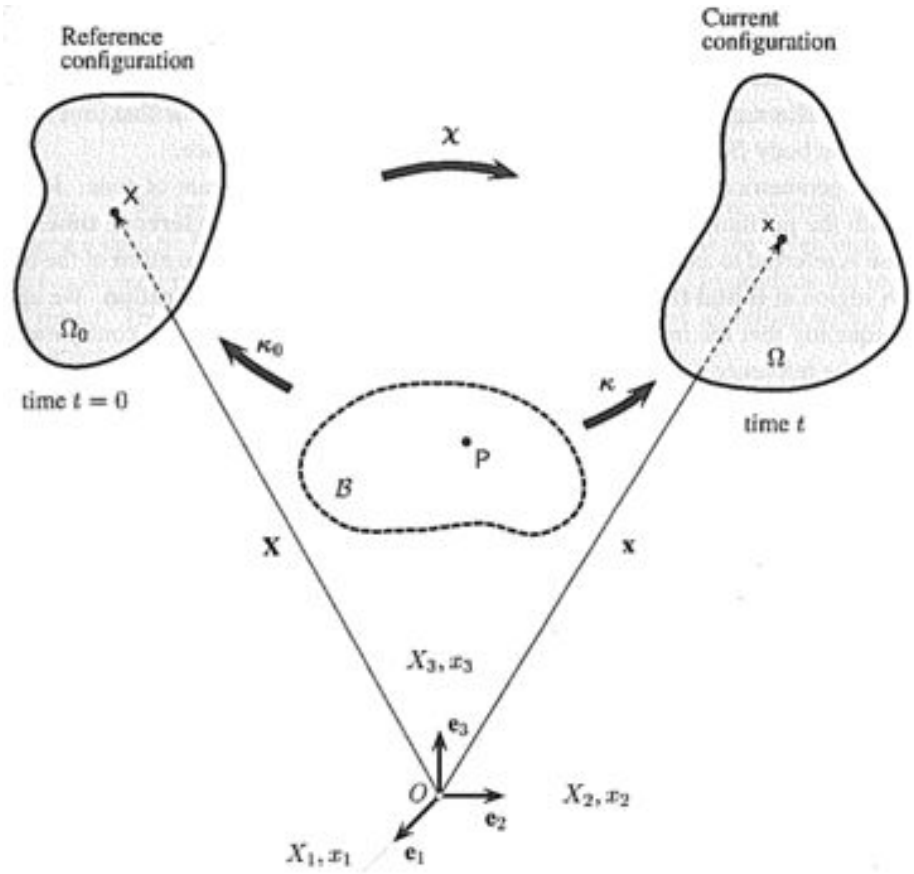

Figure 6.1: *Configuration and motion of a continuum body (from Holzapfel, 2000).*

all the quantities that are referred to the reference configuration are called material (Lagrangian description of motion), whereas all the quantities that are expressed with respect to the current configuration are named spatial (Eulerian description of motion). When possible, upper case letters will be employed for material quantities and lower case letters for spatial quantities. For the sake of simplicity, the same reference frame is employed in the following for both the referential and current configurations ($\mathbf{E}_i = \mathbf{e}_i$), so that $\mathbf{X} = X_I \mathbf{E}_I = X_I \mathbf{e}_i$.

The so called motion of body $\mathcal{B}$ is the vector field $\boldsymbol{\chi}$ that defines the

spatial position $\mathbf{x}$ for all $\mathbf{X} \in \Omega_0$ and at all times t:

$$\mathbf{x} = \boldsymbol{\chi}(\mathbf{X}, t) \ , \qquad x_i = \chi_i(X_1, X_2, X_3, t) \tag{6.1}$$

Displacement, velocity and acceleration vector fields can be derived starting from the body motion. Moreover, the motion of a body will generally change its position and orientation, in addition to its size and shape. A time-independent motion $\boldsymbol{\chi}$ is called deformation and it characterises the change in shape and size of a deformable body.

The most important measure of deformation in Continuum Mechanics is the deformation gradient, which is defined as follows:

$$\mathbf{F}(\mathbf{X}, t) = \frac{\partial \boldsymbol{\chi}(\mathbf{X}, t)}{\partial \mathbf{X}} = \operatorname{Grad} \mathbf{x}(\mathbf{X}, t) \ , \qquad F_{iI} = \frac{\partial \chi_i}{\partial X_I} = \frac{\partial x_i}{\partial X_I} \tag{6.2}$$

The deformation gradient is a second-order non-symmetric tensor, which linearly maps a material tangent vector $\mathrm{d}\mathbf{X}$ into a spatial tangent vector $\mathrm{d}\mathbf{x}$. It is a two-point tensor as it involves both the reference and current configurations, therefore it has one material coordinate index (uppercase I) and one spatial coordinate index (lowercase i). The determinant of the deformation gradient measures the change in volume between the reference and the current configuration at time t. Thus, it is called volume ratio or Jacobian determinant:

$$\mathrm{d}v = J(\mathbf{X}, t)\mathrm{d}V \tag{6.3}$$

with:

$$J(\mathbf{X}, t) = \det \mathbf{F}(\mathbf{X}, t) > 0 \tag{6.4}$$

At each point $\mathbf{X} \in \Omega_0$ and each time t, the deformation gradient $\mathbf{F}$ admits a unique polar decomposition:

$$\mathbf{F} = \mathbf{R}\mathbf{U} = \mathbf{v}\mathbf{R} \ , \qquad F_{iI} = R_{iJ}U_{JI} = v_{ij}R_{jI} \tag{6.5}$$

In Equation (6.5), $\mathbf{U}$ and $\mathbf{v}$ are unique, positive definite, symmetric tensors, which are named right (or material) stretch tensor and left (or spatial) stretch tensor, respectively. They represent a measure of the local stretching along the directions defined by their eigenvectors. $\mathbf{R}$ is a proper orthogonal two-point tensor, having properties $\det \mathbf{R} = 1$ and $\mathbf{R}^{\mathrm{T}}\mathbf{R} = \mathbf{R}\mathbf{R}^{\mathrm{T}} = \mathbf{I}$, which is called rotation tensor, because it represents a local rotation. The mutually orthogonal and normalised eigenvectors of $\mathbf{U}$ are the material

principal directions of strain, which are rotated through tensor $\mathbf{R}$ onto the corresponding spatial principal directions of strain, namely the mutually orthogonal and normalised eigenvectors of $\mathbf{v}$. Moreover, $\mathbf{U}$ and $\mathbf{v}$ share the same eigenvalues, which are the principal stretches. Since the stretch tensors are measures of pure deformation, they can be used to define strain tensors.

While displacements are measurable, strains are calculated quantities introduced to perform deformation analysis. Hence, several strain tensors have been proposed in the literature. Every strain measure should be objective, thus accounting for only relative lengths and angles changes, neglecting rigid body movements. Strain tensors that meet this requirement can be expressed in the Lagrangian and Eulerian description as:

$$\boldsymbol{\Lambda} = \log \mathbf{U} \qquad \boldsymbol{\lambda} = \log \mathbf{v} \qquad \text{if } n = 0 \tag{6.6}$$

$$\boldsymbol{\Lambda} = \frac{1}{n}(\mathbf{U}^n - \mathbf{I}) \qquad \boldsymbol{\lambda} = \frac{1}{n}(\mathbf{v}^n - \mathbf{I}) \qquad \text{if } n \neq 0 \tag{6.7}$$

where $\mathbf{I}$ is the second-order identity tensor. From Equation (6.7), setting $n = 2$ one obtains the material Green-Lagrange strain tensor:

$$\mathbf{E} = \frac{1}{2}(\mathbf{U}^2 - \mathbf{I}) = \frac{1}{2}(\mathbf{F}^{\mathrm{T}}\mathbf{F} - \mathbf{I}) \ , \qquad E_{IJ} = \frac{1}{2}(F_{iI}F_{iJ} - \delta_{IJ}) \tag{6.8}$$

where the product:

$$\mathbf{C} = \mathbf{U}^2 = \mathbf{F}^{\mathrm{T}}\mathbf{F} \ , \qquad C_{IJ} = F_{iI}F_{iJ} \tag{6.9}$$

is named right Cauchy-Green strain tensor. Both $\mathbf{E}$ and $\mathbf{C}$ are second-order symmetric tensors. Again, from Equation (6.7), setting $n = -2$ one obtains the spatial Euler-Almansi strain tensor:

$$\mathbf{e} = \frac{1}{2}(\mathbf{I} - \mathbf{v}^{-2}) = \frac{1}{2}(\mathbf{I} - \mathbf{F}^{-\mathrm{T}}\mathbf{F}^{-1}) \ , \qquad e_{ij} = \frac{1}{2}(\delta_{ij} - F^{-1}_{Ii}F^{-1}_{Ij}) \tag{6.10}$$

where the product:

$$\mathbf{b} = \mathbf{v}^2 = \mathbf{F}\mathbf{F}^{\mathrm{T}} \ , \qquad b_{ij} = F_{iI}F_{jI} \tag{6.11}$$

is named left Cauchy-Green (or Finger) strain tensor. Both $\mathbf{e}$ and $\mathbf{b}$ are second-order symmetric tensors.

Tensor type	**Push-forward**	**Pull-back**
1st-order covariant	$\boldsymbol{\chi}_*(\bullet)^\flat = \mathbf{F}^{-\mathrm{T}}(\bullet)^\flat$	$\boldsymbol{\chi}_*^{-1}(\bullet)^\flat = \mathbf{F}^{\mathrm{T}}(\bullet)^\flat$
1st-order contravariant	$\boldsymbol{\chi}_*(\bullet)^\sharp = \mathbf{F}(\bullet)^\sharp$	$\boldsymbol{\chi}_*^{-1}(\bullet)^\sharp = \mathbf{F}^{-1}(\bullet)^\sharp$
2nd-order covariant	$\boldsymbol{\chi}_*(\bullet)^\flat = \mathbf{F}^{-\mathrm{T}}(\bullet)^\flat\mathbf{F}^{-1}$	$\boldsymbol{\chi}_*^{-1}(\bullet)^\flat = \mathbf{F}^{\mathrm{T}}(\bullet)^\flat\mathbf{F}$
2nd-order contravariant	$\boldsymbol{\chi}_*(\bullet)^\sharp = \mathbf{F}(\bullet)^\sharp\mathbf{F}^{\mathrm{T}}$	$\boldsymbol{\chi}_*^{-1}(\bullet)^\sharp = \mathbf{F}^{-1}(\bullet)^\sharp\mathbf{F}^{-\mathrm{T}}$

Table 6.1: *Push-forward and pull-back operators.*

When a Lagrangian approach is used, it is always possible to obtain the spatial tensors associated to the material ones by means of the so called "push-forward" operation. Analogously, when an Eulerian approach is employed, the material tensors associated with the spatial ones can be calculated with a "pull-back" operation. Table 6.1 summarises the push-forward and pull-back operators to be applied on covariant and contravariant[1] tensors of first (vectors) and second order. For example, the Euler-Almansi strain tensor can be obtained with a push-forward operation applied on the covariant tensor $\mathbf{E}$:

$$\mathbf{e} = \boldsymbol{\chi}_*(\mathbf{E}^\flat) = \mathbf{F}^{-\mathrm{T}}\mathbf{E}\mathbf{F}^{-1} = \frac{1}{2}(\mathbf{I} - \mathbf{F}^{-\mathrm{T}}\mathbf{F}^{-1}) \tag{6.12}$$

Analogously, the Green-Lagrange strain tensor can be obtained with a pull-back operation on the covariant tensor $\mathbf{e}$:

$$\mathbf{E} = \boldsymbol{\chi}_*^{-1}(\mathbf{e}^\flat) = \mathbf{F}^{\mathrm{T}}\mathbf{e}\mathbf{F} = \frac{1}{2}(\mathbf{F}^{\mathrm{T}}\mathbf{F} - \mathbf{I}) \tag{6.13}$$

The push-forward and pull-back operations are applicable also on the stress tensor fields presented in the following section.

Finally, a decomposition of the deformation gradient other than the one in Equation (6.5) considers a multiplicative split of $\mathbf{F}$ into a dilatational

[1] Notation: covariant tensors are labeled with $\flat$, whereas contravariant tensors are labeled with $\sharp$. In the following chapters covariant strain tensors will be used in combination with contravariant stress tensors.

(volume-changing) and a distortional (volume-preserving) part:

$$\mathbf{F} = (J^{1/3}\mathbf{I})\overline{\mathbf{F}} = J^{1/3}\overline{\mathbf{F}} \tag{6.14}$$

where $J^{1/3}\mathbf{I}$ is associated to the volume-change deformation, while $\overline{\mathbf{F}}$, which is called modified deformation gradient, is such that $\det\overline{\mathbf{F}} = 1$ (volume-preserving). Tensors $\mathbf{C}$ and $\mathbf{b}$ can be decomposed analogously:

$$\mathbf{C} = (J^{2/3}\mathbf{I})\overline{\mathbf{C}} = J^{2/3}\overline{\mathbf{C}} \tag{6.15}$$

$$\mathbf{b} = (J^{2/3}\mathbf{I})\overline{\mathbf{b}} = J^{2/3}\overline{\mathbf{b}} \tag{6.16}$$

where $\overline{\mathbf{C}}$ and $\overline{\mathbf{b}}$ are named modified right and left Cauchy-Green tensors, respectively, and J is once again the volume ratio defined in Equation (6.3). This split is particularly useful for materials that behave quite differently for the bulk and shear response components. According to the definition of Holzapfel (2000), a material for which dilational changes require much higher external work than volume-preserving changes is called nearly incompressible.

6.1.2 Stress measures

In order to introduce the concepts of traction vector and stress, the deformable body $\mathcal{B}$, whose motion has been described in the previous section, is thought to be cut into two pieces in both the reference and current configurations (Figure 6.2). Let $\mathbf{x}$ be a point lying on one of the two opposite surfaces generated by the cutting in the spatial configuration Ω. Point $\mathbf{x}$ is surrounded by an infinitesimal spatial surface element $\mathrm{d}s \in \partial\Omega$ having outward normal $\mathbf{n}$. The material quantities corresponding to $\mathbf{x}$, $\mathrm{d}s$ and $\mathbf{n}$ are $\mathbf{X}$, $\mathrm{d}S$ and $\mathbf{N}$.

Since the two parts of the body interacts, forces are transmitted across the corresponding internal surfaces. The infinitesimal resultant force $\mathrm{d}\mathbf{f}$ acting on the infinitesimal surface element can be calculated with the following relationship:

$$\mathrm{d}\mathbf{f} = \mathbf{t}\mathrm{d}s = \mathbf{T}\mathrm{d}S \tag{6.17}$$

Omitting the distributed resultant couples (non-polar continuum), the Cauchy traction vector $\mathbf{t}$ and the first Piola-Kirchhoff traction vector $\mathbf{T}$ must satisfy the Cauchy's postulate, which states that the surface traction ($\mathbf{t}$ or $\mathbf{T}$)

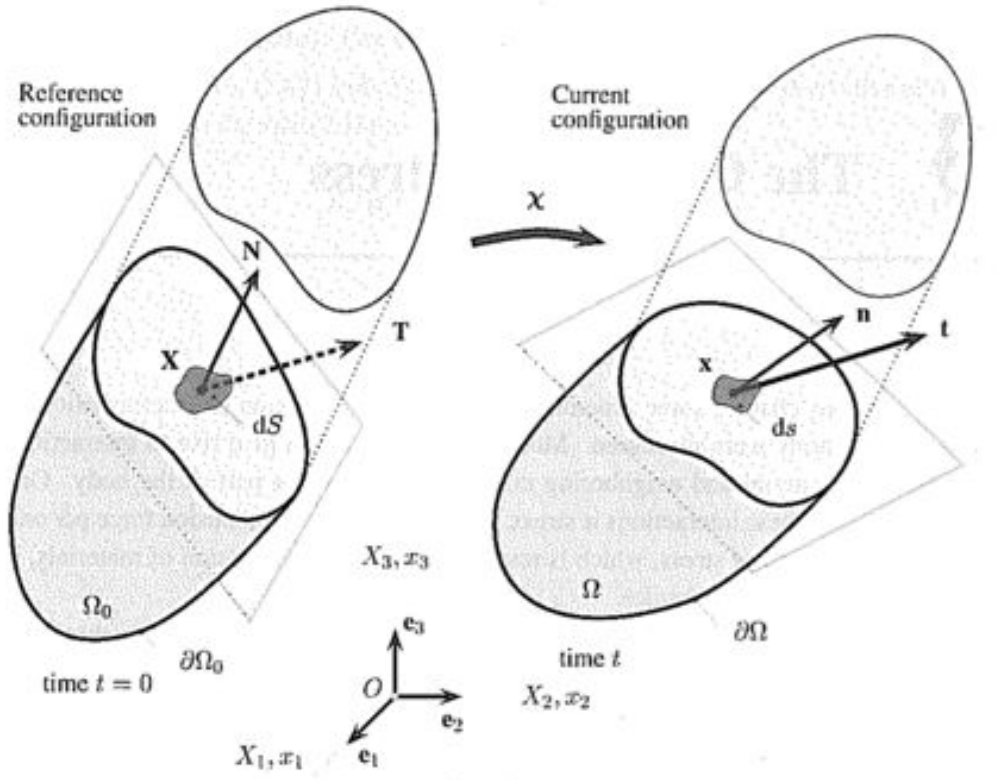

Figure 6.2: *Traction vectors acting on infinitesimal surface elements with outward unit normals (from Holzapfel, 2000).*

at a point ($\mathbf{x}$ or $\mathbf{X}$) depends on the surface ($\mathrm{d}s$ or $\mathrm{d}S$) on which the point lies only through the oriented unit normal ($\mathbf{n}$ or $\mathbf{N}$) of the surface itself at the considered point:

$$\mathbf{t} = \mathbf{t}(\mathbf{x}, t, \mathrm{d}s) = \mathbf{t}(\mathbf{x}, t, \mathbf{n}) \tag{6.18}$$

$$\mathbf{T} = \mathbf{T}(\mathbf{X}, t, \mathrm{d}S) = \mathbf{T}(\mathbf{X}, t, \mathbf{N}) \tag{6.19}$$

Vector $\mathbf{T}$ has the same direction of its spatial counterpart $\mathbf{t}$, but it measures the force per unit reference area $\mathrm{d}S$.

The second-order stress tensors $\boldsymbol{\sigma}$ and $\mathbf{P}$ are defined through the Cauchy's theorem, which states that there exist unique $\boldsymbol{\sigma}$ and $\mathbf{P}$ such that:

$$\mathbf{t}(\mathbf{x}, t, \mathbf{n}) = \boldsymbol{\sigma}(\mathbf{x}, t)\mathbf{n} \quad , \qquad t_i = \sigma_{ij} n_j \tag{6.20}$$

$$\mathbf{T}(\mathbf{X}, t, \mathbf{N}) = \mathbf{P}(\mathbf{X}, t)\mathbf{N} \ , \qquad T_i = P_{iJ}N_J \tag{6.21}$$

The spatial tensor $\boldsymbol{\sigma}$ is called Cauchy (or true) stress tensor and is symmetric as a consequence of the balance of angular momentum: its eigenvalues are the principal stresses and its eigenvectors the principal directions of stress. Moreover, its columns represent the traction vectors acting on planes perpendicular to the reference system versors. The two-point tensor $\mathbf{P}$ is named first Piola-Kirchhoff stress tensor and is not symmetric, in general. Tensors $\boldsymbol{\sigma}$ and $\mathbf{P}$ are related through the Piola transformation:

$$\mathbf{P} = J\boldsymbol{\sigma}\mathbf{F}^{-\mathrm{T}} \ , \qquad P_{iI} = J\sigma_{ij}F^{-1}_{Ij} \tag{6.22}$$

Many other stress tensors have been proposed in the literature, which not always admit a physical interpretation in terms of surface traction but show advantages when used in nonlinear analyses. Among the spatial stress tensors, it is often convenient to work with the symmetric Kirchhoff stress tensor $\boldsymbol{\tau}$, which is defined as:

$$\boldsymbol{\tau} = J\boldsymbol{\sigma} \ , \qquad \tau_{ij} = J\sigma_{ij} \tag{6.23}$$

The pull-back operation on the contravariant tensor field $\boldsymbol{\tau}$ gives the material second Piola-Kirchhoff stress tensor:

$$\mathbf{S} = \boldsymbol{\chi}_*^{-1}(\boldsymbol{\tau}^\sharp) = \mathbf{F}^{-1}(\boldsymbol{\tau})\mathbf{F}^{-\mathrm{T}} \ , \qquad S_{IJ} = F^{-1}_{Ii}\tau_{ij}F^{-1}_{Jj} \tag{6.24}$$

The second Piola-Kirchhoff stress tensor is a symmetric second-order material tensor. It is related to the first Piola-Kirchhoff stress tensor through the following expression:

$$\mathbf{P} = \mathbf{F}\mathbf{S} \ , \qquad P_{iI} = F_{iJ}S_{JI} \tag{6.25}$$

Other definitions of stress tensors exist, which are not recalled here. The reader is referred to the previously mentioned books by Holzapfel (2000), Ogden (2003) and Gurtin et al. (2010) for further insight.

6.2 Constitutive theory for strongly anisotropic solids

In Spencer (1984), a theoretical framework for the constitutive modelling of the so-called *strongly anisotropic materials* at large strains is described.

Spencer focused on composite materials that are composed by a matrix with oriented reinforcing fibres: this results in material mechanical properties that are highly dependent on direction. Even if in that case the source of anisotropy has to be identified with the systematic arrangement of fibres, the main ideas discussed by the author are applicable to strongly anisotropic materials in general sense. Specifically, the fact that Spencer's formulation is based on the presence of fibres drowned in a ground substance makes it particularly suitable to describe coated fabrics mechanical behaviour, because these are similarly made of threads and coating.

The constitutive theory defined by Spencer (1984) treats strongly anisotropic materials as an equivalent continuum. Clearly, fibre reinforced composites are not continuum bodies, since it is often possible to distinguish between matrix and reinforcement. Nethertheless, if such material is observed at a different scale, namely at the macroscale, it is possible to describe it as a continuum: this approach is allowed if the fibres are systematically arranged in the matrix and if they represent a substantial part of the composite. Again, this is what happens in coated fabrics, where the reinforcement consists of long threads that are weaved, thus they are arranged in a regular pattern with very little spacing between them.

As stated above, Spencer (1984) identifies the fibres as source of anisotropy: if the reinforcement shows one or more preferential orientations, these define the material directions of anisotropy. In the material model proposed by Spencer (1984), each group of aligned fibres is named family of fibres and its direction is characterized by a referential unit vector $\mathbf{a_{0\alpha}}$, where $\alpha = 1, \ldots, n$ denotes the family of fibres that is being considered. For instance, when there is only one preferential direction ($\alpha = 1$) the material is transversely isotropic. However, the most common pattern for coated fabrics presents two families of fibres, which are defined by the weaving directions: warp ($\alpha = 1$) and fill or weft ($\alpha = 2$).

After a transformation described by the deformation gradient tensor $\mathbf{F}$, the current orientation of the reinforcing fibres is defined through the spatial unit vector that is obtained with the push-forward of $\mathbf{a_{0\alpha}}$:

$$\mathbf{a_\alpha} = \boldsymbol{\chi}_*(\mathbf{a}^\sharp_{\mathbf{0\alpha}}) = \mathbf{F}(\mathbf{a}^\sharp_{\mathbf{0\alpha}}) \ , \qquad (a_\alpha)_i = F_{iJ}(a_{0\alpha})_J \tag{6.26}$$

Vectors $\mathbf{a_\alpha}$ also provide the stretches in the directions of the fibres (i.e. $|\mathbf{a_\alpha}|$).

In Spencer (1984) elastic and plastic behaviour at both small and large deformations are treated. For the sake of brevity, only the elastic large strains approach is summarized here: the reader is referred to the original article by Spencer (1984) for more details.

Spencer (1984) calculates the stress tensor by derivation of a strain-energy function Ψ with respect to the strain tensor, which means that the modelled material is considered to be hyperelastic (or Green-elastic). Employing a Lagrangian approach, the Helmoltz free-energy function Ψ per unit reference volume is defined as follows:

$$\Psi = \Psi(\mathbf{C}, \mathbf{A_{01}}, \ldots, \mathbf{A_{0n}}) \tag{6.27}$$

where $\mathbf{C}$ is the elastic right Cauchy-Green strain tensor defined in Equation (6.9) and $\mathbf{A_{0\alpha}}$ with $\alpha = 1, \ldots, n$ are n structural tensors, one for each family of fibres, which are defined as follows:

$$\mathbf{A_{0\alpha}} = \mathbf{a_{0\alpha}} \otimes \mathbf{a_{0\alpha}} \ , \qquad (A_{0\alpha})_{IJ} = (a_{0\alpha})_I (a_{0\alpha})_J \tag{6.28}$$

Objectivity requires that the free-energy Ψ remains unchanged if the reference configuration of the fibre reinforced composite undergoes a rotation through a proper orthogonal tensor[1] $\mathbf{Q}$. In Spencer (1984) this concept is equivalently expressed by stating that the strain-energy Ψ must be an isotropic invariant of $\mathbf{C}$ and $\mathbf{A_{0\alpha}}$, with $\alpha = 1, \ldots, n$. The requirement is satisfied if the following equation holds:

$$\Psi(\mathbf{C}, \mathbf{A_{01}}, \ldots, \mathbf{A_{0n}}) = \Psi(\mathbf{Q}\mathbf{C}\mathbf{Q}^{\mathrm{T}}, \mathbf{Q}\mathbf{A_{01}}\mathbf{Q}^{\mathrm{T}}, \ldots, \mathbf{Q}\mathbf{A_{0n}}\mathbf{Q}^{\mathrm{T}}) \tag{6.29}$$

According to Spencer (1984), in order to satisfy Equation (6.29), the free-energy must be a function of the following invariants:

$$I_1(\mathbf{C}) = \mathrm{tr}(\mathbf{C}) = \mathbf{C} : \mathbf{I} \tag{6.30a}$$

$$I_2(\mathbf{C}) = \frac{1}{2}[\mathrm{tr}(\mathbf{C})^2 - \mathrm{tr}(\mathbf{C}^2)] \tag{6.30b}$$

$$I_3(\mathbf{C}) = \det(\mathbf{C}) = J^2 \tag{6.30c}$$

$$I_{4\alpha}(\mathbf{C}, \mathbf{a_{0\alpha}}) = \mathbf{a_{0\alpha}} \cdot \mathbf{C}\mathbf{a_{0\alpha}} = \mathbf{C} : \mathbf{A_{0\alpha}} \tag{6.30d}$$

$$I_{5\alpha}(\mathbf{C}, \mathbf{a_{0\alpha}}) = \mathbf{a_{0\alpha}} \cdot \mathbf{C}^2\mathbf{a_{0\alpha}} = \mathbf{C}^2 : \mathbf{A_{0\alpha}} \tag{6.30e}$$

[1] An orthogonal tensor $\mathbf{Q}$ is a linear transformation satisfying the condition $\mathbf{Q}\mathbf{u} \cdot \mathbf{Q}\mathbf{v} = \mathbf{u} \cdot \mathbf{v}$ for all vectors $\mathbf{u}$ and $\mathbf{v}$. If $\det \mathbf{Q} = +1$, $\mathbf{Q}$ is said to be proper.

$$I_{6\alpha\beta}(\mathbf{C}, \mathbf{a_{0\alpha}}, \mathbf{a_{0\beta}}) = (\mathbf{a_{0\alpha}} \cdot \mathbf{a_{0\beta}})\mathbf{a_{0\alpha}} \cdot \mathbf{C}\mathbf{a_{0\beta}} \tag{6.30f}$$

$$I_{7\alpha\beta}(\mathbf{a_{0\alpha}}, \mathbf{a_{0\beta}}) = (\mathbf{a_{0\alpha}} \cdot \mathbf{a_{0\beta}})^2 \tag{6.30g}$$

More precisely, I_1, I_2 and I_3 are invariants of the strain tensor, while the others are named pseudo-invariants of $\mathbf{C}$ and $\mathbf{A_{0\alpha}}$, because they describe the properties of the fibre families and their interaction with other material constituents. It can be easily shown that invariants $I_{4\alpha}$ are the squares of the stretches along the fibre directions (see Holzapfel, 2000, p. 268), while $I_{5\alpha}$,$I_{6\alpha\beta}$,$I_{7\alpha\beta}$ do not display a clear physical interpretation.

Once the shape of the Helmholtz free-energy function is defined, the constitutive equation may be derived from the Clausius-Plank form of the second law of thermodynamics. For perfectly elastic materials and if thermal effects are ignored (purely mechanical theory), such inequality degenerates into the following equality:

$$\mathcal{D}_{int} = w_{int} - \dot{\Psi} = \mathbf{S} : \dot{\mathbf{E}} - \dot{\Psi} = 0 \tag{6.31}$$

where $\mathcal{D}_{int}$ is the internal dissipation or local production of entropy, which is required to be null for an elastic material; $\mathbf{S}$ is the second Piola-Kirchhoff stress tensor, defined in Equation (6.24); $\dot{\mathbf{E}}$ is the Green-Lagrange strain rate, that is the material time derivative of the Green-Lagrange strain tensor defined in Equation (6.8). $\mathbf{S}$ and $\dot{\mathbf{E}}$ represent a work-conjugate pair producing a rate of internal mechanical work per unit reference volume w_{int}. Relation $\mathbf{C} = 2\mathbf{E} + \mathbf{I}$ that holds between the right Cauchy-Green and the Green-Lagrange strain tensors may be substituted into Equation (6.31), giving:

$$\mathcal{D}_{int} = \mathbf{S} : \frac{1}{2}\dot{\mathbf{C}} - \dot{\Psi} = \left(\mathbf{S} - 2\frac{\partial \Psi}{\partial \mathbf{C}}\right) : \frac{1}{2}\dot{\mathbf{C}} = 0 \tag{6.32}$$

Since the increment of strain $\dot{\mathbf{C}}$ (or $\dot{\mathbf{E}}$) can be chosen arbitrarily, the second Piola-Kirchhoff stress tensor components can be derived from the free-energy as follows:

$$\mathbf{S} = \frac{\partial \Psi}{\partial \mathbf{E}} = 2\frac{\partial \Psi}{\partial \mathbf{C}} = 2\frac{\partial \Psi(I_i)}{\partial I_i}\frac{\partial I_i}{\partial \mathbf{C}} \ , \qquad S_{IJ} = 2\frac{\partial \Psi}{\partial C_{IJ}} \tag{6.33}$$

where summation over the dummy index i is implied.

Even if the second Piola-Kirchhoff stress tensor does not admit a physical interpretation, it is often used in the formulation of constitutive equations since it is a symmetric contravariant material tensor field parameterized by material coordinates. Through the inverse Piola transformation, it is possible to find the Cauchy (or true) stress tensor $\boldsymbol{\sigma}$, which has a clear physical meaning, since its columns represent the traction vectors acting on planes perpendicular to the reference system versors (see Section 6.1.2). The application of this transformation to Equation (6.33) leads to:

$$\boldsymbol{\sigma} = J^{-1}\mathbf{F}\mathbf{S}\mathbf{F}^{\mathrm{T}} = J^{-1}\mathbf{F}\left(2\frac{\partial\Psi}{\partial\mathbf{C}}\right)\mathbf{F}^{\mathrm{T}}\,,\ \sigma_{ij} = 2J^{-1}F_{iI}\frac{\partial\Psi}{\partial C_{IJ}}F_{jJ} \tag{6.34}$$

It can be noticed that the inverse Piola transformation is equivalent to the push-forward of the contravariant stress tensor $\mathbf{S}$ divided by the Jacobian determinant J defined in Equation (6.3). Another tensor that is often used in the Eulerian description of stress is the Kirchhoff stress tensor, which is obtained multiplying $\boldsymbol{\sigma}$ by J:

$$\boldsymbol{\tau} = J\boldsymbol{\sigma} = \mathbf{F}\left(2\frac{\partial\Psi}{\partial\mathbf{C}}\right)\mathbf{F}^{\mathrm{T}}\ ,\qquad \tau_{ij} = 2F_{iI}\frac{\partial\Psi}{\partial C_{IJ}}F_{jJ} \tag{6.35}$$

6.3 Holzapfel-Gasser-Ogden (HGO) hyperelastic constitutive model

An exisiting constitutive model that is based on Spencer's constitutive theory for fibre-reinforced materials is the one proposed by Holzapfel, Gasser and Ogden (HGO model), which is described in many journal articles (Holzapfel et al., 2000, 2002, 2004; Holzapfel & Gasser, 2001; Gasser & Holzapfel, 2002; Gasser et al., 2006; Holzapfel & Ogden, 2010). This model was proposed to describe passive mechanical response of arterial tissues, which are composed by layers of a soft matrix material (ground substance) reinforced by two families of fibres (collagen). Hence, within a macroscopic framework, arterial layers may be considered anisotropic, since they show structural properties that have strongly directional dependency. Moreover, their anisotropy is totally due to fibres, while the ground substance may be regarded as isotropic.

These characteristics are very close to the ones of coated fabrics used for membrane structure realizations and represent the main reasons why the HGO model has been used as a starting point for the development of the new constitutive law for coated fabrics proposed in this thesis. In this paragraph the HGO model for soft tissues is described in detail, while the new model for coated fabrics will be presented in the next paragraph.

Both arterial wall tissues and coated fabrics are not proper hyperelastic materials, since residual strains are often present after loads removing. Indeed, the first loading behaviour of both shows a high degree of variability. Anyway, if the material is preconditioned by performing a certain number of loading-unloading cycles, a sort of arrangement of the internal structure occurs; as a consequence, the stress-strain relationship becomes repeatable (stresses and strains are uniquely related in each loading or unloading branch of a specific cyclic process, as shown in Figure 4.35). This allows one to treat the inelastic material as an elastic material during loading and another elastic material during unloading. This is particulary convenient, because thus it is possible to define a free-energy function, from which stresses can be derived. In Fung et al. (1979) the authors name this way of modelling *pseudoelasticity* and add:

> "*Pseudoelasticity is, therefore, not an intrinsic property of the material. It is a convenient description of the stress-strain relationship in a specific cyclic loading. By its use the description of the very complex property of the artery is simplified*".

6.3.1 Free-energy function

HGO model postulates the decoupling of the Helmholtz free-energy function Ψ defined in Equation (6.27) into a volumetric (or dilational), Ψ_{vol}, and an isochoric (or deviatoric, or distortional), $\overline{\Psi}$, part:

$$\Psi = \Psi_{vol}(J) + \overline{\Psi}(\overline{\mathbf{C}}, \mathbf{A_{01}}, \ldots, \mathbf{A_{0n}}) \tag{6.36}$$

where J and $\overline{\mathbf{C}}$ are the volume ratio and the modified right Cauchy-Green strain tensor defined in Section 6.1.1.

The only requirement for $\Psi_{vol}(J)$ is that it must be a strictly convex function, with a unique minimum in $J = 1$, hence different functions has

been employed in the literature. The shape that has been most frequently utilised for compressible materials is the following:

$$\Psi_{vol}(J) = \frac{1}{D_1}\left(\frac{J^2-1}{2} - \ln(J)\right) \tag{6.37}$$

where D_1 is a constant parameter that represents the compressibility of the material, therefore it is related to the inverse of the bulk modulus and it has the the same dimension of the inverse of a stress. If an incompressible material (like arterial tissues) is considered instead, $\Psi_{vol}(J)$ is substituted by $-p(J-1)$, which is a Lagrange contribution that enforces the kinematic constraint associated with the incompressibility condition (i.e. $J = 1$) by incorporating it into the strain-energy. In that case, the volumetric part of the strain-energy $\Psi_{vol}(J)$ vanishes and scalar p may be determined only by means of equilibrium equations and boundary conditions; p represents a workless reaction to the kinematic incompressibility constraint on the deformation field.

Concerning the isochoric part $\overline{\Psi}$ of the strain-energy, the HGO model assumes an additive split into two parts, one related to the isotropic response and the other one associated with the anisotropic response. Fibres represent the source of anisotropy of the material, therefore the dependency of the free-energy on the structural tensors $\mathbf{A_{0\alpha}}$ appears only in the anisotropic term:

$$\overline{\Psi} = \overline{\Psi}_{iso}(\overline{\mathbf{C}}) + \overline{\Psi}_{aniso}(\overline{\mathbf{C}}, \mathbf{A_{01}}, \ldots, \mathbf{A_{0n}}) \tag{6.38}$$

As already seen in Section 6.2, frame invariance of the free-energy Ψ requires that it is expressed as a function of the invariants I_i defined in Equation (6.30). More precisely, $\overline{\Psi}$ should depend on the invariants $\overline{I}_i$, which are evaluated using only the distortional part of the right Cauchy-Green strain tensor. One can note that invariant $\overline{I}_3$ is constant for the incompressibility assumption, as well as $\overline{I}_{7\alpha\beta}$ because of the orthogonality of threads in coated fabrics. As a consequence, the deviatoric part of Helmholtz free-energy function $\overline{\Psi}$ may be restated in terms of invariants as follow:

$$\overline{\Psi} = \overline{\Psi}_{iso}(\overline{I}_1, \overline{I}_2) + \overline{\Psi}_{aniso}(\overline{I}_1, \overline{I}_2, \overline{I}_{4\alpha}, \overline{I}_{5\alpha}, \overline{I}_{6\alpha\beta}) \tag{6.39}$$

A further simplification of the model is proposed by Holzapfel et al. (2000), where the following reduced form of the strain-energy is considered,

in order to minimize the number of involved parameters:

$$\overline{\Psi} = \overline{\Psi}_{iso}(\overline{I}_1) + \sum_{\alpha=1}^{n} \overline{\Psi}_{aniso}(\overline{I}_{4\alpha}) \tag{6.40}$$

Based on experimental evidences, a classical neo-Hookean model is used by Holzapfel et al. (2000) to particularize the isotropic matrix contribution in Equation (6.40):

$$\overline{\Psi}_{iso}(\overline{I}_1) = \frac{\mu}{2}(\overline{I}_1 - 3) \tag{6.41}$$

where μ is a material parameter with the dimension of a stress. On the other hand, the fibres contribution is captured with an exponential function, which is suitable to catch the strong stiffening at large strains. More in detail, this is the expression proposed:

$$\overline{\Psi}_{aniso}(\overline{I}_{4\alpha}) = \frac{k_1}{2k_2} \sum_{\alpha=1}^{n} \{\exp[k_2(\overline{I}_{4\alpha} - 1)^2] - 1\} \tag{6.42}$$

where k_1 is a material parameter with the dimension of a stress and k_2 is a dimensionless parameter. They describe the mechanical behaviour of the collagen fibres and are assumed to be the same for each family of fibres. Since the reinforcing fibres can handle only tensile stresses, the energetic contribute $\overline{\Psi}_{aniso}(\overline{I}_{4\alpha})$ is activated only when the fibre stretch is greater than zero, i.e. $\overline{I}_{4\alpha} > 1$ (since $\overline{I}_{4\alpha}$ represents the squared stretch in the α^{th} fibre direction), otherwise it is disregarded.

6.3.2 Stress

The separation of the volume-dependent and volume-independent energy contributions results in an additive splitting of the second Piola-Kirchhoff stress tensor into volumetric $\mathbf{S}_{vol}$ and deviatoric $\overline{\mathbf{S}}$ stress components:

$$\mathbf{S} = \mathbf{S}_{vol} + \overline{\mathbf{S}} \tag{6.43}$$

where the volumetric stress is calculated as follows:

$$\mathbf{S}_{vol} = 2\frac{\partial \Psi_{vol}(J)}{\partial \mathbf{C}} = 2\frac{\partial \Psi_{vol}}{\partial J}\frac{\partial J}{\partial \mathbf{C}} = 2\widetilde{p}\frac{\partial J}{\partial \mathbf{C}} \tag{6.44}$$

and the deviatoric stress is evaluated as:

$$\overline{\mathbf{S}} = 2\frac{\partial\overline{\Psi}(\overline{\mathbf{C}}, \mathbf{A_{01}}, \ldots, \mathbf{A_{0n}})}{\partial\mathbf{C}} = 2\frac{\partial\overline{\Psi}}{\partial\overline{\mathbf{C}}} : \frac{\partial\overline{\mathbf{C}}}{\partial\mathbf{C}} = \widetilde{\mathbf{S}} : \frac{\partial\overline{\mathbf{C}}}{\partial\mathbf{C}} \tag{6.45}$$

with the constitutive equations for the hydrostatic pressure $\widetilde{p}$ and the fictitious second Piola-Kirchhoff stress tensor $\widetilde{\mathbf{S}}$ defined by:

$$\widetilde{p} = \frac{\partial\Psi_{vol}}{\partial J} \ , \qquad \widetilde{\mathbf{S}} = 2\frac{\partial\overline{\Psi}}{\partial\overline{\mathbf{C}}} \tag{6.46}$$

The following relations from tensor analysis (see Holzapfel, 2000, pp. 228-229) can be employed:

$$\frac{\partial J}{\partial\mathbf{C}} = \frac{1}{2}J\mathbf{C}^{-1} \tag{6.47a}$$

$$\frac{\partial\overline{\mathbf{C}}}{\partial\mathbf{C}} = J^{-2/3}\mathbb{P}^{\mathrm{T}} \tag{6.47b}$$

where $\mathbb{P}^{\mathrm{T}}$ is the transpose[1] of the fourth-order tensor $\mathbb{P}$, which is the projection tensor with respect to the reference configuration:

$$\mathbb{P} = \mathbb{I}^s - \frac{1}{3}\mathbf{C}^{-1}\otimes\mathbf{C} \ , \qquad \mathbb{P}_{IJKL} = \mathbb{I}^s_{IJKL} - \frac{1}{3}C^{-1}_{IJ}C_{KL} \tag{6.48}$$

$\mathbb{P}$ furnishes the physically-correct deviatoric operator in the Lagrangian description, thus $[\mathbb{P} : (\bullet)] : \mathbf{C} = 0$ (see, e.g., Federico, 2009).

Incidentally, the unit tensor $\mathbb{I}^s$ in equation Equation (6.48) is the fully-symmetric fourth-order identity tensor, which is different from the diagonal-symmetric fourth-order identity tensor $\mathbb{I}$. $\mathbb{I}^s$ is defined such that, for every symmetric second order tensor $\mathbf{A}^s$, $\mathbb{I}^s : \mathbf{A}^s = \mathbf{A}^s : \mathbb{I}^s = \mathbf{A}^s$. It can be written in a compact tensorial form by means of two special tensor products, the so-called *tensor-up* and *tensor-down* products: these are represented with the symbols $\overline{\otimes}$ and $\underline{\otimes}$, respectively. According to Rizzi & Carol (2001), given three second-order tensors $\mathbf{A}$, $\mathbf{B}$, and $\mathbf{C}$, the tensor-up and tensor-down products are defined as:

$$(\mathbf{A}\overline{\otimes}\mathbf{B}) : \mathbf{C} = \mathbf{A}\mathbf{C}\mathbf{B}^{\mathrm{T}} \tag{6.49}$$

$$(\mathbf{A}\underline{\otimes}\mathbf{B}) : \mathbf{C} = \mathbf{A}\mathbf{C}^{\mathrm{T}}\mathbf{B}^{\mathrm{T}} \tag{6.50}$$

[1] The transpose $\mathbb{A}^{\mathrm{T}}$ of a fourth-order tensor $\mathbb{A}$ is such that $\mathbb{A}^{\mathrm{T}}_{IJKL} = \mathbb{A}_{KLIJ}$.

so that, in Cartesian components:

$$(\mathbf{A}\overline{\otimes}\mathbf{B})_{ijkl} = A_{ik}B_{jl} \ , \qquad (\mathbf{A}\underline{\otimes}\mathbf{B})_{ijkl} = A_{il}B_{jk} \tag{6.51}$$

By using these special tensor products, the fully-symmetric fourth-order identity tensor $\mathbb{I}^s$ can be written as:

$$\mathbb{I}^s = \frac{1}{2}(\mathbf{I}\overline{\otimes}\mathbf{I} + \mathbf{I}\underline{\otimes}\mathbf{I}) = \frac{1}{2}(\mathbb{I} + \mathbb{T}) \ , \qquad \mathbb{I}^s_{ijkl} = \frac{1}{2}(\delta_{ik}\delta_{jl} + \delta_{il}\delta_{jk}) \tag{6.52}$$

It can be noticed that the identity tensor in Equation (6.52) coincides with the fourth-order tensor $\mathbb{S}$ defined in Holzapfel (2000, p. 24), which maps any second-order tensor into its symmetric part. The tensors $\mathbb{I}$ and $\mathbb{T}$ in Equation (6.52) are the fourth-order unit tensor and the transposition mapping respectively, which are defined by Rizzi & Carol (2001) and in Holzapfel (2000, p. 23) as follows:

$$\mathbb{I} : \mathbf{A} = \mathbf{A} \ , \qquad \mathbb{T} : \mathbf{A} = \mathbf{A}^{\mathrm{T}} \tag{6.53}$$

where $\mathbf{A}$ is a generic second order tensor. It may be demonstrated that the identity tensor $\mathbb{I}$ possesses only the major symmetries, whereas the fully-symmetric fourth-order identity tensor $\mathbb{I}^s$ possesses all the major and minor symmetries[1].

Going back to the stress computation, by substituting Equation (6.47a) into Equation (6.44) one obtains:

$$\mathbf{S}_{vol} = \widetilde{p}J\mathbf{C}^{-1} \tag{6.54}$$

Analogously, substituting Equation (6.47b) into Equation (6.45) the following expression of $\overline{\mathbf{S}}$ is obtained:

$$\overline{\mathbf{S}} = J^{-2/3}\widetilde{\mathbf{S}} : \mathbb{P}^{\mathrm{T}} = J^{-2/3}\mathbb{P} : \widetilde{\mathbf{S}} \tag{6.55}$$

It is possible to demonstrate the equivalence $\widetilde{\mathbf{S}} : \mathbb{P}^{\mathrm{T}} = \mathbb{P} : \widetilde{\mathbf{S}}$ in Equation (6.55) by expressing both $\widetilde{\mathbf{S}} : \mathbb{P}^{\mathrm{T}}$ and $\mathbb{P} : \widetilde{\mathbf{S}}$ in component form. The

[1] Given a fourth-order tensor $\mathbb{A}$ of components $\mathbb{A}_{ijkl}$, it may display three types of symmetries: (a) *Major symmetry*: if $\mathbb{A}_{ijkl} = \mathbb{A}_{klij}$ (b) *First minor symmetry*: if $\mathbb{A}_{ijkl} = \mathbb{A}_{jikl}$ (c) *Second minor symmetry*: if $\mathbb{A}_{ijkl} = \mathbb{A}_{ijlk}$. $\mathbb{A}$ is called *symmetric* or *diagonal-symmetric* if it displays the major symmetry and *fully-symmetric* if it possesses all the major and minor symmetries.

former looks:

$$\begin{aligned}\widetilde{\mathbf{S}} : \mathbb{P}^{\mathrm{T}} &= \widetilde{S}_{MN}\mathbb{P}_{IJHK}(\mathbf{e}_M \otimes \mathbf{e}_N) : [(\mathbf{e}_H \otimes \mathbf{e}_K) \otimes (\mathbf{e}_I \otimes \mathbf{e}_J)] = \\ &= \widetilde{S}_{MN}\mathbb{P}_{IJHK}(\mathbf{e}_I \otimes \mathbf{e}_J)[(\mathbf{e}_M \otimes \mathbf{e}_N) : (\mathbf{e}_H \otimes \mathbf{e}_K)] = \\ &= \widetilde{S}_{MN}\mathbb{P}_{IJHK}(\mathbf{e}_I \otimes \mathbf{e}_J)[(\mathbf{e}_M \cdot \mathbf{e}_H)(\mathbf{e}_N \cdot \mathbf{e}_K)] = \\ &= \widetilde{S}_{MN}\mathbb{P}_{IJHK}\delta_{MH}\delta_{NK}(\mathbf{e}_I \otimes \mathbf{e}_J) = \\ &= \mathbb{P}_{IJHK}\widetilde{S}_{HK}(\mathbf{e}_I \otimes \mathbf{e}_J) \end{aligned} \tag{6.56}$$

The latter is:

$$\begin{aligned}\mathbb{P} : \widetilde{\mathbf{S}} &= \mathbb{P}_{IJHK}\widetilde{S}_{MN}[(\mathbf{e}_I \otimes \mathbf{e}_J) \otimes (\mathbf{e}_H \otimes \mathbf{e}_K)] : (\mathbf{e}_M \otimes \mathbf{e}_N) = \\ &= \mathbb{P}_{IJHK}\widetilde{S}_{MN}(\mathbf{e}_I \otimes \mathbf{e}_J)[(\mathbf{e}_H \otimes \mathbf{e}_K) : (\mathbf{e}_M \otimes \mathbf{e}_N)] = \\ &= \mathbb{P}_{IJHK}\widetilde{S}_{MN}(\mathbf{e}_I \otimes \mathbf{e}_J)[(\mathbf{e}_H \cdot \mathbf{e}_M)(\mathbf{e}_K \cdot \mathbf{e}_N)] = \\ &= \mathbb{P}_{IJHK}\widetilde{S}_{MN}\delta_{HM}\delta_{KN}(\mathbf{e}_I \otimes \mathbf{e}_J) = \\ &= \mathbb{P}_{IJHK}\widetilde{S}_{HK}(\mathbf{e}_I \otimes \mathbf{e}_J) \end{aligned} \tag{6.57}$$

In summary, by applying Equation (6.46) to the HGO model free-energy function defined in Section 6.3.1, the following function that describes the hydrostatic pressure $\widetilde{p}$ is obtained for compressible materials:

$$\widetilde{p} = \frac{\partial \Psi_{vol}}{\partial J} = \frac{1}{D_1}\frac{J^2 - 1}{J} \tag{6.58}$$

whereas $\widetilde{p} = -p$ is the Lagrange multiplier that enforces the incompressibility constraint when an incompressible material is considered. Moreover, the fictitious second Piola-Kirchhoff stress tensor $\widetilde{\mathbf{S}}$ results to be the sum of the following contributions:

$$\widetilde{\mathbf{S}}_{iso} = 2\frac{\partial \overline{\Psi}_{iso}}{\overline{I}_1}\frac{\overline{I}_1}{\partial \overline{\mathbf{C}}} = \mu \mathbf{I} \tag{6.59a}$$

$$\widetilde{\mathbf{S}}_{aniso} = 2\frac{\partial \overline{\Psi}_{aniso}}{\overline{I}_{4\alpha}}\frac{\overline{I}_{4\alpha}}{\partial \overline{\mathbf{C}}} = 2k_1 \sum_{\alpha=1}^{n}\{(\overline{I}_{4\alpha} - 1)\exp[k_2(\overline{I}_{4\alpha} - 1)^2]\mathbf{A}_{\mathbf{0}\alpha}\} \tag{6.59b}$$

Then, by employing Equations (6.54) and (6.55), the volumetric and isochoric components of the second Piola-Kirchhoff stress tensor $\mathbf{S}$ may be

calculated:

$$\mathbf{S}_{vol} = \widetilde{p} J \mathbf{C}^{-1} \tag{6.60a}$$

$$\overline{\mathbf{S}}_{iso} = \mu J^{-2/3} \mathbb{P} : \mathbf{I} \tag{6.60b}$$

$$\overline{\mathbf{S}}_{aniso} = 2k_1 \sum_{\alpha=1}^{n} \{(\overline{I}_{4\alpha} - 1) \exp[k_2(\overline{I}_{4\alpha} - 1)^2] J^{-2/3} \mathbb{P} : \mathbf{A_{0\alpha}}\} \tag{6.60c}$$

Finally, the Cauchy stress tensor $\boldsymbol{\sigma}$, which describes the stress in the spatial configuration (true stress), may be estimated through Equation (6.34). The following push-forward operations have been employed for this aim:

$$\boldsymbol{\chi}_*(\mathbf{C}^{-1}) = \mathbf{F}\mathbf{C}^{-1}\mathbf{F}^{\mathrm{T}} = \mathbf{F}(\mathbf{F}^{\mathrm{T}}\mathbf{F})^{-1}\mathbf{F}^{\mathrm{T}} = \mathbf{F}\mathbf{F}^{-1}\mathbf{F}^{-\mathrm{T}}\mathbf{F}^{\mathrm{T}} = \mathbf{I} \tag{6.61}$$

$$\boldsymbol{\chi}_*(\mathbf{I}) = \mathbf{F}\mathbf{I}\mathbf{F}^{\mathrm{T}} = \mathbf{F}\mathbf{F}^{\mathrm{T}} = \mathbf{b} \tag{6.62}$$

$$\boldsymbol{\chi}_*(\mathbf{A_{0\alpha}}) = \mathbf{F}\mathbf{A_{0\alpha}}\mathbf{F}^{\mathrm{T}} = \mathbf{F}\mathbf{a_{0\alpha}} \otimes \mathbf{a_{0\alpha}}\mathbf{F}^{\mathrm{T}} = \mathbf{F}\mathbf{a_{0\alpha}} \otimes \mathbf{F}\mathbf{a_{0\alpha}} = \mathbf{A_\alpha} \tag{6.63}$$

where $\mathbf{b}$ is the left Cauchy-Green strain tensor defined in Equation (6.11) and $\mathbf{A}_\alpha$ is the spatial structural tensor associated with the α^{th} family of fibres. Moreover, if a material second-order tensor $\mathbf{A}$ is considered, whose correspondent spatial tensor is $\mathbf{a}$, the push-forward operation applied to the double contraction $\mathbb{P} : \mathbf{A}$ may be performed as follow:

$$\begin{aligned}
\boldsymbol{\chi}_*(\mathbb{P} : \mathbf{A}) &= \mathbf{F}(\mathbb{I}^s : \mathbf{A})\mathbf{F}^{\mathrm{T}} - \frac{1}{3}\mathbf{F}\left[(\mathbf{C}^{-1} \otimes \mathbf{C}) : \mathbf{A}\right]\mathbf{F}^{\mathrm{T}} = \\
&= \mathbf{F}\mathbf{A}^s\mathbf{F}^{\mathrm{T}} - \frac{1}{3}\mathbf{F}\left[(\mathbf{A} : \mathbf{C})\mathbf{C}^{-1}\right]\mathbf{F}^{\mathrm{T}} = \\
&= \mathbf{F}\mathbf{A}^s\mathbf{F}^{\mathrm{T}} - \frac{1}{3}\mathrm{Tr}(\mathbf{A})\mathbf{F}\mathbf{C}^{-1}\mathbf{F}^{\mathrm{T}} = \\
&= \mathbf{a}^s - \frac{1}{3}\mathrm{tr}(\mathbf{a})\mathbf{I} = \\
&= \mathbf{a}^s - \frac{1}{3}(\mathbf{a} : \mathbf{I})\mathbf{I} = \\
&= \mathbb{I}^s : \mathbf{a} - \frac{1}{3}(\mathbf{I} \otimes \mathbf{I}) : \mathbf{a} = \mathbb{P} : \mathbf{a}
\end{aligned} \tag{6.64}$$

where $\mathbf{A}^s$ and $\mathbf{a}^s$ are the symmetric parts of $\mathbf{A}$ and $\mathbf{a}$ respectively, while $\mathbb{P}$ is the spatial counterpart of $\mathbb{P}$ (i.e. fourth-order projection tensor with respect to the spatial configuration reported in Equation (6.48)), which is defined as:

$$\mathbb{P} = \mathbb{I}^s - \frac{1}{3}\mathbf{I} \otimes \mathbf{I} \ , \qquad \mathbb{P}_{ijkl} = \mathbb{I}^s_{ijkl} - \frac{1}{3}\delta_{ij}\delta_{kl} \tag{6.65}$$

$\mathbb{P}$ defines the physically-correct deviatoric operator in the Eulerian description, so that $[\mathbb{P} : (\bullet)] : \mathbf{I} = 0$ (see, e.g., Federico, 2009).

Therefore, by employing Equations (6.61) to (6.64), the Cauchy stress tensor $\boldsymbol{\sigma}$ of the HGO model results to be the sum of the following contributions:

$$\boldsymbol{\sigma}_{vol} = J^{-1}\mathbf{F}\mathbf{S}_{vol}\mathbf{F}^{\mathrm{T}} = \widetilde{p}\mathbf{I} \tag{6.66a}$$

$$\overline{\boldsymbol{\sigma}}_{iso} = J^{-1}\mathbf{F}\overline{\mathbf{S}}_{iso}\mathbf{F}^{\mathrm{T}} = \mu J^{-5/3}\mathbb{P} : \mathbf{b} \tag{6.66b}$$

$$\overline{\boldsymbol{\sigma}}_{aniso} = J^{-1}\mathbf{F}\overline{\mathbf{S}}_{aniso}\mathbf{F}^{\mathrm{T}} = 2k_1 \sum_{\alpha=1}^{n} \{(\overline{I}_{4\alpha} - 1)\exp[k_2(\overline{I}_{4\alpha} - 1)^2]J^{-5/3}\mathbb{P} : \mathbf{A}_\alpha \tag{6.66c}$$

6.3.3 Elasticity tensor

The finite element solution of nonlinear initially boundary-valued problems is usually performed by solving a series of linearised equations through the use of iterative solution techniques, e.g. of Newton's type. This solution strategy requires the linearisation of the material constitutive law in the neighbourhood of a known configuration and it is based on the assumption that small displacements from a known configuration are governed by the so-called *tangent* behaviour of the material. Within this framework, the *elasticity tensor* or *tensor of the tangent moduli*, describes how infinitesimal variations of the strain affect the stress tensor. In spite of its name, the elasticity tensor can be defined for both elastic and inelastic materials.

According to Holzapfel (2000), to determine the elasticity tensor in the material description the following total differential may be considered:

$$\mathrm{d}\mathbf{S} = 2\frac{\partial \mathbf{S}(\mathbf{C})}{\partial \mathbf{C}} : \frac{1}{2}\mathrm{d}\mathbf{C} = \mathbb{C} : \frac{1}{2}\mathrm{d}\mathbf{C} \tag{6.67}$$

where the following definition of fourth-order elasticity tensor has been introduced for the material description:

$$\mathbb{C} = 2\frac{\partial \mathbf{S}(\mathbf{C})}{\partial \mathbf{C}} \quad , \qquad \mathbb{C}_{IJKL} = 2\frac{\partial S_{IJ}}{\partial C_{KL}} \tag{6.68}$$

By using the Green-Lagrange strain tensors $\mathbf{E} = (\mathbf{C} - \mathbf{I})/2$, Equation (6.68) may be reformulated as follows:

$$\mathbb{C} = \frac{\partial \mathbf{S}(\mathbf{E})}{\partial \mathbf{E}} \quad , \qquad \mathbb{C}_{IJKL} = \frac{\partial S_{IJ}}{\partial E_{KL}} \tag{6.69}$$

It can be noticed that $\mathbb{C}$ possesses all the minor symmetries (i.e. it is symmetric in its first and second pairs of indexes), thanks to the symmetries of the right Cauchy-Green tensor $\mathbf{C}$ and of the second Piola-Kirchhoff stress tensor $\mathbf{S}$. As pointed out by Holzapfel (2000), this symmetry condition holds for all elastic materials (not only for the hyperlastic ones), because it is independent of the existence of a strain-energy function.

If a hyperelastic material is considered, the stress tensor $\mathbf{S}$ is obtainable from the free-energy derivation, which is performed by employing Equation (6.33). Thus also the elasticity tensor can be derived from the strain-energy Ψ:

$$\mathbb{C} = 4\frac{\partial^2 \Psi(\mathbf{C})}{\partial \mathbf{C} \partial \mathbf{C}} \quad , \qquad \mathbb{C}_{IJKL} = 4\frac{\partial^2 \Psi}{\partial C_{IJ} \partial C_{KL}} \tag{6.70}$$

In this case, $\mathbb{C}$ possesses also the major symmetry, which is therefore equivalent to the existence of a strain-energy function.

Finally, the elasticity tensor in the spatial description may be obtained with the following push-forward operation of $\mathbb{C}$:

$$\mathbb{c} = \boldsymbol{\chi}_*(\mathbb{C}) = \mathbb{F} : \mathbb{C} : \mathbb{F}^{\mathrm{T}} \quad , \qquad \mathbb{c}_{ijkl} = F_{iA} F_{jB} F_{kC} F_{lD} C_{ABCD} \tag{6.71}$$

where the use of the fourth order tensors $\mathbb{F} = \mathbf{F} \underline{\otimes} \mathbf{F}$ and $\mathbb{F}^{\mathrm{T}} = \mathbf{F}^{\mathrm{T}} \underline{\otimes} \mathbf{F}^{\mathrm{T}}$ permits a convenient coordinate-free expression.

Other details on HGO model may be found in Holzapfel et al. (2000, 2002, 2004), Holzapfel & Gasser (2001), Gasser & Holzapfel (2002), Gasser et al. (2006), Holzapfel & Ogden (2010).

6.4 A modified HGO model for coated fabrics

It has been largely proved by several authors that the HGO model discussed in Section 6.3 is able to describe the hyperelastic (or pseudoelastic) mechanical behaviour of soft tissues, like blood vessels. However, a large number of applications may be found in industry and structural engineering, whenever composite materials with strongly direction-dependent properties due to continuously distributed fibre reinforcement are employed. Typical applications are sporting goods construction, lightweight wheelchairs realization, prosthesis construction, automobiles and planes building, musical instruments realization and so on.

This kind of strongly anisotropic behaviour characterises also coated fabrics that are used in membrane structures and textiles façades. The decoupling of stress into an isotropic contribution related to the matrix and an anisotropic contribution due to the fibres is particularly suitable to describe PVC coated polymeric fabrics and PTFE coated glass fabrics, the materials that are most widely used in these two applications; yet, HGO model does not take into account the interaction between yarns arising from weaving, which has overall a strong influence on the mechanical response of these materials. The modification of HGO model presented in this paragraph aims at capturing this fibre interaction and at formulating a new predictive constitutive law for coated fabrics.

6.4.1 Free-energy function

The first difference between the modified HGO model proposed in this thesis and the original version by Holzapfel et al. (2000) is in the part of the free-energy function that represents the fibre contribution. Coated fabrics have two families of orthogonal fibres, warp and weft, but these are not mechanically equivalent, as widely explained in Chapter 4. Instead, warp yarns are stiffer than weft/fill yarns, because of the weaving process, which acts as a sort of pretension of warp threads and makes them less crimped. As a result, parameters k_1 and k_2 of HGO model cannot be the same for warp and weft yarns. Indeed, HGO model has been yet formulated in a more general form, with different values of the fibre parameters, for instance in application to the human cornea modelling (Pandolfi & Manganiello, 2006; Pandolfi & Holzapfel, 2008). By using labels 1 and 2 to denote the warp and fill direction respectively, Equation (6.42) becomes:

$$\overline{\Psi}_{aniso} = \sum_{\alpha=1}^{2} \frac{k_{1\alpha}}{2k_{2\alpha}} \{\exp[k_{2\alpha}(\overline{I}_{4\alpha} - 1)^2] - 1\} = \overline{\Psi}_1 + \overline{\Psi}_2 \tag{6.72}$$

where:

$$\overline{\Psi}_1 = \frac{k_{11}}{2k_{21}} \{\exp[k_{21}(\overline{I}_{41} - 1)^2] - 1\} \tag{6.73a}$$

$$\overline{\Psi}_2 = \frac{k_{12}}{2k_{22}} \{\exp[k_{22}(\overline{I}_{42} - 1)^2] - 1\} \tag{6.73b}$$

Analogously to HGO model, it has been chosen to deactivate the anisotropic energetic contributions $\overline{\Psi}_1$ and $\overline{\Psi}_2$ when the correspondent family of fibres experiences negative stretches, i.e. when $\overline{I}_{4\alpha} < 1$. This is equivalent to substitute the terms $(\overline{I}_{4\alpha} - 1)$ in Equation (6.72) with the following function:

$$f(\overline{I}_{4\alpha}) = H(\overline{I}_{4\alpha} - 1) \cdot (\overline{I}_{4\alpha} - 1) = \begin{cases} \overline{I}_{4\alpha} - 1 & \text{if } \overline{I}_{4\alpha} \geq 1 \\ 0 & \text{if } \overline{I}_{4\alpha} < 1 \end{cases} \tag{6.74}$$

where $H(\overline{I}_{4\alpha}-1)$ is the Heaviside step function. The reason for this assumption is that the reinforcing fibres can handle only tensile stresses, because their crimp increases if they are compressed. Therefore the contribution of the yarns to the stiffness of the composite is null if they are not stretched.

A more substantial modification to the HGO model is the introduction of a new energy term $(\overline{\Psi}_{12})$, which tries to capture the interaction between the fibres. Due to the weaving, the tensile behaviour of warp (fill) threads is modified by the application of a load in the transverse fill (warp) direction. For example, if a load is applied along the fill direction, the crimp level of fill yarns gradually decreases; that reduction of crimp in the transversal direction causes an increasing of crimp in the warp direction (crimp interchange), which results in a reduction of longitudinal stiffness. Therefore, the greater is the transversal load, the larger will be the stress experienced by the longitudinal yarns at an arbitrary fixed value of stretch.

The just described mechanical behaviour, which is a direct consequence of the crimp interchange between the weaving directions, would require a series of ad hoc tests to be deeply explored. For instance, several uniaxial tensile tests could be performed at different arbitrary fixed levels of stretch in the direction that is transverse to the loading axis. This series of tests should be repeated for both warp and weft directions. The use of a cruciform sample could help to obtain a uniform stress state in the central part of the specimen. The proposed procedure would require displacement control, which may easily lead to the breaking of the sample due to propagation of the slits in its arms, therefore a system for non-contact strain measurement is highly recommended, e.g. Digital Image Correlation (DIC). Moreover, the DIC could be useful to obtain the actual values of strain (or stretches) in the central square of the cross, which can be widely different from the ones measured at the clamps. Thanks to the completeness of the data provided

by this full-field measurement technique, DIC is increasingly employed for the characterization of anisotropic materials (see, e.g., Garbowski et al., 2011; Maier et al., 2013).

Because of the high demand of material needed and of the absence of a non-contact strain measurement system, which will be added to the biaxial machine available at Politecnico di Milano only later, it has not been possible to perform the described tests. Therefore, the analytical law for the additional energy term that describes the fibre interaction has been formulated empirically, by basing it on a simple observation, which is discussed further on.

The interaction between fibers due to crimp interchange is equivalent to some extent to a nonlinear Poisson's effect. Indeed, a load applied in one direction causes an increase of crimp in the transversal direction, which is equivalent to an apparent negative strain. If a biaxial loading is considered, where the forces are applied along the weaving directions, it is possible to derive a small strain approximation of the original HGO model, which looks:

$$\begin{bmatrix}\sigma_{11}\\ \sigma_{22}\end{bmatrix} = \underbrace{\begin{bmatrix}4\mu & 2\mu\\ 2\mu & 4\mu\end{bmatrix}\begin{bmatrix}\varepsilon_{11}\\ \varepsilon_{22}\end{bmatrix}}_{\text{Matrix}} + \underbrace{\begin{bmatrix}4k_{11} & 0\\ 0 & 4k_{12}\end{bmatrix}\begin{bmatrix}\varepsilon_{11}\\ \varepsilon_{12}\end{bmatrix}}_{\text{Fibres}} \tag{6.75}$$

as it will be demonstrated in Section 6.5. By observing Equation (6.75), it is easy to understand that the Poisson's effect is completely assigned to the matrix (coating), since the off-diagonal terms of the elastic matrix contain only parameter μ.

Such characteristic of the original HGO model represents a big limitation in its application to coated woven fabrics modelling. Thanks to the weaving, the Poisson's effect in these materials is extremely emphasised, because of the interaction between the yarns. Therefore, by attributing all the transverse interaction to parameter μ, an overestimation of the coating axial stiffness 4μ is obtained. As a consequence, the initial stiffnesses of the yarns (i.e. $4k_{11}$ and $4k_{12}$) are underestimated.

A modification of the HGO model is here proposed, which aims at overcoming the aforementioned issues by introducing in the elastic matrix an off-diagonal term attributed to the fibres. Since the model that is presented in this thesis is hyperelastic, the stresses must be obtained through derivation from a free-energy function, as illustrated in Section 6.3. Therefore, a

new strain-energy term $\overline{\Psi}_{12}$ has been added to capture the yarn interaction.

The idea that has been used to find a function for the additional strain-energy term $\overline{\Psi}_{12}$ is similar to the one employed by (Milani & Nemes, 2004) to model the fibre-matrix interaction, even if the solution proposed in this thesis has been thought and developed independently. In that case, the authors created the following energy term:

$$\Psi_{int} = \frac{m}{2} \underbrace{(I_1 - 1)}_{\text{Matrix}} \underbrace{[(I_{41} - 1) + (I_{42} - 1)]}_{\text{Fibres}} \tag{6.76}$$

where the matrix and fibres contributions were multiplied. In the present context, a suitable form for the new energy term is the following:

$$\overline{\Psi}_{12} = k_3 \underbrace{(\overline{I}_{41} - 1)}_{\text{Warp fibres}} \underbrace{(\overline{I}_{42} - 1)}_{\text{Fill fibres}} \tag{6.77}$$

which multiplies the warp and fill fibre contributions.

It is underlined that the proposed form of the energy term $\overline{\Psi}_{12}$ respects the condition to be null in the unstrained reference configuration, where $\overline{I}_{41} = \overline{I}_{42} = 1$. Moreover, by employing $\overline{\Psi}_{12}$ in Equation (6.77), the small strain approximation of the modified HGO model for plane stress biaxial loading, which will be derived in Section 6.5, becomes:

$$\begin{bmatrix} \sigma_{11} \\ \sigma_{22} \end{bmatrix} = \underbrace{\begin{bmatrix} 4\mu & 2\mu \\ 2\mu & 4\mu \end{bmatrix} \begin{bmatrix} \varepsilon_{11} \\ \varepsilon_{22} \end{bmatrix}}_{\text{Matrix}} + \underbrace{\begin{bmatrix} 4k_{11} & 4k_3 \\ 4k_3 & 4k_{12} \end{bmatrix} \begin{bmatrix} \varepsilon_{11} \\ \varepsilon_{12} \end{bmatrix}}_{\text{Fibres}} \tag{6.78}$$

where the new off-diagonal term $4k_3$ associated to the yarns has appeared.

Figure 6.3 represents the shape assumed by the new energy term. The function has been adimensionalised and plotted for arbitrary fixed values of the stretch ratio λ_1/λ_2. By looking at Figure 6.3(a), which represents the behaviour in warp direction, it may be noticed that the new energy term vanishes in the unstrained configuration (i.e. for $\lambda_1 = 1$). In addition, when the warp yarns are stretched ($\lambda_1 > 1$), the interaction terms diminishes if the stretch ratio increases (direction of the red arrow). On the other hand, when the warp yarns experience negative strains ($\lambda_1 < 1$), the interaction term is present, but its magnitude is limited: this behaviour is close to the physics of the problem, because the threads can increase their

level of crimp only up to a certain limit (asymptotic value), after that the crimp interchange effect does not increase further. Figure 6.3(b) shows an analogous behaviour in fill direction.

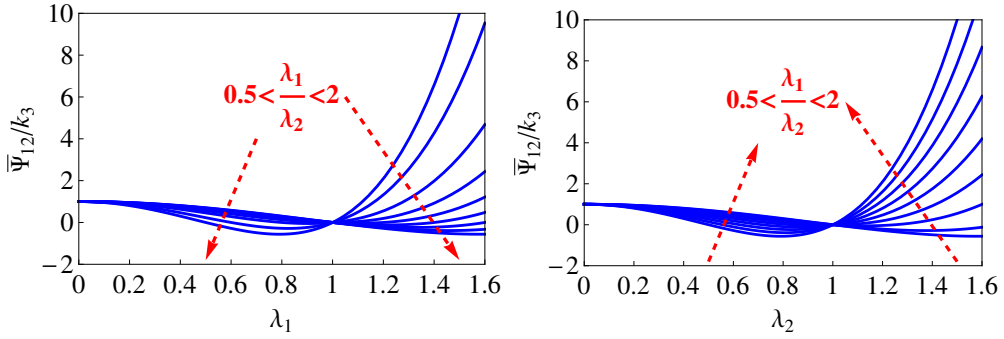

(a) Warp direction (b) Fill direction

Figure 6.3: *Shape of the new interaction energy term $\overline{\Psi}_{12}$ for increasing values of the stretch in warp and fill direction: the adimensionalised function is represented for arbitrary fixed values of the stretch ratio λ_1/λ_2 (red arrows indicate the direction of increasing values for this ratio).*

The adopted $\overline{\Psi}_{12}$ function (Equation (6.77)) results in the following deviatoric contribution to the second Piola-Kirchhoff stress tensor, which is obtained by derivation, according to Equations (6.46) and (6.55):

$$\overline{\mathbf{S}}_{12} = J^{-2/3}\mathbb{P} : \widetilde{\mathbf{S}}_{12} = J^{-2/3}\mathbb{P} : \left[2k_3(\overline{I}_{42}-1)\mathbf{A_{01}} + 2k_3(\overline{I}_{41}-1)\mathbf{A_{02}}\right] \tag{6.79}$$

One may note that the effect of a (squared) stretch in the fill direction (i.e. $\overline{I}_{42}$) on the warp yarns has been introduced in the warp stress contribution (tensor $\mathbf{A_{01}}$) through the quantity $2k_3(\overline{I}_{41}-1)$. Analogously, the effect of a (squared) stretch in the warp direction (i.e. $\overline{I}_{41}$) on the fill yarns has been introduced in the fill stress contribution (tensor $\mathbf{A_{02}}$) through the quantity $2k_3(\overline{I}_{41}-1)$.

A plot of these two stress terms is shown in Figure 6.4. This illustrates the effect in terms of stress variation of a stretch applied in the transversal direction. If the transversal stretch is $\lambda = 1$, no stress is added to the longitudinal direction, because the fibre interaction due to crimp interchange is not active. If the transversal stretch is of tension ($\lambda > 1$), an increment of

the stress in the longitudinal direction is recorded, which grows proportionally to the transversal stretch itself, because the crimp in the longitudinal direction is trying to increase against the stretch due to the applied tensile load. On the opposite side, if $\lambda < 1$, the longitudinal stress decreases.

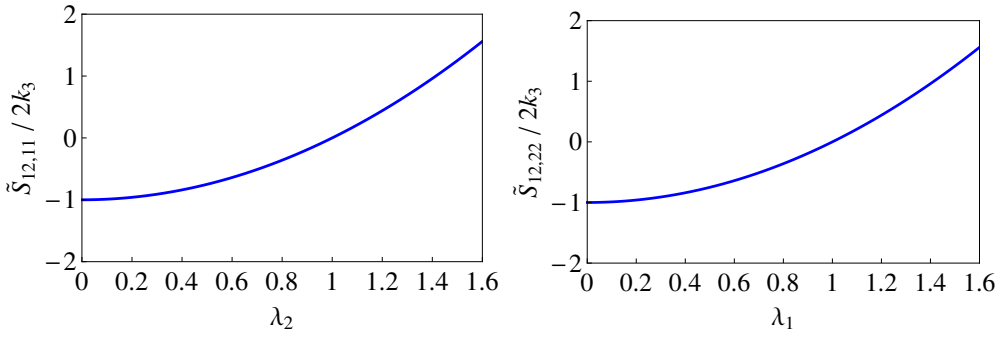

(a) Warp stress (b) Fill stress

Figure 6.4: *Plots of the warp and fill adimensionalised stress variation due to the fibre interaction, i.e.* $(\overline{I}_{42} - 1)$ *and* $(\overline{I}_{41} - 1)$.

In summary, the free-energy function adopted for the modified HGO model is the following:

$$\Psi = \Psi_{vol} + \overline{\Psi}_{iso} + \overline{\Psi}_1 + \overline{\Psi}_2 + \overline{\Psi}_{12} \tag{6.80}$$

It is the sum of several contributions, namely: the volumetric (Ψ_{vol}), the isotropic due to the matrix ($\overline{\Psi}_{iso}$), the anisotropic due to the warp fibres ($\overline{\Psi}_1$), the anisotropic due to the fill fibres ($\overline{\Psi}_2$) and the new term that captures the interaction between the two families of fibres ($\overline{\Psi}_{12}$).

The above mentioned contributions are particularised as follows:

$$\Psi_{vol} = \frac{1}{D_1}\left(\frac{J^2 - 1}{2} - \ln(J)\right) \tag{6.81a}$$

$$\overline{\Psi}_{iso} = \frac{\mu}{2}(\overline{I}_1 - 3) \tag{6.81b}$$

$$\overline{\Psi}_1 = \frac{k_{11}}{2k_{21}}\{\exp[k_{21} f(\overline{I}_{41})^2] - 1\} \tag{6.81c}$$

$$\overline{\Psi}_2 = \frac{k_{12}}{2k_{22}}\{\exp[k_{22} f(\overline{I}_{42})^2] - 1\} \tag{6.81d}$$

$$\overline{\Psi}_{12} = k_3(\overline{I}_{41} - 1)(\overline{I}_{42} - 1) \tag{6.81e}$$

where $f(\overline{I}_{4\alpha})$ is the function defined in Equation (6.74). Then, the strain energy depends on nine parameters: D_1 is a constant that has the same dimension of the inverse of a stress; μ, k_{11}, k_{12} and k_3 are material parameters with the dimension of a stress; k_{21} and k_{22} are dimensionless constants.

If an incompressible material is considered, the volumetric part $\Psi_{vol}(J)$ of the free-energy (Equation (6.81a)) vanishes and it is substituted by $-p(J-1)$, which is a Lagrange contribution that enforces the kinematic constraint associated with the incompressibility condition (i.e. $J = 1$). In that case, scalar p represents a workless reaction to the kinematic incompressibility constraint on the deformation field and may be determined only by means of equilibrium equations and boundary conditions.

The materials that are analysed in this thesis has been modelled as incompressible. Indeed, it is not easy to establish if coated fabrics employed in tensile structures are incompressible or not, because they are used as membranes, therefore measurements of the out of plane behaviour are not easily obtainable. The existence of this issue is confirmed by the fact that existing constitutive models for coated fabrics are based on opposite assumptions: for instance Xue et al. (2003) considers the material as incompressible, while Galliot & Luchsinger (2009) do not. Nevertheless, according to the authors' knowledge of the literature about the topic, there is currently no demonstration that helps to assume a definitive position on incompressibility of coated fabrics.

However, some general considerations can be made about the volumetric behaviour of coated fabrics. Unlike what happens in raw fabrics, where during tensile loading the quantity of air inside the yarns diminishes, leading to a reduction of the total volume, in coated fabrics the matrix prevents this effect. As a consequence, the threads of a coated fabric display changes in their shape that are extremely larger than their changes in volume. This is also the reason why most of the meso-scale constitutive models assume incompressibility of the yarns (see, e.g., Jeon et al., 2003; Bridgens & Gosling, 2008). In addition, polymers in general, therefore also the PVC and PTFE that are employed to coat architectural fabrics, are very similar to a liquid, because they are made of densely packed monomers. This means that they can hardly change their volume, while they can easily change their shape. According to the ABAQUS User's Manual, fibre-reinforced elastomers have very little compressibility compared to their shear flexibility, and, in applications where these materials are not highly confined, the de-

gree of compressibility is typically not crucial. In conclusion, the materials that are analysed in this thesis has been reasonably modelled by enforcing incompressibility, even if a more rigorous assessment of this property would be needed.

Finally, a difference between the modified HGO model here presented and its original version is related to the fact that the reference configuration that is created with the preconditioning cycles in a biaxial test is not stress-free. This is because the present model aims at reproducing the behaviour of an in situ fabric, which is always prestressed to avoid wrinkling, slackening or excessive tension and to providing the geometric stiffness that is sufficient to carry environmental loads. To account for this, all the stresses evaluated with the present model, hence by derivation of the free-energy, have been considered to be increments with respect to a known initial stress field.

6.4.2 Stress

As illustrated in Section 6.3, the second Piola-Kirchhoff stress tensor $\mathbf{S}$ can be obtained by deriving the strain energy function in Equation (6.80) with respect to the right Cauchy-Green strain tensor $\mathbf{C}$. In the case of the modified HGO model here presented, it is the sum of the following contributions:

$$\mathbf{S} = \mathbf{S}_{vol} + \overline{\mathbf{S}}_{iso} + \overline{\mathbf{S}}_1 + \overline{\mathbf{S}}_2 + \overline{\mathbf{S}}_{12} \tag{6.82}$$

First of all, it is necessary to evaluate the hydrostatic pressure $\widetilde{p}$ and the fictitious second Piola-Kirchhoff stress tensor $\widetilde{\mathbf{S}}$, which have been defined in Equation (6.46). The former is equal to:

$$\widetilde{p} = \frac{\partial \Psi_{vol}}{\partial J} = \frac{1}{D_1}\frac{J^2 - 1}{J} \tag{6.83}$$

whereas $\widetilde{p} = -p$ is the Lagrange multiplier that enforces the incompressibility constraint when an incompressible material ($J = 1$) is considered. The fictitious second Piola-Kirchhoff stress tensor is the sum of the following

terms:

$$\widetilde{\mathbf{S}}_{iso} = 2\frac{\partial\overline{\Psi}_{iso}}{\overline{I}_1}\frac{\overline{I}_1}{\partial\overline{\mathbf{C}}} = \mu\mathbf{I} \tag{6.84a}$$

$$\widetilde{\mathbf{S}}_1 = 2\frac{\partial\overline{\Psi}_1}{\overline{I}_{41}}\frac{\overline{I}_{41}}{\partial\overline{\mathbf{C}}} = 2k_{11}f(\overline{I}_{41})\exp[k_{21}f(\overline{I}_{41})^2]\mathbf{A_{01}} \tag{6.84b}$$

$$\widetilde{\mathbf{S}}_2 = 2\frac{\partial\overline{\Psi}_2}{\overline{I}_{42}}\frac{\overline{I}_{42}}{\partial\overline{\mathbf{C}}} = 2k_{12}f(\overline{I}_{42})\exp[k_{22}f(\overline{I}_{42})^2]\mathbf{A_{02}} \tag{6.84c}$$

$$\widetilde{\mathbf{S}}_{12} = 2\frac{\partial\overline{\Psi}_{12}}{\overline{I}_{41}}\frac{\overline{I}_{41}}{\partial\overline{\mathbf{C}}} + 2\frac{\partial\overline{\Psi}_{12}}{\overline{I}_{42}}\frac{\overline{I}_{42}}{\partial\overline{\mathbf{C}}} = 2k_3(\overline{I}_{42}-1)\mathbf{A_{01}} + 2k_3(\overline{I}_{41}-1)\mathbf{A_{02}} \tag{6.84d}$$

where $f(\overline{I}_{4\alpha})$ is the function in Equation (6.74), which deactivates the fibre contribution when the yarn is compressed.

Then, by employing Equations (6.54) and (6.55), it is possible to particularise the stress contributions in Equation (6.82) as follows:

$$\mathbf{S}_{vol} = \widetilde{p}J\mathbf{C}^{-1} \tag{6.85a}$$

$$\overline{\mathbf{S}}_{iso} = \mu J^{-2/3}\mathbb{P} : \mathbf{I} \tag{6.85b}$$

$$\overline{\mathbf{S}}_1 = 2k_{11}f(\overline{I}_{41})\exp[k_{21}f(\overline{I}_{41})^2]J^{-2/3}\mathbb{P} : \mathbf{A_{01}} \tag{6.85c}$$

$$\overline{\mathbf{S}}_2 = 2k_{12}f(\overline{I}_{42})\exp[k_{22}f(\overline{I}_{42})^2]J^{-2/3}\mathbb{P} : \mathbf{A_{02}} \tag{6.85d}$$

$$\overline{\mathbf{S}}_{12} = 2k_3(\overline{I}_{42}-1)J^{-2/3}\mathbb{P} : \mathbf{A_{01}} + 2k_3(\overline{I}_{41}-1)J^{-2/3}\mathbb{P} : \mathbf{A_{02}} \tag{6.85e}$$

It is here recalled that $\mathbb{P}$ is the fourth-order projection tensor with respect to the reference configuration, which has been defined in Equation (6.48).

Finally, the Cauchy stress tensor $\boldsymbol{\sigma}$ of the modified HGO model may be estimated as illustrated in Section 6.3.2 for the original HGO model. By employing Equations (6.61) to (6.64), it is possible to evaluate the Cauchy stress additive contributions through the push forward of the second Piola-Kirchhoff stress tensor $\mathbf{S}$:

$$\boldsymbol{\sigma}_{vol} = J^{-1}\mathbf{F}\mathbf{S}_{vol}\mathbf{F}^{\mathrm{T}} = \widetilde{p}\mathbf{I} \tag{6.86a}$$

$$\overline{\boldsymbol{\sigma}}_{iso} = J^{-1}\mathbf{F}\overline{\mathbf{S}}_{iso}\mathbf{F}^{\mathrm{T}} = \mu J^{-5/3}\mathbb{P} : \mathbf{b} \tag{6.86b}$$

$$\overline{\boldsymbol{\sigma}}_1 = J^{-1}\mathbf{F}\overline{\mathbf{S}}_1\mathbf{F}^{\mathrm{T}} = 2k_{11}f(\overline{I}_{41})\exp[k_{21}f(\overline{I}_{41})^2]J^{-5/3}\mathbb{P} : \mathbf{A_1} \tag{6.86c}$$

$$\overline{\boldsymbol{\sigma}}_2 = J^{-1}\mathbf{F}\overline{\mathbf{S}}_2\mathbf{F}^{\mathrm{T}} = 2k_{12}f(\overline{I}_{42})\exp[k_{22}f(\overline{I}_{42})^2]J^{-5/3}\mathbb{P} : \mathbf{A_2} \tag{6.86d}$$

$$\overline{\boldsymbol{\sigma}}_{12} = J^{-1}\mathbf{F}\overline{\mathbf{S}}_{12}\mathbf{F}^{\mathrm{T}} = 2k_3(\overline{I}_{42}-1)J^{-5/3}\mathbb{P} : \mathbf{A_1} + 2k_3(\overline{I}_{41}-1)J^{-5/3}\mathbb{P} : \mathbf{A_2} \tag{6.86e}$$

where it is recalled that $\mathbb{P}$ is the fourth-order projection tensor with respect to the spatial configuration, which has been defined in Equation (6.65).

In addition, if an incompressible material is considered, the second Piola-Kirchhoff and the Cauchy stress tensors may be written in a simplified form. The former, whose components have been defined in Equation (6.85), becomes:

$$\mathbf{S} = -p\mathbf{C}^{-1} + \overbrace{\mu\mathbf{I}}^{\text{Matrix}} + \left[\overbrace{2k_{11}f(\overline{I}_{41})\exp[k_{21}f(\overline{I}_{41})^2]}^{\text{Warp fibres}} + \overbrace{2k_3(\overline{I}_{42}-1)}^{\text{Fibre interaction}}\right]\mathbf{A_{01}} +$$
$$+ \left[\underbrace{2k_{12}f(\overline{I}_{42})\exp[k_{22}f(\overline{I}_{42})^2]}_{\text{Fill fibres}} + \underbrace{2k_3(\overline{I}_{41}-1)}_{\text{Fibre interaction}}\right]\mathbf{A_{02}} \tag{6.87}$$

while the latter, which is the sum of the components in Equation (6.86), is simplified as follows:

$$\boldsymbol{\sigma} = -p\mathbf{I} + \overbrace{\mu\mathbf{b}}^{\text{Matrix}} + \left[\overbrace{2k_{11}f(\overline{I}_{41})\exp[k_{21}f(\overline{I}_{41})^2]}^{\text{Warp fibres}} + \overbrace{2k_3(\overline{I}_{42}-1)}^{\text{Fibre interaction}}\right]\mathbf{A_1} +$$
$$+ \left[\underbrace{2k_{12}f(\overline{I}_{42})\exp[k_{22}f(\overline{I}_{42})^2]}_{\text{Fill fibres}} + \underbrace{2k_3(\overline{I}_{41}-1)}_{\text{Fibre interaction}}\right]\mathbf{A_2} \tag{6.88}$$

It is here recalled that the stresses evaluated by means of Equations (6.87) and (6.88) are intended as increments from an initial prestress field, which is considered to be known.

6.5 Identification of the modified HGO model parameters and preliminary validation

In this Section, the modified HGO model presented in the previous Section 6.4 is calibrated by using the biaxial test data on PVC/polyester and

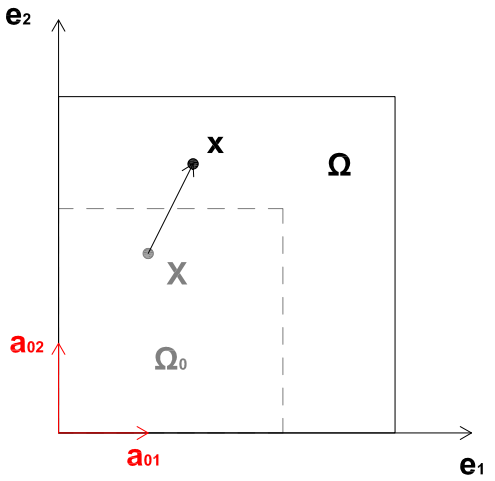

$$\begin{cases} x_1 = \lambda_1 X_1 \\ x_2 = \lambda_2 X_2 \\ x_3 = \lambda_3 X_3 = \dfrac{1}{\lambda_1 \lambda_2} X_3 \end{cases}$$

Figure 6.5: *Kinematical description of a planar biaxial test (pure homogeneous deformation, incompressible material).*

PTFE/glass fibres from Section 4.2. The results are then compared with the ones obtained in Section 5.3, where the Orthotropic Linear Elastic (OLE) model parameters were identified from the same test data. Finally, a first validation is presented in the last part of this Section, where stress-strain curves that have not been used in the calibration process are employed to check the predictive capability of the new model.

First of all, it is necessary to particularise the material stress response for a biaxial test, of which a simple geometric description is given in Figure 6.5. The load is applied along the fibre directions, namely $\mathbf{a_{01}} = [1\ 0\ 0]^{\mathrm{T}}$ (warp) and $\mathbf{a_{02}} = [0\ 1\ 0]^{\mathrm{T}}$ (fill or weft), which correspond to the principal axes of stretch. If the attention is restricted to the central part of the cruciform specimen, the test represents a case of pure deformation, because the strain magnitude does not vary with position and the principal axes of stretch do not vary in direction relative to an inertial frame either with strain or with position. Moreover, it has been widely demonstrated (Reinhardt, 1976; Bridgens, 2005; Galliot & Luchsinger, 2009) that the use of a sample with arms creates an almost homogeneous state of deformation in the central area, where the strain measurements have been performed.

Then, the matrix form of the deformation gradient tensor $\mathbf{F}$ is diagonal,

with diagonal elements being the principal stretches:

$$\mathbf{F} = \begin{bmatrix} \lambda_1 & 0 & 0 \\ 0 & \lambda_2 & 0 \\ 0 & 0 & \lambda_3 \end{bmatrix} \tag{6.89}$$

Since coated fabrics for tensile structures have been considered incompressible in this thesis, the enforcement of the incompressibility constraint $J = \det \mathbf{F} = \lambda_1 \lambda_2 \lambda_3 = 1$ results in the following form of the deformation gradient:

$$\mathbf{F} = \begin{bmatrix} \lambda_1 & 0 & 0 \\ 0 & \lambda_2 & 0 \\ 0 & 0 & \lambda_1^{-1}\lambda_2^{-1} \end{bmatrix} \tag{6.90}$$

Once the components of the deformation gradient $\mathbf{F}$ have been defined, it is possible to evaluate the left and right Cauchy-Green tensors, which read, according to Equations (6.9) and (6.11):

$$\mathbf{b} = \mathbf{F}\mathbf{F}^{\mathrm{T}} = \begin{bmatrix} \lambda_1^2 & 0 & 0 \\ 0 & \lambda_2^2 & 0 \\ 0 & 0 & \lambda_1^{-2}\lambda_2^{-2} \end{bmatrix} = \mathbf{F}^{\mathrm{T}}\mathbf{F} = \mathbf{C} \tag{6.91}$$

In addition, the structural tensors in the material configuration, which have been defined in Equation (6.28), look:

$$\mathbf{A_{01}} = \mathbf{a_{01}} \otimes \mathbf{a_{01}} = \begin{bmatrix} 1 & 0 & 0 \\ 0 & 0 & 0 \\ 0 & 0 & 0 \end{bmatrix} \tag{6.92}$$

$$\mathbf{A_{02}} = \mathbf{a_{02}} \otimes \mathbf{a_{02}} = \begin{bmatrix} 0 & 0 & 0 \\ 0 & 1 & 0 \\ 0 & 0 & 0 \end{bmatrix} \tag{6.93}$$

so that, according to Equation (6.63), their corresponding spatial counterparts are:

$$\mathbf{A_1} = \mathbf{F}\mathbf{a_{01}} \otimes \mathbf{F}\mathbf{a_{01}} = \begin{bmatrix} \lambda_1^2 & 0 & 0 \\ 0 & 0 & 0 \\ 0 & 0 & 0 \end{bmatrix} \tag{6.94}$$

$$\mathbf{A_2} = \mathbf{F}\mathbf{a_{02}} \otimes \mathbf{F}\mathbf{a_{02}} = \begin{bmatrix} 0 & 0 & 0 \\ 0 & \lambda_2^2 & 0 \\ 0 & 0 & 0 \end{bmatrix} \tag{6.95}$$

As a consequence, the pseudo-invariants $\overline{I}_{41}$ and $\overline{I}_{42}$ assume the following expressions:

$$\overline{I}_{41} = \overline{\mathbf{C}} : \mathbf{A_{01}} = \mathrm{tr}(\mathbf{A}_{\mathbf{01}}^{\mathrm{T}}\overline{\mathbf{C}}) = \lambda_1^2 \tag{6.96}$$

$$\overline{I}_{42} = \overline{\mathbf{C}} : \mathbf{A_{02}} = \mathrm{tr}(\mathbf{A}_{\mathbf{02}}^{\mathrm{T}}\overline{\mathbf{C}}) = \lambda_2^2 \tag{6.97}$$

where the relationship $\overline{\mathbf{C}} = \mathbf{C}$, which holds for the incompressibility assumption, has been used.

By employing the estimated quantities, the Cauchy stress tensor can be evaluated through Equation (6.88). In the present context (biaxial test), the true stress tensor is diagonal and its only non-zero components coincide with the principal stresses, which are:

$$\begin{cases} \sigma_{11} = -p + \mu\lambda_1^2 + 2k_{11}f(\lambda_1^2)\exp[k_{21}f(\lambda_1^2)^2]\lambda_1^2 + 2k_3(\lambda_2^2-1)\lambda_1^2 \\ \sigma_{22} = -p + \mu\lambda_2^2 + 2k_{12}f(\lambda_2^2)\exp[k_{22}f(\lambda_2^2)^2]\lambda_2^2 + 2k_3(\lambda_1^2-1)\lambda_2^2 \\ \sigma_{33} = -p + \mu\lambda_1^{-2}\lambda_2^{-2} \end{cases} \tag{6.98}$$

The prestress has been removed to simplify the identification procedure, and to stick to the assumption that the calculated stresses are increments with respect to a reference configuration which is not a natural one (i.e. it is not stress-free).

The assumption of plane stress has been adopted, therefore the Lagrange multiplier $-p$ that enforces the incompressibility constraint is such that:

$$\sigma_{33} = 0 \quad \Rightarrow \quad -p = -\mu\lambda_1^{-2}\lambda_2^{-2} \tag{6.99}$$

Eventually, the planar Cauchy stress components turn out to be described by the following functions:

$$\begin{cases} \sigma_{11} = \mu\left(\lambda_1^2 - \lambda_1^{-2}\lambda_2^{-2}\right) + 2k_{11}f(\lambda_1^2)\exp[k_{21}f(\lambda_1^2)^2]\lambda_1^2 + 2k_3(\lambda_2^2-1)\lambda_1^2 \\ \sigma_{22} = \mu\left(\lambda_2^2 - \lambda_1^{-2}\lambda_2^{-2}\right) + 2k_{12}f(\lambda_2^2)\exp[k_{22}f(\lambda_2^2)^2]\lambda_2^2 + 2k_3(\lambda_1^2-1)\lambda_2^2 \end{cases} \tag{6.100}$$

The corresponding nominal stresses, which are the components of the first Piola-Kirchhoff stress tensor $\mathbf{P}$, may be evaluated through Equation (6.22):

$$\begin{cases} P_{11} = -p\lambda_1^{-1} + \mu\lambda_1 + 2k_{11}f(\lambda_1^2)\exp[k_{21}f(\lambda_1^2)^2]\lambda_1 + 2k_3(\lambda_2^2-1)\lambda_1 \\ P_{22} = -p\lambda_2^{-1} + \mu\lambda_2 + 2k_{12}f(\lambda_2^2)\exp[k_{22}f(\lambda_2^2)^2]\lambda_2 + 2k_3(\lambda_1^2-1)\lambda_2 \\ P_{33} = -p\lambda_1\lambda_2 + \mu\lambda_1^{-1}\lambda_2^{-1} \end{cases} \tag{6.101}$$

which are further simplified, as previously done with the true stress components, by enforcing the plane stress condition ($P_{33} = 0$):

$$\begin{cases} P_{11} = \mu\left(\lambda_1 - \lambda_1^{-3}\lambda_2^{-2}\right) + 2k_{11}f(\lambda_1^2)\exp[k_{21}f(\lambda_1^2)^2]\lambda_1 + 2k_3(\lambda_2^2 - 1)\lambda_1 \\ P_{22} = \mu\left(\lambda_2 - \lambda_1^{-2}\lambda_2^{-3}\right) + 2k_{12}f(\lambda_2^2)\exp[k_{22}f(\lambda_2^2)^2]\lambda_2 + 2k_3(\lambda_1^2 - 1)\lambda_2 \end{cases} \tag{6.102}$$

Before starting with the description of the identification procedure, to better understand the physical meaning of the modified HGO model parameters, the stress components in Equation (6.100) have been reconducted to the small strain case. The Taylor's series expansion of Equation (6.100) up to the first order, evaluated at $\lambda_1, \lambda_2 \to 1^+$ (reference configuration), leads to:

$$\begin{cases} \sigma_{11}(\lambda_1, \lambda_2 \to 1^+) = \sigma_{11}|_{\substack{\lambda_1=1\\ \lambda_2=1}} + \left.\frac{\partial\sigma_{11}}{\partial\lambda_1}\right|_{\substack{\lambda_1=1\\ \lambda_2=1}}(\lambda_1 - 1) + \left.\frac{\partial\sigma_{11}}{\partial\lambda_2}\right|_{\substack{\lambda_1=1\\ \lambda_2=1}}(\lambda_2 - 1) \\ \sigma_{22}(\lambda_1, \lambda_2 \to 1^+) = \sigma_{22}|_{\substack{\lambda_1=1\\ \lambda_2=1}} + \left.\frac{\partial\sigma_{22}}{\partial\lambda_1}\right|_{\substack{\lambda_1=1\\ \lambda_2=1}}(\lambda_1 - 1) + \left.\frac{\partial\sigma_{22}}{\partial\lambda_2}\right|_{\substack{\lambda_1=1\\ \lambda_2=1}}(\lambda_2 - 1) \end{cases} \tag{6.103}$$

where:

$$\sigma_{11}|_{\substack{\lambda_1=1\\ \lambda_2=1}} = 0 \tag{6.104}$$

$$\sigma_{22}|_{\substack{\lambda_1=1\\ \lambda_2=1}} = 0 \tag{6.105}$$

as expected, since the reference configuration must be stress-free, while the other terms in Equation (6.103) look:

$$\left.\frac{\partial\sigma_{11}}{\partial\lambda_1}\right|_{\substack{\lambda_1=1\\ \lambda_2=1}} = 4\mu + 4k_{11} \tag{6.106}$$

$$\left.\frac{\partial\sigma_{22}}{\partial\lambda_1}\right|_{\substack{\lambda_1=1\\ \lambda_2=1}} = 2\mu + 4k_3 \tag{6.107}$$

$$\left.\frac{\partial\sigma_{11}}{\partial\lambda_2}\right|_{\substack{\lambda_1=1\\ \lambda_2=1}} = 2\mu + 4k_3 \tag{6.108}$$

$$\left.\frac{\partial\sigma_{22}}{\partial\lambda_2}\right|_{\substack{\lambda_1=1\\ \lambda_2=1}} = 4\mu + 4k_{12} \tag{6.109}$$

Therefore, Equation (6.103) may be rewritten as:

$$\begin{cases} \sigma_{11}(\lambda_1, \lambda_2 \to 1^+) = (4\mu + 4k_{11})(\lambda_1 - 1) + (2\mu + 4k_3)(\lambda_2 - 1) \\ \sigma_{22}(\lambda_1, \lambda_2 \to 1^+) = (2\mu + 4k_3)(\lambda_1 - 1) + (4\mu + 4k_{12})(\lambda_2 - 1) \end{cases} \tag{6.110}$$

Equation (6.110) represents the small strain approximation of the modified HGO model presented in the previous Section 6.4, which is equivalent to the following matrix form:

$$\begin{bmatrix} \sigma_{11} \\ \sigma_{22} \end{bmatrix} = \underbrace{\begin{bmatrix} 4\mu & 2\mu \\ 2\mu & 4\mu \end{bmatrix} \begin{bmatrix} \varepsilon_{11} \\ \varepsilon_{22} \end{bmatrix}}_{\text{Matrix}} + \underbrace{\begin{bmatrix} 4k_{11} & 4k_3 \\ 4k_3 & 4k_{12} \end{bmatrix} \begin{bmatrix} \varepsilon_{11} \\ \varepsilon_{12} \end{bmatrix}}_{\text{Fibres}} \tag{6.111}$$

where the isotropic contribution due to the matrix and the anisotropic term related to the fibres have been separated. Concerning the first one, by comparing it with the isotropic linear elastic model, it is easy to understand that μ is the coating shear modulus. On the other hand, consistency of the second term with the plane stress orthotropic linear elastic model gives a physical meaning to the fibre parameters: k_{11} and k_{12} represent the initial fibre stiffnesses (at small strains), while k_3 appears as an off-diagonal coefficient, which reproduces a sort of Poisson's effect. The introduction of k_3 is the most important modification to the HGO model that has been introduced in this thesis, whose aim is to capture the fibre interaction due to the weaving. In addition, it is worth noticing that the parameters k_{21} and k_{22}, which are contained in the modified HGO model at large strains, are not included in the small strains approximation, because they are related to the slope of the stress-strain curves at large strains.

Going back to the calibration of the new hyperelastic model proposed in this thesis, the identification of its parameters has been performed employing an unconstrained least square minimisation of the objective function described by Equation (5.16). The calculated values of stress that appear in Equation (5.16) has been estimated with Equation (6.102). The optimisation has been carried out by means of the MATLAB function *lsqnonlin*, which is a tool for the solution of nonlinear least squares problems. The *Levenberg-Marquardt* solution algorithm has been employed, which is a directional search method that interpolates between the Gauss-Newton and the gradient descent methods (Levenberg, 1944; Marquardt, 1963).

It is briefly recalled that the biaxial tests employed for the calibration are the followings (see Section 4.2):

- **Test A**: B18089 MSAJ;
- **Test B**: B18059 ALR;
- **Test C**: F702 MSAJ;
- **Test D**: F1202T2 ALR;
- **Test E**: VUB 001 A.

where tests A-B have been performed on PTFE coated glass fabrics, while tests C-E on a PVC coated polyester fabric. Only the first loading curves have been considered for each load ratio. Moreover, the residual strain and the prestress have been removed at the beginning of each load ratio of interest. For each loading curve, a number of 21 experimental points equally spaced in time have been considered, which is sufficient to reduce the calculation time required by the fitting procedure and the measurement noise, without loosing information about the stress-strain curves trend.

The results of the identification procedure applied to the modified HGO model presented in this thesis are shown in Table 6.2 and Figures 6.6 to 6.10. For each test, Table 6.2 reports the estimated values of the model parameters and the Residual Sum of Square (RSS), as defined in Equation (5.45). Figures 6.6 to 6.10 display the stress-strain curves of the calibrated model and compare them with the experimental data and with the OLE model, whose parameters has been calculated in Section 5.3 from the same biaxial tests.

Test	μ	k_{11}	k_{21}	k_{12}	k_{22}	k_3	RSS
	[kN/m]	[kN/m]	[1]	[kN/m]	[1]	[kN/m]	[kN^2/m^2]
A	1.32E+02	5.48E+02	1.22E+02	2.49E+02	1.09E+02	1.87E+02	3.38E+03
B	2.44E+02	6.02E+02	3.55E+01	2.79E+02	7.04E+01	2.56E+02	4.60E+03
C	4.41E+01	1.12E+02	-6.82E+01	9.28E+01	-4.37E+01	1.08E+01	1.27E+02
D	5.57E+01	2.36E+02	-1.00E+02	2.00E+02	-8.30E+00	3.09E+01	6.26E+02
E	3.74E+01	2.55E+02	-3.57E+02	1.14E+02	-1.09E+02	7.46E+00	8.18E+02

Table 6.2: *Least squares identification results for the modified HGO model: values of the best-fitting model parameters and of the Residual Sum of Squares (RSS).*

The first column of Table 6.2 reports the estimated values of μ, which is the shear modulus of the coating. A comparison between tests A and B and tests C to E shows that the shear modulus of PTFE is higher than the one of PVC. The same conclusion can be made by looking at the shear modulus values from the literature, which are summarised in the article by Galliot & Luchsinger (2010b). Therein, the authors propose a new test method for the investigation of coated fabric shear behaviour and apply it to several coated fabrics, eventually concluding that PTFE/glass fabrics have a much higher shear stiffness than PVC/polyester fabrics. However, the shear moduli estimated in this thesis are one order of magnitude grater than the ones measured by Galliot & Luchsinger (2010b), which lie in the range of 37-58 kN/m for PTFE/glass and in the range of 9-17 kN/m for PVC/polyester. Nevertheless, the empirical equation that is currently employed by engineers to calculate the shear modulus for structural fabrics (i.e. $G = E/20$, where G=shear modulus and E=Young's modulus) furnishes values that fits well the ones of μ in Table 6.2, as demonstrated by Table 6.3 (the Young's moduli E_1 are the ones from Table 5.1), especially in the case of PTFE coated glass fabrics (tests A and B).

Test	$\mathbf{G = E_1/20}$	$\boldsymbol{\mu}$
	[kN/m]	[kN/m]
A	125	132
B	130	244
C	28	44
D	49	56
E	43	37

Table 6.3: *Comparison between the values of the shear modulus obtained from the fitting of the new hyperelastic model presented in this thesis with the ones estimated by using the empirical rule adopted by engineers.*

The values of k_{11} in Table 6.2 are higher than the ones of k_{12}. This is reasonable, since warp fibres are stiffer because of the weaving process. By analysing data in Table 6.2, this difference can be quantified: it results that warp yarns show a value of k_{11} that is 216-224 % higher than the correspondent value of k_{12} for tests A, B and E. This difference is reduced to 118% in test C and 121% in test D, because the tested samples were produced with the Précontraint® technology described in Section 4.1.1. Moreover, the estimated values of the parameters k_{11} and k_{12} are larger for PTFE/glass fabrics than for PVC/polyester fabrics, which is again in accordance with the experimental behaviour of these materials.

The best-fitting values of k_{21} and k_{22}, which are the parameters related to the large strain stiffening of the yarns, appears to be of the same order of magnitude for warp and weft fibres in each test. In addition, the unconstrained least squares estimation of these parameters has lead to positive values of k_{21} and k_{22} for PTFE/glass fabrics (tests A and B) and negative values for PVC/polyester fabrics (tests C to E). Although such negative values are not compatible with the constraint $k_2 > 0$, which is setted by Holzapfel et al. (2000) in order to predict a response that is physically reasonable for arterial tissues, these may be acceptable for coated fabrics. In fact, the PTFE/glass stress-strain curves show an increment of stiffness at large strains, where, on the contrary, PVC/polyester fabrics present a decreasing slope, as it can be seen from Figures 6.6 to 6.10.

However, Holzapfel et al. (2004) demonstrated that, by assuming $k_1 > 0$ and $k_2 > 0$, convexity and material stability are guaranteed, because the strong ellipticity condition (see, e.g., Zee & Sternberg, 1983) is satisfied. Anyway, according to Holzapfel et al. (2004), more data are needed in order to assess whether or not strong ellipticity should be considered as a prerequisite condition to be satisfied by realistic material models. In addition, strong ellipticity may hold also for negative values of k_{21} and k_{22}, because the demonstration by Holzapfel et al. (2004) does not exclude this instance. A check of material stability for the new hyperelastic model presented in this thesis should be performed, but it goes beyond the goals of this work. Moreover, it is suggested that a different function for the energy contribution related to the fibres (i.e. $\overline{\Psi}_{aniso} = \overline{\Psi}_1 + \overline{\Psi}_2$) could be more appropriate to model the PVC/polyester stress-strain behaviour: for example a logarithmic term might replace the exponential one.

Again, by looking at the last column of Table 6.2, one can notice that the RSS values are larger in the case of PTFE/glass fabrics (tests A and B). The reason is in the higher nonlinearity of their behaviour with respect to the PVC/polyester fabrics, which has been ascertained also by the OLE model calibration, whose results are reported in Section 5.3.1. The poorer quality of the fitting results for the PTFE/glass fabrics can be figured out also by comparing the graphics in Figures 6.6 and 6.7 with the ones in Figures 6.8 to 6.10.

Finally, Figures 6.6 to 6.10 show also that the new hyperelastic constitutive law proposed in this thesis is able to model the material response for both PTFE/glass and PVC/polyester coated fabrics better than OLE

model. The improved quality of the fitting is confirmed by the fact that RSS values in Table 6.2 are lower than RSS values in Table 5.1 for all the five tests. This result is even more significant, because in the OLE model fitting conducted according to the Differential Solution (DS) method, part of the experimental data have been disregarded, so that the corresponding RSS values are "*artificially decreased*". In addition, by focusing on load ratios 1:0 and 0:1 in Figures 6.6 to 6.10 it is possible to see that the modified HGO model can capture the stiffening at large strain that is displayed by PTFE/glass fabrics.

Now, the next step consist in a preliminary validation of the new hyperelastic model that is proposed in this thesis (modified HGO model). Validation of a constitutive law is the process of determining the degree to which it constitutes an accurate representation of the material mechanical behaviour. More in detail, the predictive capability of the modified HGO model is assessed hereafter.

Among the biaxial tests that have been previously employed for calibration purposes, there are two tests, namely B and D, that have been performed with a particular loading profile. The peculiarity of this profile is that specimen are tested also for load ratios other than the five that are prescribed by the MSAJ/M-02:1995 Standard (see Section 4.2.2). More in detail, four additional load ratios are considered, which are intermediate between the usual five ones: they are 1:0.3, 0.3:1, 1:0.7 and 0.7:1. These have been added at the end of the typical loading profile and analogously separated by preconditioning cycles.

The stress-strain response curves for the additional load ratios in tests B and D have been constructed with the same rules employed for the other load ratios. This means that the residual strain and the prestress have been removed at the beginning of each loading curve (reference state of crimp and prestress) and that the number of experimental points has been reduced to 21 to diminish the calculation time.

Then, by using the engineering warp and fill strains from test data, the nominal stresses have been calculated according to the new constitutive law. In particular, Equation (6.102) has been employed, which represents the plane stress form for a biaxial test of the new hyperelastic constitutive model presented in Section 6.4. In Equation (6.102), the warp and fill

stretches have been evaluated with the following relations:

$$\lambda_1 = \varepsilon_1 + 1 \ , \qquad \lambda_2 = \varepsilon_2 + 1 \tag{6.112}$$

which calculate the stretches λ_1 and λ_2 as a function of the engineering strains in warp and weft direction, i.e. ε_1 and ε_2 respectively. Indeed, if L_0 is the initial distance between two points of a body and L is the final one, after stretching, the stretch comes from the following relation:

$$\lambda = \frac{L}{L_0} = \frac{L_0 + \Delta L}{L_0} = \frac{\Delta L}{L_0} + 1 = \varepsilon + 1 \tag{6.113}$$

where ΔL is the length variation and $\varepsilon = \Delta L / L_0$ is the definition of engineering strain.

Hence, the stress-strain curves that represent the model response have been represented in Figures 6.11 and 6.12. The analytical curves for both PTFE/glass (test B, Figure 6.11) and PVC/polyester (test D, Figure 6.12) fabrics show good agreement with the correspondent experimental curves. This demonstrates that the model proposed in this thesis possesses good predictive capability regarding the biaxial tensile behaviour of coated fabrics under warp to fill load ratios that have not been tested in the experiments.

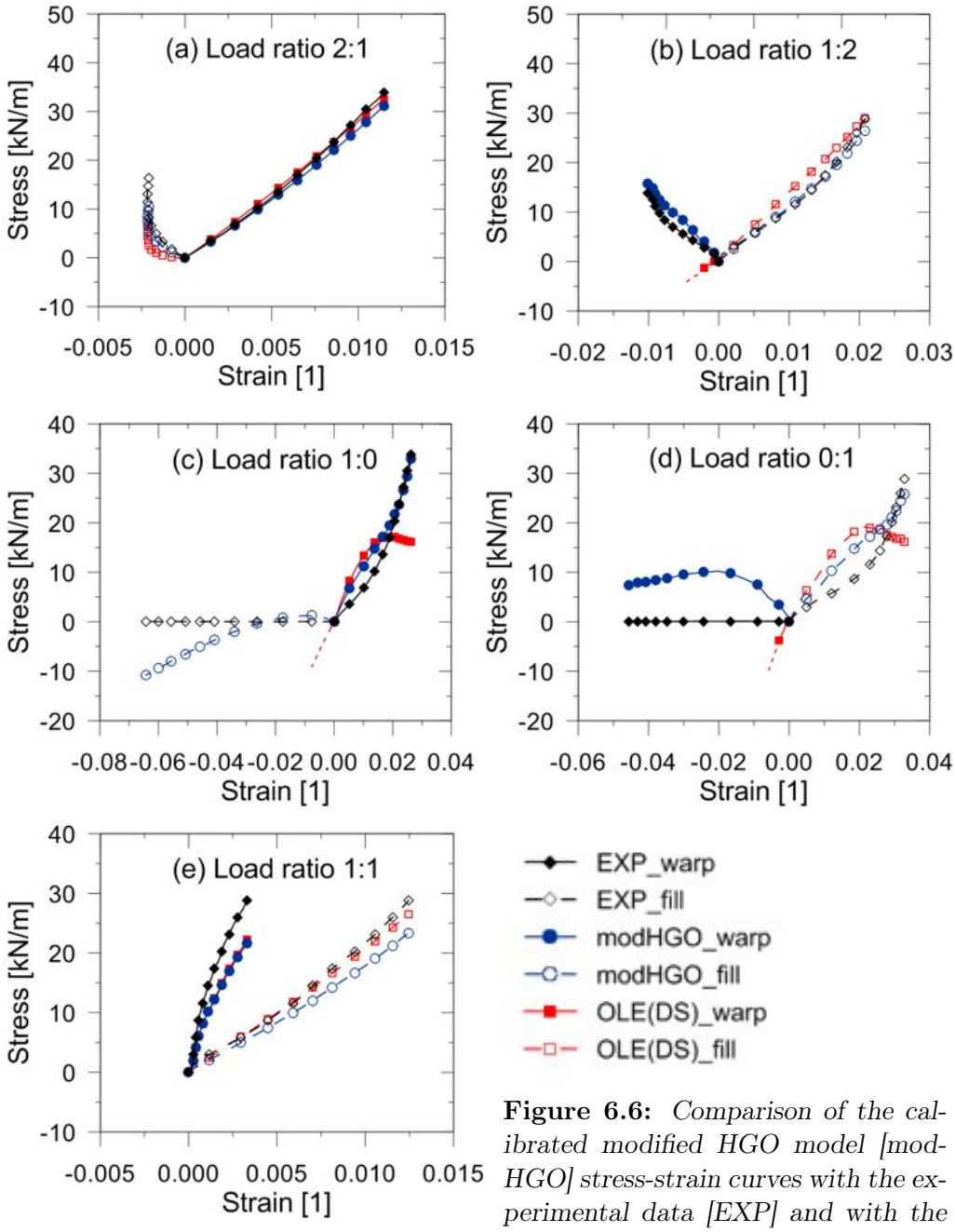

Figure 6.6: *Comparison of the calibrated modified HGO model [mod-HGO] stress-strain curves with the experimental data [EXP] and with the OLE model [OLE(DS)] calibrated in Section 5.3 (test A).*

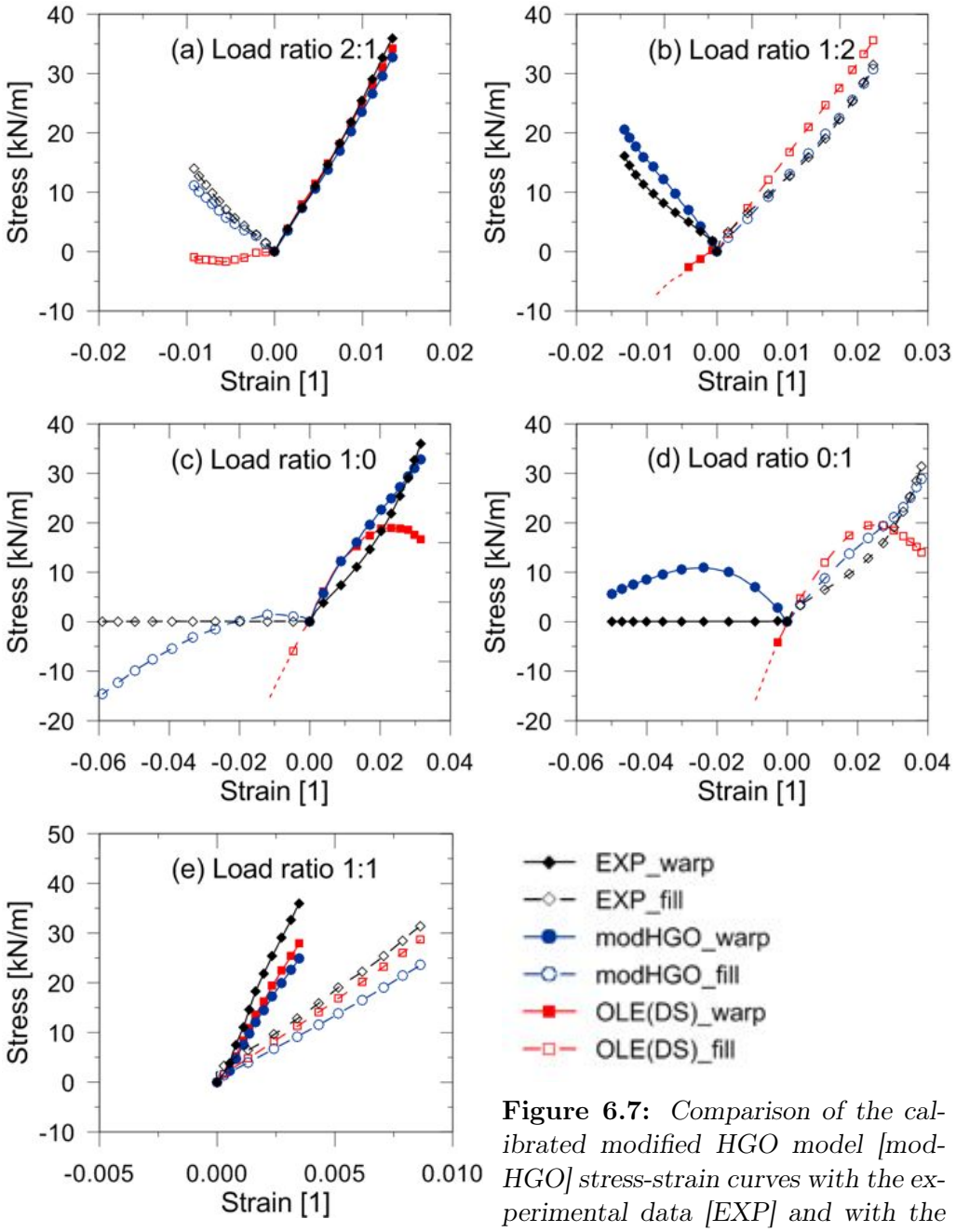

Figure 6.7: *Comparison of the calibrated modified HGO model [mod-HGO] stress-strain curves with the experimental data [EXP] and with the OLE model [OLE(DS)] calibrated in Section 5.3 (test B).*

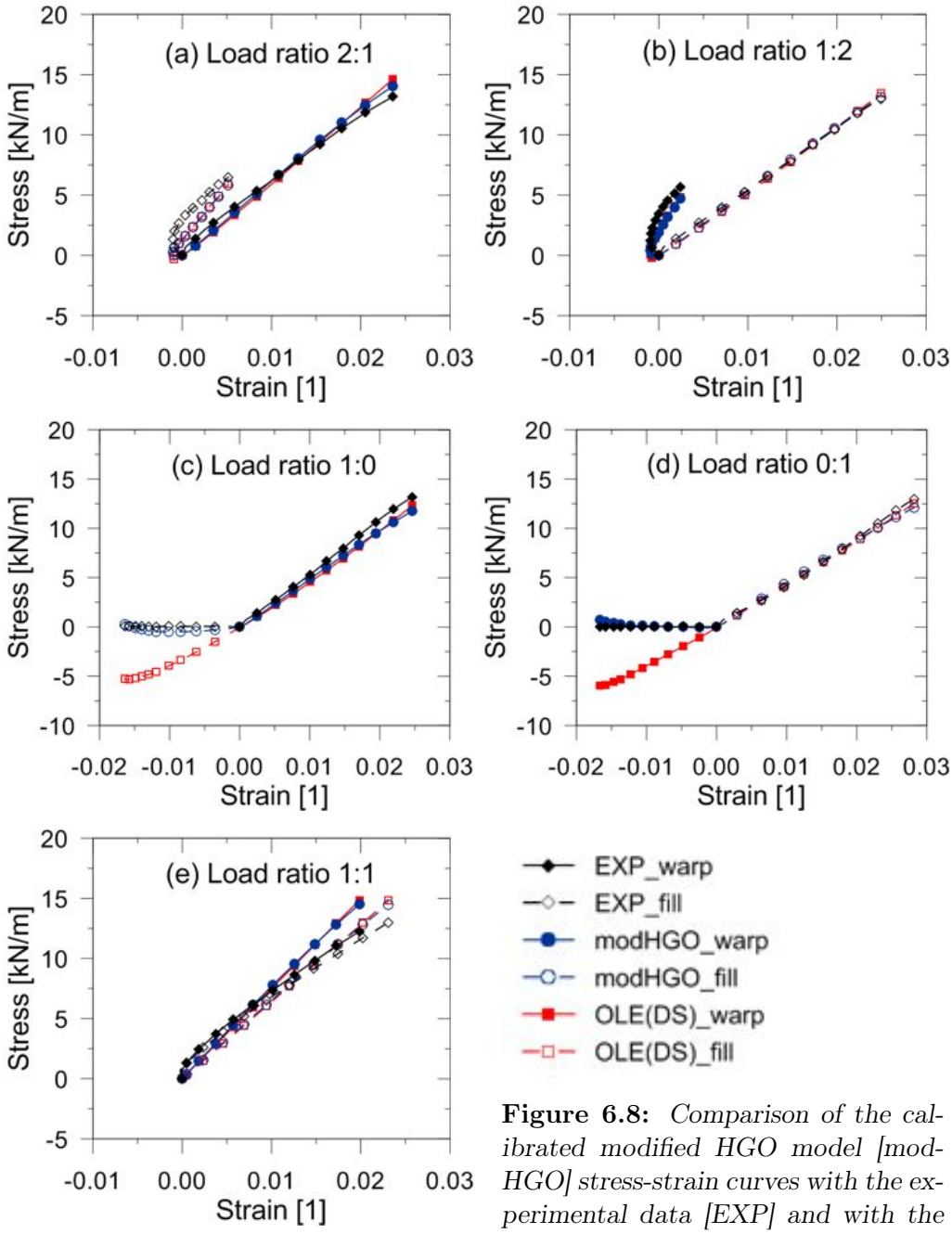

Figure 6.8: *Comparison of the calibrated modified HGO model [modHGO] stress-strain curves with the experimental data [EXP] and with the OLE model [OLE(DS)] calibrated in Section 5.3 (test C).*

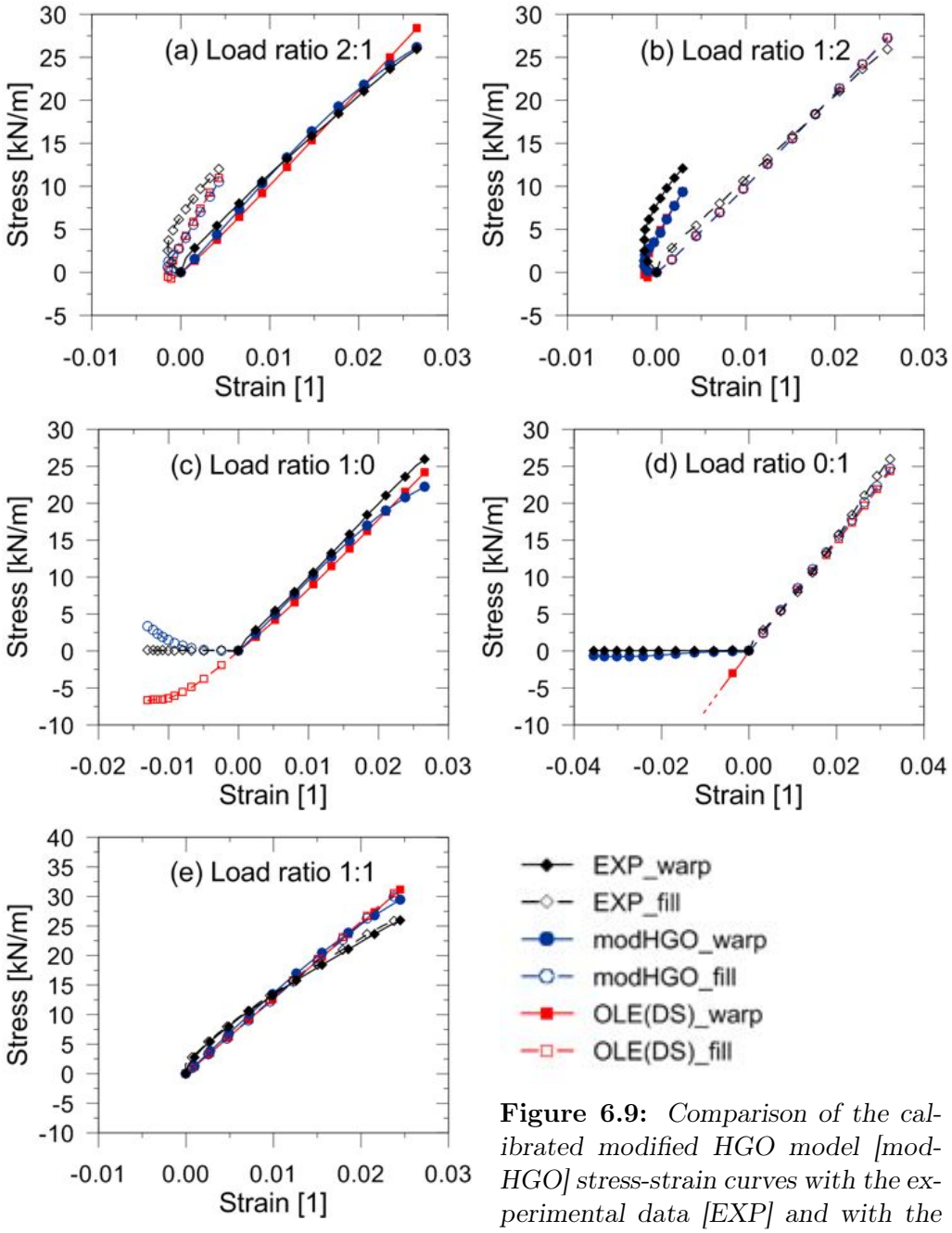

Figure 6.9: *Comparison of the calibrated modified HGO model [modHGO] stress-strain curves with the experimental data [EXP] and with the OLE model [OLE(DS)] calibrated in Section 5.3 (test D).*

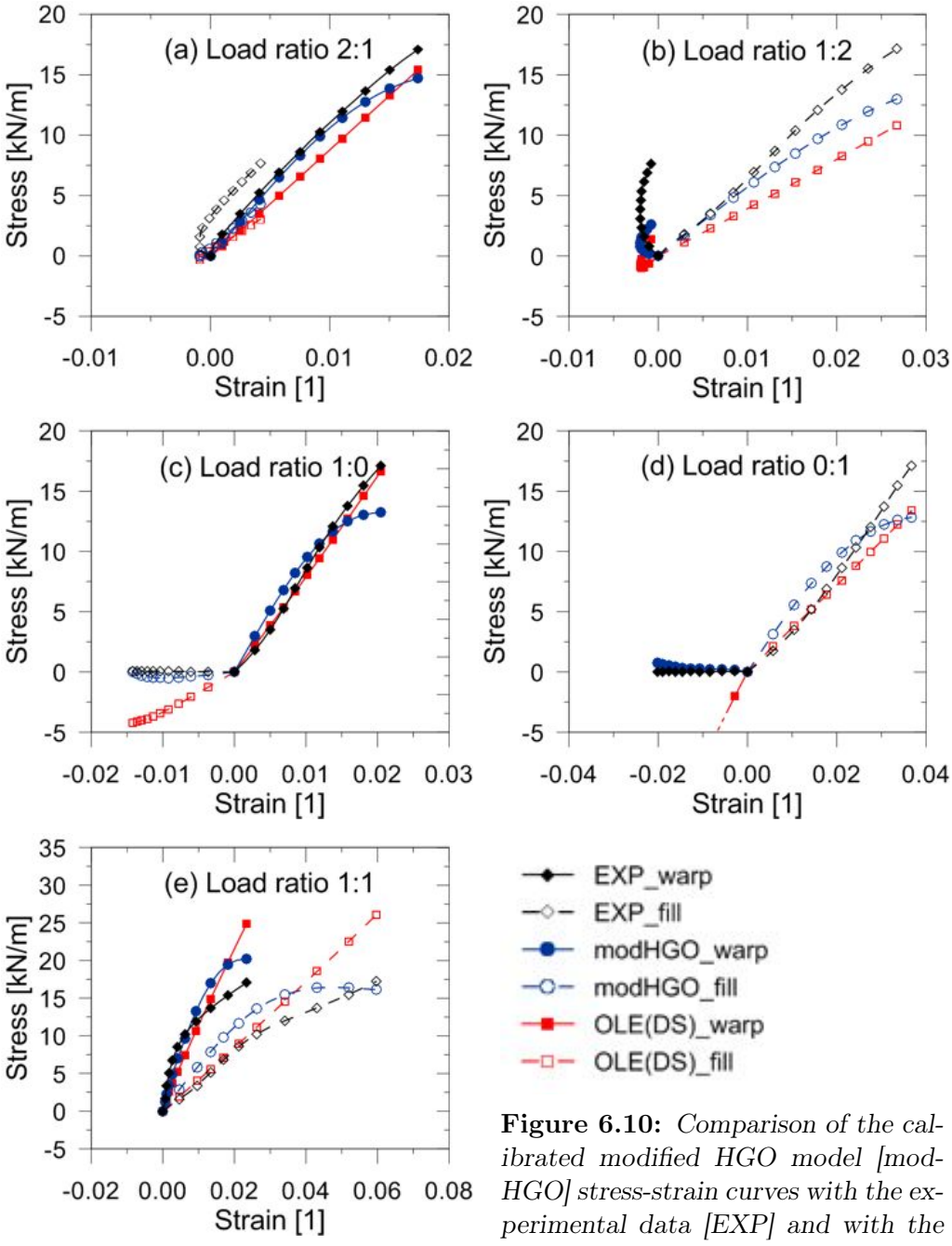

Figure 6.10: *Comparison of the calibrated modified HGO model [modHGO] stress-strain curves with the experimental data [EXP] and with the OLE model [OLE(DS)] calibrated in Section 5.3 (test E).*

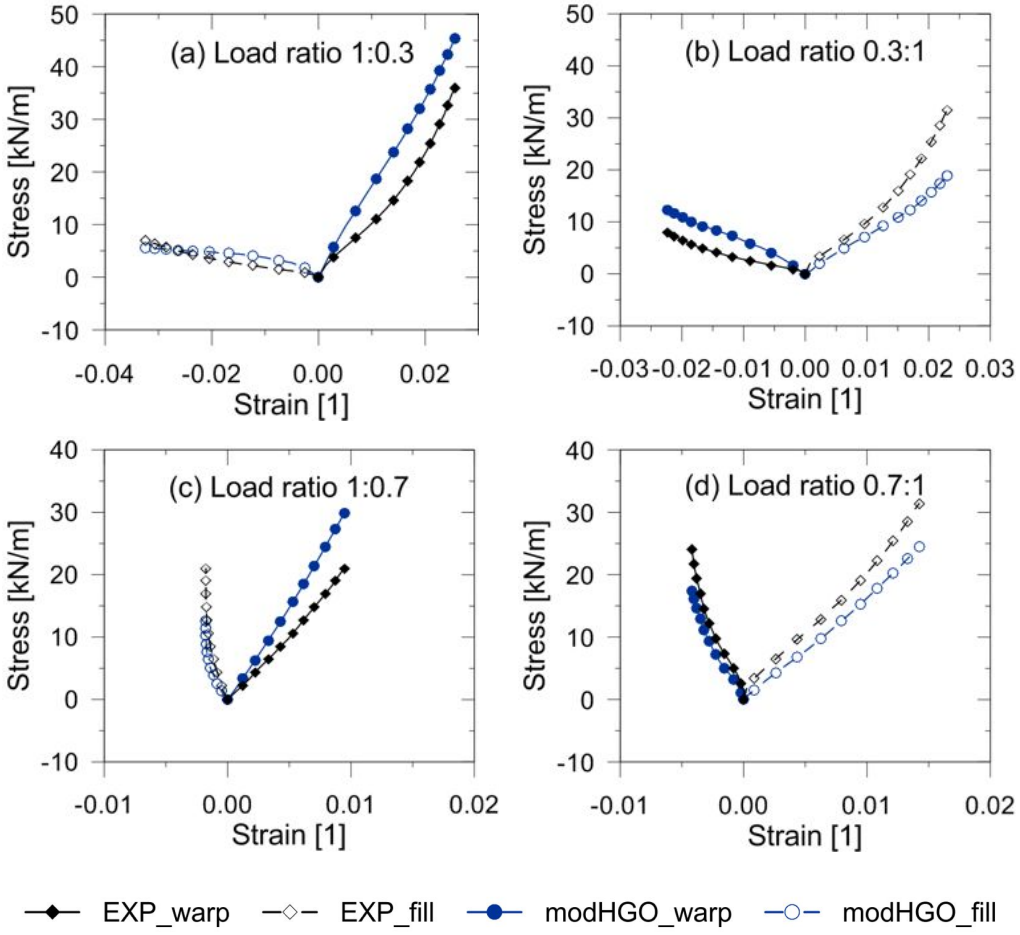

Figure 6.11: *Comparison of the calibrated modified HGO model [modHGO] stress-strain curves with the experimental data [EXP] for the additional load ratios that have not been employed in the identification of the model parameters (test B).*

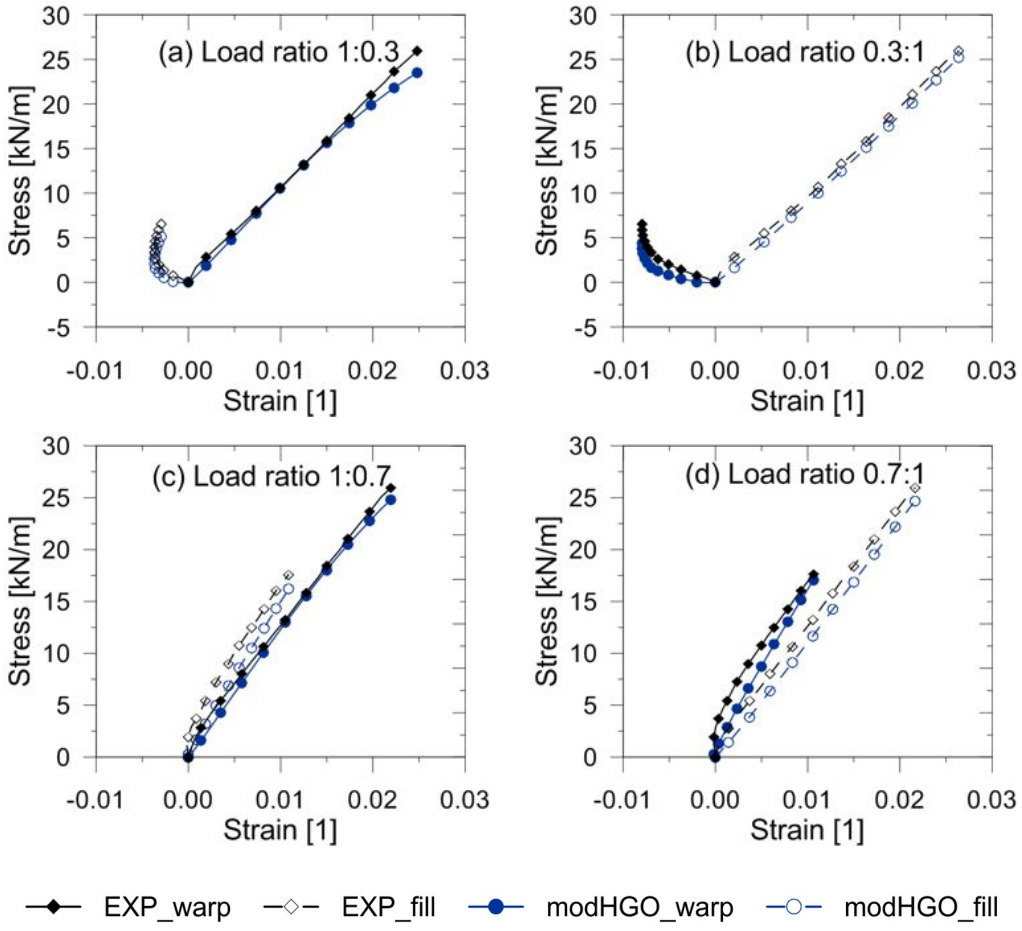

Figure 6.12: *Comparison of the calibrated modified HGO model [modHGO] stress-strain curves with the experimental data [EXP] for the additional load ratios that have not been employed in the identification of the model parameters (test D).*

7

Constitutive model implementation in ABAQUS and verification tests

At present, finite element analyses (FEA) are widely employed in the design of structures, especially when it is necessary to deal with complex behaviours at the material and/or structural level. Of course, this is the case of nonlinear problems at finite strains. Therefore, an important step is the implementation of a new constitutive model into an overall procedure of structural analysis. The new hyperelastic constitutive model for coated fabrics (modified HGO model) presented in Chapter 6 is here implemented into a general purpose commercial finite element code, namely ABAQUS.

The Holzapfel-Gasser-Ogden (HGO) model, in its original form for biological tissues, is already available in ABAQUS as embedded material, but with a limitation: the parameters that are related to the mechanical behaviour of the reinforce must be the same for each family of fibres. As discussed previously in Chapter 6, this assumption is not suitable to model architectural coated fabrics, because they display a greater stiffness of warp threads due to the weaving process. However, the embedded HGO material has been useful to validate the correct implementation of the new constitutive law. This is one of the reasons why ABAQUS has been chosen among the other popular commercial nonlinear FEA packages.

The second reason is that ABAQUS allows the user to interact with the built-in finite element solver through a series of subroutines written in FORTRAN language. This possibility represents a great advantage for research purposes. More in detail, in ABAQUS/Standard, which is the

implicit solver of the software, there are two types of constitutive user subroutines that can be employed to model anisotropic hyperelasticity: they are named UANISOHYPER and UMAT. The former is specifically conceived to model a user-defined anisotropic hyperelastic constitutive law, while the latter represents a more general tool apt to implement any kind of user material model.

The new hyperelastic model introduced previously in Chapter 6 has been implemented using UANISOHYPER. The details are reported in the next Section 7.1, together with the reasons for having chosen this type of user subroutine.

In the same Section 7.1, the verification tests that have been performed to check the correctness of the code implementation are also described. Verification consists in assessing if the code gives the correct solution to a set of benchmark problems for which analytical or highly accurate numerical solutions are available. When possible, the closed-form solution has been evaluated with an independent solver, which has been implemented by the author with Mathematica software. Some of the tests have been performed by switching off parts of the implemented user material in order to re-conduct it to a simpler built-in ABAQUS material: the numerical solution produced with the embedded material model has been employed for comparison.

7.1 User subroutine UANISOHYPER

The user subroutine UANISOHYPER is available in ABAQUS to model anisotropic hyperelastic materials. When implementing incompressible hyperelastic materials, UANISOHYPER is recommended over UMAT by the ABAQUS User's Manual. Moreover, the UANISOHYPER subroutine displays several advantages:

- it is easier to implement than UMAT, because it requires only the strain energy and its first, second and third derivatives;

- it allows the user to switch between incompressible and compressible materials, while UMAT can handle incompressibility only by means of the penalty method;

- it can be employed with both continuum and structural (for instance membrane) finite elements, without any modification of the code;
- it allows the user to define material behaviours that are dependent on field variables or state variables;
- it automatically derives the matrix of tangent moduli (elasticity tensor, in continuum mechanics);
- it supports the plane stress assumption, if needed, while UMAT must be written in a different way for plane stress or 3D stress elements.

For these reasons, it has been chosen to code the new constitutive model within a UANISOHYPER, even if it shows three drawbacks:

- it does not provide access to the Cauchy stress tensor or to the elasticity tensor, which are instead implemented directly by the user in the UMAT subroutine;
- the total deformation gradient is not available;
- it is less general than UMAT, because it allows only for modifications of the strain energy function.

Indeed, the main limit of UANISOHYPER is that it gives less control on the solution procedure, which is quite important when dealing with complex nonlinear anisotropic materials.

There are two versions of UANISOHYPER:

- UANISOHYPER_INV can be used to define the strain energy potential as a function of an irreducible set of scalar invariants;
- UANISOHYPER_STRAIN can be used to define the strain energy potential as a function of the components of the Green-Lagrange strain tensor.

Since the modified HGO model has been previously formulated in terms of invariants (see Chapter 6), the first type of subroutine has been employed.

The scalar invariants of the modified right Cauchy-Green tensor (deviatoric strain invariants), which have been defined in Equation (6.30),

Model invariants	$\overline{I}_1$	$\overline{I}_3$	$\overline{I}_{41}$	$\overline{I}_{42}$
`AINV` **invariants**	I_1^*	I_3^*	I_4^*	I_8^*

Table 7.1: *Corrispondence in the enumeration of the deviatoric strain invariants.*

are provided to the user subroutine by ABAQUS through the array `AINV`. Table 7.1 shows the correspondence in the enumeration between the invariants $\overline{I}_i$ employed in the modified HGO model and the invariants I_i^* that are contained in `AINV`.

The quantities that must be defined by the user are the strain energy potential (array `UA`) and its first (array `UI1`), second (array `UI2`) and third (array `UI3`) derivatives with respect to the deviatoric strain invariants. Firstly, the deviatoric part of the strain energy density $\overline{\Psi}$ associated with the modified HGO model, whose contributions have been defined in Equations (6.81b) to (6.81e), is stored in the second component of `UA` as follows:

$$\begin{aligned} \texttt{UA(2)} = \frac{\mu}{2}\left(I_1^* - 3\right) + \frac{k_{11}}{2k_{21}}\{\exp\left[k_{21}\langle\overline{E}_1\rangle^2\right] - 1\} + \\ + \frac{k_{12}}{2k_{22}}\{\exp\left[k_{22}\langle\overline{E}_2\rangle^2\right] - 1\} + k_3\overline{E}_1\overline{E}_2 \end{aligned} \tag{7.1}$$

where:

$$\overline{E}_1 = I_4^* - 1 \ , \qquad \overline{E}_2 = I_8^* - 1 \tag{7.2}$$

are functions of the strains in warp and weft direction respectively. The operator $\langle\bullet\rangle$ stands for the Macauley bracket and is defined as:

$$\langle\bullet\rangle = \frac{1}{2}\left(|\bullet| + \bullet\right) = \max(\bullet, 0) \tag{7.3}$$

It is employed to switch off the fibre contribution when the yarn is compressed (negative strain), therefore it is equivalent to the function in Equation (6.74).

The total strain energy density `UA(1)` is equal to `UA(2)` in the case of incompressible material. If compressibility is considered, the following term is added to the strain energy to take into account the volumetric contribution:

$$\texttt{UA(1)} = \texttt{UA(2)} + \frac{1}{D_1}\left(\frac{J^2 - 1}{2} - \ln(J)\right) \tag{7.4}$$

where D_1 is a material parameter related to the bulk modulus. The value of the volume ratio J is provided by ABAQUS among the invariants and more in detail it coincides with the invariant I_3^*.

Once the strain energy potential Ψ has been stored in the `UA` array, its first derivatives with respect to the scalar invariants ($\partial\Psi/\partial I_i^*$) are stored in the `UI1` array. Thus, the nonzero components of `UI1` in the incompressible case are:

$$\texttt{UI1(1)} = \frac{\mu}{2} \tag{7.5a}$$

$$\texttt{UI1(4)} = k_{11}\langle\overline{E}_1\rangle \exp\left[k_{21}\langle\overline{E}_1\rangle^2\right] + k_3\overline{E}_2 \tag{7.5b}$$

$$\texttt{UI1(8)} = k_{12}\langle\overline{E}_2\rangle \exp\left[k_{22}\langle\overline{E}_2\rangle^2\right] + k_3\overline{E}_1 \tag{7.5c}$$

If a compressible material is considered, the volumetric term of the strain energy adds the following term to the first derivatives:

$$\texttt{UI1(3)} = \frac{1}{D_1}\left(J - \frac{1}{J}\right) \tag{7.6}$$

Furthermore, array `UI2` contains the second derivatives of the strain energy potential Ψ with respect to the scalar invariants ($\partial^2\Psi/\partial I_i^*\partial I_j^*$). Its nonzero components result to be (incompressible case):

$$\texttt{UI2(4,4)} = k_{11}\left[H(\overline{E}_1) + 2k_{21}\langle\overline{E}_1\rangle^2\right] \exp\left[k_{21}\langle\overline{E}_1\rangle^2\right] \tag{7.7a}$$

$$\texttt{UI2(8,8)} = k_{12}\left[H(\overline{E}_2) + 2k_{22}\langle\overline{E}_2\rangle^2\right] \exp\left[k_{22}\langle\overline{E}_2\rangle^2\right] \tag{7.7b}$$

$$\texttt{UI2(4,8)} = \texttt{UI2(8,4)} = k_3 \tag{7.7c}$$

where $H(\overline{E}_\alpha)$ is the Heaviside function:

$$H(\overline{E}_\alpha) = \begin{cases} 1 & \text{if } \overline{E}_\alpha \geq 0 \\ 0 & \text{if } \overline{E}_\alpha < 0 \end{cases} \tag{7.8}$$

For compressible materials, there is another component of the array `UI2` that is not null:

$$\texttt{UI2(3,3)} = \frac{1}{D_1}\left(1 + \frac{1}{J^2}\right) \tag{7.9}$$

Finally, for compressible materials with a hybrid formulation, it is required to furnish $\partial^3\Psi/\partial I_i^*\partial I_j^*\partial J$, which are the derivatives with respect to

J of the second derivatives of the strain energy potential (i.e. the ones stored in `UI2`). Such derivatives are stored in array `UI3`, which displays only one nonzero component for the modified HGO model, namely:

$$\texttt{UI3(3,3)} = -\frac{1}{D_1}\frac{1}{J^3} \tag{7.10}$$

It is recalled that a *hybrid or mixed formulation* is a multi-field variational principle, which is employed in place of the standard displacement based method (i.e. Galerkin method) to overcome the numerical difficulties that are known as locking phenomena. These consist in poor numerical performances, such as penalty sensitivity and ill-conditioning, that arise, for example, when almost incompressible materials are modelled with a Galerkin approach, especially at large strains. In that case, a very small change in displacement produces extremely large changes in pressure, so that a purely displacement-based solution is too sensitive to be useful numerically. To solve this problem, the hybrid finite element approach discretizes the pressure stress and treats it as an independent variable, which is additional to the usual interpolated displacement field (multi-field approach). The pressure and displacement fields are coupled through the constitutive theory and the compatibility condition, with this coupling implemented by the Lagrange multiplier method. For more details about the hybrid formulation the reader is referred to the books by Zienkiewicz & Taylor (2000), Hughes (2000) or Holzapfel (2000).

7.2 Verification tests

Verification of the model implementation is extremely important. It consists in determining if the written code can accurately represent the solution to a set of benchmark problems. As suggested by Dunne & Petrinic (2005), verification of material models includes:

- development of an independent solver for uniaxial and shear problems to compare its results with that obtained using the subroutine;
- testing of a single and, where appropriate, multiple elements, for uniaxial and pure (or simple) shear conditions, using both displacement and load control;

- comparison with multiaxial problems having non uniform strain and stress distributions, for which the solution is known.

The last type of test is important, but a closed-form solution of problems that generate non uniform stress and strain fields is almost always not available. To overcome this obstacle, if it is possible to switch off parts of the implemented user constitutive law and re-conduct it to a simpler built-in material, a numerical solution produced with such embedded material model can be employed for comparison. The aforementioned verification tests have been executed and their results are presented hereafter.

7.2.1 Single element uniaxial test

A unit square (1×1 m) has been considered, which is composed by a single plane stress continuum finite element with four nodes (CPS4 in ABAQUS notation). The element has two active degrees of freedom, namely the translations in the horizontal and vertical directions (labelled with 1 and 2, respectively). A thickness of 1 mm is assigned to the cross section. Moreover, restraints are applied to the left and bottom edges of the square, to prevent horizontal displacement along the left side and vertical displacement along the bottom side.

The unit square has been subjected to different uniaxial loading conditions. Usually, the element is tested for condition of both displacement and force control: the former is used for checking the direct stress components, while the latter is employed to search for errors in the Jacobian (see, e.g., Dunne & Petrinic, 2005). Since the subroutine UANISOHYPER automatically derives the matrix of tangent moduli, only the displacement controlled tests have been carried out in this thesis.

The adopted material is the one described by the incompressible version of the modified HGO model. The material parameters in Table 7.2 have been employed, which correspond to the ones estimated for test B in Table 6.2. The warp yarns are aligned with the global direction 1, so that $\mathbf{a_{01}} = [1\ 0\ 0]^{\mathrm{T}}$, while the fill yarns are aligned with direction 2, thus $\mathbf{a_{02}} = [0\ 1\ 0]^{\mathrm{T}}$.

In the first test (Figure 7.1), a total displacement of 65 mm in direction 1 has been enforced along the right edge of the square. The external action has been applied over the step by means of linear increments, to permit the

$\boldsymbol{\mu}$ [MPa]	$\mathbf{k_{11}}$ [MPa]	$\mathbf{k_{21}}$ [1]	$\mathbf{k_{12}}$ [MPa]	$\mathbf{k_{22}}$ [1]	$\mathbf{k_3}$[MPa]
244	602	35.5	279	70.4	256

Table 7.2: *Material properties employed in the numerical analyses.*

construction of the associated stress-strain curve. This loading condition produces a uniform stress state in the plane of the element, which can be compared with a closed-form solution. This has been obtained with an independent code developed by the author with the software Mathematica.

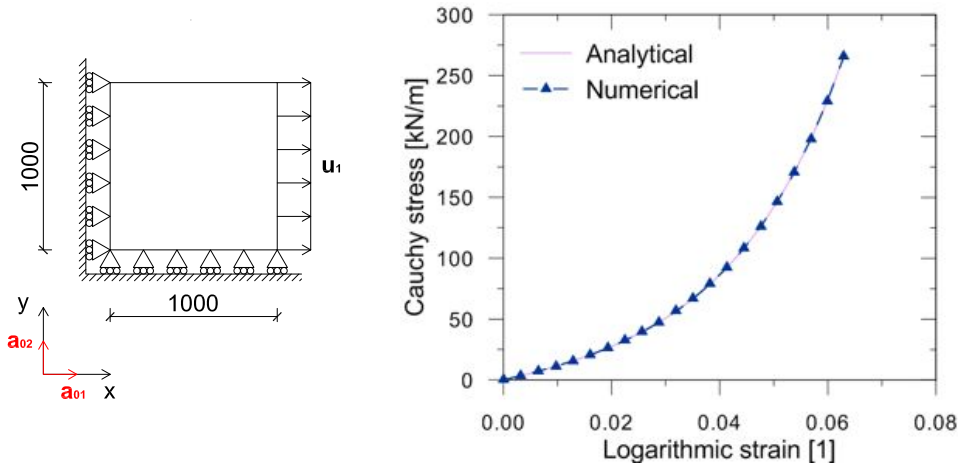

(a) Sketch (b) Stress-strain curves

Figure 7.1: *Analytical and numerical model response to an applied uniaxial displacement in direction 1.*

In Figure 7.1(b) the analytical and numerical stress-strain curves in direction 1 are reported. The numerical solution is completely overlapped to the analytical one, therefore the subroutine correctly reproduces the model response in the case of a uniaxial displacement applied in the warp direction.

An analogous test has been performed by applying the displacement in direction 2 (Figure 7.2). Once again, the resulting analytical and numerical stress-strain curves coincide. Moreover, by comparing the curves in Fig-

ure 7.2(b) to the ones in Figure 7.1(b) it is possible to notice that the fill fibres have a lower stiffness, especially at the beginning: this behaviour is consistent with the physics of the problem.

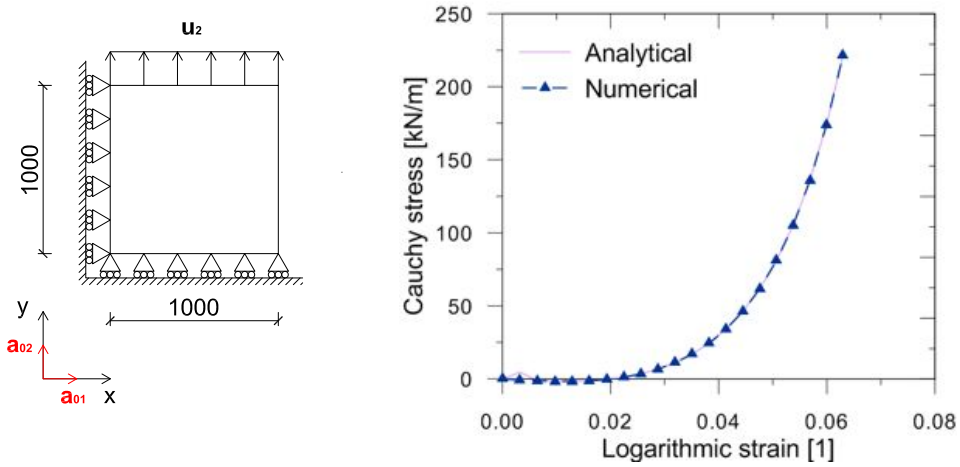

(a) Sketch (b) Stress-strain curves

Figure 7.2: *Analytical and numerical model response to an applied uniaxial displacement in direction 2.*

To test the model behaviour in a pure shear condition, the unit square of the previous examples has been subjected to a deformation that preserves the area (Figure 7.3). A horizontal displacement of 200 mm has been imposed along the right side, which has been incremented linearly over the step. At the same time, the top edge has been moved of 166.667 mm toward the bottom to enforce the conservation of the in-plane area. The warp and fill yarns, which represent the principal directions of the material, are rotated of 45 ° clockwise with respect to the horizontal direction, so that $\mathbf{a_{01}} = [\sqrt{2}/2 \ -\sqrt{2}/2 \ 0]^{\mathrm{T}}$ and $\mathbf{a_{02}} = [\sqrt{2}/2 \ \sqrt{2}/2 \ 0]^{\mathrm{T}}$.

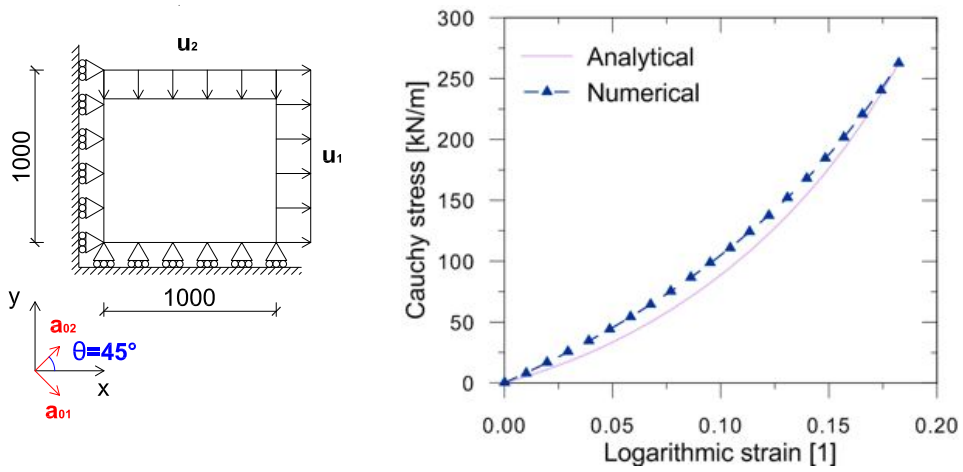

(a) Sketch (b) Stress-strain curves

Figure 7.3: *Analytical and numerical model response to pure shear loading.*

8

Validation of the new constitutive model for coated fabrics

Validation is the process of determining the predictive capability of a computational model by comparison with experimental data (Anderson et al., 2007). In this Chapter, the new hyperelastic constitutive model for coated fabrics proposed in Chapter 6 is validated through simple examples, for which experimental data are available.

When possible, the solution to these problems is found first analytically, by means of an independent solver developed by the author with Mathematica software. Then, the same problems are discretised with finite elements and solved with ABAQUS, by employing the user subroutine described in the previous Chapter 7. Finally, the analytical and numerical stress-strain curves are compared to the experimental ones and the predictive capability of the model is commented.

Firstly, in Section 8.1, the new constitutive model is tested for uniaxial and bias loading. A series of uniaxial tests are performed, having a different inclination of the fabric yarns with respect to the loading direction. The solution is compared with experimental data from the literature.

Subsequently, in Section 8.2, several biaxial tests at various load ratios are performed. The model predictions are compared with the experimental results from test B18059 ALR, which has been described in Chapter 4 and for which an estimation of the model parameters have been carried out in Chapter 5.

Finally, Section 8.3 reports some issues experienced by the author during

the numerical analyses. A possible explanation of the causes is provided and suggestions for further developments are furnished, with the aim of overcoming such difficulties in the future.

8.1 Uniaxial and bias tests

Uniaxial and bias tests have been described in Section 4.1.1. Essentially, they are the same kind of test, since they both consist in loading a strip of material along one direction. What differentiates uniaxial from bias tests is the direction of the yarns with respect to the load: in the former, the warp or fill threads are aligned with the loading direction, while in the latter, warp fibres are biased with respect to the applied force.

In a textile specimen that is stretched along one direction, the stress field is not uniform, especially in the neighbourhoods of the clamps. Anyway, in the central part of the strip, it can be approximated as homogeneous (see, e.g., Galliot & Luchsinger, 2010a). In the numerical examples that are illustrated in this paragraph, a square of unit area (1×1 m) has been considered (Figure 8.1), which simulates the mechanical behaviour in the central area of the strip. Thanks to the uniformity of the stress field, which leads to a unique value of the stress components for all the Gauss points, it has been possible to compare the numerical solution with an analytical result evaluated in the material point.

A thickness of 1 mm has been assigned to the unit square employed for the numerical analyses. Its bottom side has been constrained with rollers, which block vertical displacement. Again by means of rollers, the horizontal translation of the left edge has been prevented.

The square of unit area has been divided into 4 finite elements (2×2). Since the stress field is expected to be uniform, a single element would be enough: this subdivision has been introduced to check the capability of the numerical implementation to deal with more than one finite element (examples with an increasing number of elements have been performed, but their solution is not reported in this thesis). Plane stress continuum elements with four nodes (CPS4 in ABAQUS notation) have been employed for the mesh.

In all the considered problems, a horizontal displacement (direction 1) has been applied to the right side of the square, while the top edge has been

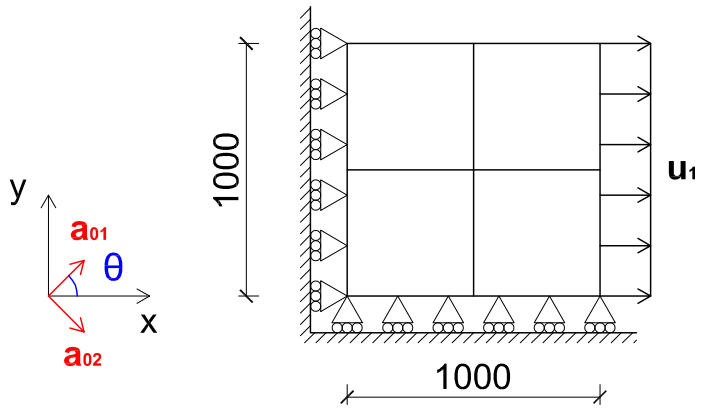

Figure 8.1: *Sketch of the geometry employed for the numerical simulations of uniaxial and bias tests.*

left free. First, the tests has been executed with the warp fibres aligned with direction 1. Secondly, the test has been repeated with the fill yarns in the direction of the load. After that, the example has been reproduced for several bias angles θ of the warp threads with respect to the applied displacement.

The material employed is a PTFE coated glass fabric, whose commercial name is B18059. The new hyperelastic model proposed in this thesis has been calibrated in Chapter 5 for this material, by using biaxial test data from Chapter 4 (test B18059 ALR). The estimated values of the material parameters are the ones reported in Table 7.2.

Since no uniaxial or bias testing results were available for the material employed in the numerical analyses, experimental data from the literature have been employed for comparison. More in detail, Zhang et al. (2010) illustrates the stress-strain behaviour of a PTFE coated glass fabric which has an ultimate tensile strength similar to the one of B18059 (Figure 4.6). Even if a quantitative comparison is not possible, Figure 4.6 has been used as reference for a qualitative assessment of the new model here proposed. It may be noticed that, in the article by Zhang et al. (2010), the bias angles are referred to the weft directions, rather than to the warp direction; thus, attention must be paid to the identification of the correct curves during the comparison with the results obtained in this Section.

Figure 8.2(b) illustrates the results of two uniaxial tests in warp (bias 0 °) and fill (bias 90 °) direction, together with the one of a 45 ° bias test. The curves represent the stress-strain behaviour in the loading direction. In the perspective of large deformation theory, it is necessary to specify the adopted measures of stress and strain: the Cauchy (or true) stress and the logarithmic strain have been employed in this graph (and in the following ones).

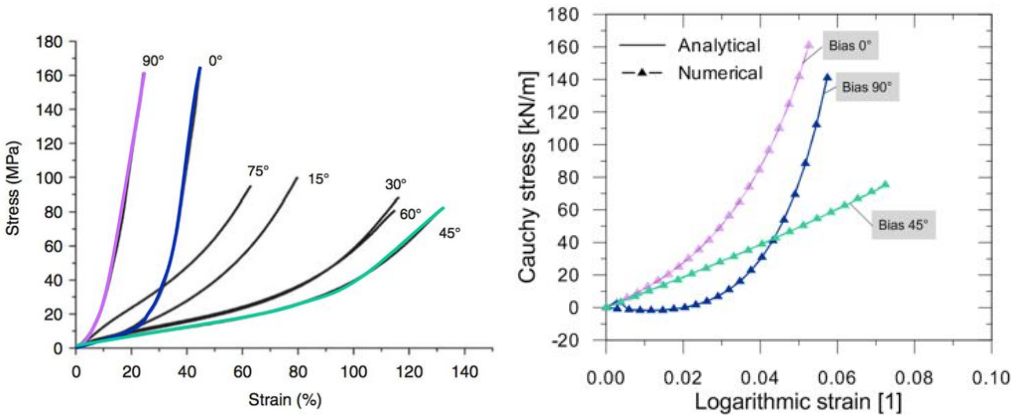

(a) Experimental data (b) Model response

Figure 8.2: *Validation of the new constitutive model for uniaxial loading in warp and fill direction, and for a 45 ° bias test.*

Figure 8.2(a) shows the experimental data obtained by Zhang et al. (2010). The stress-strain curves that correspond to the analytical and numerical solutions in Figure 8.2(b) have been highlighted with the same colors. Qualitatively, the model is able to reproduce the material behaviour in the considered cases. More in detail, the stiffness increase, due to the complete flattening of the yarns, is captured in both the uniaxial tests.

The 90 ° bias test points out that the model considers the fill yarns stiffer than they actually are, as demonstrated by the small difference between the final displacements recorded at the end of the uniaxial tests in warp and fill direction. This difference, which is lower than the one measured in the experiments, is reduced by the fact that the model parameters have been estimated on a preconditioned fabric; in fact, preconditioning cycles straighten the fill yarns, which are highly crimped in a virgin fabric, causing

an apparent increase of the stiffness. Probably, preconditioning is also the reason for the stiffer behaviour recorded at 45 °.

Figures 8.3 and 8.4 compare the experimental, analytical and numerical results for the 15 °, 75 °, 30 ° and 60 ° bias tests. Once again, the new constitutive model is able to reproduce the real behaviour of the coated fabric. As expected, the stress-strain curves in Figures 8.3 and 8.4 are intermediate between the ones of the uniaxial tests (reported in gray in the graphs). As in the previous cases, the material behaviour is stiffer than in the experiments, because of the preconditioning employed in the calibration.

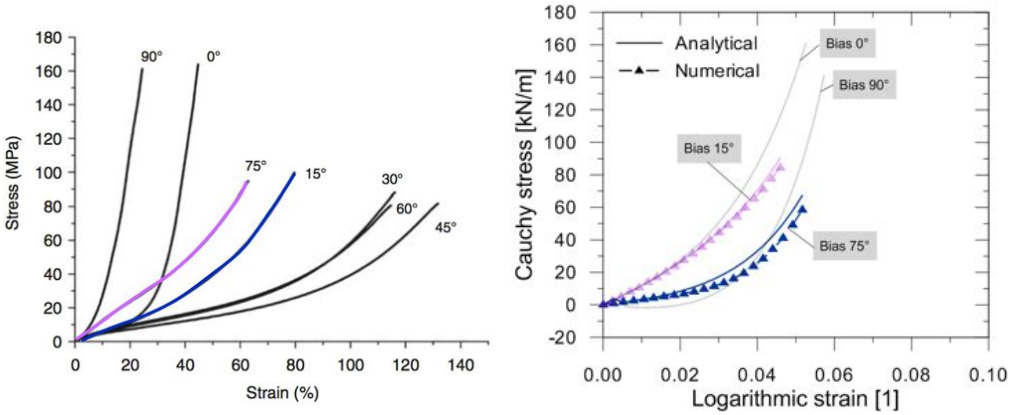

(a) Experimental data (b) Model response

Figure 8.3: *Validation of the new constitutive model for* 15 ° *and* 75 ° *bias tests.*

In conclusion, the new constitutive model presented in Chapter 6 is able to qualitatively reproduce the behaviour of a PTFE coated glass fabric. The main advantage with respect to the orthotropic linear elastic model is that the use of a large strain approach permits to capture the change in the stress-strain curve slope, which is due to the straightening of the yarns. This is done only by setting up a strain energy function, without involving evolution variables and complex plastic or viscous formulations, which are instead needed if a small strain approach is employed.

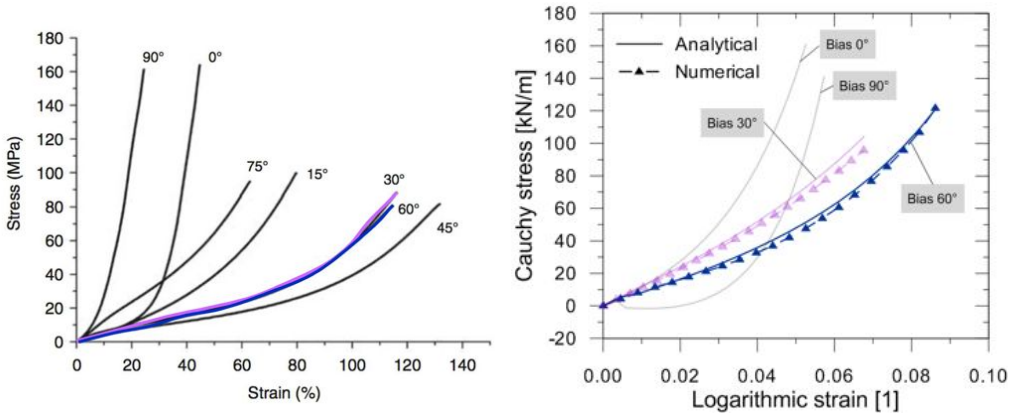

(a) Experimental data (b) Model response

Figure 8.4: *Validation of the new constitutive model for* 30° *and* 60° *bias tests.*

8.2 Biaxial tests

The tests presented in this Section have been performed using the same material of the previous Section 8.1. It is here recalled that it was a B18059 PTFE coated glass fabrics, whose model parameters, which are reported in Table 7.2, have been estimated in Chapter 5 by means of the experimental data from a biaxial test illustrated in Chapter 4, namely test B18059 ALR.

As commented in Section 4.2.2, biaxial tests are usually performed on cruciform specimens, therefore the stress field is variable over the sample. However, in the central square, where the strain measurements are performed, it can be considered uniform. For this reason, the same unit square of the previous validation tests has been employed for the biaxial simulations as well. The only difference is in the applied load, which is of course biaxial in this case.

The right edge of the square has been subjected to a horizontal displacement, while the top side has been translated upward. The imposed displacement histories have been constructed on the basis of the experimental strain measurements, which have been recorded by the extensometers placed in the central part of the sample during the test.

Different loading cases have been considered, one for each warp to fill load ratio explored in the biaxial test used as reference (test B18059 ALR

in Chapter 4). The aforementioned test has been performed according to the MSAJ/M-02:1995 Japanese Standard, which considers five load ratios (1:1, 2:1, 1:2, 1:0, 0:1); other load ratios, which are intermediate between the previous ones, have been investigated during the experiment (namely 0.3:1, 1:0.3, 0.7:1, 1:0.7). It is here briefly recalled that only the stress-strain curves obtained from the standard load ratios have been employed in the identification of the new constitutive model parameters. For further details about the test assumptions, the reader is referred to Chapter 4.

Figure 8.5 shows the legend of the graphics presented in this Section. They represent the comparison of the experimental data (EXP) to the analytical (ANA) and numerical (NUM) outputs of the adopted constitutive model.

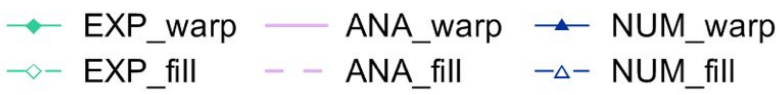

Figure 8.5: *Legend of the graphics representing the biaxial tests results.*

A biaxial test at 1:1 load ratio is illustrated in Figure 8.6. The numerical response is overlapped to the analytical one (obtained with an independent code written by the author in Mathematica), which is a proof of the correct implementation of the user subroutine. The comparison with the experimental data confirms the capability of the model of reproducing the material behaviour, at least qualitatively.

The material response for the biaxial tests 2:1 and 1:2 is almost perfectly reproduced by the model, both qualitatively and quantitatively, as shown in Figures 8.7 and 8.8.

The 1:0 and 0:1 load ratios are the most critical, as expected, because they are equivalent to a uniaxial test performed on a preconditioned and pretensioned membrane. By looking at Figures 8.9 and 8.10 it can be noticed that the model fails to predict the material behaviour in the unstressed transversal direction. However, the stress values in the stretched direction are not far from the measured ones. Moreover, the change in the curve slope is captured by the model, even if at a strain level that is larger than the actual one.

The biaxial tests considered until now are the ones associated with

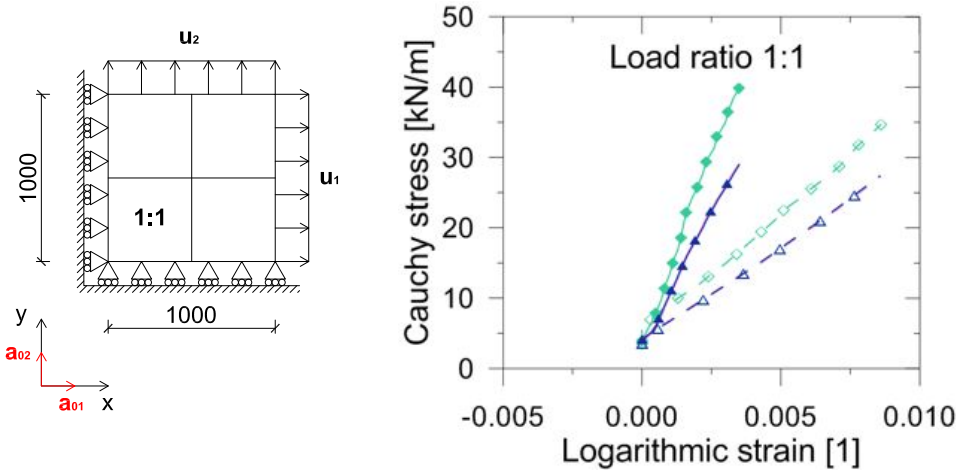

(a) Sketch (b) Stress-strain curves

Figure 8.6: *Analytical, numerical and experimental response to a biaxial loading, applied at constant warp to fill load ratio of 1:1.*

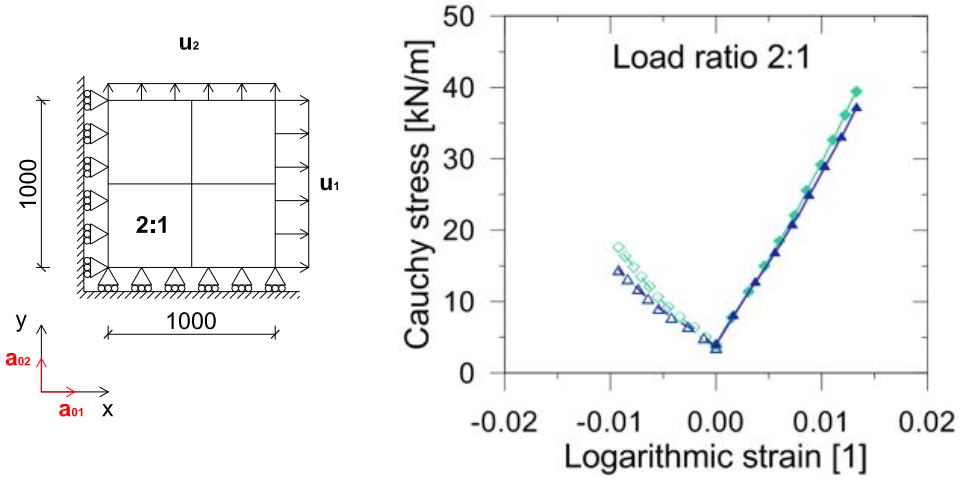

(a) Sketch (b) Stress-strain curves

Figure 8.7: *Analytical, numerical and experimental response to a biaxial loading, applied at constant warp to fill load ratio of 2:1.*

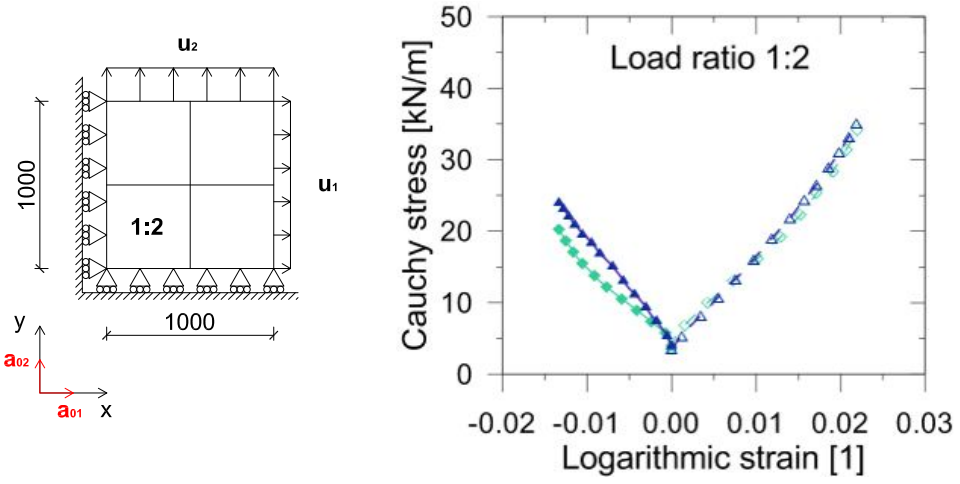

(a) Sketch (b) Stress-strain curves

Figure 8.8: *Analytical, numerical and experimental response to a biaxial loading, applied at constant warp to fill load ratio of 1:2.*

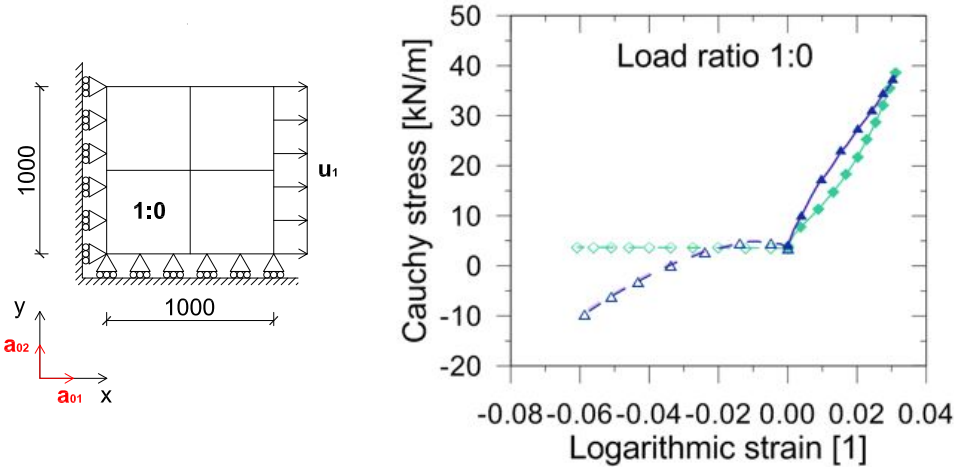

(a) Sketch (b) Stress-strain curves

Figure 8.9: *Analytical, numerical and experimental response to a biaxial loading, applied at constant warp to fill load ratio of 1:0.*

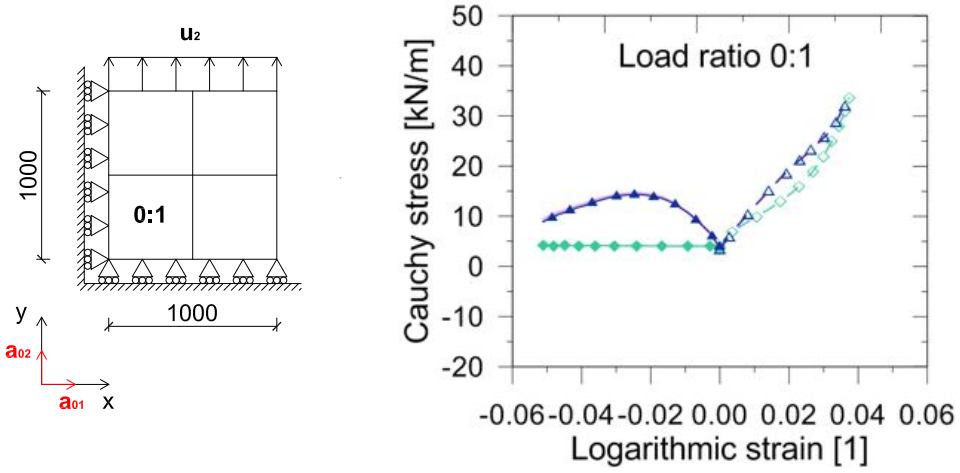

(a) Sketch (b) Stress-strain curves

Figure 8.10: *Analytical, numerical and experimental response to a biaxial loading, applied at constant warp to fill load ratio of 0:1.*

the experimental loading curves employed in the estimation of the model parameters. Therefore, they represent an assessment of the quality of the fit, more than of the predictive capabilities of the new constitutive law. In order to check this aspect, other biaxial loadings have been used, which have been excluded from the least square calibration. The results, which are illustrated in Figures 8.11 to 8.14, show good agreement between the model response (both analitycal and numerical) and the experimental data for all the considered loading cases.

In summary, the validation of the new hyperelastic constitutive law proposed in this thesis for biaxial loading has been performed in this Section. It has been demonstrated that, not only the new model is able to reproduce the material stress-strain curves for the experimental data employed in the identification of its parameters, but also it shows good predictive capabilities for biaxial loading paths not considered in the calibration procedure.

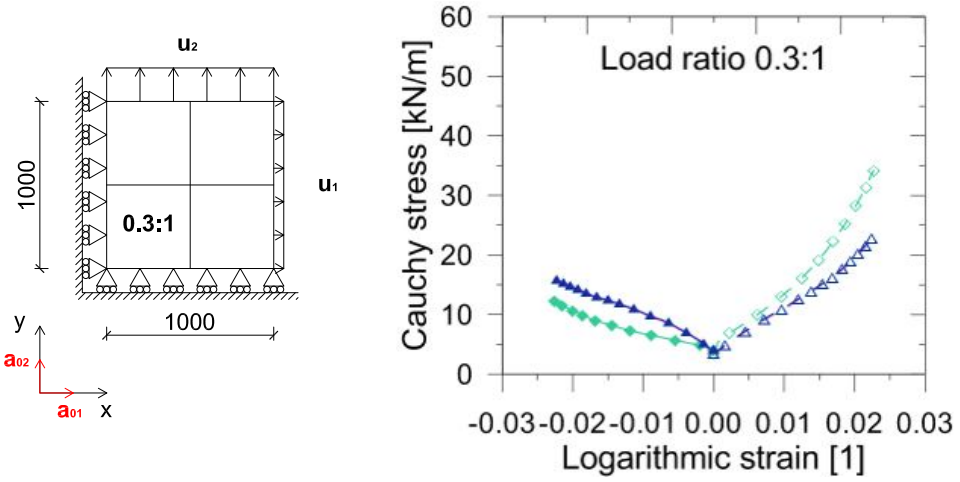

(a) Sketch (b) Stress-strain curves

Figure 8.11: *Analytical, numerical and experimental response to a biaxial loading, applied at constant warp to fill load ratio of 0.3:1.*

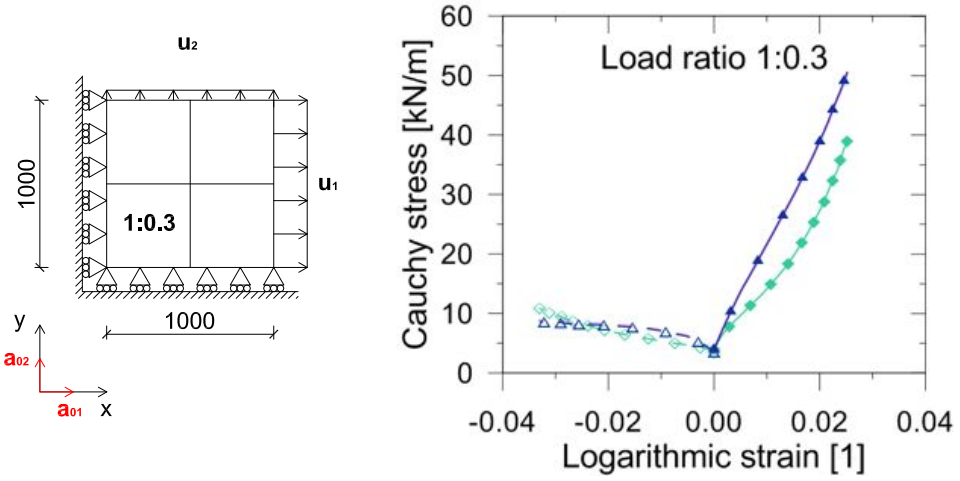

(a) Sketch (b) Stress-strain curves

Figure 8.12: *Analytical, numerical and experimental response to a biaxial loading, applied at constant warp to fill load ratio of 1:0.3.*

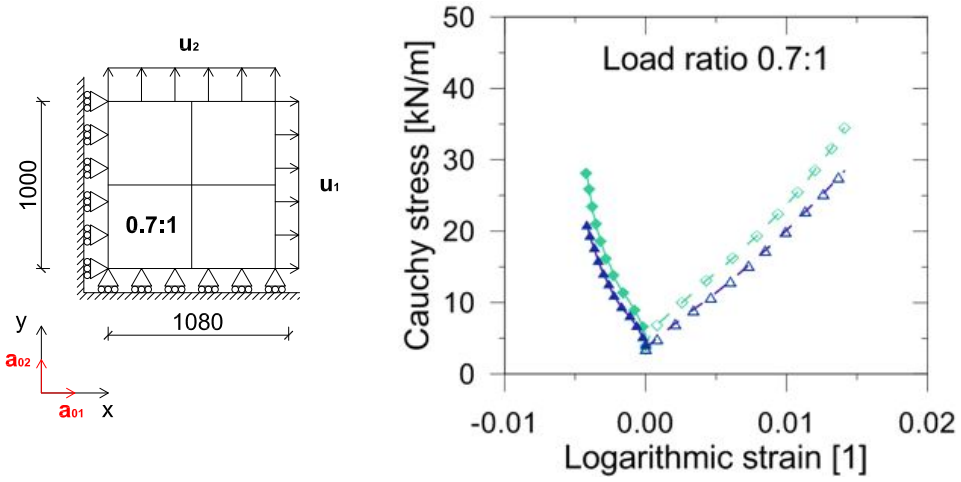

(a) Sketch (b) Stress-strain curves

Figure 8.13: *Analytical, numerical and experimental response to a biaxial loading, applied at constant warp to fill load ratio of 0.7:1.*

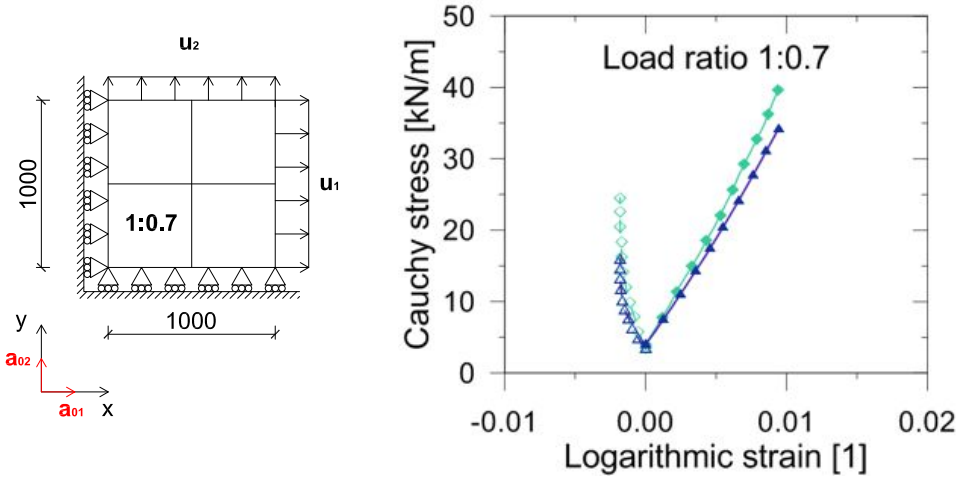

(a) Sketch (b) Stress-strain curves

Figure 8.14: *Analytical, numerical and experimental response to a biaxial loading, applied at constant warp to fill load ratio of 1:0.7.*

8.3 Numerical issues

The verification tests performed in Section 7.2 on the single finite element have been solved in ABAQUS/Standard, which is the implicit solver of the software, by executing static analyses. In that case, ABAQUS uses by default the Newton-Raphson method to solve the nonlinear equilibrium equations.

However, it has not been possible to solve the validation tests in this Chapter with the same method. In the early simulations, ABAQUS was even unable to complete the first increment. Sometimes, the required time increment was so small, that the analysis became cumbersome, especially considering that only 4 finite elements were being used.

The aforementioned numerical problem was particularly evident in the uniaxial and bias loading cases, where the displacements in one of the two in-plane directions were not imposed, so that it was task of the solver to compute the entity of the transversal contraction. Also some attempts of simulating the experiments in force control, instead of applying displacements, failed.

One of the causes of this issue may be identified in the discontinuity of the strain energy term related to the fibres. In fact, the yarns are deactivated when shortened, according to Equation (6.74). Especially at the beginning of the analysis, when the strains are small, it is possible that the solver alternatively predicts contraction or extension of the yarns, causing continuous jumping between two different values of stiffness.

To overcome such problem, the examples previously presented in this Chapter have been solved by performing quasi-static implicit dynamic analyses. For details about a such analyses the reader is referred to Section 2.1.3, where it has been described among the form-finding methods with the alternative name of dynamic relaxation. A mass density of 10^{-9} N s^2/mm^4, which is about one tenth of the steel density, has been assigned to the membrane material. Thanks to this added inertia, the solver is helped to follow a displacement path which does not oscillate between compression and tension states.

To better understand the reasons of the experienced numerical issues, the solution procedure adopted in a static analysis that employs the Newton's algorithm is summarised hereafter. The considered body is in equi-

librium if the external and internal forces are balanced at every node of the finite element discretisation. This is equivalent to a set of (usually nonlinear) equations, whose solution must respect the boundary constraints of the model.

Since the problems considered in this thesis are nonlinear, their solution cannot be found in only one large step, as in the case of linear analyses; instead, the load must be applied incrementally over the step, which is thus broken up into a certain number of increments. Within each time increment, Newton's method employs multiple iterations to find the equilibrated solution.

According to the Newton-Raphson numerical technique, the displacement correction from the initial guessed configuration is evaluated through the tangent stiffness, which is equivalent to assuming that the nodal displacements vary linearly over the increment. The configuration is then updated on the basis of the estimated correction, and the internal forces are changed accordingly. If the residual between the external and internal forces is sufficiently small, with respect to a fixed tolerance, the algorithm is stopped and the system is assumed to be in equilibrium. Otherwise, the tangent stiffness is evaluated in the updated configuration and the procedure is repeated until convergence.

Newton's method works well for convex load-displacement curves, like the one in Figure 8.15(a). This is not the case of HGO constitutive model (and of its modified version, presented in this thesis), which is characterised by concave curves of exponential type. As illustrated in Figure 8.15(b), for concave load-displacement curves, Newton-Raphson algorithm has problems in predicting reasonable values of the displacement correction. The issue is emphasised when the initial slope of the curve is very low: in that case, the displacement correction is so large that it cannot be equilibrated.

In addition, the use of exponential functions in the description of the stress-strain behaviour produces an extremely sharp increase in the stress values at large strains. Even if this is consistent with the physical behaviour of the fabric yarns, which provide further stiffness to the material once their crimp has been reduced by an applied tension, large stress values cause numerical issues. This situation exacerbates the Newton's algorithm difficulties, by reducing the range of admissible displacement corrections.

In conclusion, the numerical issues emerged during the analyses have been summarised in this Section. A possible explanation of the causes has

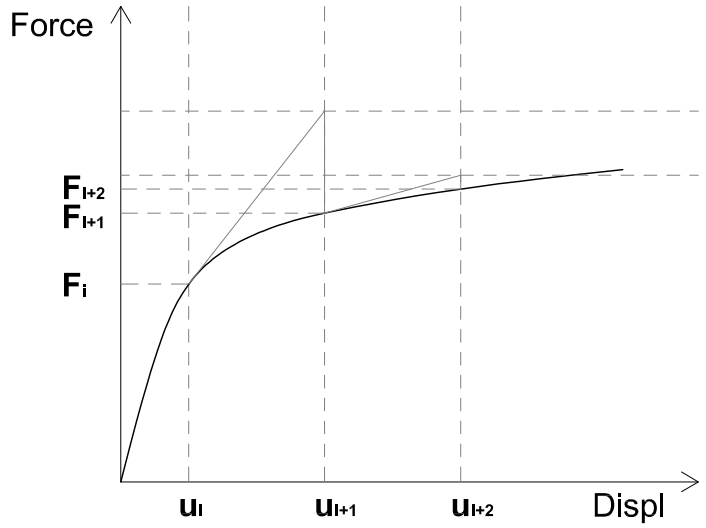

(a) Convex curve

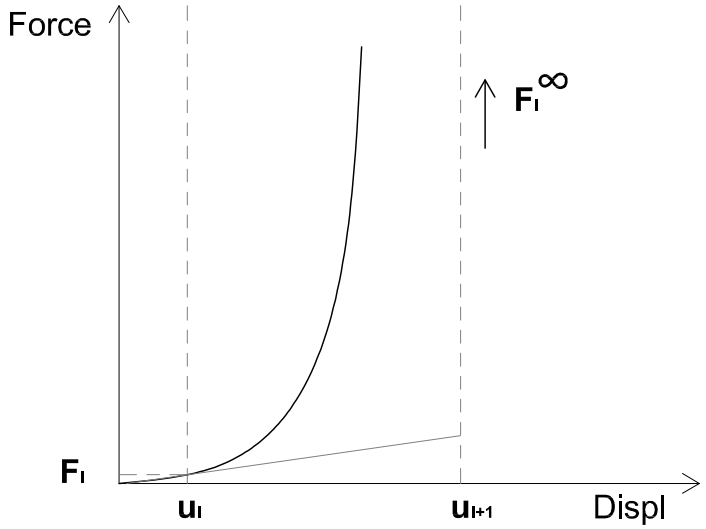

(b) Concave curve

Figure 8.15: *Issues associated with the use of Newton's method for concave load-displacement curves with low initial slope.*

been provided, which includes: large stress values due to the use of exponential stress-strain functions, difficulty of Newton's method in predicting a reasonable displacement correction when the stiffness is low, discontinuous derivatives of the strain energy due to deactivation of the shortened fibres. These issues could be overcome by employing different solution algorithms: for instance, the fictitious dynamic approach has successfully fixed the problems connected to the discontinuity of the yarn stiffness in the neighbourhood of the unstrained configuration.

9

Concluding remarks and future developments

This work has been devoted to characterise and model the mechanical behaviour of coated woven fabrics employed in tensile structures. Biaxial testing and hyperelastic constitutive modelling at large strains have been the scientific core of the thesis. Nevertheless, other contributions have been provided, which aim at enhancing the know-how about tensioned structures at Politecnico di Milano, according to the objectives of ClusTEX group.

The main results achieved may be summarised as follows:

- The state of the art about the design of tensile structures has been deeply explored with an extensive literature review. A lot of references have been found that regard the form-finding methods: these have been described in a unified framework, which shall represent a contribution to the harmonisation of the employed approaches. On the other hand, only a few articles look available about the cutting pattern generation, mostly from conference proceedings. One of the causes of the lack of information might be the absence of an accurate constitutive model for coated fabrics, which appears an essential prerequisite for the generation of cutting patterns.
- The materials used in membrane structures have been studied in detail. Since most of them are composite materials, their internal structure, as well as their production process, have been investigated, to

gather information which is useful to understand the mechanical behaviour of such materials. It has emerged that coated woven fabrics, especially PVC/polyester and PTFE/glass, are the most commonly employed for tensile structures. Therefore, the subsequent constitutive modelling has been focused on these two types of material.

- Information about the mechanical behaviour of coated woven fabrics has been collected from the literature on the topic. The main aspects that influence the highly nonlinear response of such materials are: level of crimp of the threads, crimp interchange, dependence on the load ratio between warp and fill direction (in biaxial tests), inclination of the yarns with respect to the loading direction, stiffer behaviour if the material is loaded biaxially or multi-axially, hysteresis, difference between the first loading and the subsequent loading responses. Nonlinear behaviour is more marked in PTFE coated glass fabrics than in PVC coated polyester fabrics.

- Uniaxial and biaxial tests have been performed by the author with the biaxial testing rig owned by the Research Cluster on "Innovative Textiles" (ClusTEX) of Politecnico di Milano. Several materials and different loading profiles have been investigated. Among them, four new types of PU coated fabrics have been tested according to the MSAJ/M-02:1995 Japanese Standard, to explore possible applications in the construction field. It has been found that they possess a resistance similar to the one of PVC/polyester of Type I, but they are more stretchable and cannot be welded; therefore they could be employed for tensile structures of small dimensions that require a high stretchability.

- Some biaxial tests have been also described, which have been kindly provided by the group of Prof. Peter Gosling at Newcastle University, where the author spent 5 months as visiting PhD Student in 2013. These have been executed according to the MSAJ/M-02:1995 Japanese Standard. They have been useful to calibrate the new constitutive model presented in Chapter 6, as well as to identify the elastic moduli associated to the classical orthotropic linear elastic model for comparison with the new hyperelastic one proposed here. Moreover, two of these tests have explored additional load ratios, which

have been employed for the validation of the model proposed in this thesis.

- A biaxial test on a PVC/polyester fabric, namely VUB 001 A, have been carried out by the author to investigate the effect of the preconditioning cycles. The loading profile of the MSAJ/M-02:1995 Japanese Standard has been modified by eliminating the three cycles at 1:1 load ratio that are performed before each cycle of interest. The obtained experimental data have confirmed the usefulness of the preconditioning procedure, in order to achieve the repeatability of the stress-strain curves. Moreover, the unique crimp configuration that is reached after the preconditioning cycles has been adopted as reference undeformed (but not stree-free) configuration in the subsequent constitutive modelling.

- An innovative biaxial testing procedure has been proposed, which applies to the specimen loading profiles that are driven by the extensometers placed in the central part of the crux (strain-controlled biaxial tests). Several tests have been performed by the author with this approach. It has resulted that such tests could be useful to evaluate the compensation factors for the cutting pattern generation and the subsequent installation, as well as for the retensioning procedures. Moreover, if carried out at higher levels of stress, the strain-controlled biaxial tests can give further information about the material behaviour, which is complementary to the one of classical force-controlled biaxial experiments.

- A review of the existing constitutive models for raw and coated fabrics has been presented in Chapter 5. Because of the nature of fabric reinforced composites, two different approaches are employed in their modelling: the meso-structural ones are based on the description of the geometry of a unit cell, while continuum models approximate the composite as a continuum (macro-scale). The advantages and disadvantages of both are discussed. However, in the current design practice, the orthotropic linear elastic model is the most widely used.

- An identification of the Orthotropic Linear Elastic (OLE) model parameters have been carried out for several materials. The experimen-

tal data employed in the calibration have been taken from Chapter 4. As expected, this has pointed out the limit of such an approach: the OLE model is too simple to correctly reproduce the complex nonlinear behaviour of coated woven fabrics and this has made the identification cumbersome and actually not accurate.

- The Holzapfel-Gasser-Ogden (HGO) model has been proposed as suitable to model coated woven fabric behaviour, thanks to some similarities between these materials and arterial tissues. The formulation of the HGO model has been described in detail. Nonetheless, this hyperelastic model cannot capture the interaction between the reinforcing fibres. Therefore, a new energy term has been added to the HGO free-energy function to model the interaction due to the weaving. Such new hyperelastic model operates within a large strain framework. It has been calibrated by employing the same biaxial data previously used for the OLE model. A comparison between the HGO and OLE models have demonstrated the better performance of the new hyperelastic model in predicting the coated woven fabrics stress-strain behaviour.

- The proposed new model has been implemented into a general purpose finite element code, namely ABAQUS. The code has been verified by means of several benchmark tests. This implementation opens the doors to an extensive testing of the model performances for several boundary valued problems, as well as to its future applications in the practical design of tensile structures.

- Lastly, the new hyperelastic model for coated fabrics has been validated through a series of simple reference tests. The uniaxial, bias, and biaxial responses are correctly reproduced. Some biaxial tests performed by loading the fabric at a constant load ratio have assessed also the predictive capability of the model with respect to load ratios that have not been employed in the identification of its parameters. The results are encouraging, even if some existing numerical issues have been pointed out.

9.1 Future developments

The present work represents a contribution towards the expansion of the specific expertise that is needed to design membrane structures in a reliable way. As pointed out earlier, there is currently a wide variety of design procedures and testing methods in the field of tensioned structures, which is mainly due to the absence of Standards. Therefore, the preliminary systematisation of the present know-how is fundamental, but it requires further time. Moreover, the harmonisation of the current procedures, which is being carried out through several international projects, is highlighting some issues that require further research to be solved.

Some possible future developments of the present work are listed below:

- The modelling of coated fabric behaviour requires an extensive experimental campaign, which should be specifically planned according to the modelling needs. This would be useful also in view of the development of a probabilistic approach to the design of tensile structures, where the material properties and its resistance are associated to a certain probability level.

- The new hyperelastic model for coated fabrics proposed in this thesis cannot capture the actual material response under cyclic loading. The history-dependent behaviour could be described by an enriched model endowed with appropriate evolution variables.

- The polyconvexity of the proposed free-energy function should be assessed. This mathematical requirement is extremely important in large strain elasticity, since it guarantees the global existence of the solution to the elastic problem. The involved mathematics does not look too easy, but this work is fundamental for the development of a robust formulation of the new model.

- An implementation of the new model into the more general user subroutine UMAT is essential to make possible further future enhancements (for example to add the inelastic behaviour of the material). This work has been started by the author, but results were not re-

ported in this thesis, since they represent ongoing research. One objective is of course the completion and verification of such a code.

- An extensive validation of the new constitutive model should be carried out, by solving other additional benchmark examples. More in detail, the model response to planar boundary valued problems generating non-uniform stress and strain fields should be checked (e.g. the reproduction of a cruciform biaxial test). Numerical simulations of membrane structures in the 3D space should also be performed, to assess the model performance in view of its employment in the practical design.

A

Graphical representation of biaxial test data

This Appendix contains a graphical representation of the experimental data from the biaxial tests described in this thesis. Each figure fully describes a biaxial test by furnishing three types of information within three sub-figures:

(a) Adopted loading profile, which can be in terms of applied forces (kN/m) or applied strains (%), depending on the type of control associated with the test.

(b) Visualisation of how the loading history paths cover the plane of feasible warp and fill stresses (in the case of force-controlled tests) or strains (for strain-controlled tests).

(c) Record of the measured warp and fill strain (for force-controlled tests) or stress (for strain controlled tests) histories.

In the figures associated with force-controlled tests, the capital letters (A, B, C, ...) identify a specific radial path, which is characterised by an almost constant warp to fill load ratio. On the other hand, in the graphics of strain-controlled tests, the capital letters are employed only to indicate some reference points (in red), which are used in the thesis to describe the applied strain paths.

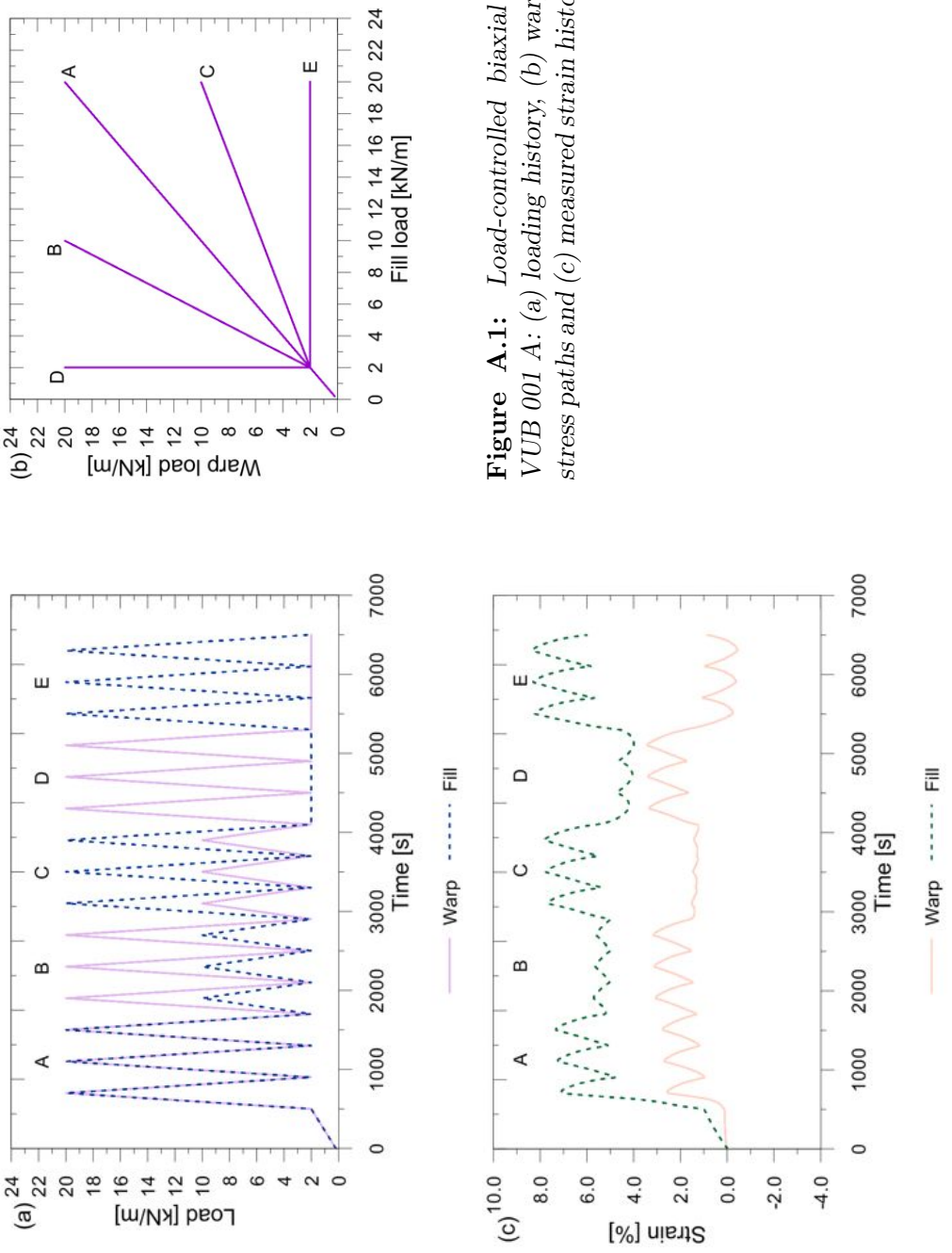

Figure A.1: *Load-controlled biaxial test VUB 001 A: (a) loading history, (b) warp-fill stress paths and (c) measured strain histories.*

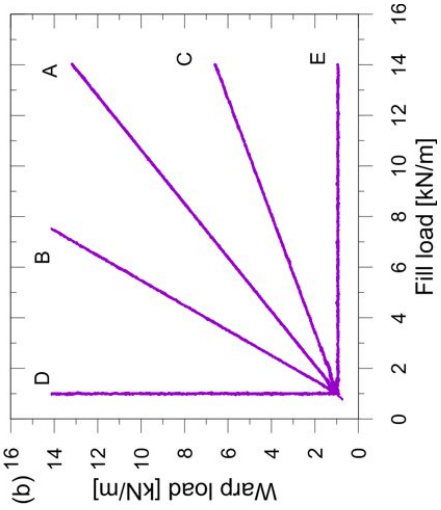

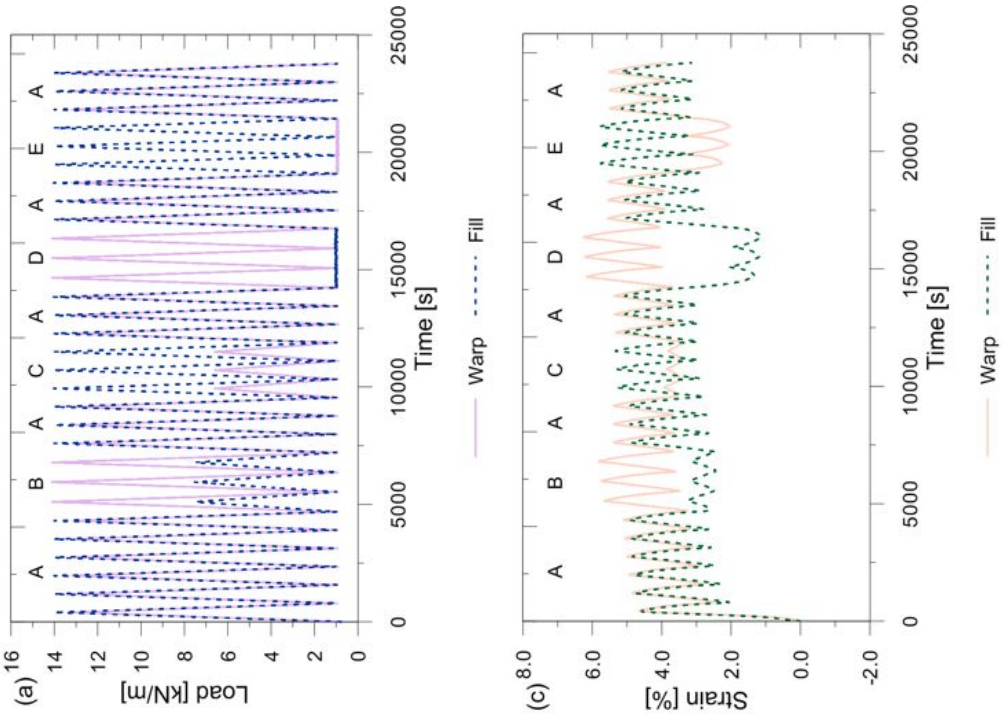

Figure A.2: *Load-controlled biaxial test F702 MSAJ: (a) loading history, (b) warp-fill stress paths and (c) measured strain histories.*

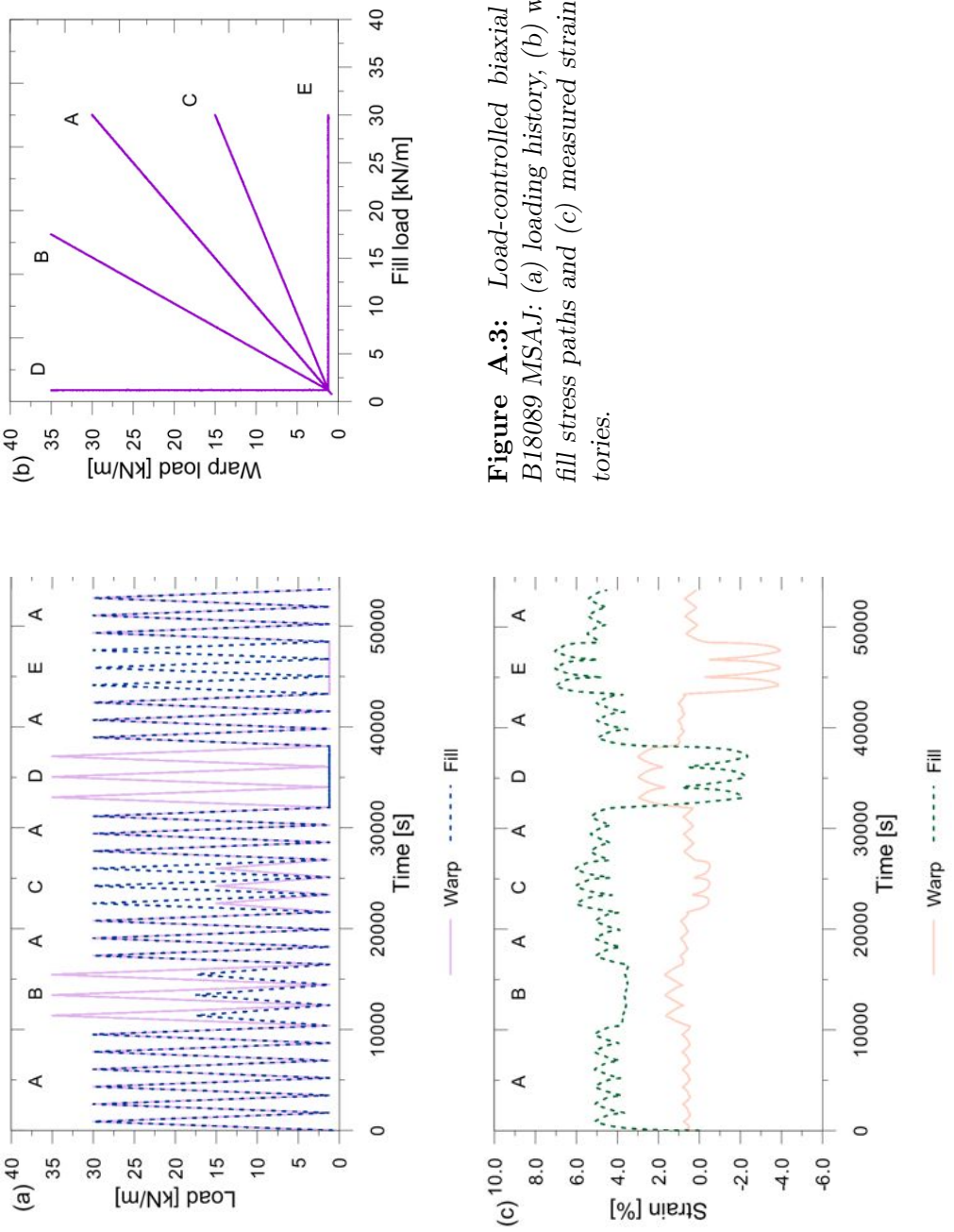

Figure A.3: *Load-controlled biaxial test B18089 MSAJ: (a) loading history, (b) warp-fill stress paths and (c) measured strain histories.*

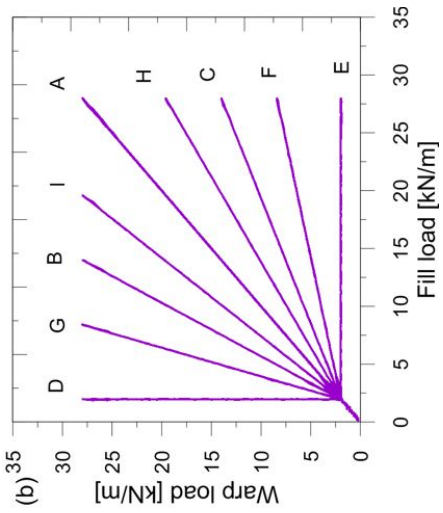

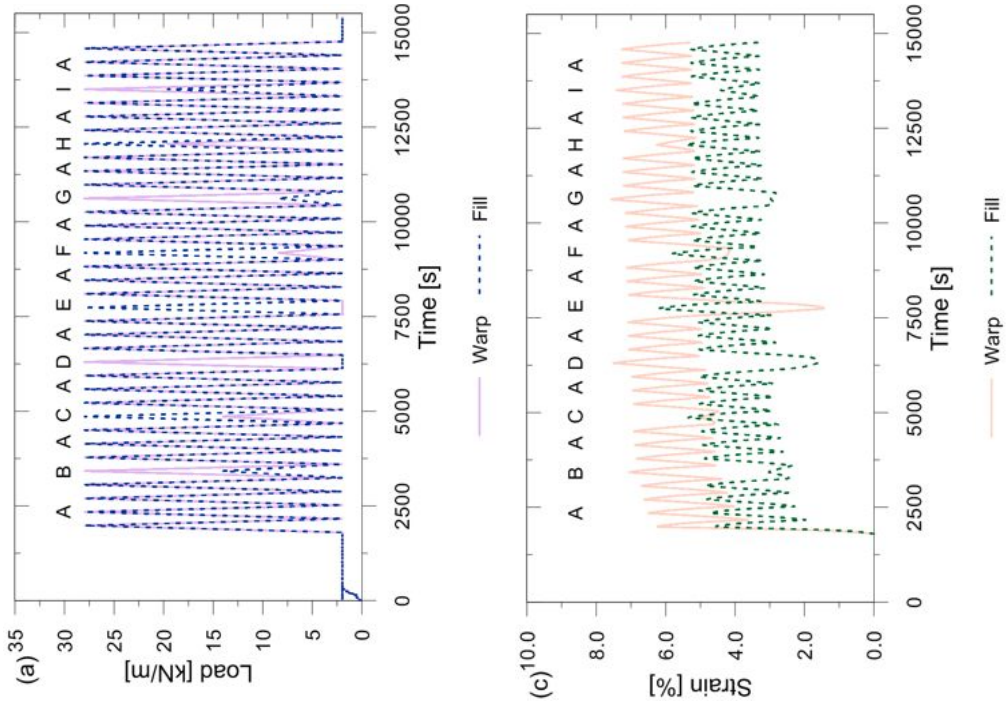

Figure A.4: *Load-controlled biaxial test F1202T2 ALR: (a) loading history, (b) warp-fill stress paths and (c) measured strain histories.*

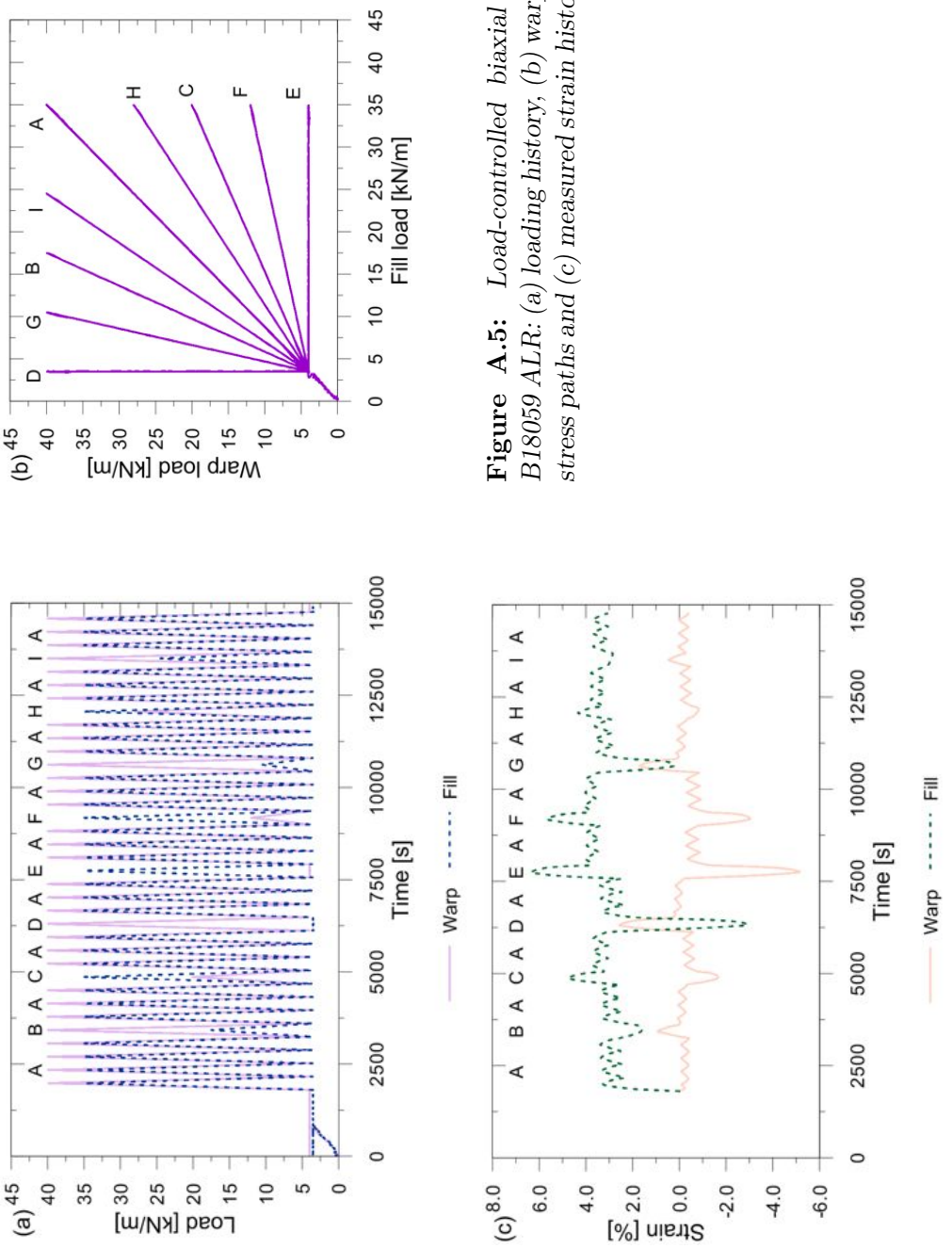

Figure A.5: *Load-controlled biaxial test B18059 ALR: (a) loading history, (b) warp-fill stress paths and (c) measured strain histories.*

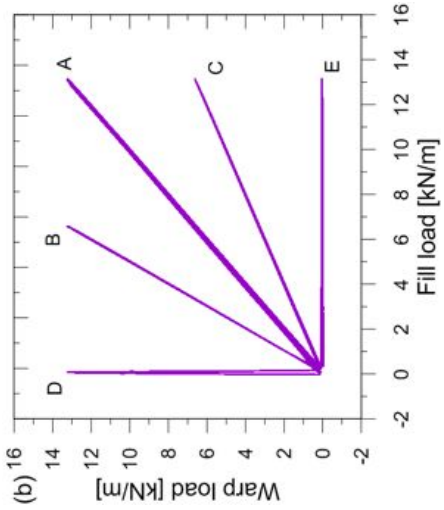

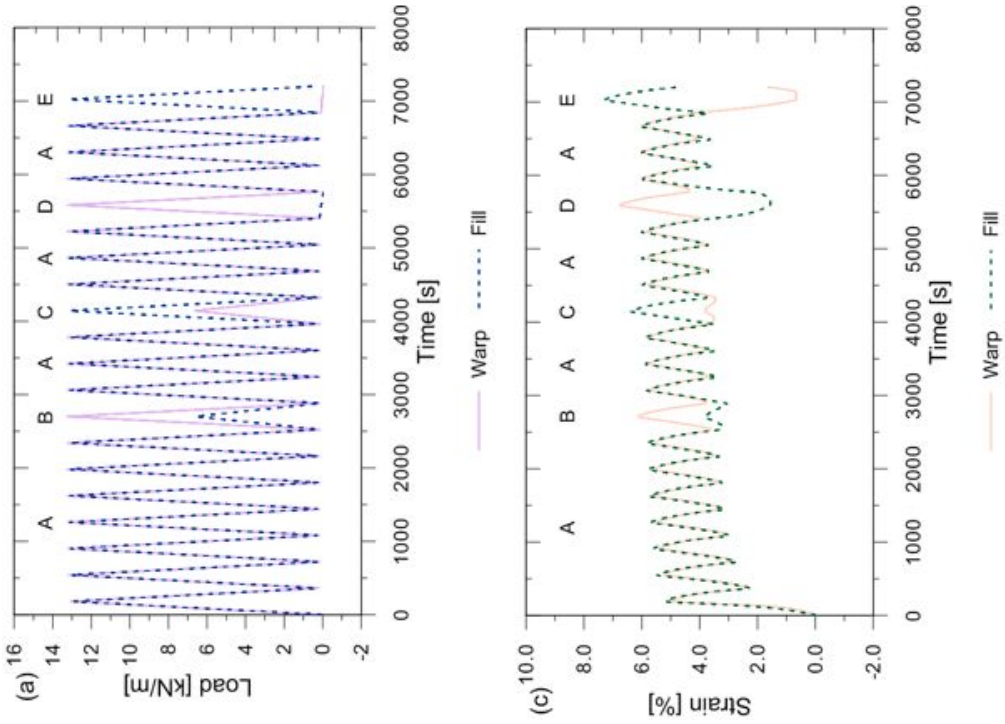

Figure A.6: *Load-controlled biaxial test NTT 011 1 BX: (a) loading history, (b) warp-fill stress paths and (c) measured strain histories.*

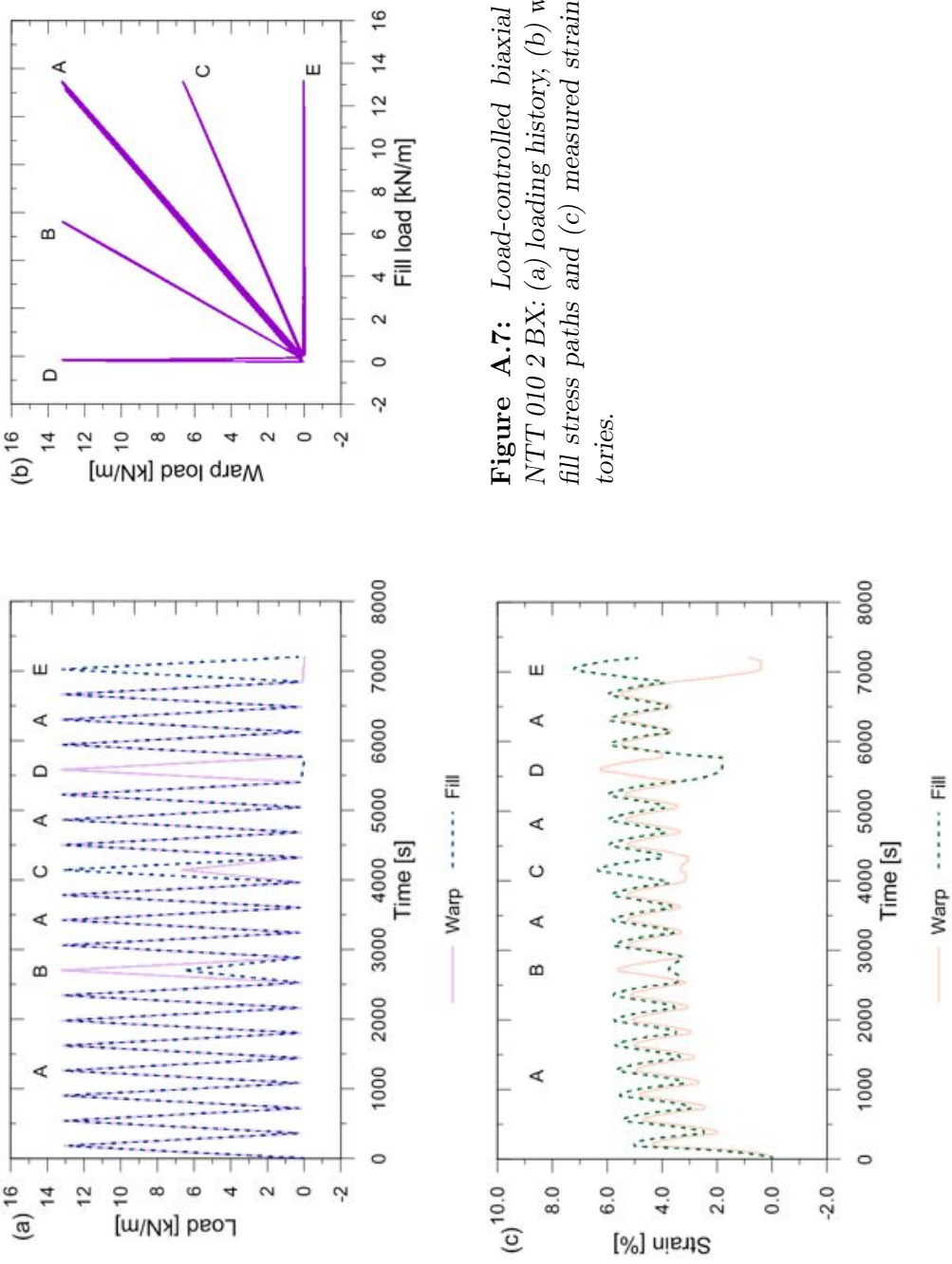

Figure A.7: *Load-controlled biaxial test NTT 010 2 BX: (a) loading history, (b) warp-fill stress paths and (c) measured strain histories.*

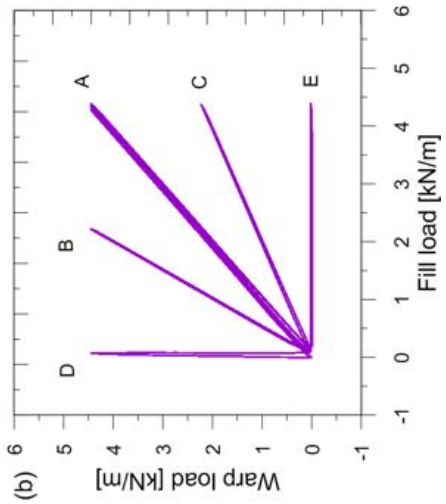

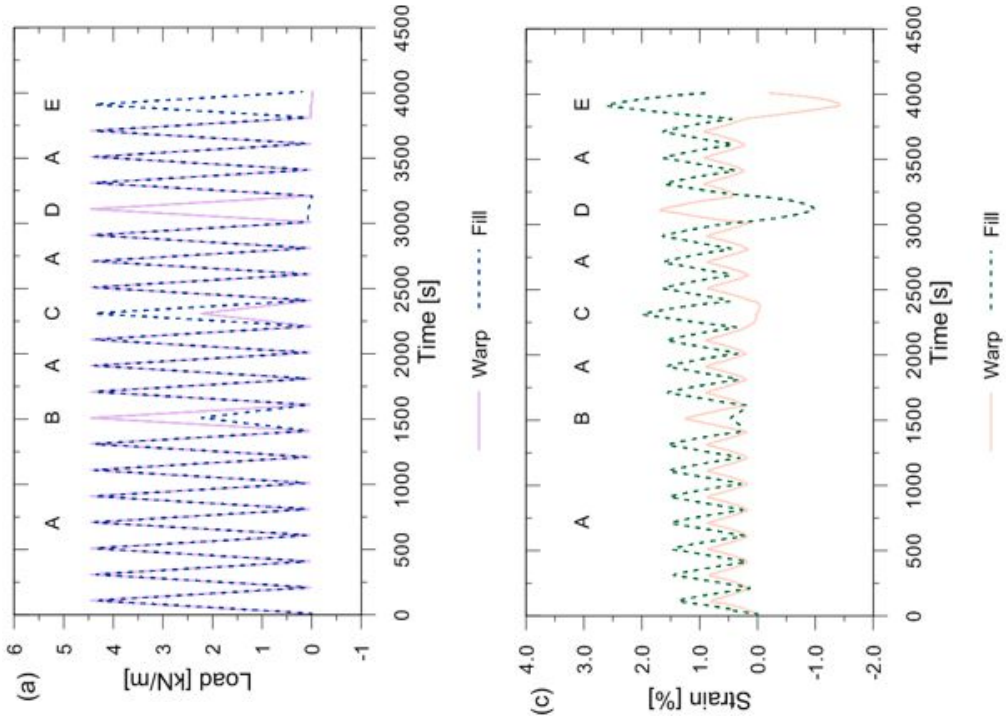

Figure A.8: *Load-controlled biaxial test NTT 001 A BX: (a) loading history, (b) warp-fill stress paths and (c) measured strain histories.*

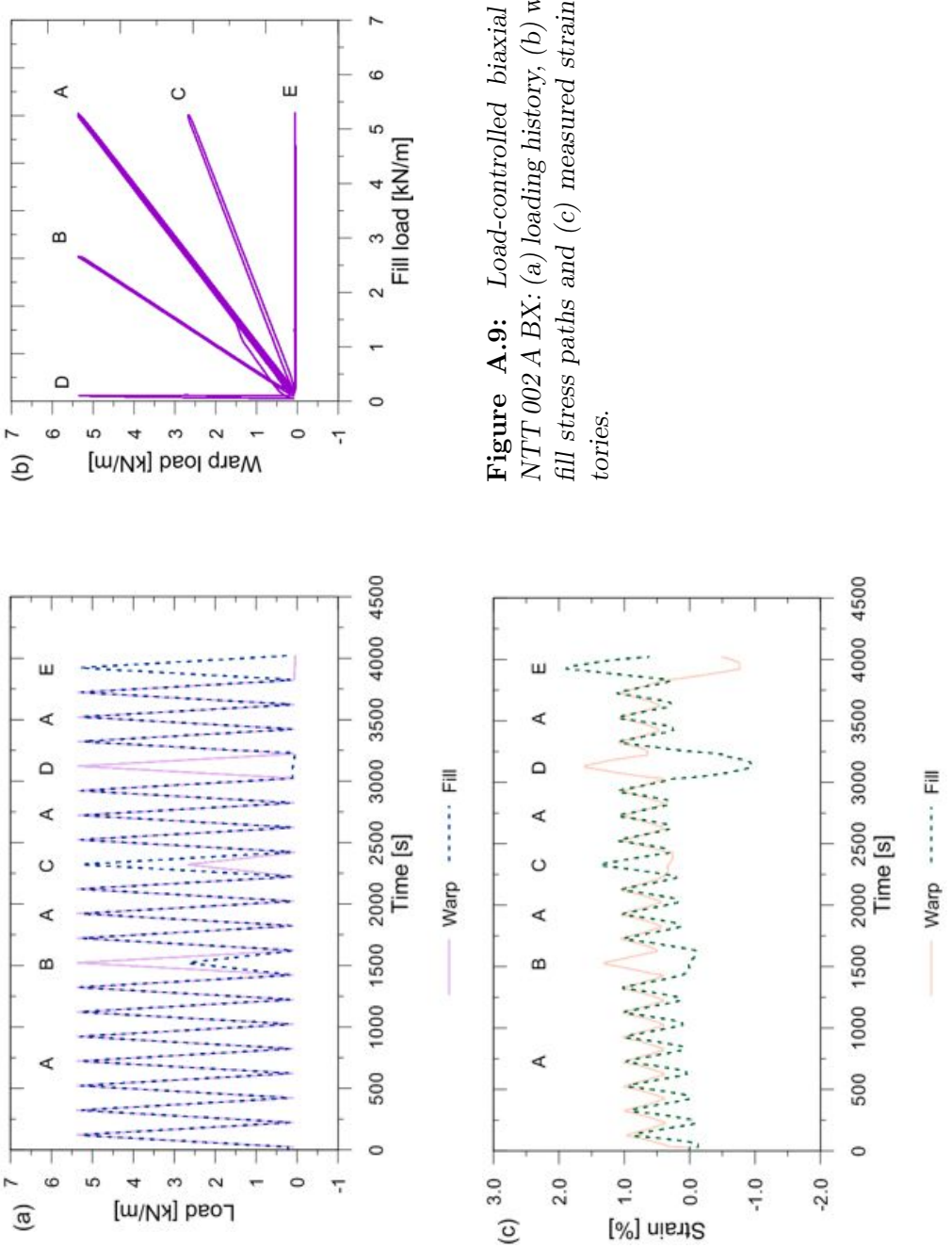

Figure A.9: *Load-controlled biaxial test NTT 002 A BX: (a) loading history, (b) warp-fill stress paths and (c) measured strain histories.*

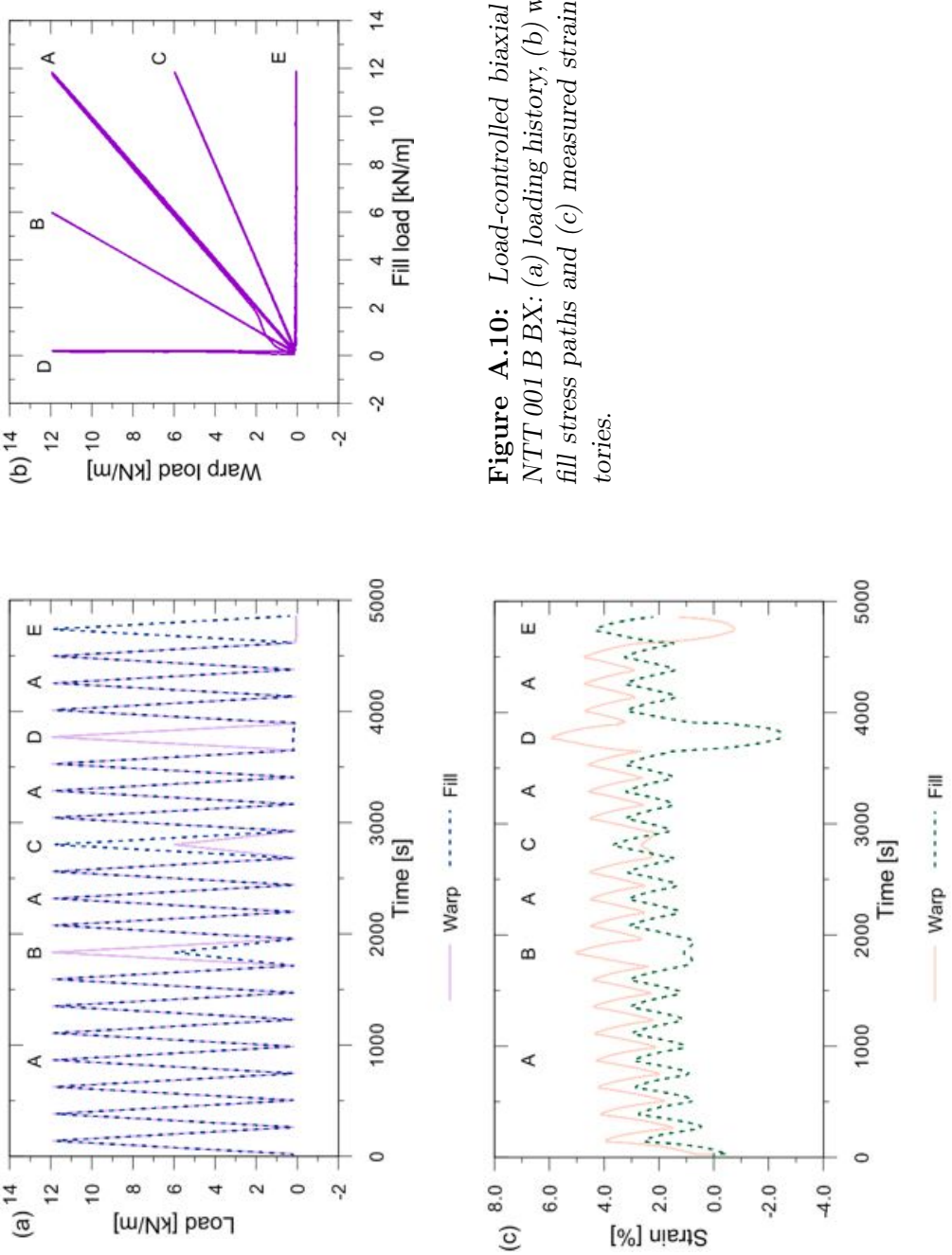

Figure A.10: *Load-controlled biaxial test NTT 001 B BX: (a) loading history, (b) warp-fill stress paths and (c) measured strain histories.*

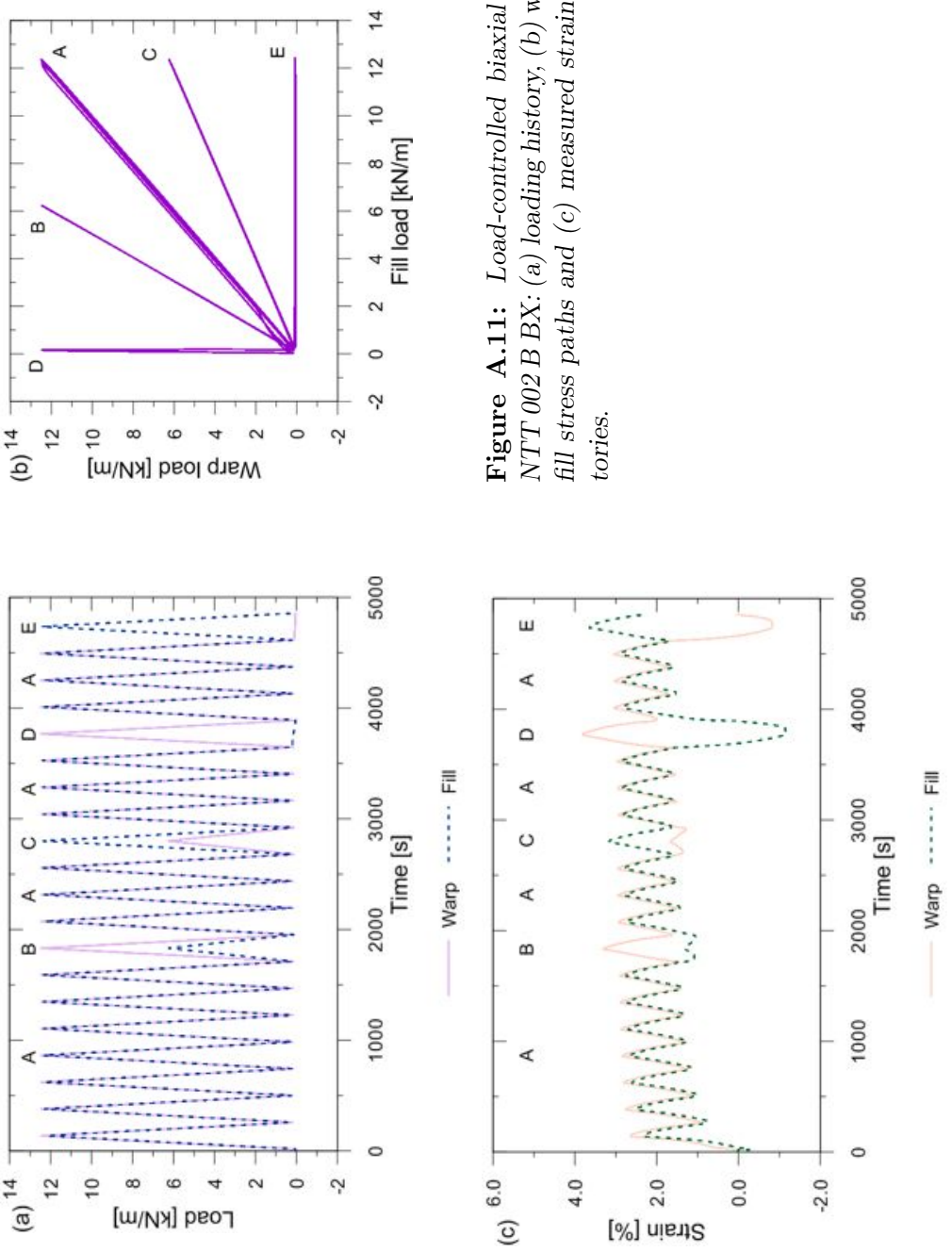

Figure A.11: *Load-controlled biaxial test NTT 002 B BX: (a) loading history, (b) warp-fill stress paths and (c) measured strain histories.*

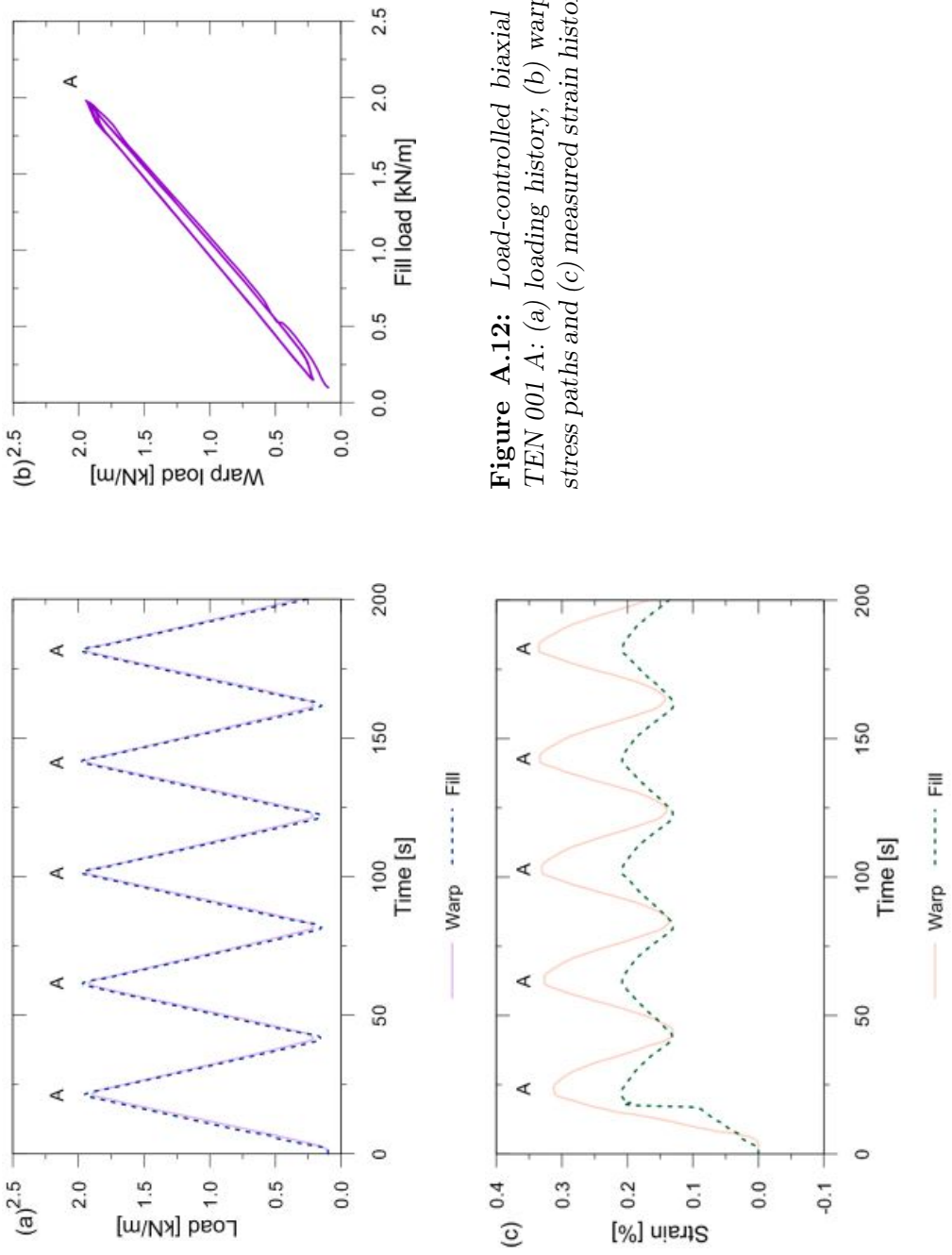

Figure A.12: *Load-controlled biaxial test TEN 001 A: (a) loading history, (b) warp-fill stress paths and (c) measured strain histories.*

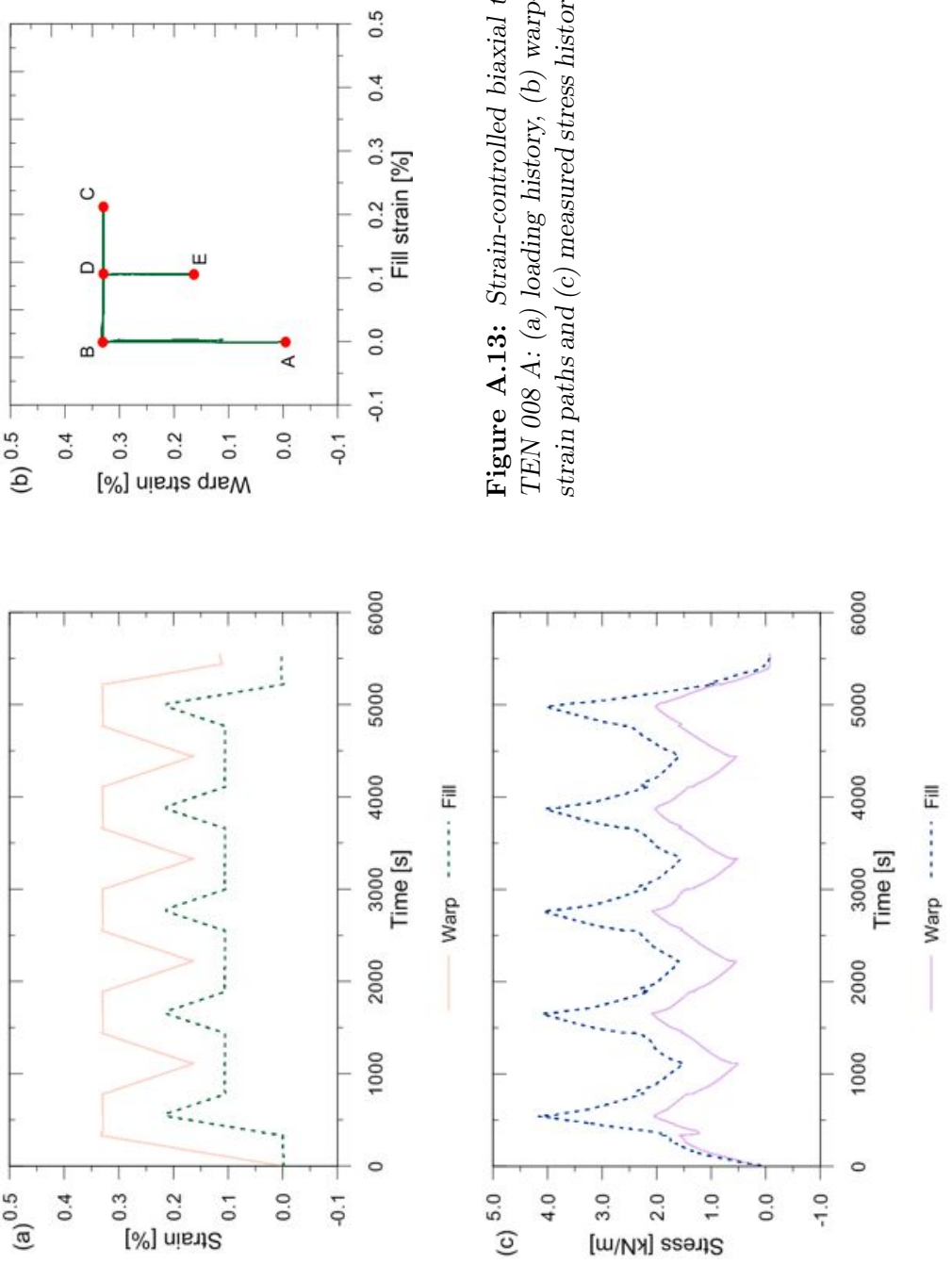

Figure A.13: *Strain-controlled biaxial test TEN 008 A: (a) loading history, (b) warp-fill strain paths and (c) measured stress histories.*

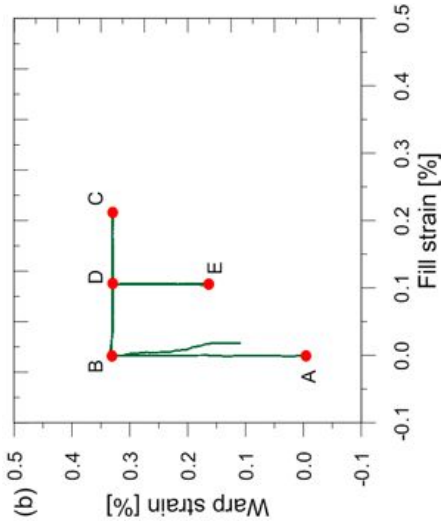

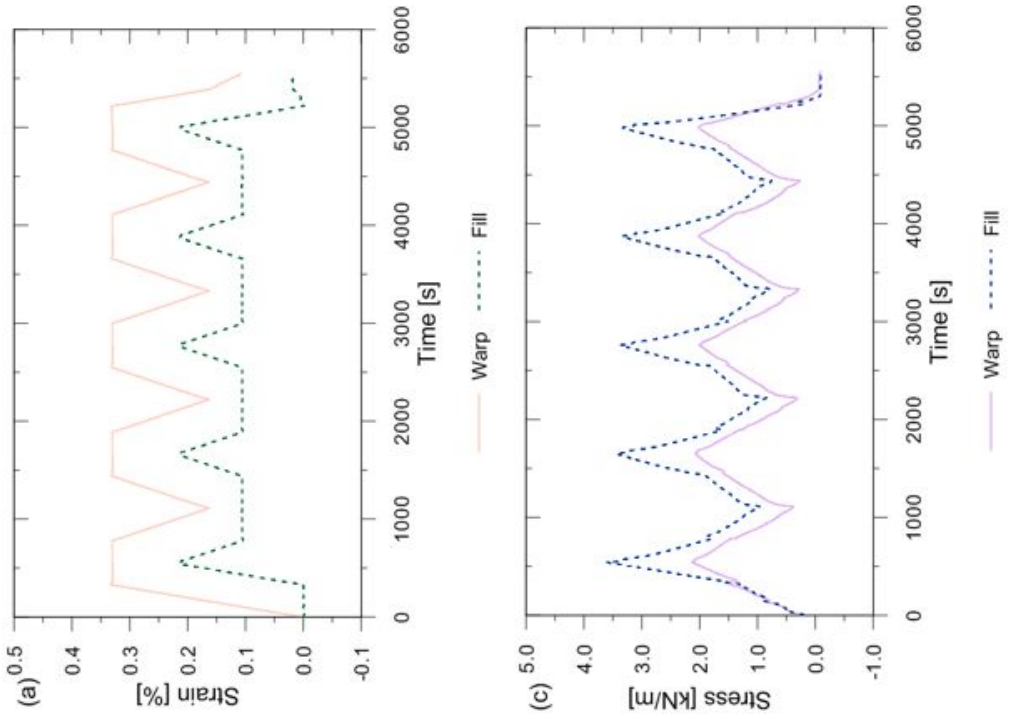

Figure A.14: *Strain-controlled biaxial test TEN 015 A: (a) loading history, (b) warp-fill strain paths and (c) measured stress histories.*

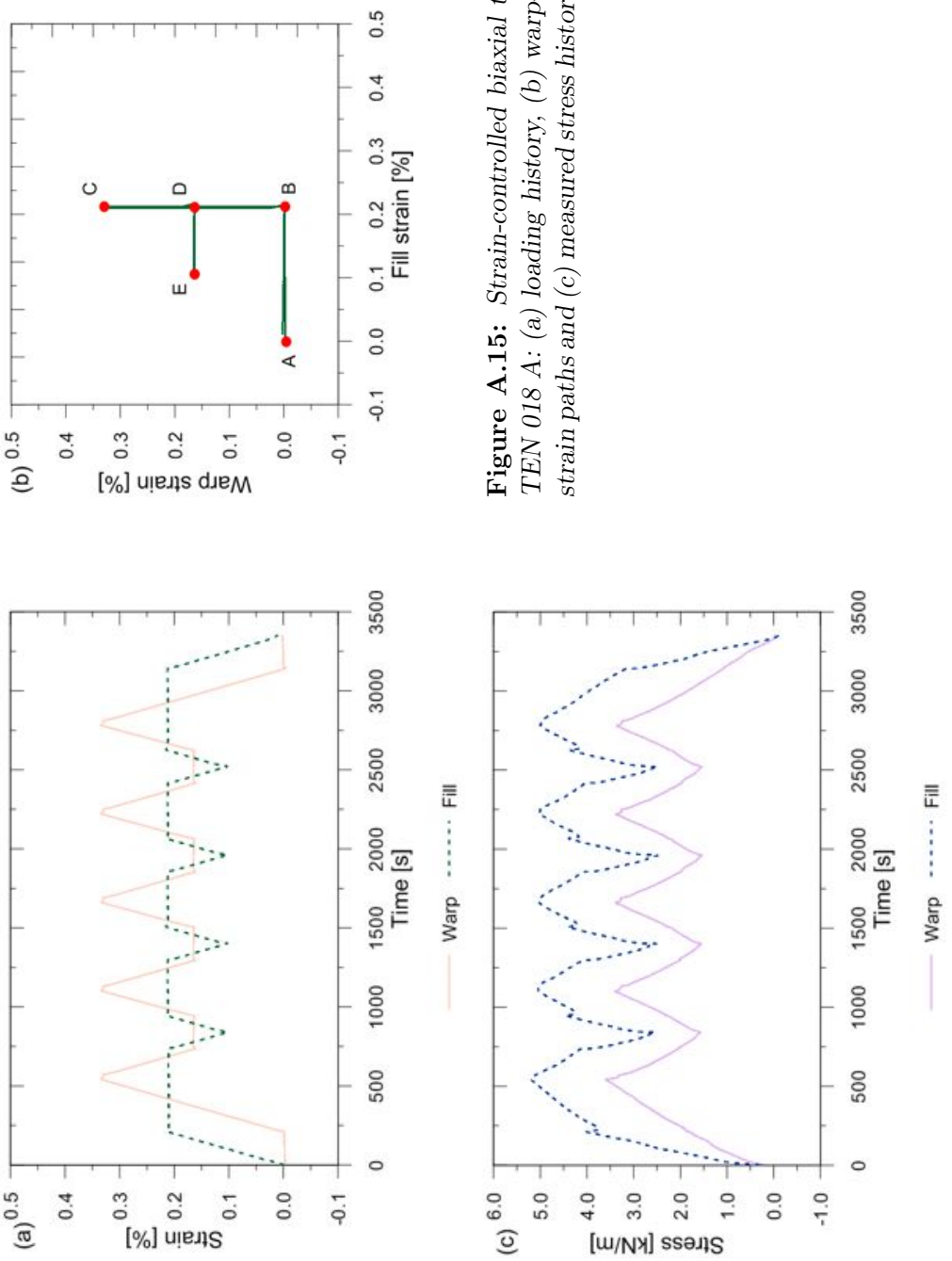

Figure A.15: *Strain-controlled biaxial test TEN 018 A: (a) loading history, (b) warp-fill strain paths and (c) measured stress histories.*

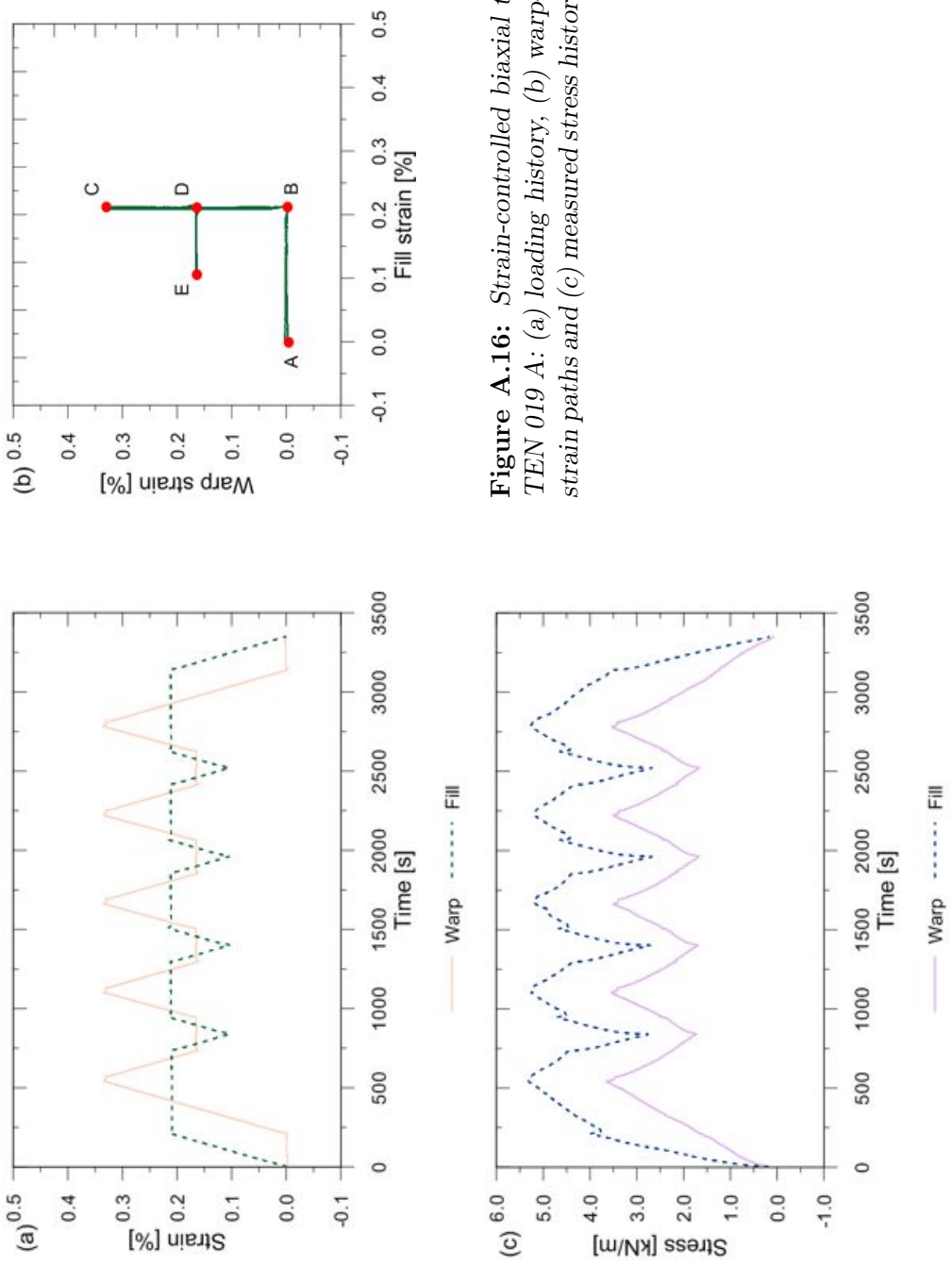

Figure A.16: *Strain-controlled biaxial test TEN 019 A: (a) loading history, (b) warp-fill strain paths and (c) measured stress histories.*

page intentionally left blank

References

Aimene, Y., Hagege, B., Sidoroff, F., Vidal-Sallé, E., Boisse, P., & Dridi, S. (2008). Hyperelastic approach for composite reinforcement forming simulations. *International Journal of Material Forming*, 1(S1), 811–814, DOI:10.1007/s12289-008-0259-x.

Aimene, Y., Vidal-Sallé, E., Hagege, B., Sidoroff, F., & Boisse, P. (2009). A hyperelastic approach for composite reinforcement large deformation analysis. *Journal of Composite Materials*, 44(1), 5–26, DOI:10.1177/0021998309345348.

Alley, V. L. & Faison, R. W. (1972). Experimental investigation of strains in fabric under biaxial and shear forces. *Journal of Aircraft*, 9(1), 55–60, DOI:10.2514/3.44321.

Anderson, A. E., Ellis, B. J., & Weiss, J. A. (2007). Verification, validation and sensitivity studies in computational biomechanics. *Computer methods in biomechanics and biomedical engineering*, 10(3), 171–84, DOI:10.1080/10255840601160484.

Antonietti, P. F., Biscari, P., Tavakoli, A., Verani, M., & Vianello, M. (2011). Theoretical study and numerical simulation of textiles. *Applied Mathematical Modelling*, 35(6), 2669–2681, DOI:10.1016/j.apm.2010.11.062.

Argyris, J. H., Angelopoulos, T., & Bichat, B. (1974a). A general method for the shape finding of lightweight tension structures. *Computer Methods in Applied Mechanics and Engineering*, 3(1), 135–149, DOI:10.1016/0045-7825(74)90046-2.

Argyris, J. H., Dunne, P. C., Angelopoulos, T., & Bichat, B. (1974b). Large natural strains and some special difficulties due to non-linearity and incompressibility in finite elements. *Computer Methods in Applied Mechanics and Engineering*, 4(2), 219–278, DOI:10.1016/0045-7825(74)90035-8.

Argyris, J. H. & Scharpf, D. W. (1972). Large deflection analysis of prestressed networks. *Journal of the Structural Division*, 98(3), 633–654.

ASCE55-10 (2010). *Tensile Membrane Structures*. Standard, American Society of Civil Engineers, Virginia, USA.

Barnes, M. R. (1975). Application of dynamic relaxation to the design and analysis of cable, membrane and pneumatic structures. In *Proc. of the 2nd International Conference on Space Structures* Guilford, Connecticut (USA).

Barnes, M. R. (1977). *Form-finding and Analysis of Tension Space Structures by Dynamic Relaxation*. Phd thesis, City University of London, UK.

Barnes, M. R. (1988). Form-finding and analysis of prestressed nets and membranes. *Computers & Structures*, 30(3), 685–695, DOI:10.1016/0045-7949(88)90304-5.

Barnes, M. R. (1994). Form and stress engineering of tension structures. *Structural Engineering Review*, 6(3-4), 175–202.

Barnes, M. R. (1999). Form finding and analysis of tension structures by dynamic relaxation. *International Journal of Space Structures*, 14(2), 89–104, DOI:10.1260/0266351991494722.

Beccarelli, P. (2010). *Testing for Designing - Biaxial Testing Procedures Supporting Design, Manufacture, Erection and Manteinance of Tension Membranes*. Phd thesis, Politecnico di Milano.

Beccarelli, P., Bridgens, B. N., Galliot, C., Gosling, P. D., Stimpfle, B., & Zanelli, A. (2011). Round-robin biaxial tensile testing of architectural coated fabrics. In *Proc. of the International Symposia IABSE-IASS 2011: Taller, Longer, Lighter - Meeting Growing Demand with Limited Resources* London, UK.

Beccarelli, P., Colasante, G., Novati, G., Stimpfle, B., & Zanelli, A. (2013). Strain-controlled biaxial tests of coated fabric membranes. In *Proc. of the Tensinet Symposium 2013 - [RE]THINKING Lightweight Structures* (pp. 53–65). Istanbul, Turkey.

Bigaud, D. & Hamelin, P. (1997). Mechanical properties prediction of textile-reinforced composite materials using a multiscale energetic approach. *Composite Structures*, 38(1-4), 361–371, DOI:10.1016/S0263-8223(97)00071-8.

Bletzinger, K.-U. & Ramm, E. (1999). A general finite element approach to the form finding of tensile structures by the updated reference strategy. *International Journal of Space Structures*, 14(2), 131–145, DOI:10.1260/0266351991494759.

Blum, R. (2002). Evaluation method for the elastic moduli. *Tensinews Newsletter September 2002*.

Boisse, P., et al. (2010). Hypoelastic, hyperelastic, discrete and semi-discrete approaches for textile composite reinforcement forming. *International Journal of Material Forming*, 3(S2), 1229–1240, DOI:10.1007/s12289-009-0664-9.

Boisse, P., Gasser, A., & Hivet, G. (2001). Analyses of fabric tensile behaviour: determination of the biaxial tension-strain surfaces and their use in forming simulations. *Composites Part A: Applied Science and Manufacturing*, 32(10), 1395–1414, DOI:10.1016/S1359-835X(01)00039-2.

Boljen, M. & Hiermaier, S. (2012). Continuum constitutive modeling of woven fabrics. *The European Physical Journal Special Topics*, 206(1), 149–161, DOI:10.1140/epjst/e2012-01596-0.

Brew, J. S. & Brotton, D. M. (1971). Non-linear structural analysis by dynamic relaxation. *International Journal for Numerical Methods in Engineering*, 3(4), 463–483, DOI:10.1002/nme.1620030403.

Brew, J. S. & Lewis, W. J. (2013). Spline-based and stress-monitored patterning of fabric structures. *Computers & Structures*, 119, 203–214, DOI:10.1016/j.compstruc.2012.11.013.

Bridgens, B. N. (2005). *Architectural Fabric Properties: Determination, Representation & Prediction*. Phd thesis, Newcastle University, UK.

Bridgens, B. N. & Gosling, P. D. (2004). Direct stress-strain representation for coated woven fabrics. *Computers & Structures*, 82(23-26), 1913–1927, DOI:10.1016/j.compstruc.2003.07.005.

Bridgens, B. N. & Gosling, P. D. (2008). A Predictive Fabric Model for Membrane Structure Design. In E. Oñate & B. Kröplin (Eds.), *Textile Composites and Inflatable Structures II SE - 3*, volume 8 of *Computational Methods in Applied Sciences* (pp. 35–50). Springer Netherlands.

Bridgens, B. N. & Gosling, P. D. (2010). Interpretation of results from the MSAJ "Testing Method for Elastic Constants of Membrane Materials". In *Proc. of the Tensinet Symposium 2010 - Tensile Architecture: Connecting Past and Future* (pp. 49–57). Sofia, Bulgaria.

Bridgens, B. N., Gosling, P. D., & Birchall, M. J. S. (2004a). Membrane material behaviour: concepts, practice & developments. *The Structural Engineer*, 82(14), 28–33.

Bridgens, B. N., Gosling, P. D., & Birchall, M. J. S. (2004b). Tensile fabric structures: concepts, practice & developments. *Structural Engineer*, 82(14), 21–27.

Bridgens, B. N., Gosling, P. D., Jou, G.-T., & Hsu, X.-Y. (2012). Inter-laboratory comparison of biaxial tests for architectural textiles. *Journal of the Textile Institute*, 103(7), 706–718, DOI:10.1080/00405000.2011.602824.

Buet-Gautier, K. & Boisse, P. (2001). Experimental analysis and modeling of biaxial mechanical behavior of woven composite reinforcements. *Experimental Mechanics*, 41(3), 260–269, DOI:10.1007/BF02323143.

Byström, J., Jekabsons, N., & Varna, J. (2000). An evaluation of different models for prediction of elastic properties of woven composites. *Composites Part B: Engineering*, 31(1), 7–20, DOI:10.1016/S1359-8368(99)00061-X.

Cao, J., et al. (2008). Characterization of mechanical behavior of woven fabrics: experimental methods and benchmark results. *Composites Part A: Applied Science and Manufacturing*, 39(6), 1037–1053, DOI:10.1016/j.compositesa.2008.02.016.

Carvelli, V. & Poggi, C. (2001). A homogenization procedure for the numerical analysis of woven fabric composites. *Composites Part A: Applied Science and Manufacturing*, 32(10), 1425–1432, DOI:10.1016/S1359-835X(01)00041-0.

Cassel, A., Kinsey, P., & Sefton, D. (1968). Cylindrical shell analysis by dynamic relaxation. In *Proc. of the Institute of Civil Engineering*, volume 39 (pp. 75–84).

Cassell, A. C. & Hobbs, R. E. (1976). Numerical stability of dynamic relaxation analysis of non-linear structures. *International Journal for Numerical Methods in Engineering*, 10(6), 1407–1410, DOI:10.1002/nme.1620100620.

Cavallaro, P. V., Johnson, M. E., & Sadegh, A. M. (2003). Mechanics of plain-woven fabrics for inflated structures. *Composite Structures*, 61(4), 375–393, DOI:10.1016/S0263-8223(03)00054-0.

Charmetant, A., Orliac, J. G., Vidal-Sallé, E., & Boisse, P. (2012). Hyperelastic model for large deformation analyses of 3D interlock composite preforms. *Composites Science and Technology*, 72(12), 1352–1360, DOI:10.1016/j.compscitech.2012.05.006.

Charmetant, A., Vidal-Sallé, E., & Boisse, P. (2011). Hyperelastic modelling for mesoscopic analyses of composite reinforcements. *Composites Science and Technology*, 71(14), 1623–1631, DOI:10.1016/j.compscitech.2011.07.004.

Chen, S., Ding, X., Fangueiro, R., & Yi, H. (2008). Tensile performance of construction membrane materials under multi-axial loads. In X. He, H. Xie, & Y. Kang (Eds.), *Proc. of the SPIE-ICEM 2008*, volume 7375 (pp. 73755V–6 pp.). Nanjing, China.

Chen, S., Ding, X., & Yi, H. (2007). On the anisotropic tensile behaviors of flexible polyvinyl chloride-coated fabrics. *Textile Research Journal*, 77(6), 369–374, DOI:10.1177/0040517507078791.

Chen, S.-H., Yu, H.-Q., Guo, Z., Fangueiro, R., & Qi, D.-P. (2011). The FEM-prediction on tensile performance of woven membrane materials

under uni and bi-axial loads. *Journal of Fiber Bioengineering and Informatics*, 3(4), 244–249, DOI:10.3993/jfbi03201109.

Courant, R., Friedrichs, K., & Lewy, H. (1928). Über die partiellen Differenzengleichungen der mathematischen Physik. *Mathematische Annalen*, 100(1), 32–74, DOI:10.1007/BF01448839.

D'Amato, E. (2001). Finite element modeling of textile composites. *Composite Structures*, 54(4), 467–475, DOI:10.1016/S0263-8223(01)00119-2.

Dasgupta, A., Agarwal, R. K., & Bhandarkar, S. M. (1996). Three-dimensional modeling of woven-fabric composites for effective thermo-mechanical and thermal properties. *Composites Science and Technology*, 56(3), 209–223, DOI:10.1016/0266-3538(95)00111-5.

Day, A. S. (1965). An introduction to dynamic relaxation. *The Engineer*, 219(5668), 218–221.

Day, A. S. (1986). Stress strain equations for non-linear bahaviour of coated woven fabrics. In *Proc. of the International Assotiation of Shell and Spatial Structures (IASS) Symposium 1986: Shells, Membranes and Space Frames* (pp. 17–24). Osaka, Japan: Elsevier.

De Laet, L., Luchsinger, R. H., Crettol, R., Mollaert, M., & De Temmerman, N. (2009). Deployable Tensairity structures. *Journal of the International Association for Shell and Spatial Structures*, 50(2), 121–128.

De Temmerman, N., Mollaert, M., Van Mele, T., & De Laet, L. (2007). Design and analysis of a foldable mobile shelter system. *International Journal of Space Structures*, 22(3), 161–168.

Douthe, C., Baverel, O., & Caron, J.-F. (2006). Form-finding of a grid shell in composite materials. *Journal of the International Association for Shell and Spatial Structures*, 47(150), 53–62.

Dunne, F. & Petrinic, N. (2005). *Introduction to Computational Plasticity*. Oxford series on materials modelling. Oxford University Press.

Durville, D. (2008). Finite Element Simulation of the Mechanical Behaviour of Textile Composites at the Mesoscopic Scale of Individual Fibers. In E.

Oñate & B. Kröplin (Eds.), *Textile Composites and Inflatable Structures II SE - 2*, volume 8 of *Computational Methods in Applied Sciences* (pp. 15–34). Springer Netherlands.

EN ISO 1421:1998 (1998). *Rubber- or plastics-coated fabrics – Determination of tensile strength and elongation at break*. Standard, International Organization for Standardization, Geneva, Switzerland.

Federico, S. (2009). Volumetric-Distortional Decomposition of Deformation and Elasticity Tensor. *Mathematics and Mechanics of Solids*, 15(6), 672–690, DOI:10.1177/1081286509105591.

Finzi, L. & Maier, G. (1964). The tension structure of the Genova Palasport (in Italian). *Costruzioni Metalliche*, 2, 61–73.

Forster, B. & Mollaert, M., Eds. (2004). *European Design Guide for Tensile Surface Structures*. Brussels, Belgium: TensiNet.

Freeston, W. D., Platt, M. M., & Schoppee, M. M. (1967). Mechanics of elastic performance of textile materials: part XVIII. Stress-strain response of fabrics under two-dimensional loading 1. *Textile Research Journal*, 37(11), 948–975, DOI:10.1177/004051756703701107.

Frieze, P. A., Hobbs, R. E., & Dowling, P. J. (1978). Application of dynamic relaxation to the large deflection elasto-plastic analysis of plates. *Computers & Structures*, 8(2), 301–310, DOI:10.1016/0045-7949(78)90037-8.

Fung, Y. C., Fronek, K., & Patitucci, P. (1979). Pseudoelasticity of arteries and the choice of its mathematical expression. *The American Journal of Physiology*, 237(5), H620–631.

Galliot, C. & Luchsinger, R. H. (2009). A simple model describing the non-linear biaxial tensile behaviour of PVC-coated polyester fabrics for use in finite element analysis. *Composite Structures*, 90(4), 438–447, DOI:10.1016/j.compstruct.2009.04.016.

Galliot, C. & Luchsinger, R. H. (2010a). The shear ramp: A new test method for the investigation of coated fabric shear behaviour - Part I: Theory. *Composites Part A: Applied Science and Manufacturing*, 41(12), 1743–1749, DOI:10.1016/j.compositesa.2010.08.008.

Galliot, C. & Luchsinger, R. H. (2010b). The shear ramp: A new test method for the investigation of coated fabric shear behaviour - Part II: Experimental validation. *Composites Part A: Applied Science and Manufacturing*, 41(12), 1750–1759, DOI:10.1016/j.compositesa.2010.08.014.

Galliot, C. & Luchsinger, R. H. (2011a). Determination of the response of coated fabrics under biaxial stress: comparison between different test procedures. In E. Oñate, B. Kröplin, & K.-U. Bletzinger (Eds.), *Proc. of the International Conference on Textile Composites and Inflatable Structures STRUCTURAL MEMBRANES 2011* Barcelona, Spain.

Galliot, C. & Luchsinger, R. H. (2011b). Uniaxial and biaxial mechanical properties of ETFE foils. *Polymer Testing*, 30(4), 356–365, DOI:10.1016/j.polymertesting.2011.02.004.

Garbowski, T., Maier, G., & Novati, G. (2011). On calibration of orthotropic elastic-plastic constitutive models for paper foils by biaxial tests and inverse analyses. *Structural and Multidisciplinary Optimization*, 46(1), 111–128, DOI:10.1007/s00158-011-0747-3.

Gasser, A., Boisse, P., & Hanklar, S. (2000). Mechanical behaviour of dry fabric reinforcements. 3D simulations versus biaxial tests. *Computational Materials Science*, 17(1), 7–20, DOI:10.1016/S0927-0256(99)00086-5.

Gasser, T. C. & Holzapfel, G. A. (2002). A rate-independent elastoplastic constitutive model for biological fiber-reinforced composites at finite strains: continuum basis, algorithmic formulation and finite element implementation. *Computational Mechanics*, 29(4-5), 340–360, DOI:10.1007/s00466-002-0347-6.

Gasser, T. C., Ogden, R. W., & Holzapfel, G. A. (2006). Hyperelastic modelling of arterial layers with distributed collagen fibre orientations. *Journal of the Royal Society / Interface*, 3(6), 15–35, DOI:10.1098/rsif.2005.0073.

Glaessgen, E. H., Pastore, C. M., Hayden Griffin, O., & Birger, A. (1996). Geometrical and finite element modelling of textile composites. *Composites Part B: Engineering*, 27(1), 43–50, DOI:10.1016/1359-8368(95)00005-4.

Gosling, P. (1992). *Numerical Modelling of Stable Minimal Surfaces*. Phd thesis, University of Warwick, UK.

Gosling, P. D. (2007). Tensinet analysis and materials working group - basic phylosophy and calling notice. *Tensinews Newsletter December 2007*.

Gosling, P. D. & Bridgens, B. N. (2008). Material testing & computational mechanics - A new philosophy for architectural fabrics. *International Journal of Space Structures*, 23(4), 215–232, DOI:10.1260/026635108786959870.

Gosling, P. D., et al. (2013). Analysis and design of membrane structures: results of a round robin exercise. *Engineering Structures*, 48, 313–328, DOI:10.1016/j.engstruct.2012.10.008.

Gründig, L. & Bäuerle, J. (1990). Automated cutting pattern determination and control for prestressed membranes. In *Proc. of Textile Composites in Building Construction* (pp. 109–120).

Gründig, L., Ekert, L., & Moncrieff, E. (1996). Geodesic and semi-geodesic line algorithms for cutting pattern generation of architectural textile structures. In T. Lan (Ed.), *Proc. of the Asia-Pacific Conference on Shell and Spatial Structures* Beijing, China.

Gründig, L., Moncrieff, E., Singer, P., & Ströbel, D. (2000). High-performance cutting pattern generation of architectural textile structures. In E. Papadrakakis (Ed.), *Proc. of IASS-IACM 2000 Fourth International Colloquium on Computation of Shell & Spatial Structures* Chania-Crete, Greece.

Gurtin, M. E., Fried, E., & Anand, L. (2010). *The Mechanics and Thermodynamics of Continua*. Cambridge University Press.

Haber, R. B. & Abel, J. F. (1982a). Initial equilibrium solution methods for cable reinforced membranes. Part I - formulations. *Computer Methods in Applied Mechanics and Engineering*, 30(3), 263–284, DOI:10.1016/0045-7825(82)90080-9.

Haber, R. B. & Abel, J. F. (1982b). Initial equilibrium solution methods for cable reinforced membranes. Part II - implementation. *Computer Methods in Applied Mechanics and Engineering*, 30(3), 285–306, DOI:10.1016/0045-7825(82)90081-0.

Happold, E., Ealey, T. A., Liddell, W. I., Pugh, J. W. E., & Webster, R. H. (1987). Discussion: the design and construction of the Diplomatic Club, Riyadh. *The Structural Engineer*, 65(1), 377–382.

Haug, E. & Powell, G. H. (1972). Analytical shape finding for cable nets. In *Proc. of the 1971 IASS Pacific Symposium Part II on Tension Structures and Space Frames* (pp. 83–92). Tokyo and Kyoto, Japan.

Hearle, J. W. S. (2001). *High-performance Fibres*. Woodhead Publishing Limited series on fibres. Textile Institute.

Hill, R. (1948). A theory of the yielding and plastic flow of anisotropic metals. *Proceedings of the Royal Society A: Mathematical, Physical and Engineering Sciences*, 193(1033), 281–297, DOI:10.1098/rspa.1948.0045.

Hivet, G. & Boisse, P. (2008). Consistent mesoscopic mechanical behaviour model for woven composite reinforcements in biaxial tension. *Composites Part B: Engineering*, 39(2), 345–361, DOI:10.1016/j.compositesb.2007.01.011.

Hivet, G., Vidal-Sallé, E., & Boisse, P. (2012). Analysis of the stress components in a textile composite reinforcement. *Journal of Composite Materials*, 47(3), 269–285, DOI:10.1177/0021998312439222.

Holzapfel, G. A. (2000). *Nonlinear Solid Mechanics: A Continuum Approach for Engineering*. John Wiley & Sons.

Holzapfel, G. A. & Gasser, T. C. (2001). A viscoelastic model for fiber-reinforced composites at finite strains: continuum basis, computational aspects and applications. *Computer Methods in Applied Mechanics and Engineering*, 190(34), 4379–4403, DOI:10.1016/S0045-7825(00)00323-6.

Holzapfel, G. A., Gasser, T. C., & Ogden, R. W. (2000). A new constitutive framework for arterial wall mechanics and a comparative study of

material models. *Journal of Elasticity and the Physical Science of Solids*, 61(1-3), 1–48, DOI:10.1023/A:1010835316564.

Holzapfel, G. A., Gasser, T. C., & Ogden, R. W. (2004). Comparison of a multi-layer structural model for arterial walls with a fung-type model, and issues of material stability. *Journal of Biomechanical Engineering*, 126(2), 264–75.

Holzapfel, G. A., Gasser, T. C., & Stadler, M. (2002). A structural model for the viscoelastic behavior of arterial walls: continuum formulation and finite element analysis. *European Journal of Mechanics - A/Solids*, 21(3), 441–463, DOI:10.1016/S0997-7538(01)01206-2.

Holzapfel, G. A. & Ogden, R. W. (2010). Constitutive modelling of arteries. *Proceedings of the Royal Society A: Mathematical, Physical and Engineering Sciences*, 466(2118), 1551–1597, DOI:10.1098/rspa.2010.0058.

Houtman, R. & Orpana, M. (2000). Materials for membrane structures. In *Proc. of Workshop Textile Roofs 2000*, volume 4 (pp. 1–7). TU Berlin, Germany.

Huang, N. C. (1979a). Finite biaxial extension of completely set plain woven fabrics. *Journal of Applied Mechanics*, 46(3), 651, DOI:10.1115/1.3424621.

Huang, N. C. (1979b). Finite biaxial extension of partially set plain woven fabrics. *International Journal of Solids and Structures*, 15(8), 615–623, DOI:10.1016/0020-7683(79)90075-1.

Hughes, T. J. R. (2000). *The Finite Element Method: Linear Static and Dynamic Finite Element Analysis*. Dover Civil and Mechanical Engineering. Dover Publications.

Ishii, K. (1999). Form finding analysis in consideration of cutting patterns of membrane structures. *International Journal of Space Structures*, 14(2), 105–119, DOI:10.1260/0266351991494731.

Ivanov, I. & Tabiei, A. (2001). Three-dimensional computational micromechanical model for woven fabric composites. *Composite Structures*, 54(4), 489–496, DOI:10.1016/S0263-8223(01)00121-0.

Jackson, A. L., Bridgens, B. N., & Gosling, P. D. (2009). A new biaxial and shear protocol for architectural fabrics. In A. Domingo & C. Lazaro (Eds.), *Proc. of the International Assotiation of Shell and Spatial Structures (IASS) Symposium 2009* (pp. 2167–2179). Valencia, Spain.

Jeon, B. S., Chun, S. Y., & Hong, C. J. (2003). Structural and mechanical properties of woven fabrics employing Peirce's model. *Textile Research Journal*, 73(10), 929–933, DOI:10.1177/004051750307301014.

Joldes, G. R., Wittek, A., & Miller, K. (2009). Computation of intra-operative brain shift using dynamic relaxation. *Computer Methods in Applied Mechanics and Engineering*, 198(41), 3313–3320, DOI:10.1016/j.cma.2009.06.012.

Joldes, G. R., Wittek, A., & Miller, K. (2011). An adaptive dynamic relaxation method for solving nonlinear finite element problems. Application to brain shift estimation. *International Journal for Numerical Methods in Biomedical Engineering*, 27(2), 173–185, DOI:10.1002/cnm.1407.

Kashiwa, M. & Onoda, J. (2009). Wrinkling analysis using improved dynamic relaxation method. *AIAA Journal*, 47(7), 1601–1607, DOI:10.2514/1.34031.

Kato, S., Minami, H., Yoshino, T., & Namita, T. (1997). Analysis of membrane structures based on fabric lattice model considering viscous characteristics. In *Proc. of the International Assotiation of Shell and Spatial Structures (IASS) Symposium 1997*, volume 1 (pp. 411–420). Singapore, China.

Kato, S., Yoshino, T., & Minami, H. (1999). Formulation of constitutive equations for fabric membranes based on the concept of fabric lattice model. *Engineering Structures*, 21(8), 691–708, DOI:10.1016/S0141-0296(98)00024-8.

Kawabata, S., Niwa, M., & Kawai, H. (1973). 3 - The finite-deformation theory of plain-weave fabrics Part I: The biaxial-deformation theory. *Journal of the Textile Institute*, 64(1), 21–46, DOI:10.1080/00405007308630416.

Kemp, A. (1958). An extension of Peirce's cloth geometry to the treatment of non-circular threads. *Journal of the Textile Institute Transactions*, 49(1), T44–T48, DOI:10.1080/19447025808660119.

Kilian, A. & Ochsendorf, J. (2006). Particle-spring systems for structural form finding. *Journal of the International Association for Shell and Spatial Structures*, 148(2), 77–84.

King, M. J., Jearanaisilawong, P., & Socrate, S. (2005). A continuum constitutive model for the mechanical behavior of woven fabrics. *International Journal of Solids and Structures*, 42(13), 3867–3896, DOI:10.1016/j.ijsolstr.2004.10.030.

Knippers, J., Cremers, J., Gabler, M., & Lienhard, J. (2011). *Construction Manual for Polymers + Membranes: Materials, Semi-Finished Products, Form-Finding, Design*. Edition Detail. Basel, Switzerland: Birkhauser Architecture.

Krieg, R. D. (1973). Unconditional stability in numerical time integration methods. *Journal of Applied Mechanics*, 40(2), 417, DOI:10.1115/1.3422999.

Kuusisto, T. K. (2010). *Textile in Architecture*. Master, Tampere University of Technology, Finland.

Leaf, G. A. V. & Anandjiwala, R. D. (1985). A Generalized Model of Plain Woven Fabric. *Textile Research Journal*, 55(2), 92–99, DOI:10.1177/004051758505500203.

Lee, E.-S. & Youn, S.-K. (2006). Finite element analysis of wrinkling membrane structures with large deformations. *Finite Elements in Analysis and Design*, 42(8-9), 780–791, DOI:10.1016/j.finel.2006.01.004.

Lempriere, B. M. (1968). Poisson's ratio in orthotropic materials. *AIAA Journal*, 6(11), 2226–2227, DOI:10.2514/3.4974.

Levenberg, K. (1944). A method for the solution of certain non-linear problems in least squares. *The Quarterly of Applied Mathematics*, 2, 164–168.

Lewis, W. J. (2003). *Tension Structures: Form and Behaviour*. Thomas Telford.

Lewis, W. J. (2008). Computational form-finding methods for fabric structures. In *Proc. of the ICE - Engineering and Computational Mechanics*, volume 161 (pp. 139–149).

Lin, J.-J. (2010). Prediction of elastic properties of plain weave fabric using geometrical modeling. In P. Dubrovski (Ed.), *Woven Fabric Engineering* chapter 7.

Linkwitz, K. (1999a). About formfinding of double-curved structures. *Engineering Structures*, 21(8), 709–718, DOI:10.1016/S0141-0296(98)00025-X.

Linkwitz, K. (1999b). Formfinding by the "Direct Approach" and pertinent strategies for the conceptual design of prestressed and hanging structures. *International Journal of Space Structures*, 14(2), 73–87, DOI:10.1260/0266351991494713.

Linkwitz, K. & Schek, H.-J. (1971). Einige Bemerkungen zur Berechnung von vorgespannten Seilnetzkonstruktionen. *Ingenieur-Archiv*, 40(3), 145–158, DOI:10.1007/BF00532146.

Linkwitz, K., Schek, H.-J., & Gründig, L. (1974). Die Gleichgewichtsberechnung von Seilnetzen unter Zusatzbedingungen. *Ingenieur-Archiv*, 43(4), 183–192, DOI:10.1007/BF00534000.

Maier, G. (1963a). Analysis of wheel-shape tension structures (in Italian). *Rendiconti dell'Istituto Lombardo di Scienze e Lettere*, 97, 527–591.

Maier, G. (1963b). Tension structures: a concise state-of-the-art (in Italian). *Costruzioni Metalliche*, 4, 180–187.

Maier, G., Buljak, V., Garbowski, T., Cocchetti, G., & Novati, G. (2013). Mechanical characterization of materials and diagnosis of structures by inverse analyses: some innovative procedures and applications. *International Journal of Computational Methods*, 11(03), 1343002, DOI:10.1142/S0219876213430020.

Marquardt, D. W. (1963). An algorithm for least-squares estimation of nonlinear parameters. *Journal of the Society for Industrial and Applied Mathematics*, 11(2), 431–441.

Maurin, B. & Motro, R. (1998). The surface stress density method as a form-finding tool for tensile membranes. *Engineering Structures*, 20(8), 712–719, DOI:10.1016/S0141-0296(97)00108-9.

Maurin, B. & Motro, R. (1999). Cutting pattern of fabric membranes with the stress composition method. *International Journal of Space Structures*, 14(2), 121–129, DOI:10.1260/0266351991494740.

Maurin, B. & Motro, R. (2013). Textile Architecture. In R. Motro (Ed.), *Flexible Composite Materials in Architecture, Constructions and Interiors* chapter 2. Basel, Switzerland: Birkhauser Architecture.

McCartney, J., Hinds, B. K., & Seow, B. L. (1999). The flattening of triangulated surfaces incorporating darts and gussets. *Computer-Aided Design*, 31(4), 249–260, DOI:10.1016/S0010-4485(99)00025-1.

Menges, G. & Meffert, B. (1976). Mechanical behaviour of PVC coated polyester fabrics under biaxial stress. *Journal of Kunststoffe German Plastics*, 66(11), 12–14.

Milani, A. & Nemes, J. (2004). An intelligent inverse method for characterization of textile reinforced thermoplastic composites using a hyperelastic constitutive model. *Composites Science and Technology*, 64(10-11), 1565–1576, DOI:10.1016/j.compscitech.2003.11.010.

Minami, H. (2006). A multi-step linear approximation method for nonlinear analysis of stress and deformation of coated plain-weave fabric. *Journal of Textile Engineering*, 52(5), 189–195, DOI:10.4188/jte.52.189.

Mollaert, M., De Temmerman, N., & Van Mele, T. (2006). Variations in form and stress behaviour of a V-shaped membrane in a foldable structure. In *WIT Transactions on the Built Environment*, volume 85 (pp. 41–50).

MSAJ/M-01:1993 (1993). *Testing Method for In-plane Shear Stiffness of Membrane Materials*. Standard, Membrane Structure Association of Japan, Tokio, Japan.

MSAJ/M-02:1995 (1995). *Testing Method for Elastic Constant of Membrane Materials*. Standard, Membrane Structure Association of Japan, Tokio, Japan.

Nouri-Baranger, T. (2004). Computational methods for tension-loaded structures. *Archives of Computational Methods in Engineering*, 11(2), 143–186, DOI:10.1007/BF02905937.

Oakley, D. R. & Knight, N. F. (1995a). Adaptive dynamic relaxation algorithm for non-linear hyperelastic structures Part I. Formulation. *Computer Methods in Applied Mechanics and Engineering*, 126(1-2), 67–89, DOI:10.1016/0045-7825(95)00805-B.

Oakley, D. R. & Knight, N. F. (1995b). Adaptive dynamic relaxation algorithm for non-linear hyperelastic structures Part II. Single-processor implementation. *Computer Methods in Applied Mechanics and Engineering*, 126(1-2), 91–109, DOI:10.1016/0045-7825(95)00806-C.

Oakley, D. R., Knight, N. F., & Warner, D. D. (1995). Adaptive dynamic relaxation algorithm for non-linear hyperelastic structures Part III. Parallel implementation. *Computer Methods in Applied Mechanics and Engineering*, 126(1-2), 111–129, DOI:10.1016/0045-7825(95)00807-D.

Odegard, G., Searles, K., & Kumosa, M. (2001). A continuum elastic-plastic model for woven-fabric/polymer-matrix composite materials under biaxial stresses. *Composites Science and Technology*, 61(16), 2501–2510, DOI:10.1016/S0266-3538(01)00168-3.

Ogden, R. W. (2003). Nonlinear elasticity, anisotropy, material stability and residual stresses in soft tissue. In G. Holzapfel & R. Ogden (Eds.), *Biomechanics of Soft Tissue in Cardiovascular Systems*, number 441 in CISM Courses and Lectures (pp. 65–108). Vienna: Springer-Verlag.

Olofsson, B. (1964). 49 - A general model of a fabric as a geometric-mechanical structure. *Journal of the Textile Institute Transactions*, 55(11), T541–T557, DOI:10.1080/19447026408662245.

Olofsson, B. (1966). Deformation properties of stretch fabrics. *Journal of the Textile Institute Transactions*, 57(9), T429–T432, DOI:10.1080/19447026608662386.

Otto, F., Trostel, R., & Schleyer, F. K. (1973). *Tensile structures: design, structure, and calculation of buildings of cables, nets, and membranes*. Number v. 1-2. The MIT Press.

Pandolfi, A. & Holzapfel, G. A. (2008). Three-dimensional modeling and computational analysis of the human cornea considering distributed collagen fibril orientations. *Journal of Biomechanical Engineering*, 130(6), 061006, DOI:10.1115/1.2982251.

Pandolfi, A. & Manganiello, F. (2006). A model for the human cornea: constitutive formulation and numerical analysis. *Biomechanics and Modeling in Mechanobiology*, 5(4), 237–46, DOI:10.1007/s10237-005-0014-x.

Papadrakakis, M. (1981). A method for the automatic evaluation of the dynamic relaxation parameters. *Computer Methods in Applied Mechanics and Engineering*, 25(1), 35–48, DOI:10.1016/0045-7825(81)90066-9.

Pargana, J. B., Lloyd-Smith, D., & Izzuddin, B. A. (2007). Advanced material model for coated fabrics used in tensioned fabric structures. *Engineering Structures*, 29(7), 1323–1336, DOI:10.1016/j.engstruct.2006.09.001.

Pauletti, R. M. O. & Pimenta, P. M. (2008). The natural force density method for the shape finding of taut structures. *Computer Methods in Applied Mechanics and Engineering*, 197(49-50), 4419–4428, DOI:10.1016/j.cma.2008.05.017.

Peel, L. D. (2007). Exploration of high and negative Poisson's ratio elastomer-matrix laminates. *Physica Status Solidi (b)*, 244(3), 988–1003, DOI:10.1002/pssb.200572717.

Peirce, F. T. (1937). 5 - The geometry of cloth strucure. *Journal of the Textile Institute Transactions*, 28(3), T45–T96, DOI:10.1080/19447023708658809.

Peng, X. & Cao, J. (2002). A dual homogenization and finite element approach for material characterization of textile composites. *Composites*

Part B: Engineering, 33(1), 45–56, DOI:10.1016/S1359-8368(01)00052-X.

Peng, X. Q. & Cao, J. (2000). Numerical determination of mechanical elastic constants of textile composites. In *Proc. of the 15th Annual Techincal Conference of the American Society for Composite* Colege Station, Texas (USA).

Peng, X. Q. & Cao, J. (2005). A continuum mechanics-based non-orthogonal constitutive model for woven composite fabrics. *Composites Part A: Applied Science and Manufacturing*, 36(6), 859–874, DOI:10.1016/j.compositesa.2004.08.008.

Potluri, P., Perez Ciurezu, D. A., & Ramgulam, R. B. (2006). Measurement of meso-scale shear deformations for modelling textile composites. *Composites Part A: Applied Science and Manufacturing*, 37(2), 303–314, DOI:10.1016/j.compositesa.2005.03.032.

Reinhardt, H. W. (1976). On the biaxial testing and strength of coated fabrics. *Experimental Mechanics*, 16(2), 71–74, DOI:10.1007/BF02328607.

Rizzi, E. & Carol, I. (2001). A formulation of anisotropic elastic damage using compact tensor formalism. *Journal of Elasticity and the Physical Science of Solids*, 64(2-3), 85–109, DOI:10.1023/A:1015284701032.

Rushton, K. R. (1968). Large deflexion of variable-thickness plates. *International Journal of Mechanical Sciences*, 10(9), 723–735, DOI:10.1016/0020-7403(68)90086-6.

Rushton, K. R. & Laing, L. M. (1968). A digital computer solution of the Laplace equation using dynamic relaxation method. *Aeronaut. Quart.*, 19, 375–387.

Sagar, T. V., Potluri, P., & Hearle, J. W. S. (2003). Mesoscale modelling of interlaced fibre assemblies using energy method. *Computational Materials Science*, 28(1), 49–62, DOI:10.1016/S0927-0256(03)00056-9.

Sánchez, J., Serna, M. A., & Morer, P. (2007). A multi-step force-density method and surface-fitting approach for the preliminary shape

design of tensile structures. *Engineering Structures*, 29(8), 1966–1976, DOI:10.1016/j.engstruct.2006.10.015.

Schek, H.-J. (1974). The force density method for form finding and computation of general networks. *Computer Methods in Applied Mechanics and Engineering*, 3(1), 115–134, DOI:10.1016/0045-7825(74)90045-0.

Seidel, M. (2009). *Tensile Surface Structures - A Practical Guide to Cable and Membrane Construction*. Berlin, Germany: Ernst & Sohn.

Sen, A. K. & Damewood, J. (2001). *Coated Textiles: Principles and Applications*. Taylor & Francis.

Siev, A. & Eidelman, J. (1964). Stress analysis of prestressed suspended roofs. *Journal of the Structural Engineering Division, ASCE*, 90(4), 103–121.

Singer, P. (1995). *Die Berechnung von Minimalflächen, Seifenblasen, Membrane und Pneus aus geodätischer Sicht*. Phd thesis, University of Stuttgart, Germany.

Skelton, J. (1976). Fundamentals of fabric shear. *Textile Research Journal*, 46(12), 862–869, DOI:10.1177/004051757604601202.

Spencer, A. J. M. (1984). Constitutive theory for strongly anisotropic solids. In A. Spencer (Ed.), *Continuum Theory of the Mechanics of Fibre-reinforced Composites*, CISM Courses and Lectures No. 282 (pp. 1–32). Wien, Austria: Springer-Verlag.

Stubbs, N. & Fluss, H. (1980). A space-truss model for plain-weave coated fabrics. *Applied Mathematical Modelling*, 4(1), 51–58, DOI:10.1016/0307-904X(80)90213-9.

Sun, W. & Sacks, M. S. (2005). Finite element implementation of a generalized Fung-elastic constitutive model for planar soft tissues. *Biomechanics and modeling in mechanobiology*, 4(2-3), 190–9, DOI:10.1007/s10237-005-0075-x.

Tabarrok, B. & Qin, Z. (1992). Nonlinear analysis of tension structures. *Computers & Structures*, 45(5-6), 973–984, DOI:10.1016/0045-7949(92)90056-6.

Takano, N., Uetsuji, Y., Kashiwagi, Y., & Zako, M. (1999). Hierarchical modelling of textile composite materials and structures by the homogenization method. *Modelling and Simulation in Materials Science and Engineering*, 7(2), 207–231, DOI:10.1088/0965-0393/7/2/006.

Tarfaoui, M. & Akesbi, S. (2001). A finite element model of mechanical properties of plain weave. *Colloids and Surfaces A: Physicochemical and Engineering Aspects*, 187-188, 439–448, DOI:10.1016/S0927-7757(01)00611-2.

Tarfaoui, M., Drean, J. Y., & Akesbi, S. (2001). Predicting the stress-strain behavior of woven fabrics using the finite element method. *Textile Research Journal*, 71(9), 790–795, DOI:10.1177/004051750107100908.

Testa, R. & Yu, L. M. (1987). Stress-strain relation for coated fabrics. *Journal of Engineering Mechanics*, 113(11), 1631–1646, DOI:10.1061/(ASCE)0733-9399(1987)113:11(1631).

Testa, R. B., Spillers, W. R., & Stubbs, N. (1978). Bilinear model for coated square fabrics. *Journal of the Engineering Mechanics Division*, 104(5), 1027–1042.

Thomas, S. & Stubbs, N. (1984). An inelastic biaxial constitutive model for fabric-reinforced composites. *Journal of Industrial Textiles*, 13(3), 144–160, DOI:10.1177/152808378401300303.

Treloar, L. R. G. (1977). Physics of textiles. *Physics Today*, 30(12), 23, DOI:10.1063/1.3037824.

Tsai, S. W. (1968). Strength theories of filamentary structures. In R. T. Schwartz & H. T. Schwartz (Eds.), *Fundamental Aspects of Fiber Reinforced Plastic Composites* (pp. 3–11). New York: Wiley Interscience.

Turvey, G. J. & Salehi, M. (1990). DR large deflection analysis of sector plates. *Computers & Structures*, 34(1), 101–112, DOI:10.1016/0045-7949(90)90304-K.

Tysmans, T., Adriaenssens, S., & Wastiels, J. (2011). Form finding methodology for force-modelled anticlastic shells in glass fibre textile

reinforced cement composites. *Engineering Structures*, 33(9), 2603–2611, DOI:10.1016/j.engstruct.2011.05.007.

Uhlemann, J., Stranghöner, N., & Saxe, K. (2014). Different determination procedures for stiffness parameters of woven fabrics and their impact in the membrane structure analysis. In E. Oñate, J. Oliver, & A. Huerta (Eds.), *Proc. of the 11th World Congress on Computational Mechanics (WCCM XI)* Barcelona, Spain.

Underwood, P. (1983). Dynamic relaxation. In T. Belytschko & T. Hughes (Eds.), *Computational Methods for Transient Analyis* (pp. 245–256). Amsterdam: Elsevier.

Van Mele, T., De Temmerman, N., De Laet, L., & Mollaert, M. (2010). Scissor-hinged retractable membrane structures. *International Journal of Structural Engineering*, 1(3), 374–396, DOI:10.1504/IJStructE.2010.033489.

Veenendaal, D. & Block, P. (2011). A framework for comparing form finding methods. In *Proceedings of the IABSE-IASS Symposium 2011* London, UK.

Veenendaal, D. & Block, P. (2012). An overview and comparison of structural form finding methods for general networks. *International Journal of Solids and Structures*, 49(26), 3741–3753, DOI:10.1016/j.ijsolstr.2012.08.008.

Vidal-Sallé, E., Florimond, C., Charmetant, A., & Boisse, P. (2014). Hypoelastic vs hyper-elastic constitutive equation for textile materials at mesoscale. In *Key Engineering Materials*, volume 611-612 (pp. 243–249).

Wang, F. (2002). Prediction method for tensile property of woven fabrics in lower loads. *Journal of Dong Hua University (English edition)*, 19(2), 6–14.

Wendling, A., Hivet, G., Vidal-Sallé, E., & Boisse, P. (2014). Consistent geometrical modelling of interlock fabrics. *Finite Elements in Analysis and Design*, 90, 93–105, DOI:10.1016/j.finel.2014.05.010.

Xue, P., Peng, X., & Cao, J. (2003). A non-orthogonal constitutive model for characterizing woven composites. *Composites Part A: Applied Science and Manufacturing*, 34(2), 183–193, DOI:10.1016/S1359-835X(02)00052-0.

Yu, G., Patrikalakis, N. M., & Maekawa, T. (2000). Optimal development of doubly curved surfaces. *Computer Aided Geometric Design*, 17(6), 545–577, DOI:10.1016/S0167-8396(00)00017-0.

Yu, W.-R., Kim, M. S., & Lee, J. S. (2006). Modeling of anisotropic creep behavior of coated textile membranes. *Fibers and Polymers*, 7(2), 123–128, DOI:10.1007/BF02908256.

Yu, W. R., Pourboghrat, F., Chung, K., Zampaloni, M., & Kang, T. J. (2002). Non-orthogonal constitutive equation for woven fabric reinforced thermoplastic composites. *Composites Part A: Applied Science and Manufacturing*, 33(8), 1095–1105, DOI:10.1016/S1359-835X(02)00053-2.

Zee, L. & Sternberg, E. (1983). Ordinary and strong ellipticity in the equilibrium theory of incompressible hyperelastic solids. *Archive for Rational Mechanics and Analysis*, 83(1), 53–90, DOI:10.1007/BF00281087.

Zhang, L. C., Kadkhodayan, M., & Mai, Y.-W. (1994). Development of the maDR method. *Computers & Structures*, 52(1), 1–8, DOI:10.1016/0045-7949(94)90249-6.

Zhang, L. G. & Yu, T. X. (1989). Modified adaptive dynamic relaxation method and its application to elastic-plastic bending and wrinkling of circular plates. *Computers & Structures*, 33(2), 609–614, DOI:10.1016/0045-7949(89)90035-7.

Zhang, Y., Zhang, Q., & Lv, H. (2012). Mechanical properties of polyvinylchloride-coated fabrics processed with Precontraint(R) technology. *Journal of Reinforced Plastics and Composites*, 31(23), 1670–1684, DOI:10.1177/0731684412459898.

Zhang, Y., Zhang, Q., Zhou, C., & Zhou, Y. (2010). Mechanical properties of PTFE coated fabrics. *Journal of Reinforced Plastics and Composites*, 29(24), 3624–3630, DOI:10.1177/0731684410378542.

Zhu, Q. (2003). Three-dimensional viscoelastic simulation of woven composite substrates for multilayer circuit boards. *Composites Science and Technology*, 63(13), 1971–1983, DOI:10.1016/S0266-3538(03)00171-4.

Zienkiewicz, O. C. & Taylor, R. L. (2000). *The Finite Element Method*. Butterworth-Heinemann.